2018

Toxicological Inhalation Effects of Metal-Based Nanoparticle Aerosols as Studied by a Portable In Vitro Exposure Cassette

Lynn E. Secondo
Virginia Commonwealth University

Toxicological Inhalation Effects of Metal-Based Nanoparticle Aerosols as Studied by a Portable In Vitro Exposure Cassette

This dissertation is submitted in partial completion of the requirements for the degree of Doctor of Philosophy at Virginia Commonwealth University.

by

Lynn Elisabeth Secondo

Bachelor of Science, Chemical Engineering, Trine University, 2012

Master of Science in Engineering, Chemical Engineering, University of Michigan, 2014

Director: Nastassja Lewinski, Ph.D.

Assistant Professor, Department of Chemical and Life Sciences Engineering

Committee in Charge:

Daren Chen, Ph.D., Professor, Department of Mechanical and Nuclear Engineering

Laleh Golshahi, Ph.D., Assistant Professor, Department of Mechanical and Nuclear Engineering

Christina Tang, Ph.D., Assistant Professor, Department of Chemical and Life Sciences Engineering

Hu Yang, Ph.D., Associate Professor, Department of Chemical and Life Sciences Engineering

Virginia Commonwealth University

Richmond, Virginia

November, 2018

Acknowledgement

First and foremost, I would like to thank my wonderful advisor, Dr. Nastassja Lewinski. Her help and support have been paramount in shaping my doctoral time. Nastassja provided me with many opportunities to present my research. Throughout my time at VCU, Nastassja consistently encouraged me to pursue my passions and helped me to discover new interests through her suggestion to pursue a Fulbright Scholarship. Her guiding hand provided me the opportunity to grow into an independent researcher while feeling supported.

I would like to thank my committee of Dr. Chen, Dr. Golshahi, Dr. Tang, and Dr. Yang who have helped to refine my work. The insights and questions provided by my committee have aided me in determining important conclusions within my research and how to explain my work across disciplines.

I would also like to thank my colleagues both at the Centre for Research and Technology Hellas in Thessaloniki who graciously hosted me during my Fulbright experience and within the Lewinski Lab. My colleagues at CERTH provided me insight into the Greek language and traditions. Thank you to the Lewinski Lab group for their support, help in the lab, and always being up for a good discussion.

Finally, I want to thank my family and friends for their unwavering support throughout my graduate years. The road has not been easy, and my family has always been supportive of my decisions. My family and friends continued to remind me of my motivation of the pursuit of this work. My brother, Ray, has been incredibly helpful in reviewing my work. Ray has pushed me to consider new ideas throughout engineering and has provided me with the opportunity to talk through many of my ideas while providing feedback. I'd also like to thank my cat, Napoleon, for always greeting me at the door after a long day with love and kitty cuddles.

Table of Contents

Table of Figures

Table of Tables

List of Abbreviations

A549 – Adenocarcinomic Alveolar Epithelial Cells
AAS – Atomic Absorption Spectroscopy
ABS - Acrylonitrile Butadiene Styrene
ABSPlus – Acrylonitrile Butadiene Styrene Plus
ALB - Albumin
ALI – Air-Liquid Interface
ALICE – Air-Liquid Interface Cell Exposure
ALP – Alkaline Phosphatase
ANOVA – Analysis of Variance
APAP – Acetaminophen
ATP – Adenosine Triphosphate
BAL – Bronchioalveolar Lavage
BALF– Bronchioalveolar Lavage Fluid
BEAS-2B – Primary Immortalized Human Bronchial Epithelial Cells
BET – Brunauer-Emmett-Teller
CERTH – Centre for Research and Technology
CFD – Computational Fluid Dynamics
CNC – Cellulose Nanocrystal
CNT – Carbon Nanotube
CPC – Condensation Particle Counter
CV – Cyclic Voltammetry
Cyt c – Cytochrome c
DC – Direct Current
DCF – Dichlorofluorescin
DCFH-DA – 2,7'-dichlorodihydrofluorescein diacetate
DEP – Diesel Exhaust Particles
DI - Deionized
DLS – Dynamic Light Scattering
DMA – Differential Mobility Analyzer
DMAS – Differential Mobility Analyzing System
DMEM – Dulbecco's Modified Eagle Medium
DMPS – Differential Mobility Particle Sizer
DMSO – Dimethyl Sulfoxide
DNA – Deoxyribonucleic Acid
DPF – Diesel Particulate Filter
EAVES – Electrostatic Aerosol In Vitro Exposure System
EDTA – Ethylenediaminetetraacetic acid
EDS – Energy Dispersive Spectroscopy
EF – Electric Field
EM – Electron Microscopy
ENP – Engineered Nanoparticle
EPDExS – Electrostatic Particulate Dosage and Exposure System
EPR – Electron Paramagnetic Resonance
ESR – Electrospin Resonance

FBS – Fetal Bovine Serum
FCS – Fetal Calf Serum
FTIR – Fourier-Transform Infrared Spectroscopy
FPG – Formamidopyrimidine DNA Glycosylase
GCS – Glucosylceramide Synthase
GM-CSF – Granulocyte-Macrophage Colony-Stimulating Factor
GSH – Glutathione (reduced)
GSSG – Glutathione (oxidized)
HBSS – Hank's Buffered Salt Solution
HEPA – High-Efficiency Particulate Air
HMOX-1 – Heme Oxygenase 1
HO-1 - Heme Oxygenase 1
HRP – Horseradish Peroxidase
HT – High Temperature Furnace
ICP-MS – Inductively Coupled Plasma – Mass Spectroscopy
ICP-OES – Inductively Coupled Plasma – Optical Emission Spectroscopy
ICRP – International Commission on Radiological Protection
IL – Interleukin
ITO – Indium Tin Oxide
LD50 – Lethal Dose, 50%
LDH – Lactate Dehydrogenase
LOAEL – Lowest-Observed-Adverse-Effect Level
LPM – Liters per Minute
LPS – Light Scattering Photometry
LSD – Low-Sulfur Diesel
MDDC – Monocyte-derived Dendritic Cells
MDM - Monocyte-derived Macrophages
MEC – Multichannel Exposure Culture
MIP- Macrophage Inflammatory Protein
MMAD – Mass Median Aerodynamic Diameter
MOUDI – Microorifice Uniform Deposit Impactor
MPPD – Multiple Path Particle Dosimetry
MTP - Microprotein
MTS - 3-(4,5-dimethylthiazol-2-yl)-5-(3-carboxymethoxyphenyl)-2-(4-sulfophenyl)-2H-tetrazolium
MTT - 3-(4,5-dimethylthiazol-2-yl)-2,5-diphenyltetrazolium bromide
MWCNT – Multiwalled Carbon Nanotube
NAA – Neutron Activation Analysis
NAC – N-acetylcysteine
NACIVT – Nano Aerosol Chamber In Vitro Toxicity
NADPH – Nicotinamide adenine dinucleotide phosphate
nDMA – nano-Dynamic Mobility Analyzer
NIST – National Institute of Science and Technology
NOAEC – No Observed Adverse Effect Concentration
NOAEL – No Observed Adverse Effect Level
NP – Nanoparticle

NR – Not Reported
OPS – Optical Particle Counter
OSHA – Occupational Safety and Health Administration
PAHs – Polycyclic Aromatic Hydrocarbons
PBS – Phosphate Buffered Solution
PEG – Polyethylene glycol
PETG – Polyethylene terephthalate glycol modified
PFT – Pulmonary Function Test
PI – Polydispersity Index
PIVEC – Portable In Vitro Exposure Cassette
PLA – Polylactic Acid
PM – Particulate Matter
PMN – Polymorphonuclear Neutrophils
PPM – Parts Per Million
PRISMA – Preferred Reporting Items for Systematic Reviews and Meta-Analyses
PSI – Pounds per Square Inch
PSL – Polystyrene Latex
PTFE - Polytetrafluoroethylene
PVP - Polyvinylpyrrolidone
QCM – Quartz Crystal Microbalance
RFS – Radial Flow System
ROS – Reactive Oxygen Species
RPM – Rotations per Minute
RPMI – Roswell Park Memorial Institute
SEM – Scanning Electron Microscopy
SDG – Spark Discharge Generator
SMPS – Scanning Mobility Particle Sizer
SOD – Superoxide Dismutase
STEM – Scanning Transmission Electron Microscopy
SRM – Standard Reference Material
T25 – 25 cm^2 flasks
T75 – 75 cm^2 flasks
TCC – Triple Co-culture
TEER – Transepithelial Electrical Resistance
TEM – Transmission Electron Microscopy
THC – Total Hydrocarbon
THP-1 – Human Monocytic Cells
TNF – Tumor Necrosis Factor
TP – Total Protein
UFP – Ultrafine Particle
UV-VIS – Ultraviolet – Visible Spectroscopy
VOC – Volatile Organic Compound
XRD – X-Ray Diffraction
XOD – Xanthine Oxidase

List of Symbols

A, A_{cell}, A_{ALI} - Area

° - Degree

V, V_{neb}, V_C - Volume

η - Deposition Efficiency

N, N_{dep} – Particle Number

Re – Reynolds Number

S - Distance between aerosol inlet and stagnation plate

W – Aerosol Inlet Diameter (Width)

L – Aerosol Inlet Throat Length

P - Pressure

T - Temperature

r, r_0, r_{crit} – Radius, Inlet Radius, Critical Radius

c_p, c_m – Particle Number Concentration, Mass Concentration

u, u_p, u_S, u_E, u_{TS} – Velocity, Particle Velocity, Settling Velocity, Electrical Drift Velocity, Terminal Settling Velocity

t – Time

d_p – Particle Diameter

μ– Kinetic Viscosity

C_c – Cunningham Correction Factor

C_D – Particle Drag Coefficient

ρ, ρ_p, ρ_0 – Density, Particle Density, Initial Density

a,b,n – Constants provided by Fujitani et al. 2006

A, B, C, d_0, E, m_0 – Constants from Comouth et al. 2013

D – Diffusivity

τ– Residence Time

k_B - Boltzmann constant

φ – Electric Potential

Z_p – Electrical Mobility

Q – Flow Rate

f_{ALI} – Fraction of Internal Area Covered by Cells at the ALI

F_{sample} – Fluorescence Signal

M, M_c – Mass, Mass Collected

g – Gravitational Constant

F_B – Brownian Force

I – Ionic Strength

n_E – Number of Charges Carried by Particle

Φ - Deposition

λ - Particle Mean Free Path

q – Electron Charge Constant

n – Number of Transferred Electrons

F – Faraday's Constant

i – Current

Γ – Molar Enzyme Concentration

N – Cyclic Voltammetry Scan Rate

ABSTRACT

TOXICOLOGICAL INHALATION EFFECTS OF METAL-BASED NANOPARTICLE AEROSOLS AS STUDIED BY A PORTABLE IN VITRO EXPOSURE CASSETTE

Lynn E. Secondo, Ph.D.

This dissertation is submitted in partial completion of the requirements for the degree of Doctor of Philosophy at Virginia Commonwealth University.

Virginia Commonwealth University, 2018

Director: Nastassja Lewinski, Ph.D., Assistant Professor, Chemical and Life Sciences Engineering

The toxicology of aerosols in occupational settings is often performed through particle collection on a filter followed by reconstitution into cell culture media which can alter the biological effects. Current *in vitro* exposure systems require additional instruments to control temperature and humidity, making the system bulky and difficult to take to the field. The Portable *In Vitro* Exposure Cassette (PIVEC) was designed for personal monitoring, characterized using copper nanoparticles, tested with alveolar cells, and set-up for real-time monitoring. Three differently sized copper nanoparticles, 40-800 nm, were dispersed as a dry aerosol and measured gravimetrically and on a number concentration basis to determine the deposition efficiency of the PIVEC. A549 cells, a human alveolar adenocarcinoma epithelial line, were exposed to the aerosols and oxidative stress and cell viability were monitored post-exposure. The deposition efficiency ranged from 0.5% to 18% depending on method of analysis and size of particle. Oxidative stress increased within the first two hours post exposure, however there was no significant difference in cell viability at the four hour time point at deposited doses up to 1.63 mg/cm^2.

Validation of the PIVEC was done in the laboratory using diesel exhaust. Metal oxide fuel additives are used to reduce emissions; however, additives have been shown to increase emitted nanoparticles. The PIVEC was used to determine the potential cytotoxicity and oxidative activity changes in A549 cells after exposure to either model particles or exhaust generated with or without a commercial, nano-cerium oxide based additive. Acellular experiments suggest a correlation between the deposition and the type of fuel used for the newly designed PIVEC. Cellular results suggest a decrease in cytotoxicity and no statistically significant effect on reactive oxygen species generation with the use of the nano-cerium oxide additive.

Rapid monitoring of oxidative stress was performed using an enzyme-based biosensor. The functionalized biosensor uses cytochrome c to measure reactive oxygen species through electrochemical detection during aerosol exposures. When compared to a traditional biological assay, the biosensor response was similar. The PIVEC is a unique device, designed to monitor aerosols using air-liquid interface *in vitro* techniques including a real-time monitor for oxidative stress.

CHAPTER 1: MOTIVATION AND INTRODUCTION

1.1 Motivation

With the ever growing use of nanomaterials in everyday life the determination of toxicology of these compounds is critical for safe use. On average, nanoparticles will deposit in the alveolar region of the lungs with an efficiency near 20%. Once deposited, particles will take on the order of days to months to clear from the lungs. The ability to directly capture nanoparticles in aerosols to achieve realistic biological responses *in vitro* at the source of emission or within the breathing zone is difficult or nearly impossible using current exposure systems.

There are many exposure systems available to the use of ALI models, however the major limitation of these systems is the large, bulky nature that prevents the systems from moving to the source of emission. To perform *in vitro* tests, cells must remain near body temperature, 37°C, with a reasonably high relative humidity, >50%, to stay viable and systems require a vacuum pump in order to create flow for exposure. The addition of a pump, temperature system, and humidifier can add significant size to an exposure system. There is a gap in personal monitoring of aerosol exposure using evaluation at the ALI. The Portable In Vitro Exposure Cassette (PIVEC) design will allow the user to take the lab to the field to collect aerosol samples at the air-liquid interface (ALI) and then perform subsequent analyses in the lab while retaining a small portable size. By establishing a correlation between a common filter design and the PIVEC wells, the deposited dose, which better represents the dose linked to the response, will be easier

to determine. Through the development of a highly portable *in vitro*, ALI exposure system, the biological responses induced by occupational aerosols can be realized. The sampler developed in this work will be able to be used at the site of emission to gauge the initial concentration of complex mixtures and particles being released into the atmosphere, as well as in the breathing zone to monitor one's exposure levels.

1.2 Introduction

There are four main routes of nanoparticle exposure: ingestion, dermal, injection, and inhalation. Occupational exposure increases the exposure due to inhalation[1] making inhalation a target for considerable research to identify potential health effects. Nanoparticles have the ability to deposit over 20% in the lower regions of the lungs[2–4].

After depositing in the lungs, particles can interact with lung epithelial and phagocytic cells as well as translocate into the body[5–11]. The particles enter the cells, through phagocytosis or endocytosis, crossing through to blood stream where the particles can either travel to the lymph nodes, liver, brain, or other organs and accumulate, or be excreted through the kidneys to the urine and feces. Modeling the translocation and clearance of particles after deposition *in vivo* is difficult due to the lack of many clearance mechanisms within the *in vitro* systems. Bachler et al.[12] used citrate coated gold to study the uptake kinetics through both monocultures and co-cultures with three lung cell types and determined that the uptake kinetics were similar for both models. Similarly, Rothen-Rutishauser et al.[13] investigated particle interactions through translocation in a co-culture system reporting the necessity of dendritic cells in a co-culture system. To determine the most appropriate *in vitro* models for studying particle translocation, Geiser et al.[2] and Braakhuis et al.[14] investigated ALI systems and mono- and co-cultures and recommended that co-cultures be used for studies. *In vivo*, silver was found to translocate after

inhalation by rats to the liver and the brain by Ji et al.[15] and systemic distribution in rats by Takenaka et al.[16]. Ravenzwaay et al.[17] noted titanium dioxide translocation to the mediastinal lymph nodes after inhalation exposure in rats as well. This translocation can lead to eventual health effects in other areas of the body that were not within the route of exposure such as cancer or cardiovascular disease.

In nanotoxicology, there are many approaches to determine the health effects from exposure to an aerosol. The simplest method is to use *in vitro* suspension studies, where the aerosol is captured, suspended in culture media, and added to cells. After a defined exposure duration, biological endpoints are observed. While this method is very straightforward to perform, low in cost, and quick, there is much debate as to how well the results model real exposures. When aerosol particles are added to liquid, there is a higher potential for agglomeration of particles which affects deposition [18–21]. A protein corona may form around particles or compounds in the liquid may interact with the particles, which can influence the biological response [22–24]. Another, more expensive, option is to use an organism of choice to study the biological effects. *In vivo* studies are very useful in determining the effects of the aerosol on the whole organism or the entire system of interest. For example, the whole respiratory system can be studied instead of a certain area via cell type. However, it can be difficult to determine the proper biological endpoints to capture, what model to use, and the model may limit the types of studies that can be performed, for example mice are nose-only breathers while humans are nose and mouth breathers. A model that is more physiologically relevant than the suspension models, yet less expensive *in* vivo are the ALI *in vitro* models.

The ALI model allows for the aerosol to be administered directly to the cells through the air as in a real exposure scenario, yet it is more cost-effective and less time intensive than *in vivo*

studies while mimicking the air-liquid barriers such as the eyes, skin, and lungs. Lung cells grown at the ALI have the ability to generate a differentiated cell monolayer [7,25–27], which produces physiological traits that closely resemble the *in vivo* lung epithelium, including mucus and surfactant production in specific bronchial or alveolar cell lines, cilia beating [26], tight junctions [8,26], and cell polarization [25]. Changes such as these can affect the cellular response measured in toxicity studies [28–30] In addition, through a literature review of engineered nanoparticle aerosols interacting with lung cells, ALI *in vitro* model results are able to model acute *in vivo* inhalation toxicity and are often more sensitive than suspension models[31].

An additional model variation comes from the selection of cell type used, whether primary or immortalized, and if using a cell line, monoculture or co-culture. Primary cells, those that come directly from donors, are ideal as these models include multiple cell types and that the cells have a longer experimental lifespan. These cells can be purchased in 3D scaffolds for use and in either normal or diseased models. Immortalized cells, also known as cell lines, are more reliable in culture and are often used in toxicity studies. Just as primary cells, however, immortalized cells may provide varied results between experiments and also should be verified to confirm the line type. Monocultures, using only one cell line, can be useful to determine the interaction of particles with a cell type such as epithelial or macrophages, however the lack of multiple cells does not adequately represent the lungs as there are over forty different cell types present. Including multiple cell types in a co-culture allows for the study of particle interaction that is more physiologically representative.

Throughout literature, there are few choices of exposure systems available commercially (Vitrocell, Cultex) and multiple choices developed independently (ALICE, EAVES, MEC II, MINUCELL, NACIVT). Three flow profiles are used throughout the systems: perpendicular,

where the flow impacts directly with the cells, parallel, where the flow is indirect, and cloud settling, where the aerosol acts like a single unit and slowly settles on the cells. The choice of exposure system depends on the area of the lungs being investigated and the deposition desired.

Diffusion and sedimentation are the main forces that interact with the particles to induce deposition. Larger particles have higher sedimentation rates, while smaller particles are mainly driven by diffusion. Unfortunately, physiologically there are forces such as impaction also involved. In the bronchioles, the main force of deposition is impaction, whereas in the alveolar region the main force is diffusion. These forces influence which size particles will deposit in the area. In addition, the flow profile directly affects the deposition of the particles. Assisted deposition, such as thermal precipitation [32] or electrostatic precipitation [33–37], increase the deposition of particles by changing the forces through temperature effects or charging of the particles.

There are many exposure systems available for use. Ideally, *in vitro* exposure systems should allow mimicking of the physiological aspects of a realistic exposure, including temperature, flow rate, humidity, and gas composition. The exposure duration should allow for a realistic deposition of nanoparticles into the lungs in order to investigate typical exposure scenarios. Unfortunately, there is no consistent methodology in the *in vitro* nanotoxicology community for exposure testing regarding models, exposure duration, doses, or endpoints. There are a variety of exposure systems used for many lengths of experimental duration to achieve multiple doses characterizing numerous endpoints. There is a large need for experimental data collected *in vitro* at the source of emission. Generally, ambient particles have been collected using filters and then reconstituted into a suspension in the laboratory for testing[38,39].

By exposing the cells to aerosol directly at the source of emission, we can better understand the effects of all gases, semi-volatile compounds, and particles involved in the mixture. When the mixture is collected on a filter, the gases and semi-volatile compounds are not captured and the mixture as a whole cannot be explored. In addition, the reconstitution of particles into a powder or liquid suspension can change particle morphology or size by scraping or lead to aggregation or particle-fluid interactions in liquid suspension. These changes to the particle and mixture can affect the outcome of toxicological experiments. Immediately post-emission, there becomes a spatial variance in particle concentration. This grows with time as the particles disperse throughout the atmosphere and these effects can change based on the ambient conditions, such as temperature, pressure, wind, and sun. Particle concentration and dispersal rates are affected by the topography; higher concentrations will be found in canyons and tunnels, where dispersion effects are slowed, and lower concentrations can be found where there is a large area for dispersion. These changes in dispersion rates can have significant effects on human health and can been seen when comparing the number of asthmatic adults living in urban versus in rural settings [40].

The current methods for measuring aerosols in the breathing zone are filter based, capturing particles over a given sampling period and using the filters to conduct further testing. The breathing zone, the area encompassing the head and chest, is crucial for understanding deposition and effects in the lungs of nanoparticles. As the toxicological community has found, cells exposed at the ALI tend to be more sensitive than those exposed in suspension[29,41–43], therefore an ALI exposure system that is able to perform measurements within the breathing zone a natural next step.

1.3 Research Questions, Specific Aims, and Overview of Work

Research Questions:

1. What design characteristics are important to mimic *in vivo* exposures?

2. Do model particle exposures mimic real-world exposures?

3. Do kinetic studies of biological endpoints reflect time point studies?

This work investigates these research questions via the induction of inhalation effects of metal-based nanoparticles as determined by *in vitro* studies using a new ALI sampler. To do this, the following three specific aims have been identified:

1. Design, characterize, and optimize, an air-liquid interface, in vitro exposure system that is highly portable to collect nanoparticle aerosols
2. Validate ALI sampler in laboratory and toxicity tests of nanoceria diesel exhaust
3. Incorporate real-time monitoring into the ALI sampler to measure a biological endpoint

To this end, the following chapters will discuss the design, characterization, and use of a portable, *in vitro* exposure device for cells cultured at the ALI. A thorough background of ALI exposure methods and comparisons between *in vitro* exposure and *in vitro-in vivo* exposures is presented in Chapter 2. Chapter 3 will discuss the design, optimization, and characterization of the device as designed to capture nanoparticle aerosols. In Chapter 4, use of this device for comparison of a model particle system to a real-world exposure scenario is performed and the device is compared to an available ALI exposure system using a differing flow profile. As limitations of this device are recognized, Chapter 5 seeks to incorporate real-time monitoring of an important biomarker, oxidative stress, within the system through the use of an enzymatic biosensor. In the final chapter of this dissertation, conclusions regarding the current device will be discussed and the future prospects of this work will be investigated.

CHAPTER 2: INTRODUCTION TO IN VITRO NANOPARTICLE EXPOSURES AT THE AIR-LIQUID INTERFACE[1]

2.1 Introduction

Engineered nanoparticles (ENPs) are incorporated in over 1000 consumer products[44] and over 100 clinical trials, producing over 50 approved nanomedicines[45–47]. As a consequence of increasing human contact with nanoparticulate matter, considerable research is being conducted to identify potential health effects due to exposure. Among the routes of human exposure to nanoparticles, inhalation is highly significant as it is the route of highest exposure[1] and nanoparticles are deposited at efficiencies over 20% in the alveolar region of the lungs[2–4].

The need for *in vitro* models predictive of inhalation toxicity and lung disease formation in humans is well recognized by the respiratory research community[1,2,4,8,30,48–54]. While traditional toxicity studies *in vivo* have the advantage of reconstituting organ- and organism-level functions, given the costs, ethical concerns, and questionable human relevance of animal studies, it is arguable that modern *in vitro* testing techniques may reduce and possibly replace certain animal tests if adequate systems are developed and correlated to the *in vivo* human response[12,48,49,55]. Scientific panels have reviewed the status of *in vitro* lung cell models and provided several recommendations for improving the methodology of *in vitro* alternatives to

[1] This chapter is adapted from Secondo et al. Crit Rev Tox. 2016.

animal models[51,56]. The use of cells grown and exposed at the air-liquid interface is currently the prevailing approach. The air-liquid interface (ALI) is also known as the air-interface culture.

ALI cell culture involves seeding cells, typically of lung, skin, or eye origin, on permeable membrane supports allowing for cells to receive nutrients from culture media touching the basolateral side while exposing the apical side to air. While traditional liquid cover cell cultures are still widely used in inhalation studies due to relative ease of handling, suspension exposures are poorly representative of aerosol inhalation in humans[56,57]. Conversely, lung cells grown at the ALI produce a better differentiated cell monolayer[7,25–27], and assume physiological traits that more closely resemble the *in vivo* lung epithelium, including mucus and surfactant production in specific bronchial or alveolar cells, cell polarization[25], ciliary beating[26], and tight junctions[8,26]. These changes have been shown to affect cellular responses in toxicity studies[4,28,29].

It has been suggested that suspension and air-liquid interface exposures differ fundamentally in their dose-response pattern[41,58], although this has been contested[43]. Cells grown at the ALI may be directly exposed to aerosols eliminating particulate agglomeration or dissolution that can occur when transferring aerosol compounds into cell culture media or buffer[43,59]. In addition, mixtures of particles and gases, such as diesel exhaust and cigarette smoke, can be tested in air-liquid interface exposures but not suspension exposures[29,60–66]. However, the reliability of the dose-response relationships obtained under ALI conditions can be limited by the method in which the aerosol is introduced to the cells. The forces acting on particles in aerosols are subject to the size of the particle and the flow profile used[6,50,67]. Possible flow profiles include (1) parallel flow, where the aerosol flows over the cells and the major forces of deposition are diffusional and gravitational, (2) perpendicular flow, where the aerosol

flows directly onto the cells and diffusional, gravitational, and impaction forces influence deposition, (3) cloud settling, where there is no flow and deposition occurs by diffusion and gravitational settling. A review on the differences between suspension and ALI exposures is presented in Cohen et al.[68] including the changes that particles can undergo when added to suspension, the proportionality between administered and deposited dose for suspension exposure, and the advantages for ALI exposures as the particles do not have to deposit through a media layer.

Furthermore, many biological and kinetic changes to particles occur while suspended in cell media, including surface adsorption of molecules in the medium and uncontrolled agglomeration of nanoparticles in suspension [22–24], leading to changes in particle size that significantly alter dose-response relationships [69,70]. Diffusional losses in submerged conditions and increased tendency to agglomerate can result in size-biased particle deposition in submerged systems[19–21,71]. Consequently, the reliability of dose–response relationships obtained under submerged conditions is limited unless all parameters (particle/agglomerate size, height of the medium above the cells, etc.) are well controlled[67,72,73].

Although ALI cell exposure is the preferred method to assess the toxicity of ENPs when using *in vitro* lung models, the growing literature in this area demonstrate a wide range in the culturing conditions, exposure parameters, experiment controls, and most importantly the dosimetry of aerosolized ENPs used when conducting these experiments. The purpose of this review is to critically examine the different approaches that have been used to date to assess the inhalation toxicity of aerosolized ENPs *in vitro*. Prior to assessing the literature collected, the authors set forth questions to consider regarding the methodology of ALI *in vitro* studies.

- Does the administered dose or the deposited dose better correlate with the biological response?
- Is there a difference between the ALI exposure systems when depositing the same dose?
- Are the results generated for nanomaterials with similar physiochemical properties consistent?
- Does the deposited dose *in vitro* correlate to the deposited dose *in vivo*?
- Can ALI studies reliably predict acute toxicity *in vivo*?

In addition to comparing the different ALI cell exposure chambers employed, the advantages and disadvantages of the various methods used to determine the dose of ENPs are discussed.

2.2 Methods

Literature for this review was collected from PubMed and Web of Science with the most recent search date of January 4, 2016, to include articles through 2015. Search terms included nano*, lung*, "air-liquid interface" OR "air-cultured interface", "in vitro", and "in vivo". The literature was explored using the PRISMA framework set forth by The PRISMA Group[74] and evaluated via reliability ranking influenced by Klimisch et al.[75] and Linkov et al.[76]. The reliability standards chosen were based on those set forth by Klimisch et al.[75], in which reliability is assessed by judging the description of the study methodology and results. Additionally, the authors considered weighted factors for uncertainty and other decision-making criteria discussed by Linkov et al.[76]. Literature providing data from a standardized method that has been compared to other values would have high reliability and a high weighting factor; whereas abstracts were immediately excluded due to lack of information. A total of 163 results related to *in vitro* and 10,078 related to *in vivo* literature were screened using the document title and abstract. From these 251 results were excluded due to duplicate publications, non-human or rodent cells used in

study, exposure to a non-ENP substance, exposure to a non-nanoscale substance or lack of *in vivo* exposure; thus allowing 297 results for further assessment. Cells must have been grown and exposed at the ALI to man-made nanoscale materials, and *in vivo* studies were limited to rodent or human inhalation studies containing exposures to the same criteria described in the *in vitro* inclusion criteria. Of the literature collected, 56 papers related to *in vitro* studies of ENP and 54

papers related to in vivo studies of ENP. For more information of the literature search process, see Figure 1.

2.3 Dosimetry

Dosimetry of nanoparticles differs from that of small molecules due to particle

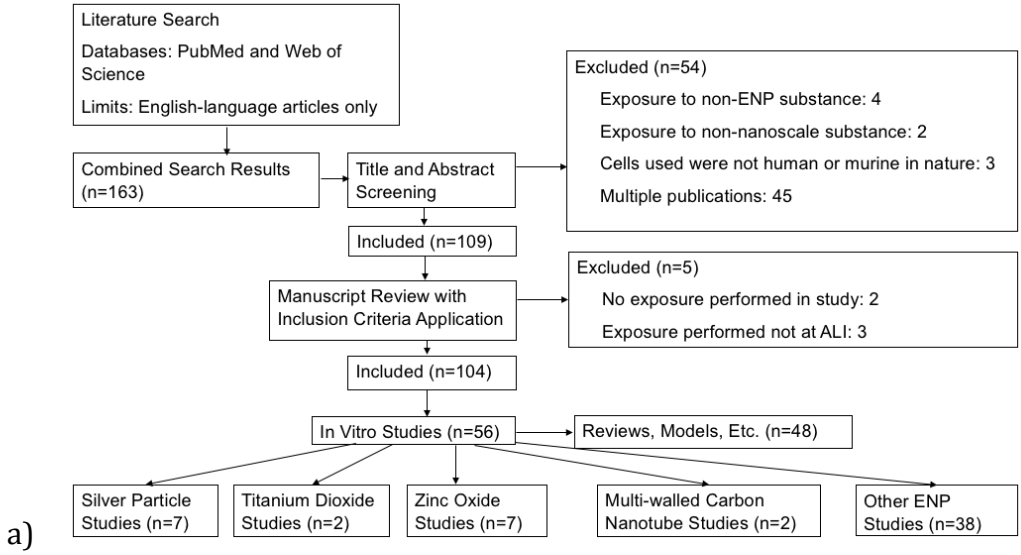

a)

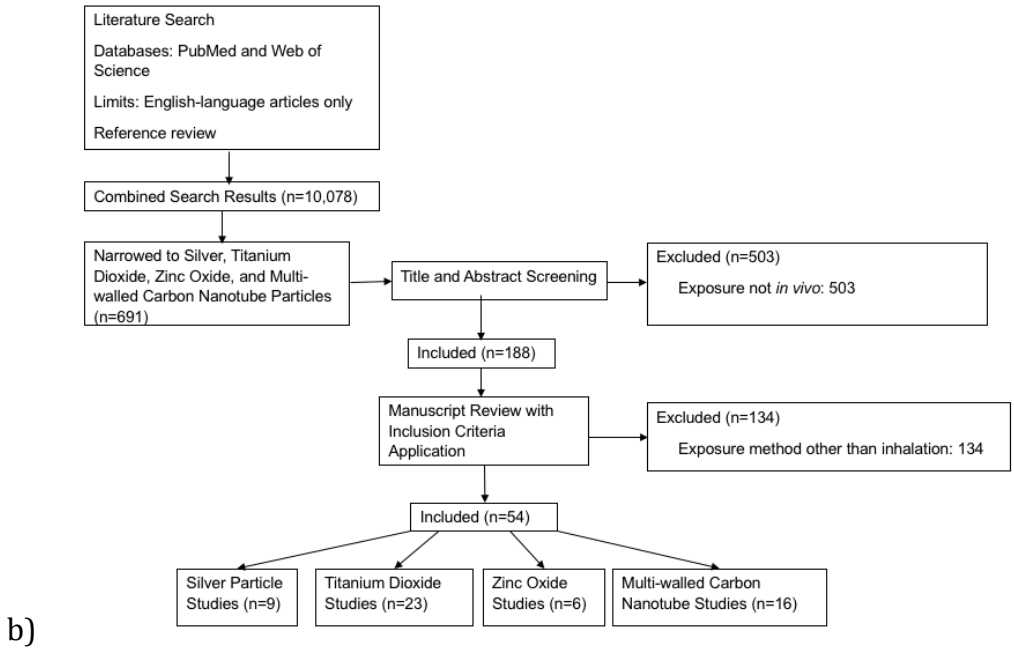

b)

Figure 1. Literature review based on PRISMA model. a) In Vitro b) In Vivo.

agglomeration, diffusion, settling, and physico-chemical changes that can alter transport to and

into cells. The current paradigm for ENP dosimetry names three dose classifications: (i) *administered dose*, or the nonspecific total dose reflected in the media exposed to cells, (ii) *deposited dose*, reflecting the dose of ENPs that makes contact and adsorbs to the cell, and (iii) *cellular dose*, the most specific dose referring to the dose of ENPs internalized[67,72,77]. While these definitions were created to describe dosimetry of nanoparticles in suspension, they also are useful in the discussion of dosimetry at the ALI.

Since the early 2000s, there has been an evolution of dosimetry measurements of aerosolized ENPs. Initial efforts in dosimetry began with measurement of administered dose through the characterization of the aerosols, with few attempts to investigate cells after exposure. Early approaches to determine the deposited dose included theoretical calculations using basic transport models[78] and theoretical calculations following aerosol characterization with light scattering photometry[60,63,66], as well as observation of cells using scanning electron microscopy (SEM) following exposure[79]. A review on strategies for the characterization of nanomaterials, provided by Oberdörster et al.[4], shed light on many additional techniques for aerosol characterization not previously discussed. Techniques such as transmission electron microscopy (TEM), inductively coupled plasma mass spectrometry (ICP-MS), atomic absorption spectroscopy (AAS), and gravimetric analysis increased greatly in the following years, as indicated in Table 1. The quartz crystal microbalance (QCM) has become an important apparatus for determining gravimetric dosage in real-time through the use of vibration displacement of a sample versus reference crystal to determine the deposited mass. These techniques combined with deposition models, are the most used for dosimetry determination, see Table 1.

Table 1. Methods to Quantify Dose

Detection Method	Aerosol	Deposited Aerosol	Internalized Aerosol	Used By
Aerosol Particle Mass Analyser	x			[80,81]
Cascade Impactor	x			[82]
Condensation Particle Counter	x			[1,29,41,65,79,80,83–96]
Differential Mobility Analyser	x			[80,81,92]
Light Scattering Photometry	x			[60,63,66]
Scanning Mobility Particle Sizer	x			[65,84,87,91]
Computational Analysis		x		[89,97–101]
Energy Dispersive Spectroscopy		x		[102]
Fluorescent Spectrophotometry		x	x	[41,43,81,84,102,103]
Gravimetric Analysis		x		[104–107]
Laser Scanning Fluorescence Confocal Microscopy		x		[35,59,80,88,92,108–112]
Neutron Activation Analysis		x		[71]
Quartz Crystal Microbalance		x		[28,59,86,101,112–116]

Table 1 Con't

Detection Method	Aerosol	Deposited Aerosol	Internalized Aerosol	Used By
Scanning Electron Microscopy		x		14,43,86,93
Transmission Electron Microscopy		x	x	^{18,33,88,89,91,93,108,110,112,113,116,117,41,118–120,59,60,64,71,81,85,86}
X-Ray Diffraction Spectroscopy		x		91
Atomic Absorption Spectroscopy			x	^{58,85,121–126}
Inductively Coupled Plasma-Atomic Emission Spectroscopy			x	17,99,126,127
Inductively Coupled Plasma-Mass Spectroscopy			x	14,35,86,89,91,99,115,116,128,129
Inductively Coupled Plasma-Optical Emission Spectroscopy			x	130,131

Additionally, there also exists inconsistency in the units used to quantify dose. Considerations of ease of measurement, ease of understanding, and usefulness are highly debated within the nanotoxicology community. Taking measurements of particle numbers or number concentrations are easily understood and straightforward to perform both during and post-exposure with condensation particle counters (CPC) and imaging methods, such as electron microscopy (EM). However, the actual information provided by particle number concentrations would be best complimented with additional information such as size distribution, surface area, or mass. Size is important due to differences in deposition rates, uptake, and translocation of nanoparticles[30]. Size distribution can be a crucial measurement to aid in determining deposition[50]. Mass spectrometry and gravimetric techniques can be used for quantifying dose based on mass, but mass measurements are best coupled with either size or number measurements to be most useful in predicting and determining the types of particles depositing. Another metric of dose uses surface area as the basis, yet even this is debated[72]. Brunauer-Emmett-Teller (BET) analysis can be used to generate surface area measurements, especially for ENPs that are irregular in shape. However additional options include using projected spherical areas for mobility sizes, or an active surface area related to ion mass transfer. While surface area measurements have been suggested as the most relevant dose metric for nanoparticle toxicity[30], they are time-intensive, generally requiring additional off-line BET analysis. Few published studies describing ALI cell exposures to ENPs report surface area dose metrics [81,83].

2.3.1 Administered Dose

The most easily measured and reported dose measurement, *administered (exposure) dose*, in ALI exposure refers to the measurement of nanoparticle mass, surface area, or number of particles that is added to the medium (air or liquid) during exposure. Although metrics in mass[108] and surface area concentrations[93,115,132] have been reported, administered dose is most commonly reported in particle number concentrations measured using scanning mobility particle sizer/condensation particle counters (SMPS/CPC)[1,33,58,84,93,117,132,133]. Occasionally, other online particle sizers are used, such as fast mobility particle sizer (FMPS) and diffusion size classifiers like the DiscMini[1,58]. The average background concentration of airborne particles is on the order of 10^4 particles/cm^3 or 10 μg/m^3 [56,134,135]. The administered dose of ENPs reported in studies is much higher, see Table 2, with concentrations ranging up to 3 orders of magnitude greater[85].

Table 2. In Vitro Nanoparticle Exposures

Nanoparticle	Size (nm)	Surface Coating	Cell Line	Exposure System	Exposure Duration (hr)	Deposition Efficiency Reported	Administered Dose	Deposited Dose	Results Summary	Ref.
Ag	SMPS: 5.5 ± 1.5 TEM: 8	Bare	Mono Mac 6 (mouse), human alveolar macrophages (lavage)	Direct	0.167	NR	~10^8/cm^3	3.4 mg/cm^2	No reduction in cell viability but cell cycle arrest found 48 hr post exposure, all 3 NP types cause significant DNA damage	113
	Manufacturer: 20 DLS: 33.4 ± 0.2	Citrate	TCC1	ALICE	0.25	24 µg/mL: 50%, 240 µg/mL: 47%	No Online Characterization Reported	30±6.6 ng/cm^2 278±43.6 ng/cm^2	No cytotoxicity or change in IL-8, TNF-α secretion after exposure to Ag NPs alone, but increased IL-8 & TNF-α secretion when exposed with LPS	59
	Geometric: 32 SMPS: 169 DLS: 20, 68	PVP	A549	Custom electrostatic precipitation chamber	2, 3	50 nm: 38.2% 75 nm: 63.3% 100 nm: 63.5%	0.7 µg/cm^2	NR	Ag exposure did not result in significant cytotoxicity or inflammation.	41
	DLS: 116 ± 7	PVP	A549, MDM, MDDC	ALICE	NR	50%	2.4 mg	0.03 µg/cm^2 0.3 µg/cm^2 3 µg/cm^2	Comparing submerged to AIC, submerged shows stronger response	53
	SMPS: 20	Bare	BEAS-2B	NACIVT	1	40%	2x10^6/cm^3	NR	Approximately two thirds of AgNPs were cell associated within 4 hours of exposure.	35

Table 2 con't

Nanoparticle	Size (nm)	Surface Coating	Cell Line	Exposure System	Exposure Duration (hr)	Deposition Efficiency Reported	Administered Dose	Deposited Dose	Results Summary	Ref.
Ag	Surface Enhanced Fluorescence: 140.2 ±7.04 SMPS: 148.7 ± 2.86	Silica shell encapsulating rhodamine fluorophore	A549	Custom electrostatic preparation chamber	1	NR	0.01 mg/m^3 10.0 mg/m^3	Flux: 4E5 part/cm^2/min with screen, 3.1E6/cm^2/min no screen	Compared multiple analytical, experimental, and simulation options, good agreement in all	136
	SMPS: 20 ± 1.5 TEM: 20	NR	HBE, BEAS-2B	NACIVT	0.01, 0.1, 1	40%	2 x10^6/cm^3	1.76 ng/cm^2 17.56 ng/cm^2 175.76 ng/cm^2	Increased cytotoxicity and pro-inflammatory cytokines except TNF-α	120
Au	SMPS: 8 ± 2 TEM: 8	Bare	Mono Mac 6 (mouse), human alveolar macrophages (lavage)	Direct	0.167	NR	~10^8/cm^3	5.4 mg/cm^2	No reduction in cell viability but cell cycle arrest found 48 hr post exposure, all 3 NP types cause significant DNA damage	113
	Manufacturer: 15	Citrate	A549	ALICE	0.17	Total: 57%, 6 well: 7.2%, 12 well: 3.1%, 24 well: 2.1%	1.4x10^{12}/mL	NR	No significant impairment of cell viability due to ALI exposure.	114
	Manufacturer: 15 Gel Electrophoresis: 25	Citrate, PEG	A549	ALICE	0.33	NR	No Online Characterization Reported	16.1x10^9/cm^2 (bare) 14.1x10^9/cm^2 (PEG)	Same as below just focused on TEM	18
	Manufacturer: 15 DLS: 15	Citrate	A549, TCC1	ALICE	0.33	61% 55%	No Online Characterization Reported	61±5.5 ng/cm^2 561±48.5 ng/cm^2	No mRNA induction due to particles observed for all markers, no synergistic effect due to Au+LPS	71

Table 2 con't

Nanoparticle	Size (nm)	Surface Coating	Cell Line	Exposure System	Exposure Duration (hr)	Deposition Efficiency Reported	Administered Dose	Deposited Dose	Results Summary	Ref.
Au	TEM: 5.1 5.5 6.7 6.9	NR	None tested	NACIVT	NR	NR	SDG: $2x10^8/cm^3$, 7 mg/m^3, HT: $1x10^8/cm^3$, 27 mg/m^3 (1575°C), 49 mg/m^3 (1625°C)	NR	The methods used for particle generation are tunable and can be used for toxicity studies	83
	UV-Vis: 2 7 18 46 80	Citrate	A549, MLE-12, 16HBE14o-, TCC1	ALICE	0.25	NR	170 µg 300 µg 200 µg 220 µg 200 µg	25 ng/cm^2 50 ng/cm^2 100 ng/cm^2 150 ng/cm^2 200 ng/cm^2	Translocation through cell monolayer and triple co-culture had similar kinetics, therefore monoculture should suffice for study of translocation	12
Carbon	SMPS: 16-673	Bare	A549	MINUCELL	6	2%	$(1.9±0.2)x10^6/cm^3$	44±4 ng, 87±23 ng ~ $(2.6±0.3)x10^8/cm^2$, 230±70 ng	94.9±9.5% viability after 6 hr exposure to low, mid, and high doses, no difference between change in IL-6, IL-8 and TNF from clean air and exposure, HO-1 increased	93
	Manufacturer: 14	NR	A549	ALICE	0.17	Total: 57%, 6 well: 7.2%, 12 well: 3.1%, 24 well: 2.1%	NR	18 $µg/cm^2$	Carbon was used as a calibration for the QCM.	114

Table 2 con't

Nanoparticle	Size (nm)	Surface Coating	Cell Line	Exposure System	Exposure Duration (hr)	Deposition Efficiency Reported	Administered Dose	Deposited Dose	Results Summary	Ref.
Carbon	NR	NR	A549	Cultex RFS	0.25, 0.5, 1	NR	$6.856x10^5$ - $7.156x10^5$ or 484 ± 20.03 µg /L	25 µg/cm^2 50 µg/cm^2 100 µg/cm^2	Comparison of inter and intra lab results, decreased viability	36
	SMPS: 1.65	NR	HBE, BEAS-2B	NACIVT	0.025, 0.33, 1	40%	$7x10^6$ or $1x10^7$/cm^3	0.33 ng/cm^2 33.13 ng/cm^2 189.33 ng/cm^2	Increased cytotoxicity and pro-inflammatory cytokines except TNF-α	120
Cellulose Nanocrystals	TEM: 168 ± 72 x 19 ± 7	NR	None tested	ALICE	0.0028, 0.0056, 0.0111, 0.0222	NR	1 mg	NR	CNCs could be used for in vitro experiments	110
CeO_2	TEM: 5-20 XDC: 19 ± 1.49	Bare	A549	Glove box	0.16, 0.33, 0.5	NR	NR	$0.95x10^{12}$/cm^2 ~ 0.012 mg Ce/cm^2 $1.43x10^{12}$/cm^2 ~ 0.019 mg Ce/cm^2 $1.9x10^{12}$/cm^2 ~ 0.024 mg Ce/cm^2	Reduced TEER at highest concentration, induction of 8-oxoguanine production	108
	BET: 8.9 XDC: 24 ± 1.45	Bare	A549	Glove box	0.08, 0.17, 0.33, 0.5	NR	NR	1.5±0.4 µg/4.2 cm^2 5.3±0.1 µg/4.2 cm^2 7.8±0.1 µg/4.2 cm^2	CeO_2 particles are internalized quickly and deposited mass causes no necrosis of epithelial cell cultures.	115
	NR	NR	A549	Cultex RFS	0.25, 0.5, 1	NR	$6.856x10^5$ - $7.156x10^5$ or 484 ± 20.03 µg /L	25 µg/cm^2 50 µg/cm^2 100 µg/cm^2	Comparison of inter and intra lab results, decreased viability	36

Table 2 con't

Nanoparticle	Size (nm)	Surface Coating	Cell Line	Exposure System	Exposure Duration (hr)	Deposition Efficiency Reported	Administered Dose	Deposited Dose	Results Summary	Ref.
Cu	DMPS: 80 180	Bare	A549	Cultex CG	4	0.05-1.1%	No Online Characterization Reported	Constant flow: 80 nm: 0.01 μg/cm^2 180 nm: 1.6-7.6 μg/cm^2 Pulsed flow: 80 nm: 0.01-0.05 μg/cm^2 180 nm: 0.3-2.6 μg/cm^2	Air exposed cells had 87±5% viability, 4 hr of constant exposure to 180 nm Cu exposure had cytotoxicity (44±7% viability), pulsed did not and 80 nm Cu did not	85
CuO	SMPS: 9.2 ± 0.2 TEM: 17.6 ± 12.0	Bare	A549, HBEC	Vitrocell	0, 2, 4	50%	2.27 x10^7/cm^3	74 ng/cm^2 148 ng/cm^2	A549 more affected than HBEC by CuONP toxicity (increased LDH and ROS, decreased viability), NAC reduced cytotoxicity through inhibited generation of ROS, comparison of AIC to in vivo study found in "good agreement"	91

Table 2 con't

Nanoparticle	Size (nm)	Surface Coating	Cell Line	Exposure System	Exposure Duration (hr)	Deposition Efficiency Reported	Administered Dose	Deposited Dose	Results Summary	Ref.
CuO	Manufacturer: 25 TEM: 12 ± 1 SMPS: 30.2 ± 1.92	Oxidized shell	A549	Vitrocell	CuO: 8 (two 4 hr) Fluorescein: 2	70.3 ± 3.4%	1.0 μg/cm^2	262 ± 9.5 ng/cm^2 1.7±0.1μg /4.7 cm^2	Reduced cell viability (73%), increased LDH, ROS, and IL-8 amounts after exposure to Cu NPs. 63% of delivered Cu was found in basolateral medium	86
	NR	NR	A549	Cultex RFS	0.25, 0.5, 1	NR	6.856x10^5 - 7.156x10^5 or 484 ± 20.03 μg /L	25 μg/cm^2 50 μg/cm^2 100 μg/cm^2	Comparison of inter and intra lab results, decreased viability	36
Cu_2O	Manufacturer: 40-80 5μm	NR	A549	Cultex RFS	0.25, 0.5, 1	NR	25 μg/cm^2/15min	Chamber 1: 535 ± 11 μg Chamber 2: 540 ± 12 μg Chamber 3: 539 ± 16 μg	Cu compounds had significant dose related cytotoxicity	34
Fe	SMPS: <10-100	Bare	Mono Mac 6 (mouse), human alveolar macrophages (lavage)	Direct	0.167	NR	~10^8/cm^3	10.2 mg/cm^2	No reduction in cell viability but cell cycle arrest found 48 hr post exposure, all 3 NP types cause significant DNA damage	113
Fe_3O_4 Fe_2O_3	STEM: 32 ± 11 35 ± 12 25 ± 5	Silica	BEAS-2B	Custom exposure device with magnet	0.75	NR	No Online Characterization Reported	8.2-59.9 μg	No cytotoxicity alone but cytotoxicity with ammonium bisulfate, citric acid, and sulfuric acid	133

Table 2 con't

Nanoparticle	Size (nm)	Surface Coating	Cell Line	Exposure System	Exposure Duration (hr)	Deposition Efficiency Reported	Administered Dose	Deposited Dose	Results Summary	Ref.
NiO	Manufacturer: 10-20	Bare	A549	Custom electrostatic precipitation chamber	2, 3	NR	2.1 μg/cm^2	NR	NiO had reduced cell viability with higher extent at AIC than submerged	41
MgO_2	NR	NR	A549	Cultex RFS	0.25, 0.5, 1	NR	6.856x10^5 - 7.156x10^5, or 484 ± 20.03 μg /L	25 μg/cm^2, 50 μg/cm^2, 100 μg/cm^2	Comparison of inter and intra lab results, decreased viability	36
MWCNT	Manufacturer: <8, 20-30, >50 x 0.5-2 μm	Carboyxl	A549	Vitrocell, Microsprayer	1	Vitrocell: CNT8 8.81 ± 0.92% CNT50 1.25 ± 0.07% Microsprayer: CNTs 25 ± 2.5%.	No Online Characterization Reported	Vitrocell/Pariboy:PSPs: CNT: ~0.02 μg/cm^2; Microsprayer: CNTs: 66.37 μg/cm^2	Amine modified PSL caused 98% cell death when exposed to 89 μg/cm^2 delivered via microsprayer	111
	TEM: 30 ± 10.3 x 3.4 ± 2.2 μm	NR	A549, A549 +MDM, TCC1	ALICE	NR	NR	25, 125, 250 μg/mL (single exposures), 250 μg/mL (three times in one day or once for three days)	0.14 μg/cm^2, 0.2 μg/cm^2, 0.39 μg/cm^2, 1.15 μg/cm^2 for all repeated exposures	Observed no cytotoxic or inflammatory effect at the given doses in mono or co-cultures	112

Table 2 con't

Nanoparticle	Size (nm)	Surface Coating	Cell Line	Exposure System	Exposure Duration (hr)	Deposition Efficiency Reported	Administered Dose	Deposited Dose	Results Summary	Ref.
Polystyrene	Manufacturer: 196 SEM: 196	NR	NR	Modified MINUCELL	0.62 h	NR	1.6E4/cm^3 ± 20%	Calculated: 1.1E4 /mm^2 ± 35%, Measured: 1.3E4/mm^2 ± 40%	Developed a stagnation point flow model	79
	Manufacturer: 50 100 150 200 300 400 600	Bare	BEAS-2B, porcine lung macrophages	NACIVT	2	100 nm: 32.121±4.404%, 400nm: 14.395±5.693%	10^4/cm^3	3x10^6 /cm^2	No significant increase in LDH or cytokine levels were observed upon exposure to PSL at AIC	117
	Manufacturer: 300	NR	C10	EPDExS	NR	Equation 2	NR	NR	Developed and tested deposition with PSL and used PSL as negative control	96
	Manufacturer: 200 500	Fluorolabeled	A549	EAVES	1	200 nm: 35.16±9.32%, 500 nm: 47.04±9.84%	1.71 mg/m^3 2.36 mg/m^3	1.96±0.50 µg /cell 4.11±0.84 µg /cell	No change in LDH or IL-8 after 9 hr post exposure to Polystyrene	33
	Manufacturer: 50 DLS: 40.4 ± 3.1	Bare	CF41o-, CF45o-, wild type airway epithelial, 16HBEo-	PennCentury microsprayer	1 spray	55+/-9%	3.6x10^6/cm^2 or 0.1 mg/cm^2	NR	No change in TEER, no cytotoxicity by PI staining, NP exposure before ozone does not cause different cytotoxicity and IL-8 release	109

Table 2 Con't

Nanoparticle	Size (nm)	Surface Coating	Cell Line	Exposure System	Exposure Duration (hr)	Deposition Efficiency Reported	Administered Dose	Deposited Dose	Results Summary	Ref.
Polystyrene	Manufacturer: 100 ± 1.04 SMPS: 111 152	NR	A549	Thermal Precipitator	1	17-20%	85000 ± 2000/cm^3	1 mg/m^3	Developed a thermal precipitator, tested cell viability using air and saw no significant effect, tested deposition with PSL	32
	SMPS: 100 2000	NR	None	Vitrocell	5	0.17-4%	(1.1±0.2) x 10^6 (4.0±0.8) x 10^{10}	(1.4±0.4) x $10^4/cm^2$ (1.5 ± 0.4) x $10^7/cm^2$	Developed and validated deposition model based on Vitrocell, very good agreement to experimental data	119
	Manufacturer: 20 40 100 200	Carboxyl	A549	Vitrocell, Microsprayer	1	Vitrocell: 40-200 nm: 0.038 ± 0.0068% 0.029 ± 0.0073%, Microsprayer: 28 ± 1.96%	No Online Characterization Reported	Vitrocell/Pariboy:PSPs: ~0.0001 µg/cm^2, Microsprayer: 148.67 µg/cm^2	Amine modified PSL caused 98% cell death when exposed to 89 µg/cm^2 delivered via microsprayer	111
	Manufacturer: 200	Bare	BEAS-2B	NACIVT	1	40%	Polystyrene Latex: 2x$10^3/cm^3$	NR	No cytotoxicity for PSL	35
	Manufacturer: 200 TEM: 214	Fluorescent	A549	Gillings Sampler - electrostatic device	91.7min	NR	1 mg/m^3	NR	Developed an electrostatic deposition chamber, tested deposition with PSL	137

Table 2 con't

Nanoparticle	Size (nm)	Surface Coating	Cell Line	Exposure System	Exposure Duration (hr)	Deposition Efficiency Reported	Administered Dose	Deposited Dose	Results Summary	Ref.
Polystyrene	Manufacturer: 29	NR	None tested	Vitrocell	29 nm: 2.5	6.82 ± 3.70%	31159±9700	2124 ± 943	Developed and validated deposition model based on Vitrocell, good agreement to experimental data, more flexible.	90
	48				48 nm: 2	2.88 ± 2.72%	16502 ±7080	475±400		
	100				100 nm: 2	0.71±0.47%	56171 ±1414	396±261		
	196				196 nm: 8	0.19±0.34%	36316±17447	68±118		
	309				309 nm: 10	0.19 ± 0.23%	31212±3204	58±73		
	603				603 nm: 3	1.97 ±1.17%	21669±870	428±253		
	814				814 nm: 8.5	2.49±1.08%	31754±6359	790±306		
	1005				1005 nm: 6.5	3.53±2.81%	14145±3612	499±376		
SiO_2	Nanosight: 89 ± 7	Fluoprobe532	A549	MEC II	1	35%	40,000/cm^3	NR	No significant ROS generation	84
	Manufacturer: 29	NR	None	Vitrocell	5	0.17-4%	(1.1±0.2) x 10^6	(1.4±0.4) x 10^4/cm^2	Developed and validated deposition model based on Vitrocell, very good agreement to experimental data	119
	53									
	92						(4.0±0.8) x 10^{10}	(1.5 ± 0.4) x 10^7/cm^2		
	140									
	1600									
	TEM: 54 ± 3	Bare	A549	Vitrocell	5, 7	11 ±3%	No Online Characterization Reported	52 ± 26 µg/cm^2	Silica NPs induced cytotoxicity and inflammation under submerged conditions, increased response with AIC	81
	7-100							~(2.0 ±0.8) x 10^8/cm^2, 117 ± 46 µg/cm^2		
								~(1.4±0.3) x 10^9/cm^2, 0.14 ±0.05 µg/cm^2		
								~(6±2) x 10^8/cm^2		

Table 2 con't

Nanoparticle	Size (nm)	Surface Coating	Cell Line	Exposure System	Exposure Duration (hr)	Deposition Efficiency Reported	Administered Dose	Deposited Dose	Results Summary	Ref.
SiO_2-Rhodamine	Manufacturer: 50	NR	Tetraculture A549, THP-1, EA.hy926, HMC-1	Vitrocell	0.5	NR	No Online Characterization Reported	NR	SiO_2-Rhodamine found inside THP-1	8
TiO_2 (Aeroxide P25 80/20 anastase/rutile)	NR	NR	A549	Cultex RFS	0.25, 0.5, 1	NR	$6.856x10^5$ - $7.156x10^5$ or 484 ± 20.03 µg /L	25 µg/cm^2 50 µg/cm^2 100 µg/cm^2	Comparison of inter and intra lab results, decreased viability	36
	Manufacturer: 25	NR	A549	Cultex RFS	0.25-1	NR	NR	25 µg/cm^2 50 µg/cm^2 100 µg/cm^2	Dose dependent cytotoxicity.	37
ZnO	Manufacturer: 24-71 SMPS: 141 ± 12 DLS: 350, 900	Bare	A549	ALICE	0.17	Total: 57% 6 well: 7.2% 12 well: 3.1% 24 well: 2.1%	0.3 mg 1.5 mg 7.5 mg	0.3 µg/cm^2 1.9 µg/cm^2 8.5 µg/cm^2	No significant impairment of cell viability due to exposure at AIC, biological endpoints only assessed for ZnO	114
	FMPS: 100	Bare	TCC2	Glove box	0.5	NR	~10^8 /mL	22 sec.: 1.3±0.7 µg/cm^2 45 sec.: 2.9±0.6 µg/cm^2 90 sec.: 6.1±0.2 µg/cm^2 270 sec.: 31.1±4.8 µg/cm^2	No cytotoxicity, no change in SOD-1 or TNF-α but increase in HO-1 protein expression	58
	Reported: 25 DLS: 288.2 ± 2.4	Bare	C10	Vitrocell	0.17-0.33	NR	933 aggregates/20 µm^2 106 aggregates/20 µm^2	46.5 aggregates/µm^2 2.7 aggregates/µm^2	Cytotoxicity measured at conc. above 500 aggregates/20 µm^2	43

Table 2 con't

Nanoparticle	Size (nm)	Surface Coating	Cell Line	Exposure System	Exposure Duration (hr)	Deposition Efficiency Reported	Administered Dose	Deposited Dose	Results Summary	Ref.
	Manufacturer: 24-71	Bare	A549	MINUCELL	3	From Model, Bitterle et al. 2006: 2%, Submerged: 100%	AIC: Low:(3.5 ± 0.45) × 10^5/mL High: (9.5 ± 0.9) × 10^5/mL Submerged: Low: 0.7 µg/cm^2 High: 2.5 µg/cm^2	AIC: Low: 0.7 µg/cm^2 High: 2.2 µg/cm^2 Submerged: Low: 0.7 µg/cm^2 High:2.5 µg/cm^2	AIC exposure causes significant fold increases in IL-6, GM-CSF, and IL-8 mRNA levels, much more dramatic than submerged	132
	Manufacturer: 25 EM: 117 ± 2.17 DLS: 73.78 ± 1.6	Bare	C10	Vitrocell	0.17	NR	0 mg/mL, 0.05 mg/mL 0.2 mg/mL 0.3 mg/mL 0.5 mg/mL 1 mg/mL 1.5 mg/mL	0 µg/cm^2 2.44 µg/cm^2 3.01 µg/cm^2 3.39 µg/cm^2 4.13 µg/cm^2 6.00 µg/cm^2 7.87 µg/cm^2	Focused on the dissolution of NPs into zinc ions. Observed a possible threshold of zinc ions prior to toxic effects.	42
ZnO	TEM: 30-40 DLS: 138 ± 62	NR	A549	ALICE	0.25	48 ± 3% 68 ± 2%	0.5 mg 4.25 mg	0.62 +/- 0.04 µg/cm^2 6.23 +/-0.22 µg/cm^2	Doses in submerged and AIC were designed to be equal, cytotoxicity increased for AIC at all time points and doses but not for sub, Same for IL8	138

CNC: Cellulose Nanocrystals

While administered dose is relatively easy to measure in comparison to deposited dose or cellular dose, it does not accurately represent the particle dose that cells experience due to loss in the system. Administered dose does not account for particles that exit the exposure chamber never contacting cells, particles lost to the exposure device, and other particles that remain in the exposure chamber without making contact with cells, as none of these particles exert a direct effect on cell behavior. Only the first limitation is addressed by characterizing both the inlet and outlet streams of the device, reporting the ratio as the "collection efficiency" of the device. For this reason, measurements of administered dose do not give a direct indication of the effective dose cells interact with, and are often regarded as a measurement of "exposure" rather than "dose"[56]. In suspension exposures, differences between nominal media concentrations and cellular dose were observed to be as great as three to six orders of magnitude[67,77]. The characterization of administered dose is necessary in ensuring that cells are being exposed to the test aerosol, but should be supplemented with more specific metrics such as deposited dose or cellular dose.

Administered dose can be converted to deposited dose by using the deposition efficiency, a dimensionless number. This refers to the fraction of original particles that either remain in the chamber with the cells or that the cells are assumed to directly contact. Unfortunately, this number can change in a single exposure system due particle type or different chemical species completely[111,119]. The deposition efficiencies of the exposure systems discussed can be found in Table 3 and may be used to convert between administered and deposited doses.

Table 3. ALI Exposure Systems

Exposure System	Used By	Exposure	Flow Direction	Experimental Flow Rate (L/min) [Min-Max]	Aerosolization Method	Forces Used for Deposition	Charge Neutralization?	Max Exposure Wells
ALICE	[12,18,53,59,71,103,110,112,114,138]	Batch	Cloud	NA	Vibrating membrane nebulizer (PARI Pharma GmbH)	Cloud settling	no	12
Glove box	[58,108,115]	Batch	Cloud	NA	Flame spray synthesis reactor	Cloud settling	no	NA
PennCentury Microsprayer	[109,111,113]	Batch	Perpendicular	NA	Direct	Diffusional and gravitational forces	no	NA
Custom exposure device with magnet	[133]	Flow through	Parallel	0.8	PARI LC STAR Nebulizer	Magnetic	no	NA
EAVES	[33,82]	Flow through	Parallel	1 [1-4]	Pocket nebulizer (Retec X-70/N)	Electrostatic precipitation, diffusional and gravitational forces	no	9
MEC II	[84]	Flow through	Parallel	5 [2-5]	1-jet Collision nebulizer (BGI)	Diffusional and gravitational	no	36

Table 3 con't

Exposure System	Used By	Exposure	Flow Direction	Experimental Flow Rate (L/min) [Min-Max]	Aerosolization Method	Forces Used for Deposition	Charge Neutralization?	Max Exposure Wells
Cultex CG	[60–63,65,66,85]	Flow through	Perpendicular	0.6 [1.38E-4-0.6]	High temperature furnace, Rotating brush generator	Diffusional and gravitational	no	3
Cultex RFS	[34,36,37]	Flow through	Perpendicular	1.5 [1.5-8]	Powder cake scrapping	Electrostatic precipitation	no	3
MINUCELL	[79,93,132]	Flow through	Perpendicular	0.25 [0.25-1.5]	Spark discharge generator (GFG 1000, Palas), Dry powder disperser (TOPAS Model SAG 410)	Diffusional and gravitational forces	no	12
NACIVT	[35,64,83,87,117,120]	Flow through	Perpendicular	0.05 [0.025-2]	Custom nebulizer (critical orifice), Spark discharge generator (GFG 1000, Palas)	Electrostatic precipitation, diffusional and gravitational forces	Kr-85 charger	24
Vitrocell	[8,43,81,86,90,91,111,119]	Flow through	Perpendicular	0.6 [0.01-4.75]	Vibrating membrane nebulizer (Aeroneb Lab nebulizer system, Aerogen), PARI LC SPRINT Baby Nebulizer (PARI BOY)	Diffusional and gravitational forces	no	6

2.3.2 Deposited Dose

A more specific dose metric is the *deposited* (*delivered) dose*, referring to particles that adsorb to the cell surface and remain associated with the cell monolayer. Measurements of deposited dose are generally more time-intensive than measurements of administered dose, but more accurately reflect the amount of nanoparticles that cells interact with, and have been observed to produce more accurate dose-response curves in the literature[34,37,67,78,82,91,139]. A potential issue with deposited dose is dissolution of soluble particles. The release of ions can change the deposited dose and alter the way the particle interacts with the cell. Methods of measuring deposited dose may again be split into those measuring particle number dose, mass dose, and surface area dose, although as of yet, only one computational and no experimental determinations of deposited surface area dose has yet been published for ENPs[4,133]. A summary of these methods is presented in Table 1.

2.3.2.1 Particle dose determination methods

The most frequently reported particle number-based methods for determination of cell-deposited dose are SEM, TEM, and fluorescence microscopy. In general, visual methods, specifically microscopy, have been vastly more popular than mass or surface area dose determination methods due to their ability to provide visual confirmation of particle deposition, while simultaneously obtaining information about deposited particle size and morphology. In addition, microscopy methods generally are not material-dependent (except fluorescence microscopy which requires inherently fluorescent or fluorophore-tagged particles), as opposed to direct methods like ICP-MS and AAS. TEM generally allows for the visualization of smaller particles than SEM, yet both techniques are time intensive, often yielding smaller samples.

However, visual methods are limited in that they may not provide sufficient resolution to distinguish small agglomerates from individual particles, leading to underestimations of particle number concentration. For this reason, visual methods like EM are becoming more popular as non-quantitative visual confirmation for deposition, completed along with another analytical technique[33,41,59,85,86,113–115,117,132,133]. In addition, studies have been conducted to investigate the deposition of particles in the ALICE[110] and modified versions of the NACIVT[83,87] without investigating biological endpoints. These studies have used multiple methods such as SMPS, TEM, laser scanning microscopy, and fluorescence to determine deposition within the exposure system, see Table 1.

2.3.2.2 Mass-dose/direct determination methods

Among direct techniques used to determine mass deposited and intracellular dose, AAS, ICP-MS, and QCM are common in use. Unlike microscopy methods, mass-based or composition-based methods for analyzing deposited dose cannot distinguish between agglomerates and single nanoparticles, and thus cannot give a more direct comparison between administered dose and deposited dose. Post-exposure AAS and ICP-MS give a direct measurement of total metal or particle content in cell samples. However, these methods require metal content in the nanoparticles for quantification and have a limit of detection and saturation for the technique. For example, Elihn et al.[85] experimentally quantified the deposition of copper NPs through AAS, Herzog et al.[59] and Raemy et al.[115] used ICP-MS to determine silver and cerium oxide dosing, respectively. Kim et al.[102] used fluorescence to first optimize control parameters in the Vitrocell system used for exposure with ammonium fluorescein particles, then ICP-MS to confirm the predicted copper oxide dose. QCM is advantageous because it is not material-dependent like ICP-MS, AAS, or neutron activation analysis (NAA), and QCM crystals

placed in cell inserts can provide a time-resolved kinetic view of particle deposition. Lenz et al.[114] utilized a QCM to determine the deposition kinetics of the different nebulized suspensions, specifically ammonium sulfate, sodium chloride, carbon black, and zinc oxide, and correlated the measurements to gravimetric filter readings. Another approach to calibration of QCM includes using the detection of fluorescence of labeled particles[140]. A drawback of QCM, however, is the difference in surface type in which dose is determined. QCM does not respond linearly when covered with a liquid film[114], as cells may be at the ALI. In order for QCM to be predictive, the surface must be dry and the particles may interact very differently than they would with a cell surface as particles may stick to a wet surface. TEM is often used as a starting point for deposited dose or deposition in models such as those developed by Comouth et al.[119] and Fujitani et al.[90] where, by counting particles on electron micrographs, initial deposition efficiency can be determined. Gravimetric analysis of deposited dose is simple and often applied[34,37,91,114,133], as it is not limited by the particle composition, only the precision of the balance used. Deposited dose is also determined mathematically through use of mass balances to calculate deposition, such as by Bitterle et al.[93] or Rothen-Rutishauser et al.[108].

2.3.2.3 Computational methods

While models have been developed for the determination of deposited dose of nanoparticles delivered via suspension, notably by Teeguarden et al.[67] and Hinderliter et al.[77], little attention has been directed towards modeling dosimetry at the air-liquid interface. The few models developed were adapted and validated concurrently with experimental methods above, resulting in dose models that are exposure system-specific and not able to be generalized across studies.

Bitterle et al.[93] used a computational model, equation 1, previously described by Tippe et al.[79] using the same exposure system, where deposited number of ultrafine carbon particles is proportionally related to the 'critical' radius (r_{crit}), the flow velocity (u), the exposure time, and the concentration of the aerosol administered, c_p.

$$N_{dep} = 2r_{crit}^2 \pi u t \quad (1)$$

The critical radius is defined by a specific inner cylindrical flow region within an adapted MINUCELL system[79]. Using quantitative SEM grid analysis, a 2% deposition efficiency was determined that matched computed values reported by Tippe et al.[79].

Similarly to the model by Tippe et al.[79], Desantes et al.[141] generated a model based on a modified design that was used to study the deposition of NPs from diesel exhaust aerosol. Solving discretized Navier-Stokes equations, Desantes et al.[141] included Brownian motion, gravity, and drag on each particle, forces discussed in detail in a review paper by Grass et al.[6]. Equation 2 is the initial equation of motion before discretization.

$$\frac{du_p}{dt} = \frac{18\mu}{\rho_p d_p^2}\frac{1}{C_C}\left(u - u_p\right) + \frac{\rho_p - \rho}{\rho_p} g + F_B \quad (2)$$

The left side of the equation is the rate of change of position of the particles and the right side is broken into three terms, the first relating to drag, the second to gravitational pull, and the third to Brownian forces. In this equation, u_p is the particle velocity, μ is the fluid viscosity, ρ_d is the particle density, C_c is the Cunningham correction factor, ρ is the fluid density, and F_B are the Brownian forces per unit particle mass. The model accuracy was compared to Tippe et al.[79]. The model and data matched well for the particle sizes described[141].

Following the work done by Desantes et al.[141], Fujitani et al.[90] generated a similar model using Brownian motion, gravity, and drag forces on polystyrene latex particles in the Vitrocell exposure system. The deposition efficiency was determined over radius, r, through computational fluid dynamic (CFD) and Monte Carlo simulations and then fit with the following, equation 3, where a and b are fitting parameters and r_0 is the radius of the aerosol inlet, to determine the deposition efficiency, η .

$$\eta(\%) = a\exp[-\left(\frac{r}{r_0}\right)^n] \quad (3)$$

Validation of the model was performed using TEM measurements showing good agreement. Comparing results to previous studies, the maximum deposition efficiency of 7% is similar to those reported[79,141]. The approach to the model described by both Desantes et al.[141] and Fujitani et al.[90] is the same, including comparison to data given by Tippe et al.[79], however Fujitani et al. also compared the described model to experimental data.

Comouth et al.[119] have generated a comprehensive CFD model based on the Vitrocell system. The delivered dose was determined through initial TEM grid analysis of polystyrene and silicon dioxide particles and extrapolated using the cell culture insert surface size and the volumetric flow rate or determined through deposition efficiency. After evaluation of test particle densities and linearity of deposition throughout the cell culture insert, the final total deposition efficiency (η) equation (equation 4) was determined for the given experimental set up of T=37-38°C, P=atmospheric, volumetric flow=100 mL/min, aerosol outlet distance to cell culture insert = 2mm, with particle diameter d_p, and aerosol inlet radius, r_0:

$$\eta = A\left(\frac{d_p}{d_0}\right)^B + \frac{2\left(Ce^{\rho_p E} + m_0\right)^2 d_p^2}{r_0^2} \quad (4)$$

Using least square fits, the parameters for polystyrene and silicon dioxide are determined as follows: A = 8.81 x 10^{-13}, B = -1.133618, C = -905.207, E = 9.71 x 10^{-5} m^3/kg, d_0 = 1 m, m_0 = 1015.43. Due to software limitations, the CFD model is only applicable to particles between 20 nm and 2μm as Brownian motion is neglected. Fractal-like agglomerates are handled through fractal formalism and impact the model in limiting cases only. The model was validated using silicon dioxide particles and through comparison to Desantes et al.[141] and Tippe et al.[79]. Predictions of the size distributions and deposition efficiencies of silicon dioxide result in very good agreement, where the simulation is within experimental error at each data point, resulting in less than a 20% deviation. Additionally, the simulation generated matches qualitatively with those generated by Desantes et al.[141] and Tippe et al.[79] and the changes in exposure system geometry, the Vitrocell used by Comouth et al.[119] and Desantes et al.[141] and MINUCELL used by Tippe et al.[79], and flow rate that could lead to discrepancies between the models.

Grabinski et al.[52] studied the deposition of rhodamine encapsulated silica coated silver nanoparticles through experiments, simulations, and analytical expressions in a custom perpendicular flow chamber with and without electrostatic deposition. Without an electric field, the deposition of particles is dependent on diffusion and gravitational settling alone, yielding equation 5.

$$\eta = 1 - \exp\left(\frac{-\sqrt{2D\tau}}{S}\right) \text{ or } 1 - \exp\left(\frac{-u_s\tau}{S}\right) \tag{5}$$

$$D = \frac{C_C k_B T}{3\pi\mu d_p} \tag{6}$$

$$\tau = \frac{V_C}{Q} = \frac{\pi(r_o^2 + r_o r + r^2)S}{3Q} \tag{7}$$

$$u_s = \frac{\rho_p d_p^{\,2} g C_c}{18\mu} \tag{8}$$

Where S is the distance between the outlet of the aerosol delivery and the ALI, D is the diffusivity, k_B is Bolzmann's constant, T is the temperature, τ is the residence time, V_c is the volume of the chamber, Q is the flow rate, r_o is the inlet radius, r is the deposition radius, and u_s is the settling velocity.

In addition, the voltage can be applied in either a direct current, holding a constant voltage, or an alternating current, switching between positive and negative voltage. The inclusion of the alternating current is more computationally extensive and thus simple, analytical equations are often difficult to determine. With an electric field, the equations change to include the electrostatic forces [52]. Equation 9 formulates the theoretical deposition efficiency with an electric field, where u_E is the electrical drift velocity, Z_p is the electrical mobility, φ the electric potential, q the electron charge constant, and n_E the number of charges carried by the particle.

$$\eta = \frac{u_E \tau}{1.35S} \tag{9}$$

$$u_E = \frac{Z_p \phi}{S} \tag{10}$$

$$Z_p = \frac{q n_E C_C}{3\pi\mu d_p} \tag{11}$$

The advantages of creating computational dosimetry models include the ability to predict deposited dose based on simulated experimental parameters, and to compare predicted doses across exposure systems. However, the current efforts described rely on experimentally determined parameters for deposition efficiency dependent on the specific exposure setup used,

and cannot be generalized for the bulk of ALI studies. In addition, many of these studies fail to provide experimentally quantitative support for their models, weakening their validity. It may be necessary to determine new parameters that account for differences in flow profile and cell surface area utilized by different systems before computational derivations of dose can be used to compare deposition across studies.

2.3.3 Cellular Dose

Cellular dose, sometimes referred to as the "internal deposited dose"[115] or intracellular dose, may be the hardest dose measure to assess, but is also the most specific, representing the dose of nanoparticles actually internalized into the cells, and is most important for evaluation of toxicity as it is influenced by surface functionality of nanoparticles[142]. Few published studies to date report measurements of intracellular dose. Generally, the preferred method of detecting nanoparticle uptake in cells is TEM, visually separating particles adsorbed to the membrane and those internalized in the cytoplasm. While some studies, such as Schaudien et al.[143], report TEM sectioning of cells, then manually counting and calculating the number of internalized particles, others, like Brandenberger et al.[18,71], report estimating intracellular dose using TEM with stereology and extrapolating intracellular dose found in 2D sections to determine cellular uptake efficiency over the entire cell. Instead of the TEM method, Raemy et al.[115] used ICP-MS to determine the intracellular dose. However, this approach is limited in that it cannot differentiate between strongly adherent and intracellular nanoparticles or between intact and degraded nanoparticles. Several studies additionally report cellular doses as the sum of the intracellular dose and adhered particles[19,72,143]; as this is also the deposited dose, standardization of dose definitions may be necessary to limit confusion.

The culture model plays a role in dosimetry as well through differences in cell lines, including cell-cell signaling, and clearance methods, such as phagocytosis through macrophages. State of the art ALI models often include multiple cell lines in co-culture, a format more representative of the physiology of the lungs[7,8,13,25,144]. Klein et al.[7,8] has investigated deposition within co-cultures of epithelial, macrophages, mast, and endothelial cells and subsets thereof. Through the investigation of increase of reactive oxygen species (ROS) production at the ALI, Klein et al.[8] reported lower responses from double and tetra co-cultures, than from monocultures. This could be due to the increase in antioxidants with an increased number of cells as well as the lower dose per cell. Rothen-Rutishauser et al.[13] used a triple co-culture with epithelial cells, macrophages, and dendritic cells and evaluated the particle uptake using fluorescence. With the additional clearance through macrophages, nanoparticles were found within the dendritic cells seeded on the basal side of the membrane, unexposed to the aerosol. The complexities of the co-cultures systems may make it difficult to determine cell-type specific response mechanisms.

Cellular dose is less consistent than deposited dose, due to its dependence on uptake kinetics related to the exposure time and especially the post-incubation times utilized after exposure. Notably, Schaudien et al.[143] and Raemy et al.[115] both observed significant increases in cellular dose over post-incubation periods of up to 24 hours. In addition, translocation rates of nanoparticles are an additional factor in cellular dose as the outflow of particles from cells is important to consider *in vivo* when there may be accumulation in secondary organs[12,26,145], and *in vitro* where translocation may alter the biological response. These alterations are accentuated in the case of cellular necrosis, where internalized nanoparticles are released to the nearby medium. Initial studies have found similar translocation rates of nanoparticles *in vivo* as *in vitro*, as well as relatively constant rates of translocation up to 24 hours post exposure[18]. Translocation often

occurs through the mucocillary escalator and phagocytosis *in vivo*[1,26,146]; however, *in vitro* the cell culture is limited to phagocytosis.

2.3.4 Deposition Efficiency

Many exposure systems will use the deposited dose to determine the efficiency of the device, reporting the deposition efficiency. This dimensionless number is dependent on factors relating to the particles administered such as the number of particles entering the system, the properties of the flow of the particles, particle type and size, and factors relating to the chamber and method of administration such as the deposition area, the volume of the chamber, the exposure duration, and many others. For example, Fröhlich et al.[111] observed a 200-fold difference in deposition efficiency using the same experimental set up in the Vitrocell, changing only ENPs from fluorospheres to carbon nanotubes, from 0.02% to 4.2%. Similarly, an increase in the particle diameter by 25 nm led to 30% increase in deposition efficiency observed by Holder & Marr[41]. The deposition efficiencies may be used to convert between administered and deposited doses, but without a standardized formula or concept, the efficiency calculated may include more than solely what is deposited on the cells.

Particle number concentrations are often used to determine the deposition efficiency. By characterizing the inlet and outlet streams for particle number concentrations, $c_{p,in}$ and $c_{p,out,}$ respectively, and the fraction of internal area covered by cells at the ALI, f_{ALI}, a rough estimate of the deposited dose (η) can be found (equation 12)[84,147,148].

$$\eta(\%) = \frac{c_{p,in} - c_{p,out}}{c_{p,in}} (f_{ALI})(100) \qquad (12)$$

Instead of characterizing the concentration of particles in the inlet and outlet streams, Fröhlich et al.[111] considered the fluorescent signal, F, given by the tagged particles in both the sample and the initial solution, equation 13. This equation also takes into account the dilution, C, of each the sample and the initial solution.

$$\eta(\%) = \frac{F_{\text{sample}} C_{\text{sample}}}{F_{\text{nebulized}} C_{\text{nebulized}} V_{\text{nebulized}}} (100) \quad (13)$$

Jeannet et al.[35] report an alternate formula utilizing the number of deposited particles, N_{dep}, the flow rate, Q, the particle concentration, c_p, and the exposure time, t, (equation 14).

$$\eta(\%) = \frac{N_{\text{dep}}}{Q c_{\text{p}} t} (100) \quad (14)$$

Similarly, to Jeannet et al.[35], Grabinski et al.[52] perform a material balance on the particles and report a formula including the area that the ALI occupies and the total area, A_{ALI} and A, respectively, (equation 15).

$$\eta(\%) = \frac{N_{\text{dep}} A_{\text{ALI}}}{A Q c_{\text{p}} t} (100) \quad (15)$$

Stevens et al.[96], present a formula based on the electrostatic deposition chamber used in their study, where the flow rates, Q, are differentiated for the total aerosol, the condensation particle counter, and the exposure chamber (equation 16).

$$\eta(\%) = \frac{N_{dep}}{c_{p,in} t} \frac{Q_{aerosol}}{Q_{CPC} Q_{chamber}} (100) \quad (16)$$

Zavala et al.[137] base deposition efficiency on mass collected, M_c, instead of number metrics, the particle concentration, and the total volume of sampled, V_t (equation 17). The deposition can be increased in electrostatic systems by cycling or pulsing the voltage, as done by Zavala et al.[137], thereby capturing oppositely charged particles or forcing particles to deposit through the reduction of charging effects.

$$\eta(\%) = \frac{M_c}{c_p V_t}(100) \tag{17}$$

Although the equations appear different, the basic structure is the amount collected over the input amount. These values are expressed through signal, number, or mass, and may have factors to adjust for the exposure system in the form of areas of the ALI system or volume or aerosol added. To determine a standard factor, the influence of four variables on deposition efficiency were considered on a system operating at steady state: exposure time, volume of the exposure system, area of ALI exposure, and internal surface area of the exposure system. In flow through systems, exposure time should not have an effect on an overall deposition efficiency. The factors pertinent to the exposure system, such as volume and internal surface area, will increase the possibility for system losses, having a negative influence on deposition efficiency. ALI exposure area is directly proportional to the deposition efficiency. These results are synthesized in equation 18, where the volume is the product of the flow rate and exposure duration for flow through systems.

$$\eta(\%) = \frac{N_{dep}}{c_p}\frac{A_{ALI}}{AV}(100) \tag{18}$$

Measurements of the administered amount, deposited amount, and flow rates are important for determination of deposition efficiency which can be related to the physiologic deposition of nanoparticles in the lungs.

2.3.5 Exposure Duration

Dose is not only dependent on the aerosol particle concentration, but also on the exposure duration. As a result, increases in the duration of exposure can cause changes in the administered, deposited, and intracellular dose of particles. For example, Raemy et al. documents a positive correlation between exposure duration ('reactor runtime') and resulting deposited dose for a zinc oxide aerosol[58]. The exposure duration can ideally be adapted to match the real-life application of concern; e.g. short exposures to high doses can be used to mimic the exposure of lungs using an inhaler, while long exposures to trace amounts of aerosol can be used to model chronic exposures in occupational settings. However, apart from being time-intensive, a more important factor currently limiting long exposure durations at the ALI include limited lifetime of cells in the incubator, overgrowth of cells beyond a monolayer, increased risk of contamination, and loss of viability due to dehydration[102]. Consequently, it is unsurprising that the vast majority of published ALI studies use exposure durations less than 1 hour, see Table 2. Additional research in exposure methodologies to increase cell viability is required before effects of long-term exposures of cells to nanoparticle aerosols may be accurately measured at the ALI.

2.4 Exposure Systems

Many ALI cell exposure systems have been developed including the commercial Vitrocell and Cultex systems, and independently produced ALICE and MEC systems[34,60,84,114,147,149]. In addition, microsprayers have been used for direct deposition onto cells[109,111]. A summary of these systems is presented in Table 3.

ALI exposure systems currently employed utilize different flow profiles (e.g. direct, indirect, see Figure 2) that can lead to different delivered doses of particles to cells[79]. Whereas the diffusional and gravitational particle displacements are well-known values which can be obtained from literature, the convective transport of nanoparticles depends upon the experimental layout, or the exposure system used[79]. The Vitrocell, MINUCELL, CULTEX CG and RFS, and NACIVT systems widely used in the literature utilize direct flow where the aerosol directly collides onto the cells[36,85,93,117], as opposed to indirect flow of the aerosol parallel to the cell surfaces of the MEC and EAVES systems[33,84]. The direct flow systems may lead to greater nanoparticle deposition, which facilitates higher dosing but is representative of physiological deposition of particles in the lung where impaction is the main force of deposition such as the bronchi. In addition to flow-through systems, batch systems, such as the ALICE, deposit aerosols onto cells through cloud settling dynamics[114,150], which is representative of deposition during breath holding.

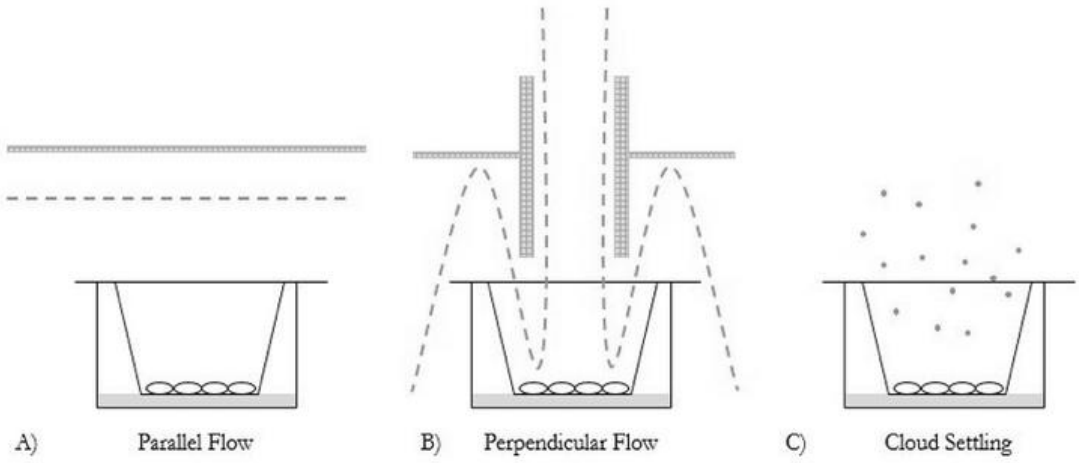

Figure 2. Flow profiles for exposure systems. Dashed lines represent flow profiles. a) Parallel flow. b) Perpendicular flow. c) Cloud settling.

There are many advantages and disadvantages to the current exposure systems available, including number of exposed samples, stress on the cells, and availability. For batch systems, the ALICE is the most widely used throughout literature, as observed in Table 3, and is a more controlled system than a glove box. A microsprayer provides a larger dose of particles but also induces a higher physical stress onto the cells like the cells experience in perpendicular flow through systems. Currently there are no parallel flow systems available commercially, however the Vitrocell and CULTEX systems are available for perpendicular flow with options for dry aerosol generation from CULTEX and multiple cell culture insert sizes from Vitrocell. The MEC II and NACIVT have the highest number of samples available for exposure, which is important for high throughput screening.

As observed in Table 3, many systems use nebulization methods for aerosol generation. The droplets generated by nebulizers are often on the order of microns and therefore may not reach the alveolar region of the lungs to represent a realistic scenario. Droplets from a nebulizer should be dried prior to entrance into the exposure system to reduce size while preserving sample from loss to the sample. In addition to the droplet size, for particles with high solubility, such as metals or metal oxides, there is the possibility of increased dissolution during delivery to the cells[36,42,43,91,132]. This can change the deposited dose and the experiment is then no longer measuring solely particle interactions. For these highly soluble particles, a dry generation of aerosols would be more realistic, such as in the CULTEX RFS and the MINUCELL systems. Lenz et al.[132], using the MINUCELL, and Xie et al.[43], using the Vitrocell, investigated the toxicity at the alveolar region using both the ALI and submerged techniques with similarly sized bare zinc oxide particles. While different biological endpoints were evaluated and different doses deposited, both groups agreed that the ALI was more sensitive than the submerged

technique[43,132 43,132]. In another case, Steinritz et al.[36] and Jing et al.[91] studied the cytotoxicity of copper (II) oxide on the well-studied, A549 alveolar cell line. The dry dispersal technique of the CULTEX RFS had a higher deposited dose and lead to a high toxic response [36] while the longer exposure duration and lower deposition of the Vitrocell lead to a lesser, but similar, response [91]. A concern with using a dry aerosol generation device *in vitro* is to not dry out the cells exposed as the respiratory tract has natural humidification; therefore a completely dry aerosol generation would not be appropriate for toxicological study.

Despite the variation of exposure methodologies used, most current ALI systems have limited nanoparticle deposition efficiencies, as low as 0%[85,90] to 2% of all administered particles reaching the cells[34,85,93,114,117]. These low efficiencies require administration of high particle concentrations and limit the range of doses that can be reported in a dose-response curve, reducing their utility. The low deposition may be appropriate for the study of cellular response mechanisms. At lower doses, response may be different compared to cells that have been over-dosed. For example, it is known that small amounts oxidative stress can disrupt the cell cycle but not lead to cell death, yet when the amount is increased cell death can occur and the pathway may change based on the amount of stress the cell incurs due to exposure[151].

Several methods have been used to experimentally increase deposited dose, including treating particles with charge neutralizers prior to deposition[102], application of electrostatic forces to charged particles[33,96,117,137] and magnetic forces to iron oxide nanoparticles[133,152], generation of a temperature gradient to induce thermal precipitation[32], as well as utilization of a microsprayer to directly deposit increased particle doses, albeit at unrealistically high kinetic deposition rates[109,111]. These methods resulted in increased deposition efficiencies ranging from 25-98%[33,82], enabling determination of toxicity values such as the LC_{50}, or the dose lethal to 50% of cells

studied. Changes in deposition due to particle size and deposition method can be seen in Figure 3. With each change in the exposure device there is an addition of uncertainty due to the specifics of the device itself, such as flow profile or deposition efficiency, which affect repeatability. These sources of variability can be seen in Figure 4. Drawbacks of the exposure systems described above include the inability to incorporate more complexity, such as pressure fluctuation, biomechanical stretching, and interstitial flow in the lung model. Microfluidic devices, more specifically Lung-on-a-Chip devices have the capacity to more accurately model the dynamic environment of the lung *in vitro* than any comparable system[54,153,154]. The response of lung cells exposed to nanoparticles using the Lung-on-a-Chip device has been reported; however, the alveolar epithelia was exposed via injection of a nanoparticle suspension followed by aspiration of excess media, more closely resembling a submerged exposure than an ALI

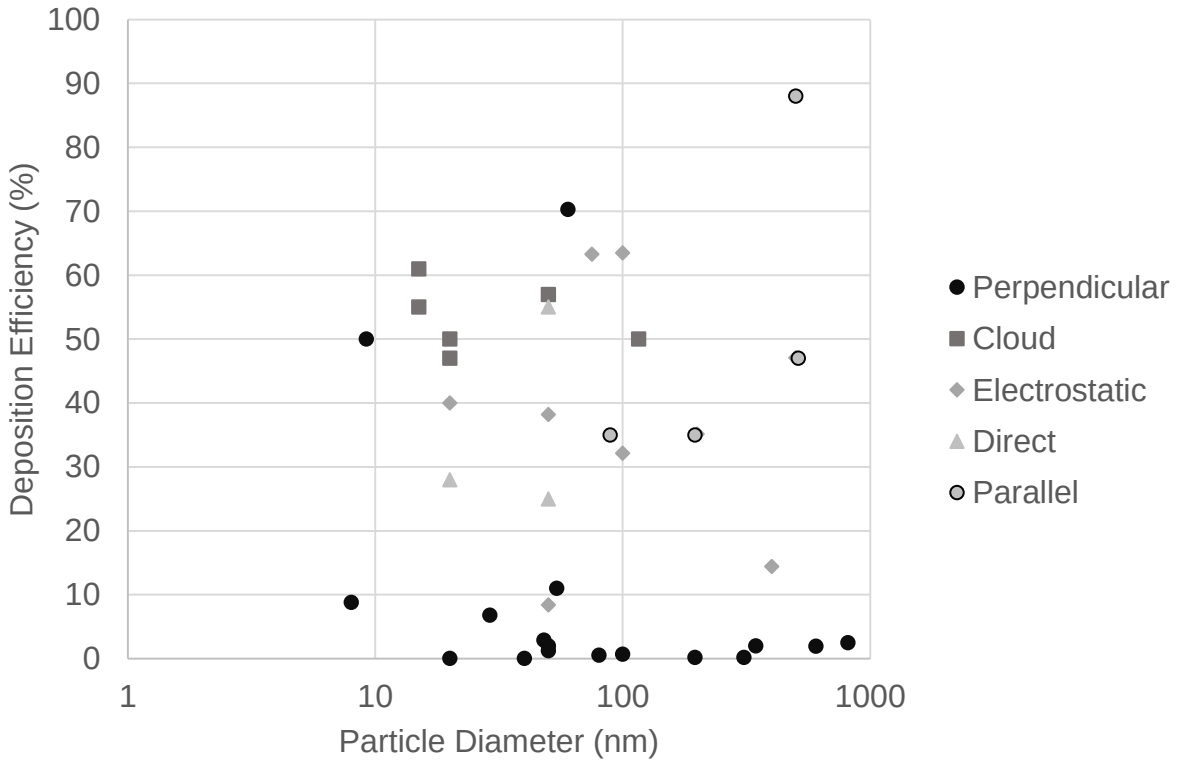

Figure 3. Exposure system reported deposition efficiencies.

exposure[54]. More work is needed to deliver particles in aerosol form before the Lung-on-a-Chip can realistically model ALI exposure.

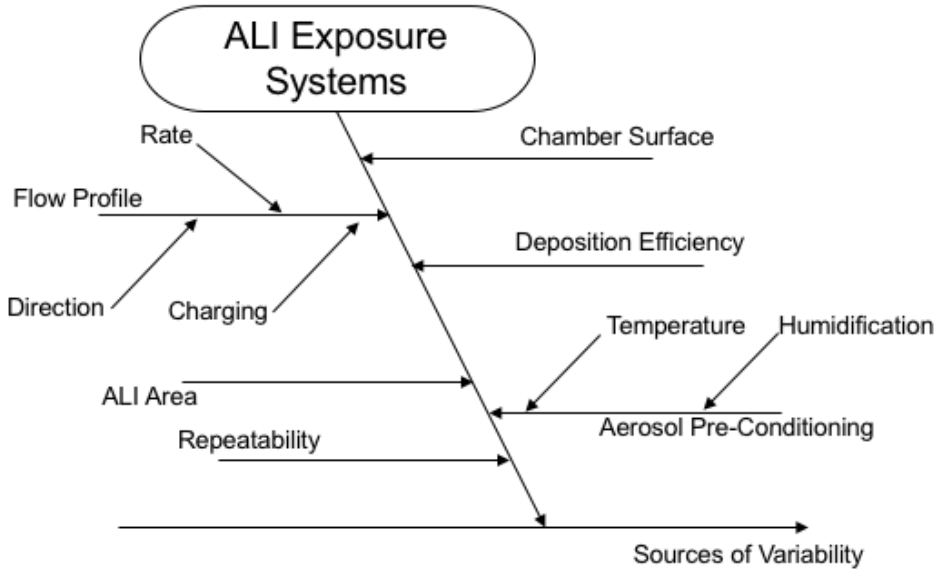

Figure 4. Cause and effect diagram including sources of variability specific to ALI exposure systems.

2.4.1 Characterization of Deposition Efficiency Using Polystyrene

Due to the spherical, inert nature of polystyrene, it is often chosen as a model substance for characterization of exposure systems. Many groups reported plots or data of deposition efficiency versus particle diameter for polystyrene alone [35,90,111,117,119], however the deposition efficiency can change based on the particle material. The data was similar to the general trends presented in Figure 3. For example, Savi et al.[117] and Jeannet et al.[35] used electrostatic deposition in the NACIVT system and overall achieved higher deposited doses than Fröhlich et al.[111] who used the Vitrocell. Although polystyrene appears to follow the general trend of deposition efficiencies of the reported data collected, the data presented by Comouth et al.[119] on the

deposition of polystyrene and silica appears that it may be necessary to re-characterize deposition for new substances.

Five studies reported cell responses after exposure to polystyrene particles for approximately one hour. Each study used a different exposure system, including the NACIVT[35,117], EAVES[33], Vitrocell[109,111], and microsprayer[111]. No change in lactate dehydrogenase (LDH) release[33,117] and interleukin 8 (IL-8) response[33,109] was observed following ALI exposure to polystyrene particles. Fröhlich et al.[111] determined that carboxyl functionalized polystyrene did not induce cytotoxicity in ALI exposure; however, amine functionalized polystyrene particles generated significant cytotoxicity at the ALI. Significant monolayer integrity disruption was measured via reduction in transepithelial electrical resistance (TEER) values for ALI versus suspension exposed cells to doses as low as 31 $\mu g/cm^2$ [111]. Fröhlich et al. compared mass dose needed to generate a cytotoxic response in cells using 20 nm fluorescent polystyrene particles and found that submerged cultures exhibited greater viability than ALI cultures measured through LDH release when exposed to the same dose of amine-functionalized polystyrene particles[111].

2.4.2 Case Studies: Comparison of Nanoparticle Exposures In Vitro

The comparison of data between laboratories is integral for nanoparticle toxicity screening, yet is also currently difficult due to the lack of standardization throughout ALI exposure studies. Although many groups have reported dosimetry of ALI and suspension exposures alone, few have in the same study conducted both types of exposures using comparable dosimetry. This is surprising because a wealth of literature exists on the toxicology of nanoparticles delivered via suspension, and dose-response analyses could benefit by relating the suspension and ALI delivery of nanoparticles. Comparisons of ALI and suspension dose

responses should satisfy two requirements: (1) equivalent deposited nanoparticle dose, and (2) comparable agglomeration states in both conditions[58]. In current studies reporting comparisons of ALI and submerged dose-response patterns, one or both of these requirements is generally not satisfied. Despite this limitation, two ENPs most frequently tested at the ALI, zinc oxide and silver, were chosen for further discussion on the correlation between suspension and ALI exposure results.

2.4.2.1 Zinc oxide

Seven studies investigating ZnO nanoparticle exposures were compared[42,43,58,114,116,132,143]. No cytotoxic responses were observed in monocultures with deposited doses up to 4.13 μg/cm^2 [42] nor in triple co-cultures exposed at the ALI[58]. Significant inflammatory and oxidative stress responses to ALI exposures occurred at deposited doses over 1.0 μg/cm^2 [114]. The higher dose necessary for a cytotoxic response could be due to a necessary threshold of zinc ions, as discussed by Mihai et al.[42]. Xie et al.[43] and Lenz et al.[132] determined that the inflammatory and oxidative stress responses to ZnO ENPs were higher at ALI than suspension given the same deposited dose.

Deposited dose of ZnO ENPs was determined in each of these studies through various methods including QCM, AAS, SEM, and use of the model developed by Bitterle et al.[43,58,93,114,132]. In addition, Schaudien et al.[143] dosed multiple lung cell lines, both bronchial and alveolar epithelial, grown at the ALI to ZnO ENPs in suspension and monitored the deposited and cellular dose visually using TEM analysis. It was determined that, within an hour after deposition, particles were either on the cell surface or few had entered into the cell. It can be seen in Figure 5d, that in relation to the pro-inflammatory release of the cytokine interleukin 8, the

deposited dose is more informative than the administered dose, observed in Figure 5c, providing a dose-response relationship to the deposited dose.

Based on the 56% deposition efficiency for the ALICE system previously determined for ZnO ENPs using QCM[114], Lenz et al.[132] administered the corresponding ZnO ENP dose in suspension to cells. It was experimentally observed that all particles in the media reached the cells within the exposure time frame of 3 hours. The minimum mass deposited/cell to produce significant changes in mRNA encoding pro-inflammatory cytokines such as IL-8, interleukin 6 (IL-6), or the granulocyte macrophage colony-stimulating factor (GM-CSF) and oxidative stress markers, such as heme oxygenase (decycling) 1 (HMOX1), superoxide dismutase 2, mitochondrial (SOD-2), and glucosylceramide synthase (GCS), was reported to be generally greater for submerged cultures than for ALI[132]. Also using the ALICE, Stoehr et al.[116] compared ALI experiments to submerged cultures utilizing a modified Stoke's law to determine the settling time of the ZnO ENPs. Responses for cytotoxicity from LDH was higher for ALI cells, as was the IL-8 response [138]. Overall, ZnO ENP doses over 1.0 $\mu g/cm^2$ were necessary to produce biological responses in ALI studies, yet similar doses did not produce responses under submerged conditions, even after entering the cell.

2.4.2.2 Silver

Herzog et al.[53] investigated the effects of Ag nanoparticles in suspension and at the ALI on cytotoxicity and cytokine release using the ALICE exposure system. Cytotoxicity was determined through LDH release. No significant response was measured in the ALI tests; yet, a significant response was measured in suspension tests. Similarly, no significant increase in IL-8 release was measured for ALI exposure, yet there was an increase in IL-8 release in suspension after 24 hours of exposure. Although this study directly compared the two exposure scenarios,

the deposited doses at post-exposure measurements were not comparable. For ALI exposure, the QCM measured deposited doses were 0.03, 0.3, and 3 μg/cm^2. In suspension, the administered doses were 10, 20, and 30 μg Ag/mL, and the deposited dose was calculated using the *in vitro* sedimentation, diffusion, and dosimetry model, developed by Hinderliter et al.[77]. Four hours after exposure, 24% of the administered dose deposited, and twenty-four hours post-exposure, 71% of the administered dose deposited, providing doses of 0.6, 1.1, and 1.7 μg Ag/cm^2, and 1.7, 3.4, and 5.1 μg Ag/cm^2, respectively. The change in deposited dose with post-exposure time and the higher deposited doses compared to the ALI doses could explain the dramatic difference in responses between the ALI and suspension exposures[28].

Holder and Marr[41] also performed a direct *in vitro* suspension versus ALI comparison study with Ag ENPs. For suspension exposures, all particles were assumed to deposit onto cells within 5 hours, administering 2.6, 6.6, and 13.2 μg/cm^2 Ag ENPs. Similar to Herzog et al.[53], in this study the deposited dose for the suspension tests was also found to be higher than the deposited ALI dose, 0.7 μg/cm^2. In attempt to rectify these discrepancies, Lenz et al.[132] propose a relationship (equation 19) between the deposited dose in both the ALI and submerged scenarios. In this equation, M_c is the mass collected or deposited dose, c_m, is a mass concentration, averaged for the ALI and in the stock solution for the submerged technique, V is the volume of stock solution, and A_{cell} is the area covered by cells being exposed to nanoparticles.

$$M_c = \frac{c_m Q t \eta}{A_{cell}} = \frac{c_m V \eta}{A_{cell}} \quad (19)$$

Increasing administered dose also leads to increased agglomeration in suspension and, when combined with size-dependent settling, produce size-biased deposition patterns that make control

of ENP dose in suspension difficult. For example, recall that Herzog et al.[53] compared exposures to Ag ENPs of co-cultures in both ALI, using the ALICE, and suspension conditions. Additional aggregates were found in the cells exposed via suspension, and, unlike the ALI exposure, the doses were not well controlled, leading to the highest suspension dose exceeding the highest ALI dose by nearly 70%.

Comparing the Ag ENPs exposure studies gives an opportunity to assess inter-laboratory and intra-laboratory differences through changes in exposure systems, particle sizes, and particle surface coatings. Exposure systems used include custom exposure systems[41,113], the ALICE [53,59], and the NACIVT [35,120], which varied in flow pattern (cloud or perpendicular) and use of external force (electrostatic deposition). Using the ALICE system, Herzog et al.[53,59] observed no cytokine release or cytotoxicity for a range of different exposure durations, confirming earlier reports of negligible cytotoxicity of silver particles at the ALI[41,52,113]. Contradictorily, Jeannet et al.[120] observed significant increases in cytotoxicity and pro-inflammatory cytokines after exposing bronchial epithelial cells to silver nanoparticles. Herzog et al.[53], Holder and Marr[41], and Grabinski et al.[52] each studied particles larger than the 20 nm bare silver particles studied by Jeannet et al.[35,120]. Smaller particles can penetrate the cellular membrane easier and may have enhanced release of toxic silver ions due to the higher surface area to volume ratio [102]. In addition, the citrate coating on particles studied by Herzog et al.[59] would add a negative charge, inducing repulsion between the particles and cells, potentially leading to the negligible toxicity compared to results using bare particles of the same size[102]. These effects can be observed in Figure 5 as the low cytotoxicity of silver is observed throughout the dose range and inflammation reported by IL-8 is constant over a range of doses.

Intra-laboratory comparison of data is crucial to the study of engineered nanoparticles *in vitro*. In multiple studies the ALI model was generally more sensitive than submerged conditions, reporting higher cytotoxic or pro-inflammatory responses at lower deposited doses than submerged conditions[41–43,132]. Standardized metrics for dosimetry, including a method for determining deposition efficiency, and reporting will increase the ease of exchange of knowledge across the discipline.

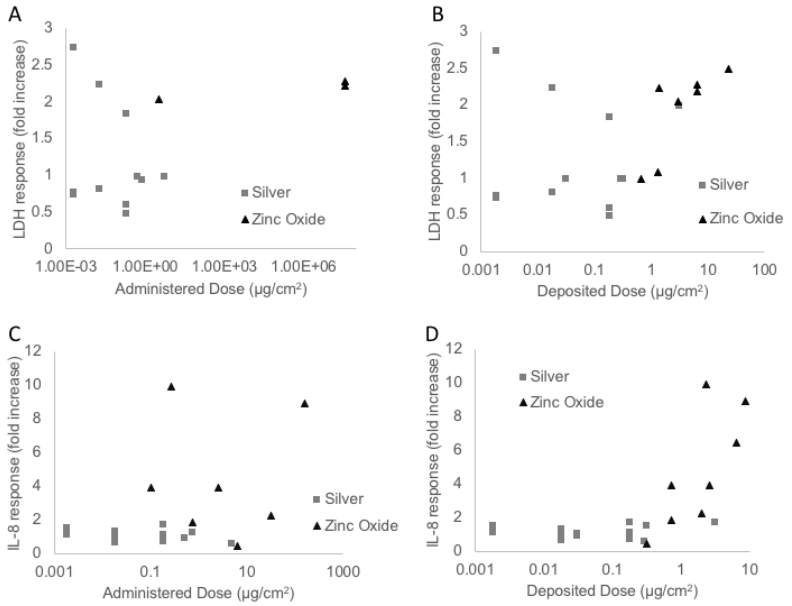

Figure 5. In vitro biological responses for silver and zinc oxide. LDH release (a and b) and pro-inflammatory cytokine IL-8 response (c and d) based on administered dose (a and c) or deposited dose (b and d).

2.5 In Vitro - In Vivo Comparisons

In general, there exist many differences between *in vitro* and *in vivo* exposure experiments. While dose *in vitro* depends on the flow rate used in the cell exposure chamber, inhalation dose *in vivo* depends on the respiratory minute volume of the animals instead of the aerosol flow rate, which simply serves to prevent dilution of the aerosol concentration in the exposure chamber. Gernand et al.[155] performed a review of two popular modes of *in vivo*

exposure, instillation and inhalation, and found that the exposure method was minimally influential on toxicological outcomes. However, in addition to being a non-physiological route of pulmonary exposure, instillation is also believed to overestimate toxicity due to an increase in lung damage compared to inhalation exposure, as determined by the review done by Krug et al.[156].

In vitro ALI exposure platforms currently lack major components of the respiratory defense system that are intact in *in vivo* animal studies. Although rodent models lack the reflex protection of humans (e.g. cough reflex), *in vitro* models cannot approximate the effect of the mucociliary elevator, alveolar macrophage clearance, nor entering leukocytes and lymphocytes. It is only in high dose, long-term *in vivo* studies, when these defense mechanisms are overwhelmed, that the direct effect of the nanoparticles on the epithelium is revealed, leading to observations that correlate with *in vitro* findings. In practical settings, these exposure doses and durations are generally too high to be relevant in representing human occupational or environmental exposures.

2.5.1 Case Studies: Nanoparticle Exposure Comparisons

Notwithstanding the inability of current *in vitro* models to physiologically imitate the *in vivo* lung, there remain associations between the toxicity measures collected *in vitro* and pathophysiological endpoints observed *in vivo* such as the ability to measure LDH release, inflammation, and oxidative stress. The comparison of *in vitro* and *in vivo* biological responses remains important to reduce the number of animals used for toxicological testing. Through comparison of biological endpoints, the toxicological predictive capability of ALI exposure can be considered. Four ENPs often tested by *in vivo* exposures were chosen to be discussed further: silver, zinc oxide, titanium dioxide, multi-walled carbon nanotubes (MWCNTs). These case

studies provide a framework for the discussion of results between inter- and intra-laboratory *in vitro* and *in vivo* studies, and highlight the necessity for consistent measurement and reporting of dose measures. For the same ENPs tested in the same exposure scenario, the results were generally consistent. Silver did not generate cytotoxicity, zinc oxide required higher than expected doses to produce biological responses *in vitro* yet produced inflammation *in vivo*, and MWCNTs and titanium dioxide each readily produced inflammatory responses. For a complete set of *in vivo* literature reviewed on these ENPs, see Table 4.

Table 4. In Vivo Nanoparticle Inhalation Exposures

Nanoparticle	Size (nm)	Surface Coating	Model, subject	Exposure Duration	Deposition Efficiency	Administered Dose	Pulmonary Dose	Results	Ref.
Ag	Microscopy: 20 110	Bare	Rat (n=4)	6h	NR	133 µg Ag/m^3	7.2 µg	Inhalation lead to systemic distribution of silver after rapid clearance from the lungs.	[16]
	TEM: 14-15 DMA: 14-15	Bare	Rat (n=10)	28 d, 6 h/d	NR	Low: 1.66 x 10^4/cm^3 Med: 1.60 x 10^5/cm^3 High: 1.63 x 10^6/cm^3	Males- Control : 0.89 ± 0.2 ng/g wet Low : 0.32± 0.2 ng/g Med : 1.25±-0.16 ng/g High : 1180.76 ± 110.97 ng/g Female- Control : 0.27 ± 0.21 ng/g wet Low : 0.45 ± 0.16 ng/g Med : 1.19 ± 0.07 ng/g High : 1496.64±384.72 ng/g	No significant health effects at the doses studied. However observed a calcium increase in the serum of both sexes at the high dose. In addition observed translocation of NPs to liver, olfactory bulb, and brain.	[15]
	SMPS: 18	Bare	Rat (n=10)	90 d, 6 h/d	NR	Low: 0.7 x 10^6/cm^3 Mid: 1.4 x 10^6/cm^3 High: 2.9 x 10^6/cm^3	NR	Overall, a dose-dependent inflammatory response was induced. Exposure did not result in changes in total cell counts found in BALF. However, reductions in tidal volume, minute volume (PFTs) were observed and BALF inflammatory cytokines (LDH) were increased in the high-dose female rats. Histopathological exam indicated dose-dependent increases in lesions related to silver nanoparticle exposure, such as infiltrate mixed cell and chronic alveolar inflammation, including thickened alveolar walls and small granulomatous lesions.	[122]

Table 4 con't

Nanoparticle	Size (nm)	Surface Coating	Model, subject	Exposure Duration	Deposition Efficiency	Administered Dose	Pulmonary Dose	Results	Ref.
Ag	TEM: 18-19	Bare	Rat (n=20)	90 d, 6 h/d	NR	Low: 0.664 x 10^6/cm^3 Mid: 1.43 x 10^6/cm^3 High: 2.85 x 10^6/cm^3	NR	Determined a NOAEL of 100 µg/m^3 which is consistent with the current silver dust standard.	123
	TEM: 5	Adventitious Carbon	Mouse (n=5)	10 d, 4 h/d	15%	2.4-4.0 mg/m^3	31 µg/g lung	No significant effect from this dose of silver. Some potential evidence though of silver dissolution in the lungs.	106
	DMAS: 18-20	Bare	Rat (n=10)	4h	NR	Low: 0.94 x 10^4/cm^3 Mid: 1.64 x 10^6/cm^3 High: 3.08 x 10^6 /cm^3	NR	No toxicity found.	124
	TEM: 14-15	Bare	Rat (n=29)	90 d, 6 h/d	NR	Low: 0.66 x10^6/cm^3 (49mg/m^3) Med: 1.41 x 10^6/cm^3 (117mg/m^3) High: 3.24 x10^6/cm^3 (381mg/m^3)	0 weeks - Low: 80.65 ± 8.54 ng/g lung Med: 417.40±32.08 ng/g lung High: 4715.28±212.13 ng/g lung	An exposure-related lung function decrease was measured in the male rats after the exposure period, whereas, the female rats did not show a consistent decrease. The histopathology showed a gradual recovery from the lung inflammation in the female rats, whereas the male rats in the high-dose group exhibited persistent inflammation. Results suggest a potential persistence of lung function changes and inflammation induced above the NOAEL.	125
	SEM: 15	Bare	Rat (n=6)	4 d, 6 h/d	27%	179 µg/m^3 (3.8 x 10^6/cm^3)	2.1 µg (7.9 x 10^6 particles/mm^3)	Exposed rats had high lung neutrophils, a doubling of cellular damage markers, increase in pro-inflammatory cytokines and increase in glutathione 24 h post exposure. All observed effects disappear 7 days post exposure.	89

Table 4 con't

Nanoparticle	Size (nm)	Surface Coating	Model, subject	Exposure Duration	Deposition Efficiency	Administered Dose	Pulmonary Dose	Results	Ref.
MWCNT	Manufacturer: 10-20 nm x 5-15 µm	Bare	Mouse (n=6)	7 d or 14 d, 6 h/d	NR	0.3 ± 0.1 mg/m^3 1.0 ± 0.1 mg/m^3 5.3 ± 0.6 mg/m^3	NR	Exposed mice underwent systemic immunosuppression (reduced NK and T-cell activation when challenged) without lung inflammation or tissue damage observed. Increased macrophage counts observed in histology (engulfing particles) and in BALF.	157
	Manufacturer: 13 nm x 1 µm	Depleted Co using HCl	Rat (n=6)	6h	NR	0.53% Co: 11.0 ± 1.3 mg/m^3 241.3 ± 24.4 mg/m^3 0.11% Co: 10.7 ± 1.6 mg/m^3	NR	Observed similar gene expression deregulations for MWCNT and quartz. Believe that BAL is the most sensitive method to probe for short and long-term sequelae induced by MWCNT.	105
	TEM/SEM: 30-50 nm x 0.3-50 µm	NR	Mouse (n=10)	6 h	10% (predicted)	1 mg/m^3 30 mg/m^3	0.2 mg/kg 4 mg/kg	MWCNTs at 30 mg/m^3 embed in the subpleural wall and within macrophages, and resulted in mononuclear cell aggregates (giant cell foci). Sub-pleural fibrosis increased after 2 and 6 weeks following inhalation. None of these effects were seen in mice that inhaled carbon black nanoparticles or a lower dose.	158
	TEM/SEM: 30-50 nm x 0.3-50 µm	NR	Mouse (n=40)	6h	30%	100 mg/m^3 (10mg/kg)	12 mg/kg mouse	Inhaled MWCNT are phagocytosed by macrophages, and do not cause a decrease in cell viability (measured by LDH or total lung protein). Inhalation causes transient neutrophilia (increase in PMNs). Inflammatory cytokines are not increased as a result of NP administration.	158

Table 4 con't

Nanoparticle	Size (nm)	Surface Coating	Model, subject	Exposure Duration	Deposition Efficiency	Administered Dose	Pulmonary Dose	Results	Ref.
MWCNT	Manufacturer: 10-15 nm x 1-10 µm	Bare	Rat (n=14)	5 d, 6 h/d	NR	0.1 mg/m^3 0.5 mg/m^3 2.5 mg/m^3	NR	Increased neutrophils, macrophages, and total protein in BALF. Particles were found in macrophages, and some animals exhibited foci of minimal granulomatous inflammation.	159
	TEM: 13 nm x 1 µm	Bare, contained Co	Rat (n=60)	90 d, 6 h/d	5.70%	0.1 ± 0.02 mg/m^3 0.45 ± 0.06 mg/m^3 1.62 ± 0.2 mg/m^3 5.98 ± 0.8 mg/m^3	NR	Pulmonary inflammation (BAL response) and changes in Co lung burdens did not change in concert as the authors expected. Began observing toxicity in a concentration-dependent manner at 0.4 mg/m^3.	97
	SEM: 10-15 nm x 20 µm	NR	Rat (n=10)	5 d, 6 h/d	NR	0.16 mg/m^3 0.34 mg/m^3 0.94 mg/m^3	NR	Exposure to high doses of caused significant increases in lung DNA damage relative to controls as measured by comet assay. MWCNTs were deposited on the alveolar walls and were ingested by the lung macrophages.	160
	SEM: 20-70 nm x 1.5 µm	Bare	Mouse (n=8)	2 d, 5 h/d 4 d 5 h/d 8 d, 5 h/d 12 d, 5 h/d	2 d: 13.8% 4 d: 13.5% 8 d: 12.1% 12 d: 10.7%	10 mg/m^3	2 d: 16.6 ± 1.3 µg/lung 4 d: 32.5 ± 1.6 µg 8 d: 58.0 ± 3.9 µg 12 d: 76.7 ± 3.0 µg	Dose-dependent increase of neutrophil-mediated pulmonary inflammation and LDH. Lavage albumin indicates broken integrity of AIC in lung. Histopathology revealed bronciolocentric deposition and inflammation, bronchiolar epithelial hyperplasia and hypertrophy, fibrosis of the lung parenchyma, and vascular changes. Pleural penetration and translocation to lymph nodes after >8d exposure.	161

Table 4 con't

Nanoparticle	Size (nm)	Surface Coating	Model, subject	Exposure Duration	Deposition Efficiency	Administered Dose	Pulmonary Dose	Results	Ref.
MWCNT	SEM: 44 nm x 1 µm	NR	Rat (n=6)	5x (microspra yer)	NR	50 ug cumulative 1250 µg cumulative	NR	Two types of MWCNTs tested both induced abundant macrophage-mediated pulmonary inflammation, hyperplastic proliferative lesions of visceral mesothelium as well as inflammatory cell infiltration and inflammation-induced fibrosis of pleural tissue.	162
	SEM: 10-15 nm x 0.1-10 µm	Bare	Rat (n=11)	5 d, 6h/d	NR	0.15 ± 0.05 mg/m^3 0.57 ± 0.10 mg/m^3 2.86 ± 0.82 mg/m^3 Total at highest dose: 0.1287 mg	Highest dose: 0.03 mg/mg lung	Increases of lavage markers indicative for inflammatory processes started at exposure concentration of 0.5 mg/m^3. Consistent with the changes in lavage fluid, microgranulomas were observed at 2.5 mg/m^3 multi-wall carbon nanotubes. In order to evaluate volumetric loading of the lung as the key parameter driving the toxicity, deposited particle volume was calculated, taking into account different methods to determine the agglomerate density. However, the calculated volumetric load did not correlate to the toxicity, nor did the particle surface burden of the lung.	98
	SEM: 49 ± 13.4 nm x 3.86 µm	NR	Mouse (n=NR)	12 d, 5 h/d	NR	5 mg/m^3	28.1 µg	Progressive and persistent fibrotic response. Rapid increase in inflammation and damage (LDH).	163

Table 4 con't

Nanoparticle	Size (nm)	Surface Coating	Model, subject	Exposure Duration	Deposition Efficiency	Administered Dose	Pulmonary Dose	Results	Ref.
MWCNT	Manufacturer: 5-15 nm x 0.1-10 µm	NR	Rat (n=NR)	90 d	NR	0.1 mg/m^3 0.5 mg/m^3 2.5 mg/m^3	NR	No increase in connective tissue from exposure. MWCNTS were observed within the alveolar macrophages. This produces lesions in the lungs similar to those after inhaling asbestos.	164
	Manufacturer: 88 ± 5 nm x 5.0 ± 4.5 µm	Bare	Rat (n=10)	10 d, 6 h/d	NR	0.2 mg/m^3 1 mg/m^3 5 mg/m^3	NR	MWCNT exposure induced granulomatous changes in the lung at 5 mg/m^3, goblet cell hyperplasias in the nasal cavity and nasopharynx were observed in the rats exposed to 1 and 5 mg/m^3, and increased neutrophils, macrophage, ALP, total protein, and ALB in rat BALF. These elevations were maintained throughout a four week post-exposure period. Toxic changes were observed at the lowest dose studied.	165
	TEM: 90.1 nm x 5.7 µm	Bare	Rat (n=10)	65 d, 6 h/d	0.591% 0.745% 0.857% (calculated)	0.2 mg/m^3 1 mg/m^3 5 mg/m^3	2.765 µg/lung 17.45 µg/lung 100.3 µg/lung	MWCNT exposure led to gender-dependent deposition, with more particles found in male rats. There is a dose-dependent increase in lung weight, BALF neutrophil and macrophage count, LDH, ALP, and TP markers. Histopathology revealed dose dependent granulomatous changes, focal fibrosis of the alveolar wall, and inflammatory infiltration in the visceral pleural and subpleural areas.	166

Table 4 con't

Nanoparticle	Size (nm)	Surface Coating	Model, subject	Exposure Duration	Deposition Efficiency	Administered Dose	Pulmonary Dose	Results	Reference
MWCNT	TEM: 10-15 nm x SEM: 200 µm	NR	Rat (n=25)	20 d, 6 h/d	NR	0.17 mg/m^3 0.49 mg/m^3 0.96 mg/m^3	NR	Exposure to MWCNT resulted in DNA damage. No change in inflammatory cytokine levels was found post exposure in the BAL fluid.	[167]
	TEM: 90.7 nm x 5.7 µm	NR	Rat	13 wk, 5 d/wk, 6 h/d	NR	0 mg/m^3 0.2 mg/m^3 1 mg/m^3 5 mg/m^3	Males: Females: NR NR 3.23 µg/lung 2.30 µg/lung 21.2 µg/lung 13.7 µg/lung 120.3 µg/lung 80.3 µg/lung	Focal fibrosis increase starting at 1 mg/m^3. Gender dependent granulomatous changes. Inflammatory infiltration observed at highest dose.	[168]
	TEM: 13 nm x 1 µm	Bare, contained Co	Rat (n=6)	6 h	Empirical: dry: 3.67%, wet: 8.15% MPPD2: dry: 3.1%, wet: 8.2%	25-30 mg/m^3	Empirical: 58 µg (dry dust),166 µg (wet dispersal) MPPD2: 49 µg/lung (dry dust), 167 µg/lung (wet dispersal)	Response was dependent on aerosol generation method. Dry dust feeder aerosols resulted in normal gross appearance and increased alveolar macrophages in distal airways. Wet nebulizer generated aerosols resulted in grey discoloration of the lungs and clusters of macrophages near the bronchiolo-alveolar junction. In both scenarios, the alveolar macrophages engulf the deposited particles.	[100]

Table 4 con't

Nanoparticle	Size (nm)	Surface Coating	Model, subject	Exposure Duration	Deposition Efficiency	Administered Dose	Pulmonary Dose	Results	Ref.
TiO_2	Manufacturer: 21	Bare	Rat (n=6)	28d, 6 h/d	Low: 5.56% Med: 9.52% High: 5.78% (calculated)	Low: 0.11 mg/m^3 Med: 1.05 mg/m^3 High: 10.1 mg/m^3	1 week post-exposure- Low: 4.4 ± 0.8 µg/g lung (total = 8.8 µg) Med: 72 ± 16 µg/g lung (total = 144 µg) High: 440 ± 50 µg/g lung (total = 840 µg)	With lung burdens up to 750 µg/g lung, the TiO_2 elicited no changes in BALF parameters at any time by either method of exposure, nor was any histopathology observed.	121
	Manufacturer: 20	Bare	Rat (n=3)	90 d, 6h/d	NR	23.5 mg/m^3	NR	Fibrosis apparent in exposed rats vs. controls and larger particles. As well as increase macrophage count.	169
	SMPS: 22 ± 1.7	Bare	Rat (n=5)	1 h	NR	NR	4–5 µg/rat (reported estimate)	Inhaled TiO_2 particles deposit within the lung parenchyma, within the alveolar epithelium (PNII cells) as well as within capillary endothelium.	170
	SMPS: 22	NR	Rat (n=10)	1 h	673-842% (calculated)	0.11 mg/m^3 (7.3 x 10^6/cm^3)	4–5 µg/rat (reported estimate)	Inhaled ultrafine titanium dioxide particles were found on the luminal side of airways and alveoli, in all major lung tissue compartments and cells, and within capillaries. Particle uptake in vitro into cells did not occur by any of the expected endocytic processes, but rather by diffusion or adhesive interactions.	171
	SMPS: 20	NR	Rat (n=6)	1 h	NR	0.1 mg/m^3 (7.2 ± 0.5 x 10^6/cm^3)	NR	Uptake of 0.06 to 0.12% ultrafine TiO_2 particles by lung-surface macrophages within 24 hours of acute exposure.	95

Table 4 con't

Nanoparticle	Size (nm)	Surface Coating	Model, subject	Exposure Duration	Deposition Efficiency	Administered Dose	Pulmonary Dose	Results	Ref.
TiO_2, anastase	Manufacturer: 21	NR	Rat (n=3-4)	90d, 6 h/d	5.02% (calculated)	23.5 ± 3.2 mg/m^3	5.1 mg	Localization to the lymph nodes of lungs apparent, increase in PMN count in BALF starting from first month of exposure.	172
	Manufacturer: 20	NR	Rat (n=64)	84d, 6 h/d	5.42% (calculated)	22.3 ± 4.2 mg/m^3	5.22 ± 0.75 mg	TiO_2 ultrafine elicited a persistently high inflammatory reaction in the lungs of the animals compared to particles greater than >100 nm, characterized by increase in total cell counts in BALF, coupled by increases in BAL LDH and ß-glucuronidase concentrations vs. controls. In the long term, pulmonary overload results in impaired macrophage clearance.	173
	Manufacturer: 5 TEM: 3.4 ± 1.0	Bare	Mouse (n=6)	4 h 10d, 4 h/d	NR Sub-acute- 20% (reported estimate)	0.77 mg/m^3 7.22 mg/m^3 8.88 ± 1.98 mg/m^3	NR Sub-acute- 154 µg (from assumed efficiency)	Minimal lung toxicity or inflammation at low dose. Increased total cell count, and alveolar macrophage count, indicating a dose-dependent acute phase inflammatory response. However, no increase in LDH, or cytokine (IL-1, IL-6, TNF-α) amounts was observed relative to negative controls. Sub-acute exposure (8.88 mg/m^3) and necropsied had higher counts of total cells and alveolar macrophages in the BALF compared with sentinels. Increase in cell counts subsides by 3 weeks post exposure.	174

Table 4 con't

Nanoparticle	Size (nm)	Surface Coating	Model, subject	Exposure Duration	Deposition Efficiency	Administered Dose	Pulmonary Dose	Results	Ref.
TiO_2, anastase	Manufacturer: 5 TEM: 3.5 ± 1.0	Bare	Mouse (n=6)	4 h	20% (reported estimate)	0.77 mg/m^3 7.22 mg/m^3	1.3 µg 12.5 µg (from assumed efficiency)	No significant difference in total cell count, total protein, or LDH vs. controls at low dose. Increase in macrophage count, without increase in PMNs, significant increase in total cell count, but no change in total protein, or LDH vs. controls.	175
	Manufacturer: 25	Bare	Rat (n=14)	5 d, 6 h/d	5d post exposure- Low: 9.08%, Med: 12.6%, High: 13.7% (calculated)	Low: 2.4 ± 0.5 mg/m^3 Med: 12 ± 0.5 mg/m^3 High: 50 ± 1.6 mg/m^3	At 5 d- Low: 118.4 µg Med: 544.9 µg High: 1635 µg At 21-29 d- Low: 93.4 µg Med: 400.3 µg High: 1340 µg	Inflammation results in histiocytosis, visible via microscopy, with neutrophilia.	159
	Manufacturer: 5	Bare	Rat (n=6)	6 h	7.45% (calculated)	2 mg/m^3	14.3 µg	TiO_2 agglomerates <100 nm caused cytotoxic effects (1.8 x LDH), increase in macrophage count, and oxidative stress (cytokines).	101

Table 4 con't

Nanoparticle	Size (nm)	Surface Coating	Model, subject	Exposure Duration	Deposition Efficiency	Administered Dose	Pulmonary Dose	Results	Ref.
TiO_2, 86/14 anastase/rutile	TEM: 25.1 ± 8.2	Hydrophobic	Rat (n=6)	5d, 6 h/d	Low: 27.4% Med 25.0% High: 18.2% (calculated)	Low: 2.4 ± 0.5 mg/m^3 Med: 12.1 ± 0.5 mg/m^3 High: 50.0 ± 1.6 mg/m^3	Immediately post exposure- Low: 118.4 µg/lung Med: 544.9 µg/lung High: 1634.7 µg/lung	Dose-dependent inflammatory response characterized by increases in BALF total cell and neutrophil counts, total protein content, enzyme activities and levels of a number of cell mediators following exposure. Cell replication was increased at all nano-TiO_2 dose levels in large/medium bronchi and terminal bronchioles. Effects prominent immediately post exposure, with some endpoints returning to control levels by 16 d post exposure.	127
TiO_2, P25, 80/20 anatase/rutile	Impactor: 15-40	Bare	Rat (n=288)	2 yr	7.43% (calculated)	10.00 mg/m^3	24 mo exposure- 39287 ± 7364 µg/lung	60% of rats exposed to TiO_2 died at 24 mo, 90% at 130 wk (post-recovery). Increase in LDH in BAL vs. controls. Lung tumors (adenocarcinoma, squamous cell carcinoma) in 32% of rats, representing a large increase vs. controls.	176
	Impactor: 15-40	Bare	Mouse (n=160)	13.5 mo.	3.37% (calculated)	10.00 mg/m^3	12 mo exposure- 5.2 mg/lung	Mortality in mice to TiO_2 was 33% at 13.5 mo and 50% at 17 mo (post recovery). Lung tumor rates were not changed relative to clean air controls.	176
	Manufacturer: 21 MOUDI: 1.37 µm	Bare	Rat (n=25)	90d, 6h/d	Low: 17.9% Med: 18.2% High: 23.5% (calculated)	0.5 mg/m^3 2.0 mg/m^3 10 mg/m^3	Low: 0.42 mg/g lung Med: 1.7 mg/g lung High: 11 mg/g lung	Inflammation, dose-related increase in total cell count, marked by increase in macrophage and PMN count. High dose group showed elevation in total protein and LDH. Development of particle-induced lesions (emphysema) and metaplastic epithelium in high dose group only.	131

Table 4 con't

Nanoparticle	Size (nm)	Surface Coating	Model, subject	Exposure Duration	Deposition Efficiency	Administered Dose	Pulmonary Dose	Results	Ref.
TiO_2, P25 80/20 anastase/rutile	Manufacturer: 21 MOUDI: 1.37 µm	Bare	Mouse (n=25)	90d, 6h/d	Low 4.62% Med: 4.48% High: 6.73% (calculated)	0.5 mg/m^3 2.0 mg/m^3 10 mg/m^3	Low: 0.36 mg/g lung Med: 1.4 mg/g lung High: 10.5 mg/g lung	Inflammation, dose-related increase in total cell count, marked by increase in macrophage and PMN count. High dose group showed elevation in total protein and LDH.	131
	Manufacturer: 21 MOUDI: 1.37 µm	Bare	Hamster (n=25)	90d, 6h/d	Low: 2.31% Med: 1.83% High: 1.28% (calculated)	0.5 mg/m^3 2.0 mg/m^3 10 mg/m^3	Low: 0.18 mg/g lung Med: 0.57 mg/g lung High: 2 mg/g lung	Inflammation without increase in total cell counts, only increase in PMN count. No elevation in LDH or total protein. No histopathology noted other than pigment laden macrophages. Supports previous study suggesting hamsters have improved particle clearance rates.	131
	Manufacturer: 21 TEM: 18 ± 4	Bare	Mouse (n=6)	4 h	20% (reported estimate)	0.62 mg/m^3 7.16 mg/m^3	1.1 µg 12.4 µg (from assumed efficiency)	Significant increase in total cell count, but no change in total protein, or LDH vs. controls at both doses. At higher dose, increase in macrophage count, without increase in PMNs, even more so than in 5 nm particles.	175

Table 4 con't

Nanoparticle	Size (nm)	Surface Coating	Model, subject	Exposure Duration	Deposition Efficiency	Administered Dose	Pulmonary Dose	Results	Ref.
TiO_2, P25 80/20 anastase/rutile	Manufacturer: 21 SMPS: 100 ± 2.2	Bare	Rat (n=8)	4 h 12 h	min: 9.72%, low: 10.4%, high: 10.4%, max: 26.0% 12 h: 10.4% (calculated)	Min: 1.5 mg/m^3 Low: 3 mg/m^3 High: 6 mg/m^3 Max: 12 mg/m^3 12 h: 10 mg/m^3	Min: 7 µg Low: 15 µg High: 30 µg Max: 150 µg 12 h: 150 µg	Rats exposed showed no evidence of pulmonary inflammation or lung damage. However, particle-containing macrophages were frequently seen in intimate contact with the alveolar wall. However, there was significant arteriolar vasodilation in the NP-exposed group with respect to the control group. These findings strongly suggest that cardiovascular effects may occur at lower concentrations or particle size distributions than for pulmonary toxicity associated with cytologic changes. Whether similar cardiovascular effects occur in our animal model of NP exposure is presently unknown.	126
	Manufacturer: 21 TEM: 25.3	Bare	Mouse (n=12)	24 d, 1 h/d	NR	Low: 1 mg/m^3 High: 10 mg/m^3	NR	Nanoparticle exposure led to inflammatory infiltration and fibrosis of the lungs, with apparent collagen deposition visible on EM. Alveoli architecture was obliterated at both low and high doses.	177
	Manufacturer: 25	Bare	Rat (n=3-5)	4h 4d, 4h/d	NR	Low: 13 ± 1 mg/m^3 High: 33 ± 4 mg/m^3 Repeated: 13 ± 1 mg/m^3	Low: 44.56 ± 2.85 µg High: 170.25 ± 9.15 µg Repeated: 197.89 ± 8.89 µg	No TiO_2 found in blood at any time point. Compared to inhalation, the instillation experiments over predicted toxicity.	107

Table 4 con't

Nanoparticle	Size (nm)	Surface Coating	Model, subject	Exposure Duration	Deposition Efficiency	Administered Dose	Pulmonary Dose	Results	Ref.
TiO_2, P25 80/20 anastase/rutile	Manufacturer: 21	Bare	Rat (n=7-8)	0s (microsprayer)	NR	4 mg/kg (wt) 10 mg/kg 20 mg/kg	NR	Exposure to TiO_2 resulted in transient increases in LDH, Leukotriene C4, and decreases in peak expiratory flow rate as measured by pulmonary function tests. These form part of an inflammatory response abrogated by treatment using a leukotriene receptor antagonist indicating that inflammatory changes occur via a lipoxygenase-mediated mechanism.	178
TiO_2, 70/30 anastase/rutile	TEM: 20-30	NR	Rat (n=17)	5 d, 6 h/d	6.30% (reported), 6.39% (calculated)	88.0 ± 6.4 mg/m^3 (88 x 10^4/cm^3)	Day 5: 2025 µg day 19: 1547 µg	Translocation to the mediastinal lymph nodes was noted, although to smaller amounts than following inhalation of pigmentary TiO_2, but much higher amounts than after exposure to quartz. The (agglomerate) particle size of lung deposited nano-TiO_2 was virtually the same as in the test atmosphere. Changes in BALF composition and histological examination indicated mild neutrophilic inflammation and activation of macrophages. The effects were reversible with recovery.	17
TiO_2, 74/26 anastase/brookite	TEM: 21	NR	Mouse (n=6)	5 d, 4 h/d	Low: 9.0% Mid: 5.45% High: 8.24% (reported)	Low: 0.8 mg/m^3 Mid: 7.2 mg/m^3 High: 28.5 mg/m^3	Low: 2.7 µg Mid: 18 µg High: 84 µg	Exposure at the highest dose increased the number of neutrophils found in the BALF. No significant effect on the level of DNA damage in lung epithelial cells or micronuclei in polychromatic erythrocytes was observed, suggesting no genotoxic effects after a 5-day inhalation exposure to nano-TiO_2.	128

Table 4 con't

Nanoparticle	Size (nm)	Surface Coating	Model, subject	Exposure Duration	Deposition Efficiency	Administered Dose	Pulmonary Dose	Results	Ref.
TiO_2, rutile	MMAD: 1.44 ± 0.09 Geometric: 1.71 ± 0.23	Bare	Rat (n=65)	90d, 6h/d	Low: 15.0% Med: 19.2% High: 10.3% (calculated)	10 mg/m^3 50 mg/m^3 250 mg/m^3	Immediately post-exposure -(Approx.) Low: 7 mg/g lung Med: 45 mg/g lung High: 120 g/g lung	Pulmonary overload was achieved at the exposure levels of 50 and 250 mg/m^3. Increases in macrophage and neutrophil numbers and in soluble indices of inflammation in BALF. Prominent pulmonary lesions (centriacinar) characterized by destruction of parenchyma.	130
	MMAD: 1.39 ± 0.04 Geometric: 1.72 ± 0.29	Bare	Mouse (n=73)	90d, 6h/d	Low: 3.40% Med: 6.79% High: 4.23% (calculated)	10 mg/m^3 50 mg/m^3 250 mg/m^3	Immediately post-exposure -(Approx.) Low: 5.3 mg/g lung Med: 53 mg/g lung High: 165 mg/g lung	Pulmonary overload was achieved at the exposure levels of 50 and 250 mg/m^3. Increases in macrophage and neutrophil numbers and in soluble indices of inflammation in BALF.	130
	MMAD: 1.36 ± 0.07 Geometric: 1.50 ± 0.11	Bare	Hamster (n=73)	90 d, 6h/d	Low: 1.60% Med: 1.79% High: 2.82% (calculated)	10 mg/m^3 50 mg/m^3 250 mg/m^3	Immediately post-exposure - (Approx.) Low: 2.5 mg/g lung Med: 14 mg/g lung High: 110 mg/g lung	Less pulmonary overload than in mice or rats, suggesting hamsters have improved clearance mechanisms. Increases in macrophage and neutrophil numbers and in soluble indices of inflammation in BALF, but disappear as overload disappears over recovery time.	130

Table 4 con't

Nanoparticle	Size (nm)	Surface Coating	Model, subject	Exposure Duration	Deposition Efficiency	Administered Dose	Pulmonary Dose	Results	Ref.
TiO_2, rutile	TEM: 15 x 50 µm	Alumina and dimethicone/ methicone copolymer	Rat (n=5)	5d, 6 h/d	12.4% (reported) 13.2% (calculated)	Low: 0.6 ± 0.1 mg/m^3 Mid: 2.0±0.1 mg/m^3 High: 10.7±1.2 mg/m^3	459.0 ± 71.3 µg/lung	Inhalation of nano-TiO_2 caused mild pulmonary inflammation that was not fully reversible, with a NOAEC of 0.5 mg/m^3. This is observed as dose-dependent increases in neutrophil and monocyte/macrophage counts in the BALF, accompanied by increased total cell counts, enzyme and total protein levels that remain elevated three weeks post-exposure (i.e. in the recovery groups). Histological examination reveals pigment-loaded alveolar macrophages are responsible for this response. Treatment did not result in changes to pulmonary epithelial architecture, upper airways (i.e. nasal cavity, larynx level, trachea, and carina) or mediastinal lymph nodes.	[99]

Table 4 con't

Nanoparticle	Size (nm)	Surface Coating	Model, subject	Exposure Duration	Deposition Efficiency	Administered Dose	Pulmonary Dose	Results	Ref.
ZnO	SMPS: 40 291	NR	Human (n=12)	3 d, 2h/d	0.79	NR	500 µg/m^3	No measured response in any parameters studied (symptoms, physiologic, hematologic, cardiac electrophysiologic) true for both fine and UFP.	104
	TEM: 90	NR	Rat (n=5)	1 or 3 h	NR	25 mg/m^3 50 mg/m^3	NR	3 hr inhalation resulted in transient dose-dependent pulmonary inflammation in rats, characterized by increase in PMNs, LDH, and MTP in BALF.	179
	Manufacturer: 60	Bare	Rat (n=14)	5 d, 6 h/d	NR	0.5 mg/m^3 2.5 mg/m^3 10 mg/m^3	5d- 33.9 mg 123.4 mg 428.2 mg 21-29d- 25.4 mg 26.3 mg 28.4 mg	Early inflammation and necrosis.	159
	SMPS: 35 TEM: 35	NR	Rat (n=6)	6 h	NR	Low: 2.4 mg/m^3 Mid: 3.7 mg/m^3 High: 12.1 mg/m^3	NR	Dose-dependent increase in total cells, PMN count in BALF. Increase in LDH and total protein in BAL of high dose group. Increase in 8-hydroxydeoxyguanosine (oxidative stress marker) in highest dose group.	180

Table 4 con't

Nanoparticle	Size (nm)	Surface Coating	Model, subject	Exposure Duration	Deposition Efficiency	Administered Dose	Pulmonary Dose	Results	Ref.
ZnO	Manufacturer: 10 TEM: Lot 1 - 15 ±4 Lot 2 – 26 ± 11 SMPS: Subacute – 46 ±1.8 Subchronic – 36 ± 1.8	Carbonates	Mouse (n=11 subacute; n=17 subchronic)	Subacute: 14d, 4 h/d Subchronic: 90d, 4 h/d	24% (reported estimate)	Subacute: 3.6±0.5 mg/m^3 Subchronic: 3.3±0.6 mg/m^3	Subacute: 51 µg Subchronic: 306 µg (reported estimate)	Zinc was elevated in BAL immediately after exposure but returned to control levels within 3 wks. Sub-acute exposure to ZnO caused an increase in total cellularity and macrophages in BALF and a moderate increase in IL-12(p40) and MIP-1α, but no other inflammatory or toxic responses. Increase in BAL total cellularity was observed immediately post-exposure sub-chronically. Following both sub-acute and sub-chronic exposures, pulmonary mechanics were no different than sham-exposed animals.	[129]
	TEM: 20-200	Triethoxyca pryl silane	Rat (n=5)	5d, 6 h/d	8.6% (reported)	Low: 2.5 mg/m^3 High: 12.5 mg/m^3	428.2 ± 19.4 µg/lung at 5 d, 28.4±4.1 µg/lung at recovery period	Pulmonary inflammation (increased PMN, lymphocyte counts) which was dose dependent. Increased BALF enzymes, total proteins, chemokine, and cytokine concentrations. Histology shows PMN, macrophage, lymphocyte infiltration. Most effects reversible on recovery. Necrosis apparent in upper respiratory tract. Increased cell proliferation in terminal bronchiole.	[99]

ALB: Albumin, APAP: Acetaminophen, ATP: Adenosine Triphosphate, BALF: Bronchoalveolar Lavage Fluid

2.5.1.1 Silver

At similar doses of silver and time points, the rodent *in vivo* biological responses of little or no cytotoxicity or inflammation correlate to results presented by groups performing *in vitro* work[15,16,41,53,59,113,124] as observed in Figure 6a. As the dose is repeated in *in vivo* studies, there is a transient inflammatory response marked by an increase in alveolar macrophages and neutrophils found in bronchoalveolar lavage fluid (BALF) at higher doses[122,125], yet this response resolved quickly back to control levels post exposure[14]. Smaller silver particles lead to higher clearance and translocation. This data is very consistent with the *in vitro* data. The smaller particles produced more of an effect, but no damage to the cells.

2.5.1.2 Zinc Oxide

In vivo rodent exposures of zinc oxide resulted in a dose-dependent neutrophil-mediated inflammatory response within 24 hours post exposure, which was reversible following a recovery period with no aerosol exposure[179,180]. This effect is consistent through the *in vivo* literature[99,129,159,179,180] and the *in vitro* studies[42,43,58,116,132]. Warheit et al.[179] compared *in vitro* and *in vivo* experiments, with results that the *in vitro* model is not predictive of the *in vivo*, yet the doses applied to the models were different as observed in Figure 6b. Only the highest dose, a three-fold particle overload, of a co-culture of epithelial and macrophages increased cytotoxicity. Beckett et al.[104] performed a human study using one-tenth of the permissible exposure limit as an administered dose. After 24 hours, no significant effects were seen throughout the 170 endpoints tested. This could be explained given the concept that was presented by Mihai et al.[42] where there may be a threshold level that must be reached prior to observing toxic effects, since zinc

releases ions in solution.

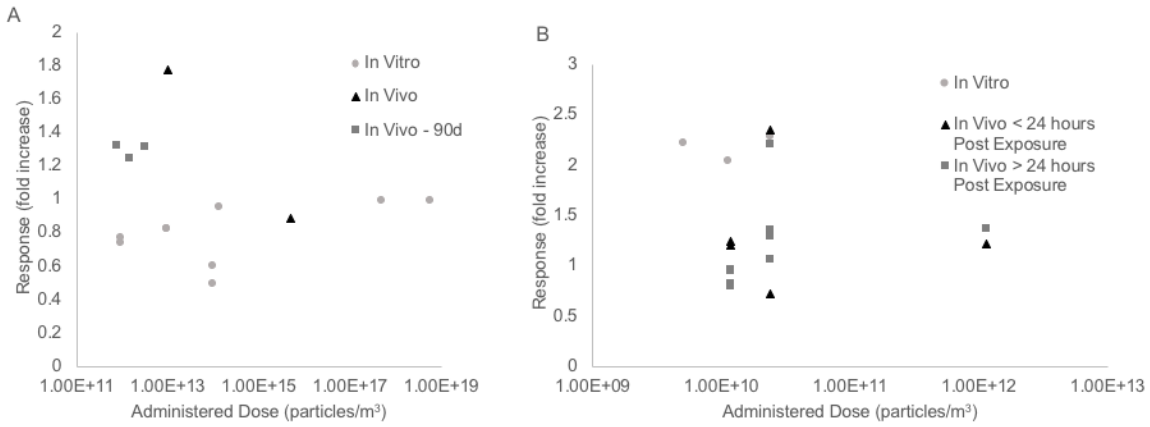

Figure 6. LDH cytotoxicity in vitro comparison to in vivo. a) Silver. b) Zinc oxide.

2.5.1.3 Titanium Dioxide

Documented responses to TiO_2 nanoparticle inhalation *in vivo* are variable, depending on the animal model used, administered dose, and exposure duration, as well as the post-exposure recovery time employed prior to analysis. In general, both *in vivo* and *in vitro* studies support the role of TiO_2 as a persistent pulmonary irritant. *In vivo*, exposure appears to initiate epithelial injury to activate neutrophils and macrophages, which in turn creates an inflammatory milieu supporting the long-term development of fibrosis and cancer. *In vitro*, TiO_2 exposures result in dose-dependent decreases in lung cell viability.

Bermudez et al.[130] in a larger study of rats found that high doses of inhaled TiO_2 nanoparticles led to evidence of centriacinar parenchymal destruction, resulting in disruption of the air-liquid interface and further recruitment of inflammatory agents. Longer exposures at increased doses, as well as persistent inflammation[173], likely overwhelms clearance mechanisms, leading to direct effects of TiO_2 upon the alveolar epithelium. *In vitro* exposures to TiO_2 support the ability of nanoparticles to induce direct damage at the air-liquid interface, as two *in vitro*

studies using Aeroxide^{TM} TiO_2 P25, an archetypal titanium dioxide particle also utilized in 8 of the 18 *in vivo* studies reviewed, demonstrated dose-dependent decreases in lung cell viability, falling from ~75% to <50% compared to controls over a one-hour exposure[36,37].

2.5.1.4 Multi-walled Carbon Nanotubes (MWCNTs)

While there remains disagreement about the *in vivo* effects of MWCNT inhalation, a majority of studies report that MWCNTs are engulfed by alveolar macrophages following deposition in the lung[100,157,159,160,168] leading to downstream inflammation mediated by macrophages, neutrophils, and cytokines measureable in the BAL fluid[97,100,158,162,165,166,181,182]. In several studies[158,159,165,166,181] (Kasai et al. 2010; Umeda et al. 2010), giant cells or mononuclear aggregates were observed indicating the presence of granulomatous inflammation. Fibrosis secondary to this inflammatory response was also documented in other studies[162,182] (Porter et al. 2012). Conflictingly, other groups observed negligible cytotoxicity or inflammation at the doses tested[157,167,183,184]. Indeed, Kim et al. [160] suggests phagocytosis by alveolar macrophages does not lead to lung parenchymal inflammation but rather DNA damage and genotoxicity, a hypothesis which is supported by other studies in the literature[105,167]. The majority of *in vivo* exposures of MWCNTs utilize acute or subchronic inhalation exposure models, and little is known about the long-term effects of MWCNT inhalation.

While Chortarea et al.[112] and Frohlich et al.[111] both investigated cytotoxicity of MWCNTs at the ALI, differences in endpoint testing impedes comparison of both *in vitro* exposures to the *in vivo* scenarios. It is difficult to tell if there is *in vitro* prediction for *in vivo* responses given the dose differences, however responses observed, such as particle uptake into macrophages, appear to correlate [98,112,159,161,164,184].

Identical biological endpoints are necessary for ideal comparison; however, correlations of endpoints that measure the same properties can be described as well. Often, the same endpoints are not measured between *in vitro* and *in vivo* studies, making comparisons difficult. In addition, there is a need for more homogeneous dosing metrics between *in vivo* and *in vitro* studies allowing for simple toxicological comparison of biological responses.

2.6 Recommendations for ALI Experiment Design

Recognizing the great diversity of methods currently used, the following elements for inclusion in nanoparticle aerosol ALI exposure experiments are recommended to facilitate improved inter-laboratory comparison of generated biological response data and advancement in the field. Many doses applied *in vitro* are folds higher than the permissible limit of nuisance dust in one hour set by OSHA at 5 mg/m^3, which translated into a particle concentration using the same assumptions made by Geiser & Kreyling[2] of a 50 nm particle, gives approximately $4.7x10^8$ $particles/cm^3$.

(1) Matching of aerosol flow profile to exposure mechanism in humans/animals

Differences in the methods of introducing the aerosol to cells may lead to different biological responses. Many doses applied *in vitro* are folds higher than the permissible limit of nuisance dust in one hour set by OSHA at 5 mg/m^3, which translated into a particle concentration using the same assumptions made by Geiser & Kreyling[2] of a 50 nm particle, gives approximately $4.7x10^8$ $particles/cm^3$. Due to the unique properties of the nano size range, it can be difficult to determine appropriate doses to investigate when compared to the bulk materials. The exposure system as well as the cell type studied should be appropriate for the question being investigated. For example, the deposition efficiency of the system directly influences the deposited dose which affects the utility of using certain systems for studying different

toxicological responses, such as dose-response or mechanistic effects. The deposited dose is affected by the flow profile given a constant administered dose. For dose-response studies which can require high particle deposition, the use of electrostatic deposition, thermal precipitation, direct dosing, and cloud settling may be more suitable. Mechanistic studies, which do not require the ability to deposit high doses, may be done with a lower deposition system as sublethal interactions between nanoparticle and cell are under investigation. The flow pattern of the system is also an important factor to consider when planning an ALI study. Perpendicular flow may be appropriate for modeling the impaction of nanoparticles at bifurcations in the respiratory system, such as in the bronchi. Parallel flow may be more characteristic of the air flow in the lower airways, as air entering the lungs does not hit the epithelial lung cells with high force, and allows for study of the sedimentation and diffusion of particles during inhalation. Studies performed in an environment without air flow do not fully mimic the mechanics of breathing. Flow through systems capture more aerosol dynamics, and further coordination of flow direction and rate would be worthwhile. Despite the influence of flow pattern (e.g. perpendicular versus parallel) on particle deposition, currently there is no evidence reported in the literature of negative cellular effects from flow or deposition forces used in the various exposure systems that have been reviewed. Additionally, there is no evidence in the literature that charging the particles upon entrance to the exposure system influences cell viability, particle charging is not expected during normal breathing *in vivo* in addition to particles charged prior to inhalation.

(2) Measurement and reporting of the deposited dose

It is recommended that estimation of dose be done by means of deposited dose, however multiple doses should be reported to aid in inter-laboratory comparison. Administered dose does not always correlate well to cell response, and currently developed methods of measuring

cellular dose are time consuming and difficult to perform. It is debatable whether reporting deposited dose or cellular dose is more useful in dose-response curves. However, deposited dose is more conveniently and reliably measured by comparison, as it is not dependent on post-exposure incubation/internalization. Ideally, deposited dose measurements can be collected using QCM as the data can be time resolved, is not material-dependent, and can be confirmed visually. Additionally, exposure duration is a key factor in the determination of deposited dose and should be reported in experimental protocols.

As the particle size appears to have the most influence on deposition, the deposition efficiency should be characterized over multiple particle sizes. With deposition efficiency curves, the ability to convert between administered and deposited dose exists instead of needing to measure the deposition for each experiment as many deposition efficiency equations reported include the amount collected and the amount administered. The uptake kinetics of nanoparticles into cells may be able to link the deposited dose to cellular dose; however, further studies in this area are necessary.

(3) Matching experiment parameters and methodologies *in vitro* and *in vivo*

When comparing submerged cultures to ALI cultures, the same methods should be used whenever possible, including using cell culture inserts for the culture of submerged cells and measuring both apical and basal supernatant concentrations of biomarkers. It is also important to use similar doses when comparing the responses of each culture[58]. The deposition of nanoparticles in suspension can increase with time due to sedimentation and diffusion, whereas ALI exposures have a fixed deposited dose at the end of administration. When this is considered, along with aggregation states, the dose can be compared.

In addition to experimental parameters, cell types should also match when comparing *in vitro* and *in vivo* studies. There are over forty different cell types present in the respiratory tract including mobile and stationary cells. Cell lines that have been immortalized through transformation, while predictive, easy to work with, and more reliable for lab to lab comparison, have a short lifespan under culture and, alone, only provide one potential pathway of interaction. Using cell lines only, a co-culture is a more physiologically representative model than a monoculture and mobile macrophages should be included, if possible. An alternative to cell lines are primary cells, such as EpiAirway from Mattek or MucilAir from Epthelix, which can be purchased in normal or diseased states and increase the experimental lifespan of the cells as well as include potential clearance pathways using mobile cells and ciliary beating. The additional lifespan can aid in the comparison of time course and transitioning to chronic studies which will better simulate everyday exposures and *in vivo* exposures rather than the high-dose acute studies that are often used to locate a toxic amount.

The pulmonary dose *in vivo* is rarely measured and instead is often calculated based on computational models that provide average parameters given the subject model. Changes in weight of the target organs may be evaluated and, in combination with composition-based measurements, the amount of ENP in the organ at the time of sacrifice can be determined. When evaluated over the same post exposure period, biological responses, such as LDH release, are often similar between *in vivo* and *in vitro* ALI exposures. However, as observed in Figure 6, there are very few data points that can be compared. Long-term exposure studies are limited by cell viability in current exposure systems. Further development of these systems is needed in order to study the sub-acute and chronic responses to nanoparticle exposure. Another option

includes performing multiple consecutive exposures, which have been investigated by few groups and would be an initial step toward long-term exposures.

Uncertainty needs to be considered throughout the choices of exposure systems and biological assays used to quantify endpoints. In addition to the sources of variability discussed by Rösslein et al.[185], the authors recommend consideration of the sources in Figure 4 that are identified as specific to ALI exposure systems. Inherent in each biological assay is uncertainty; the 3-(4,5-dimethylthiazol-2-yl)-5-(3-carboxymethoxyphenyl)-2-(4-sulfophenyl)-2H-tetrazolium, (MTS) assay has been described in literature[185,186], however the two endpoints widely used throughout the literature described in this review, LDH and IL-8, has not. By standardizing experimental protocols and generating reference materials the uncertainty can be reduced.

2.7 Conclusions

Through the weight of evidence suggested by the case studies reviewed, ALI studies do predict acute toxicity for the same ENPs as seen in *in vivo*. In case studies of four nanoparticle classes used in *in vitro* and *in vivo* exposures: silver, zinc oxide, multi-walled carbon nanotubes, and titanium dioxide, the biological responses for cytotoxicity and inflammatory responses to each particle type were similar. While *in vitro* studies may be unable to capture the full physiological complexity of the lungs, the simplified model can be utilized to predict *in vivo* acute toxicity response and remains an important tool for risk assessment of nanoparticle aerosols.

The ability to compare studies across laboratories is crucial for assessment of nanoparticles. Exposure durations, leading to changes in dose, and different biological endpoint investigations are the largest sources of protocol variation. In this paper, we presented recommendations for standardizing dose measurements to ease comparison of intra-laboratory

and inter-laboratory findings. To enable meta-analyses and potential validation of results, deposition data and toxicity measurements gathered could be placed into an open database. Lastly, differences in the exposure system used also lead to inter-laboratory disparities. Availability of an inexpensive and easy-to-use ALI exposure system would allow for a more unified approach to ALI exposures.

CHAPTER 3: DESIGN, CHARACTERIZATION, AND OPTIMIZATION OF A HIGHLY PORTABLE, AIR-LIQUID INTERFACE AEROSOL EXPOSURE SYSTEM[2]

3.1 Introduction

Personal sampling using *in vitro* techniques could provide comprehensive information regarding the biological effects of aerosols in the workplace.[187] Exposures to contaminants in the air include exposures to the chemical itself, to collected air samples, under submerged conditions where the gas is introduced to the cell suspension, intermittent exposures using a device such as a rocker, or direct exposures at the air-liquid interface (ALI).[188] Many of these techniques are performed with cells grown in suspension or the collection of samples prior to exposure, each of which can affect the toxicological study due to potential changes in the aerosol.[29,50,58] To avoid these changes, the laboratory can be brought to the field using several *in vitro* ALI culture exposure systems that are used in literature,[33,34,60,79,84,111,113,114,117,189] however few are commercially available.[34,60,111] These systems are often bulky, especially when including instruments to regulate the temperature and humidity of the cellular environment and the flow rate of the sample aerosol. By using the PIVEC, aerosol exposures can be performed outside of a traditional lab setting or within the breathing zone while mimicking inhalation conditions.

The determination of aerosol deposition *in vitro* is important to the investigation of health effects due to inhalation. The breathing zone, the area within 30 cm from the mouth and nose,[190]

[2] This chapter is adapted from Secondo et al. Journal of Visualized Experiments. In Press.

is crucial for understanding exposure to nanoparticles and for linking to the biological effects in the lungs.[188] Often, the deposition on cells is defined as a deposition efficiency, the particles deposited onto and taken up by the cells divided by the particles administered to the system[84,90,120] or on a mass basis of the same amounts.[85,114] The current methods for measuring aerosols in the breathing zone are filter based, capturing particles over a given sampling period and using the filters to conduct further testing.[191] Personal monitoring requires a small system that comes with the tradeoff of fewer samples.

There are many approaches to determine the health effects from exposure to an aerosol. The ALI model allows for the aerosol to be administered directly to the cells through the air as in a real exposure scenario, yet it is more cost-effective and less time intensive than *in vivo* studies while mimicking the air-liquid barriers such as the eyes, skin, and lungs. Lung cells grown at the ALI have the ability to generate a differentiated cell monolayer,[7,25–27] which produces physiological traits that closely resemble the *in vivo* lung epithelium, including mucus and surfactant production in specific bronchial or alveolar cell lines, cilia beating,[26] tight junctions,[8,26] and cell polarization.[25] Changes such as these can affect the cellular response measured in toxicity studies.[28–30] In addition, ALI *in vitro* model results are often more sensitive than cells exposed via suspension models[29,31,41–43] and are able to model acute *in vivo* inhalation toxicity.[49,192–194] Therefore, an ALI exposure system that is able to perform measurements within the breathing zone is a natural next step.

By exposing the cells to aerosol directly at the source of emission, investigation of the effects of all gases, semi-volatile compounds, and particles involved in the mixture occurs. When the mixture is collected on a filter, the gases and volatile compounds are not captured and the whole mixture cannot be investigated. In addition, reconstitution of particles into a powder or

liquid suspension can lead to aggregation or particle-fluid interactions, such as dissolution, in liquid suspension.[20,21] When aerosol particles are added to liquid, there is a higher potential for agglomeration,[18–21] formation of a protein corona,[22–24] or interaction with compounds in the liquid, which can affect deposition and influence the biological response.[29,58]

Exposure at the ALI is based on three main aerosol profiles, cloud settling, parallel flow, and perpendicular flow, as discussed in Chapter 2. Many of these exposure systems are large and bulky, requiring excess systems for aerosol pre-conditioning, pumps for flow, or even heating chambers for incubation of cells. This large size decreases the portability of the system. Instead of sampling directly at the source of emission, these systems often have samples brought to the lab or model aerosols generated for analysis. The complexity of the emitted aerosol can be lost in translation from the field to the lab.

The large size of current exposure systems also decreases the ability to perform sampling to investigate spatial gradients in concentrations. This resolution is key when determining toxicological effects of many potential environmental and occupational hazards such as vehicular exhaust particulate matter or workplace activities where aerosolization occurs. Immediately post-emission, there becomes a spatial variance in particle concentration. This grows with time as the particles disperse throughout the atmosphere and these effects can change based on the ambient conditions, such as temperature, pressure, wind, and sun. Particles can begin to age and oxidize as well once emitted[195–198] and dispersal rates are affected by the topography; higher concentrations will be found in canyons and tunnels, where dispersion effects are slowed, and lower concentrations can be found where there is a large area for dispersion.[199–201] These changes in dispersion rates can have significant effects on human health and can been seen when comparing the number of asthmatic adults living in urban versus in rural settings.[40] While many exposure

systems provide multiple samples at once, multiple systems are necessary with an abundance of large equipment to perform spatial resolution.

By bringing the lab to the field, the time of analysis can be decreased by using the whole cell as a sensor. Following known biological mechanisms and endpoints can aid in determination of the aerosol composition and size. Due to slow clearance methods, including mucociliary clearance, phagocytosis, and translocation, these particles are often interacting with cells for approximately days to weeks[146,202,203] generating oxidative stress, inflammation, and even cell death. These biological endpoints can be the starting points for adverse outcome pathways for cardiovascular disease or chronic obstructive pulmonary disease. In addition, Wiemenn et al. performed an array of *in vitro* assays to compare with literature values for short term *in vivo* inhalation toxicity.[204] *In vivo* response was predicted with two of four positive results from testing cytotoxicity via lactate dehydrogenase release, oxidative stress from glutathione reduction and hydrogen peroxide formation and release, and inflammation potential from the tumor necrosis factor alpha gene. Out of ten nanosized metal oxides tested, six tested as active (titanium oxide, zinc oxide, and four different cerium oxide) using *in vitro* exposures with confirmation *in vitro*.

To study the effects of aerosols in an occupational setting, the Portable *In Vitro* Exposure Cassette (PIVEC) was developed for exposures in the field. Additionally, the PIVEC can be worn for personal sampling to monitor and investigate inhalation exposure like the 37 mm filter cassette[205] or multiple systems can be used to achieve spatial resolution within a given area. In this chapter, the design, optimization process, characterization, and use of the PIVEC for cellular exposures is discussed. The design is adapted from the 37 mm closed-case filter cassette design to maintain cells cultured at the ALI. Optimization was determined using similar ALI exposure device designs and available models. Particle deposition was characterized using aerosols

containing copper nanoparticles of 40 nm, 100 nm, and 800 nm in diameter. Copper is used for sensors[206], catalysts[207], and semiconductors[208], as well as electronic cigarettes[209] and welding[210,211], where copper can be found in the aerosols, making inhalation toxicity a concern. Toxicological experiments with the same copper nanoparticles were performed using human lung epithelial cells at the ALI. After exposure, the cytotoxicity was measured by the release of lactate dehydrogenase (LDH) and oxidative stress was measured using the oxidation of 2',7'-dichlorodihydrofluoroscein diacetate.

3.2 Design

The exposure of cells is done either in batch methods or flow-through processes, using one of a few flow profiles. The flow profiles are the cloud settling, where the aerosol is added to the system to form a single cloud and then allowed to settle as a unit onto the cells, parallel flow, where the direction of aerosol flow is across the cells, allowing for the major forms of deposition to be diffusion and sedimentation, and finally, perpendicular flow, where the direction of aerosol flow is onto to the cells, and the major form of deposition includes impaction along with diffusion and sedimentation. These deposition forces can affect the biological endpoints observed.

For quick, rapid prototyping of the exposure system, 3D printing was used to generate PIVEC pieces for design characterization in acrylonitrile butadiene styrene (ABS), ABSPlus, polylactic acid (PLA), and polyethylene terephthalate glycol (PETG). Advantages and disadvantages for these plastics are found in Table 5. These plastics are not able to be autoclaved and therefore were sterilized through ultraviolet light exposure after rinsing with 70% ethanol solution. All plastic thicknesses were kept at 2 mm to increase stability and strength. Due to high volume resistivity, these plastics will likely collect nanoparticles throughout the exposure

duration. To prevent leaks in the PIVEC, Teflon tape, duct tape, and silicon was used to seal connections. While rapid prototyping is ideal for quick and easy changes to designs, there are often deformations with the printed plastics that constitute leaks, poor fittings, or other problems.

Table 5. Comparison of 3D printer filaments used for PIVEC prototyping.

Filament Name	**Acrylonitrile Butadiene Styrene Plus**	**Acrylonitrile Butadiene Styrene**	**Polylactic acid**	**Polyethylene Terephthalate Glycol**
Common Name	ABSPlus	ABS	PLA	PETG
Extruder Temperature	240 ± 20 °C	230 ± 10 °C	205 ± 15 °C	245 ± 10 °C
Bed Temperature	90 ± 10 °C	90 ± 10 °C	40 ± 15 °C	60 ± 10 °C
Advantages	Strong material Easy post-processing Decreased warping	Strong material Lightweight Wear and heat resistant	Odorless during printing Biocompatible Good for low stress projects	Strong material Odorless during printing FDA approved for food use
Disadvantages	Brittle material Little odor during printing	Odor during printing Non-biodegradable material	Dissolves in water Brittle material Often clogs printer nozzle	Nozzle and printer bed temperatures must be fine-tuned for best results

The closed-face 37 mm polystyrene filter cassette has been adapted to hold a cell culture insert with culture media for a highly portable, *in vitro* ALI nanoparticle aerosol exposure system. The

PIVEC is designed as a three-piece system, shown in Figure 7: a top that connects to the inlet piece of the 37 mm filter cassette, an adapter which is designed to hold a cell culture insert of a 6 well or 24 well size, and a bottom that connects to the outlet of the 37 mm filter cassette. The outlet connects to a vacuum pump, protected by a filter, to generate flow. The pulled flow simulates inhalation through the system and mimics in vivo exposure through depositing particles in the air phase onto lung cells grown in air interfaced culture through impaction, diffusion, and sedimentation. Temperature is kept at 37°C ± 1°C using aluminum foil insulation around a battery powered resistive heater which wraps around the PIVEC. Prior to entering the PIVEC, the relative humidity of the aerosol is increased to over 60% as it passes through a length of wet 10 micron porous hydrophilic tubing (Scientific Commodities, Inc.). Perpendicular flow mimics the deposition forces in the bronchial region of the lungs and allows the system to be compact while maintaining a similar design to the 37 mm cassette.

A.  B.  C. 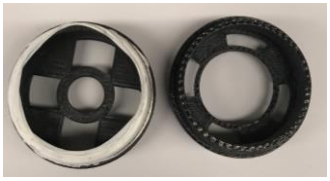 D. 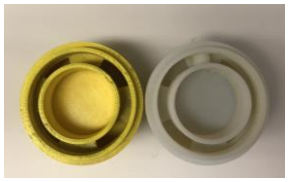

Figure 7. PIVEC Design. A. 37 mm filter cassette. B. Top piece. C. Cell adapter for either a 24 well (left) or 6 well (right) cell culture insert. D. Bottom piece.

3.3 Design Optimization

The optimization of the PIVEC system is dependent on the deposition efficiency of the system. The ideal deposition of the system is approximately 20% of particles with a diameter under 100 nm, based on an average from the International Commission on Radiological Protection human respiratory model[212]. To achieve this amount, the design of the aerosol inlet was altered based on models and current exposure systems.

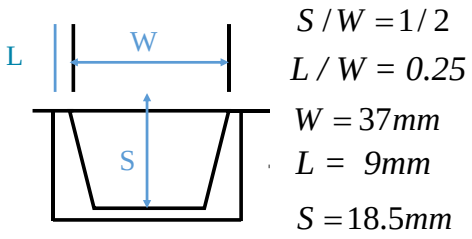

Figure 8. Impactor design and calculation for round jets given in the 37 mm filter cassette.

Marple and Willeke[213] discuss an impactor design model that uses a stagnant point flow to determine the design of the system and size of particles that deposit. The impactor design is based from three parameters observed in Figure 8, L, the aerosol inlet length, W, the aerosol inlet diameter, and S, the distance between the aerosol inlet and the stagnation plate.

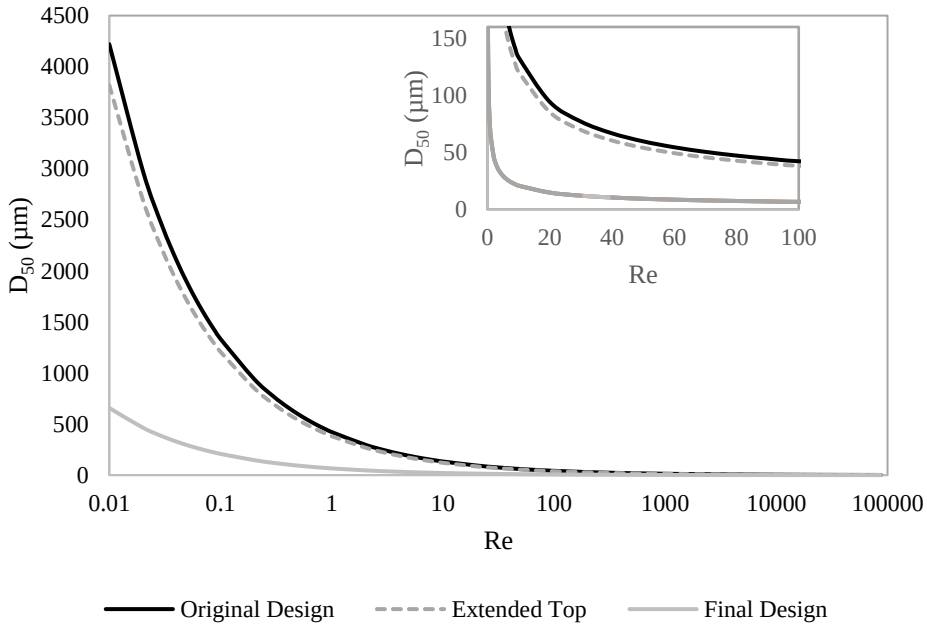

Figure 9. Diameter of deposited particles at 50% efficiency as a function of Reynolds number based on different PIVEC designs.

As the flow rate changes, the cutoff diameter of particles that deposit changes proportionally, allowing larger particles to deposit with a higher flow rate. To keep with the 37 mm cassette design, the W was held at 37 mm and the L was increased to 37 mm. This allows for an increase in the size of deposited particles and lowers the Reynolds number, Re, observed in Figure 9. Theoretically with larger particles depositing, the depositing mass is increased, which also increases the mass based deposition efficiency. In order to decrease Re of the vehicle to a maximum of 1 with the final design, the flow rate must be a maximum of 3.92×10^{-8} LPM, the equivalent of less than 1 mL/day. Alternatively, using a flow rate of 10 mL/min, the same as the lowest reported for the Vitrocell system for a single well{Formatting Citation}, the aerosol inlet diameter would need to be over 60 m in diameter to achieve a maximum Re of 1. As neither of these designs are physically feasible, the final design was chosen to maintain the small system size.

Using available ALI exposure systems to consider alternative design options, found in Figure 10, to increase the deposition efficiency, the PIVEC design was altered to reflect the Vitrocell and MINUCELL design and models set forth by Desantes et al.[141] and Grabinski et al.[136]. The aerosol inlet diameter and deposition distances were decreased, mimicking the trumpet-like inlet of the Vitrocell and MINUCELL systems. In addition, a PIVEC design was prototyped with only the aerosol inlet diameter decreased and a design was prototyped with the deposition distance increased, observed in Figure 4. Deposited efficiency is generally increased

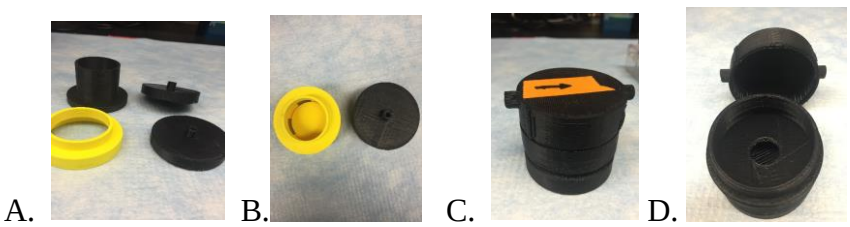

Figure 10. Alternative PIVEC Designs. A. Various Top Designs. B. Various Bottom Designs. C. Parallel Flow Design. D. Internal Parallel Flow.

to approximately 35% when the flow profile is parallel to the cells, thus this method was also investigated.

As the throat length increases in relation to the aerosol inlet width, smaller particles can be collected. However, significant increases must be made to obtain small reductions in particle size. With a 400% increase in throat length, there is only a 10% reduction in particle size from 8583 microns to 7720 microns observed between the original PIVEC design and the extended top design. No change in the particle deposition profile is observed with a 42% increase in throat length between the design that mimicked the Vitrocell and MINUCELL exposure systems and the PIVEC final design. A significant change in particle size is observed, however, between the original design and final design, from 8583 microns to 447 microns. In addition, smaller particles are collected as the aerosol becomes more streamlined, either by bringing the outlet of the aerosol closer to the desired area for deposition, not allowing time for the flow to develop, or by narrowing the inlet diameter to increase the Reynolds number.

The influence of these inlet parameters was also determined experimentally using measurements of mass based deposition efficiency. These measurements were performed using saline solutions at 1%, 5%, and 10%, mass basis. Saline solutions are used throughout aerosol exposure literature to determine deposition in exposure chambers due to operating conditions[35,114,214]. Lenz et al.[114] determined the uniformity and efficiency of deposition in the ALICE using saline solutions between 2-10%, mass basis. The set-up for these experiments is found in Figure 11, using a BGI 3-jet nebulizer and diffusion dryer to control droplet size. Following best practices discussed in the *Aerosols Handbook*[191] and *Air Monitoring Methods*[215], gravimetric analysis of deposited aerosol particles was performed using glass fiber filters 1.0 μm pore size (SKC 225-7). To minimize fluctuations, the filters were kept in an environmental

chamber to regulate humidity and weighed three times prior to and post exposure using a micro-balance (A&D, Model BM-22) to determine the total mass of particulate matter collected. Filters

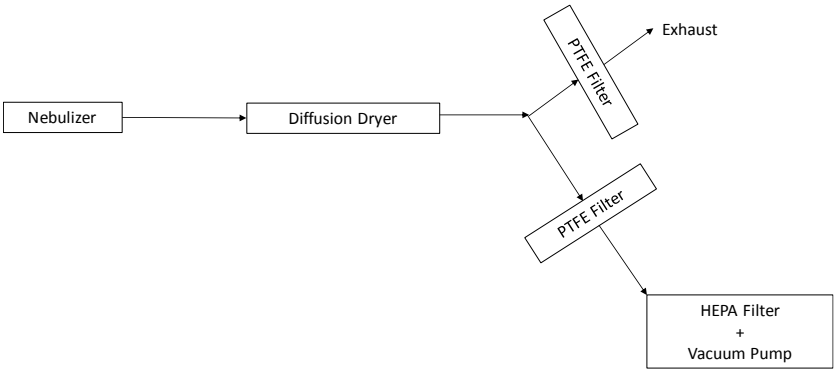

A.

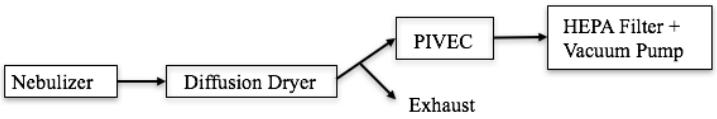

B.

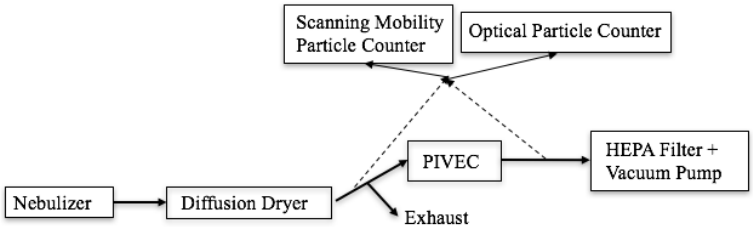

C.

Figure 11. Deposition Set-Ups. A. Flow Diagram of Set-up. B. Initial Flow Diagram of Aerosol Push Set-Up. C. Flow Diagram with Particle Counters. Dashed lines represent connections that can be set up prior to or post PIVEC to determine number and size depositions.

were exposed for a duration of 1 hour to saline solution. The same is performed with cell culture inserts containing filters in the PIVEC system using 6-well and 24-well insert sizes. For the 24-well insert, the design was tested using both a medical nebulizer (LC Plus, Pari) and a research nebulizer (BGI 3-jet, CH Technologies USA).

The extended top and original have the same aerosol inlet diameter, however the extended top throat length follows the design recommendations from Marple and Willeke[213] and is nearly four times longer than the original, leading to an increase in deposition by over 400%, observed in Table 6. The increase in deposition efficiency can be described through the loss in velocity with the lengthened aerosol inlet, which results in larger particles depositing and therefore a higher deposition amount. When comparing the smaller diameter of 4 mm, deposition efficiencies of 0.1% for the short length inlet are observed. As described above, it is possible that smaller particles are depositing at a similar overall efficiency, which would result in this decrease in mass based deposition efficiency measured. A prototype using parallel flow was used and observed to have a significantly decreased deposition efficiency of 0.02% compared to the alternative prototypes. As the parallel system would require longer lengths for the deposition area and therefore would make the system much larger, this design was not pursued further.

The final design parameters were decided based on adjusting the size of deposited particles to better match the goal of 20% deposition efficiency for nanoparticles. As observed through theory and experimental results, a more streamlined aerosol is preferred within an extended aerosol inlet length. This was achieved by using a porous tube that serves as an aerosol inlet and provides additional humidity to the aerosol sample in conjunction with the original

A.  B. 

C. 

Figure 12. Design of PIVEC. A. Full design. B. PIVEC with temperature and humidity control. C. Worn PIVEC by a model student.

PIVEC design, Figure 12. This PIVEC design was used for deposition characterization using dry aerosol particles, discussed in Section 3.5.

Table 6. Mass-based deposition efficiency determined from various PIVEC designs. Characterized through 5% saline deposition on a 24 well sized cell culture insert. A. Original Universal Design, η=0.20 ± 0.15%. B. Decreased Aerosol Inlet Diameter, η=0.10 ± 0.03%. C. Increased Aerosol Inlet Length, η=0.88 ± 0.12%. D. Parallel Flow Design, η=0.02 ± 0.01%.

A.

Original	Difference (mg)	Stdev (mg)	Administrated (mg)	% deposited
Run 3	1.64	0.04	454.05	0.36%
Run 4	0.82	0.05	908.1	0.09%
Run 5	0.95	0.01	706.3	0.13%
Average	1.14	0.03	689.48	**0.20%**
Stdev	0.44	0.02	227.49	**0.15%**

B.

Small Top	Difference (mg)	Stdev (mg)	Administrated (mg)	% deposited
Run 1	0.44	0.05	403.6	0.11%
Run 2	0.66	0.05	504.5	0.13%
Run 3	0.59	0.17	877.83	0.07%
Average	0.57	0.09	595.31	**0.10%**
Stdev	0.11	0.07	249.82	**0.03%**

C.

Extended Top	Difference (mg)	Stdev (mg)	Administrated (mg)	% deposited
Run 1	1.36	0.04	201.8	0.67%
Run 2	2.62	0.06	252.25	1.04%
Run 3	3.69	0.04	403.60	0.91%
Average	2.56	0.05	285.88	**0.88%**
Stdev	1.17	0.01	105.02	**0.18%**

D.

Parallel	Difference (mg)	Stdev (mg)	Administrated (mg)	% deposited
Run 1	0.13	0.04	403.6	0.03%
Run 2	0.07	0.05	504.5	0.01%
Run 3	0.09	0.03	504.50	0.02%
Average	0.10	0.04	470.87	**0.02%**
Stdev	0.03	0.01	58.25	**0.01%**

3.4 Modeling

To model a deposition system, considerations of methods of deposition, the geometry, and the size scale are very important. While there are few literature references when considering similar deposition systems to the PIVEC, such as the Minucell [79] and Vitrocell [90,141,216], it can be helpful to consider more fundamental physics such as impaction modeling [213,217,218] and the flow regime of the aerosol.

Following the work of Lucci et al.[219] that designed an analytical deposition model for diffusion/sedimentation-driven flows largely based on *Aerosol Technology* by William C. Hinds[220]. Lucci et al.[219] present a deposition model for the Vitrocell exposure system geometry operating within the Stokes's flow regime. The Stokes regime occurs when the particle Reynolds number is below 1, where viscous forces are non-negligible compared to inertial forces. Sedimentation deposition (Φ_s^{dep}, pt/s) is approximated by equation 20, where $c_{p,in}$ is the administered particle concentration, A_{ALI} is the area of interest for deposition, C_C is the Cunningham correction factor, ρ_p is the particle density, d is the particle diameter, g is the

$$\Phi_{s,i}^{dep} = c_{p,in} A_{ALI} C_C \frac{\rho_p d_p^2}{18\mu} g \tag{20}$$

gravitational acceleration constant, and μ is the viscosity of the aerosol vehicle. The Cunningham correction factor accounts for drag forces on small particles and can be calculated using equation 21 where λ is the particle mean free path. The deposition due to diffusion (Φ_D^{dep}, pt/s) is dependent

$$C_C = 1 + \frac{2\lambda}{d_p}\left(1.257 + 0.4e^{-1.1\frac{2\lambda}{d_p}}\right) \tag{21}$$

on the size-dependent particle diffusivity and the Brownian displacement during a characteristic time, t_c. Equation 22 approximates the diffusive deposition, where k_B is the Boltzmann constant, T is the experimental absolute temperature, S is the distance between the aerosol inlet and the deposition area, and Q is the volumetric flow rate of the aerosol.

$$\Phi_{D,i}^{dep} = A_{ALI} c_{p,in} \frac{C_C k_B T}{3\pi\mu d_p} \frac{1}{\sqrt{2\frac{C_C k_B T}{3\pi\mu d_p} A_{ALI} S/Q}} \tag{22}$$

However, within the PIVEC system, the small aerosol inlet of 4 mm generates a flow that is outside of Stokes's regime and therefore the sedimentation deposition must be handled differently. In addition, the influence of deposition through impaction will be discussed.

Within the transition region of the particle Reynolds number, between 1 and 1000, the settling velocity of the particle must be calculated using equation 23, where C_D is the particle drag coefficient. As the drag coefficient is dependent on the particle Reynolds number, equations 24 and 25, and therefore the settling velocity, these equations must be solved iteratively. The

$$u_{TS} = \sqrt{\frac{4\rho_p d_p g}{3 C_D \rho_g}} \tag{23}$$

$$C_D = \frac{24}{Re}\left(1 + \frac{Re^{\frac{2}{3}}}{6}\right) \tag{24}$$

$$Re = \frac{\rho_p W u_{TS}}{\mu} \tag{25}$$

acceptance criteria for the square of the error between the assumed and calculated settling velocities for iterative solving was set to less than or equal to 1 x 10^{-6} cm^2/s^2. Impaction is difficult to adequately model without the aid of computational methods as analytical methods do not fully describe the particle streamlines within the system. This deposition force can be

described as the ability for particles to exit the vehicle streamline and deposit within the system. For this work, impaction was described using the relationship of inertial and viscous forces found in equation 26. The maximum theoretical deposition is the sum of deposition through sedimentation, diffusion, and inertial impaction.

$$\Phi_{Imp,i}^{dep} = A_{ALI} c_{p,in} \frac{\pi}{2} \frac{\rho_p d_p^2 u C_C}{9\mu \frac{W}{2}} \quad (26)$$

Using the values for an aerosol of copper particles within air flowing at 0.5 liters per minute (LPM) through the PIVEC, the following relationships were observed in Figure 13. The effect of impaction within the PIVEC is low, although non-negligible for particles above 5 micron in diameter. As the particle size increases, impaction and sedimentation become more influential. Diffusion is the dominating force for particles below 10 nm in diameter, as these particles are too small to leave the streamline and deposit through impaction and too light to have significant gravitational forces.

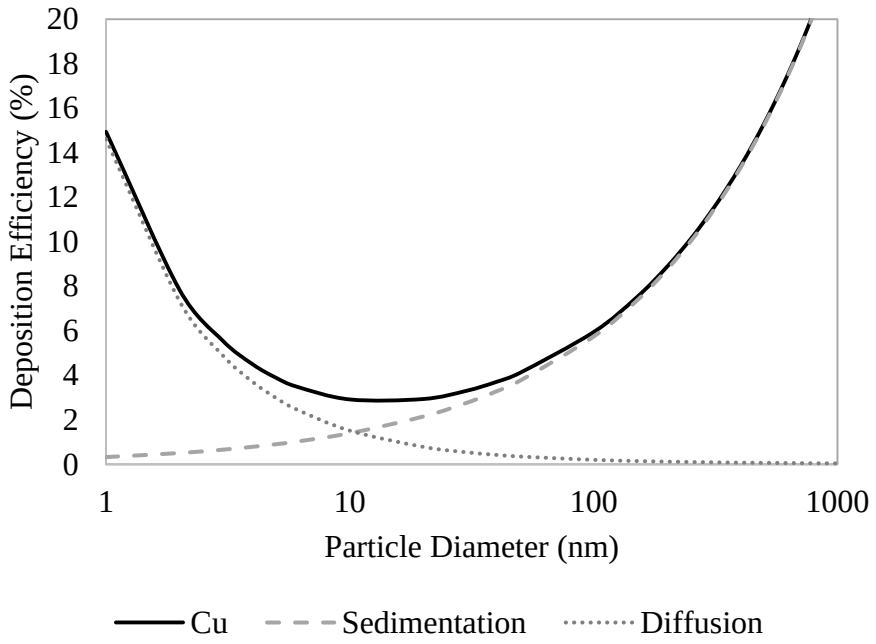

Figure 13. Relationship of deposition methods within PIVEC for an aerosol of copper particles in air at 0.5 LPM.

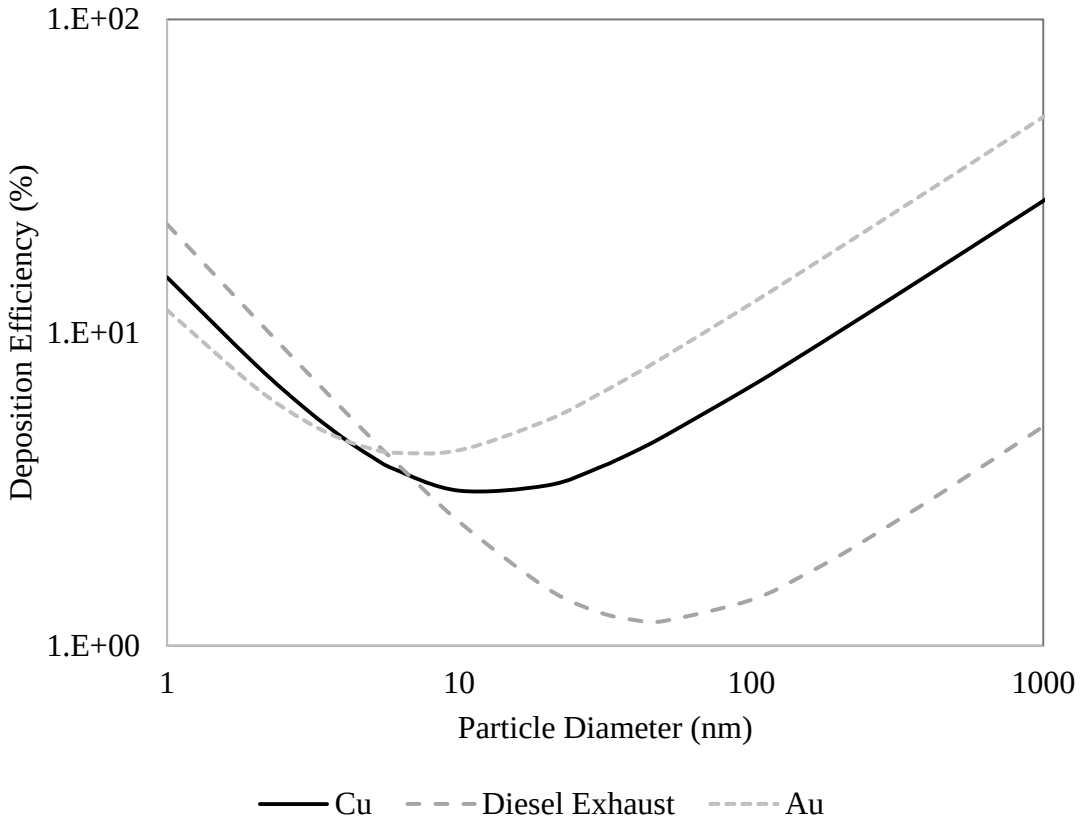

Figure 14. Influence of particle composition and size on deposition within PIVEC.

It is well known that particles of different sizes and compositions will deposit with different amounts within the same system[221]. Figure 14 presents the deposition efficiency within the PIVEC for three particles of varying densities, copper (ρ_p = 8.96 g/cm^3), diesel exhaust (ρ_p = 1.2 g/cm^3), and gold (ρ_p = 19.35 g/cm^3), two of which will be used throughout this dissertation. Below 10 nm, as the deposition is dominated by diffusive forces, deposition efficiency of the particles is dependent on the density of the particle with the lightest particles depositing in the greatest numbers. After this region, when inertial forces begin to outweigh the viscous forces, the particles with the highest molecular weight deposit with the greatest efficiency. The experimental values of number based deposition are approximately 20% of the theoretical

values, computed using the dry aerosol size distribution. This predictive analysis will be helpful for working with varying particle types.

3.5 Characterization of PIVEC using Deposition Efficiency

The deposition efficiency is a good choice for a characterization metric as it is commonly reported for available ALI exposure devices allowing easy comparison and provides for conversion between administered and deposited doses. However, as discussed in Chapter 2, the deposition can be influenced by multiple factors including particle properties and method of administration. Perpendicular flow patterns generally have a deposition efficiency under 10% for all particle sizes, observed in Figure 3. To determine the deposition efficiency of the PIVEC in regards to administration method, characterization of the system was performed with both a wet and dry aerosol, a saline solution and copper nanoparticles (U.S. Research Nanomaterials Inc.), respectively. Multiple sizes of copper nanoparticles were used to investigate the effect of particle size on deposition efficiency within the PIVEC, as a real-world aerosol will be comprised of many sizes of particles. The target deposition efficiency for the PIVEC is 20%, determined from an approximated average value of percent deposition of nanoparticles within the alveolar region of the lungs.

Particle deposition was characterized through particle number and gravimetric analysis. Particle number and size were determined using a scanning mobility particle sizer (NanoScan SMPS 3910, TSI Inc.), which measures particles with geometric mean diameters ranging from 10-420 nm, and an optical particle sizer (OPS 3330, TSI Inc.), which measure particles with geometric mean diameters of 300-10,000 nm. Particle number deposition was determined through measurements before and after the PIVEC, which includes particles collected within the insert and deposited within the PIVEC or tubing. This is taken into account when calculating the deposition

efficiency. Gravimetric analysis was performed using glass fiber filters with 1.0 μm pore size (SKC 225-7) and 25 mm diameter Nucleopore filters with 1.0 mm pore size (Whatman #110610). Filters were kept in an environmental chamber to regulate humidity and weighed three times prior to and post exposure using a micro-balance (A&D, Model BM-22) to determine the total mass of particulate matter collected. Comparisons between the 37 mm filter cassette set up and the PIVEC design were performed to relate the total deposition.

Dry dispersals of aerosols were also used to characterize the PIVEC. Dry dispersions were performed using a homemade system based on Tiwari et al.[222], Figure 15, to produce aerosols using 40 nm, 100 nm, and 800 nm copper particles (U.S. Research Nanomaterials, Inc.) to determine deposition efficiency as it is well known that the deposition can change based on particle size[31]. The copper nanoparticles were characterized through TEM (JOEL JEM-1230) and dynamic light scattering (DLS, Malvern Zetasizer Nano ZS) after suspension in water. The mass based deposition efficiency can be determined through the ratio of particles collected on a filter and amount administered, equation 27. Alternatively, the number based deposition efficiency can be measured through the initial particle concentration, the number of particles deposited, and the ratio of area available for desired deposition to the total area available for deposition, using equation 28[31].

$$\eta(\%)_{mass} = \frac{M_c}{c_m}(100\%) \tag{27}$$

$$\eta(\%)_{number} = \frac{N_{dep}A_{ALI}}{c_p AV}(100\%) \tag{28}$$

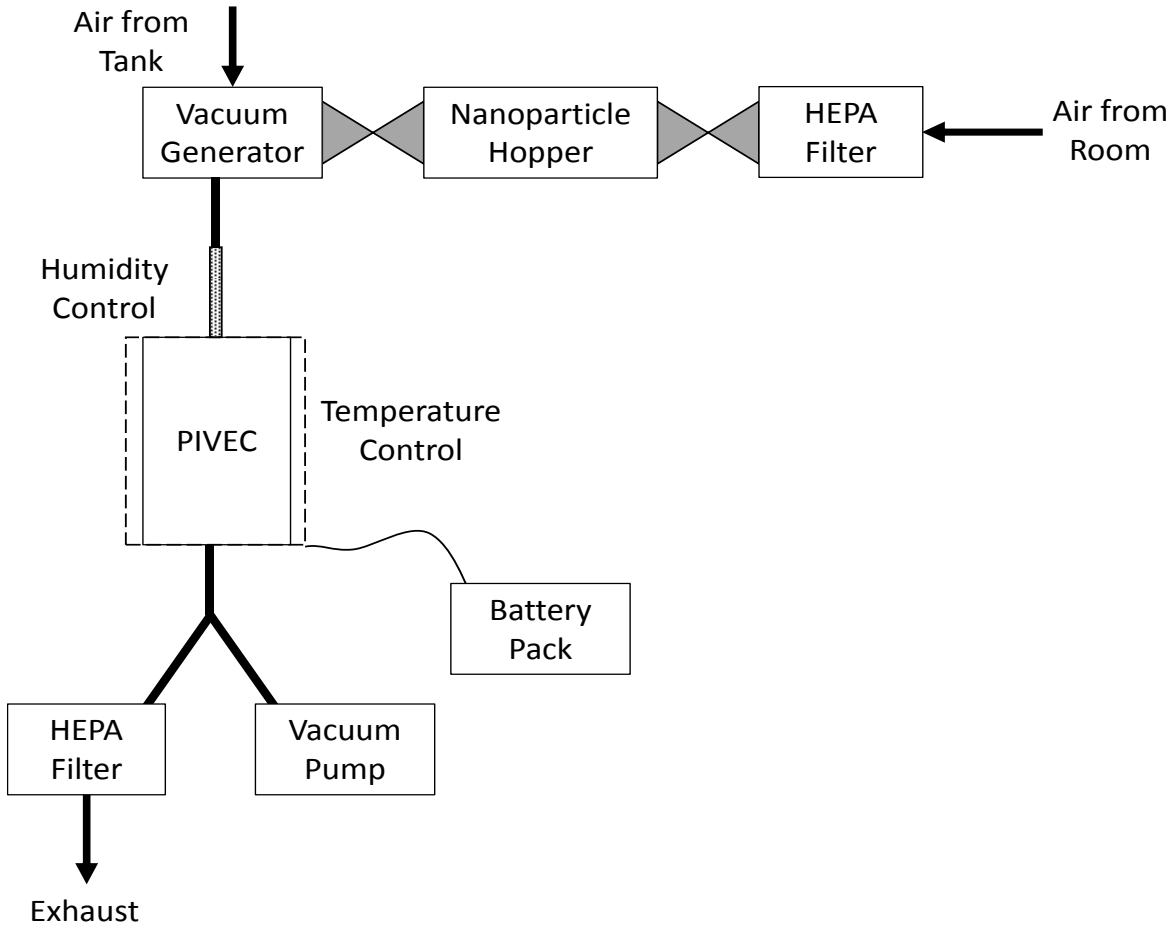

Figure 15. Schematic of dry dispersal system and experimental design.

In addition to the deposition efficiency in the PIVEC system, the deposition percentage of the PIVEC compared to the 37 mm filter. This was considered a crucial step in the characterization of the PIVEC with the design basis of the 37 mm filter cassette. Through the relation of the filter and cell depositions, the analysis of cell deposition post-exposure can be expedited. The 37 mm filter cassette and the PIVEC can be run in parallel and once the filter is weighed, the deposition of particles on the cells will be known.

3.5.1 Characterization Results

The PIVEC is a highly portable, *in vitro* ALI aerosol exposure system designed as an adapter to the 37 mm filter cassette commonly used by exposure scientists and industrial hygienists. Through perpendicular flow, the device mimics inhalation and deposition of particles onto the lung cells with a low deposition efficiency between 0.5% and 18%, depending on particle size and measurement method. The aerosol is conditioned through the addition of humidity as it passes through a wetted, porous tube. Temperature of the cells during exposure is maintained through a battery powered, resistive heater. Characterization of the system allows for determination of the deposited dose onto the cells which can then be correlated to cellular response.

Using the LC Plus and no vacuum pump, therefore only pushing the particles, out of the 400 mg nebulized, 26.72 mg were collected by a filter, and 0.82 mg of NaCl deposited within the PIVEC, resulting in 0.2% deposition efficiency within the PIVEC. When the BGI nebulizer was used with the vacuum pump, approximately 331 mg of NaCl was nebulized, and 19.91 mg was collected by the filter, but only 0.07 mg was collected in the PIVEC, which decreased the collection percentage dramatically to 0.02%. Although approximately 6% was deposited onto the filters by each system, the difference in PIVEC deposition efficiency suggests that there is a difference in the size of particles produced by the nebulizer. The deposition efficiency as measured by the saline solution is dependent on the concentration of salt in the solution. As observed by Lenz et al.[114], the deposited mass increases with increasing mass concentration. However, this trend is only observed slightly.

When the particle number concentration was used to measure deposition efficiency, the value was approximately 100x higher than using the particle mass. To determine this value, the particle number concentration was measured using a particle sizer and counter, such as an SMPS

or CPC, and the total particle count was determined through integration. The PIVEC design was considered with a ratio of the ALI area to the internal surface area. An increase in the ALI area alone should lead to a higher deposition efficiency, whereas a larger internal surface area will lead to more losses of particles due to electrostatic and other deposition forces. With these considerations, for a 5% saline solution in the original design, the PIVEC system has a particle number based deposition efficiency of 4.2%.

The deposition efficiency of the PIVEC has been determined through two methods, gravimetric analysis and particle number counting. Equations 27 and 28 were used to determine the deposition efficiencies in Table 7 using filter based, SMPS, and OPS measurements, Figure 16. Increased deposition is observed overall for the 24 well design than the 6 well design and slightly decreases for 100 nm in comparison to 40 nm and 800 nm copper particles.

Table 7. PIVEC Deposition Efficiency.

		Number Based Deposition Efficiency (%)	Mass Based Deposition Efficiency (%)
6 well	40 nm	17.83 ± 32.13	5.85 ± 0.85
	100 nm	0.47 ± 4.06	5.11 ± 0.94
	800 nm	3.70 ± 35.00	6.39 ± 1.01
24 well	40 nm	1.43 ± 2.43	12.61 ± 1.34
	100 nm	1.37 ± 19.45	2.95 ± 0.75
	800 nm	6.98 ± 3.93	15.95 ± 0.53

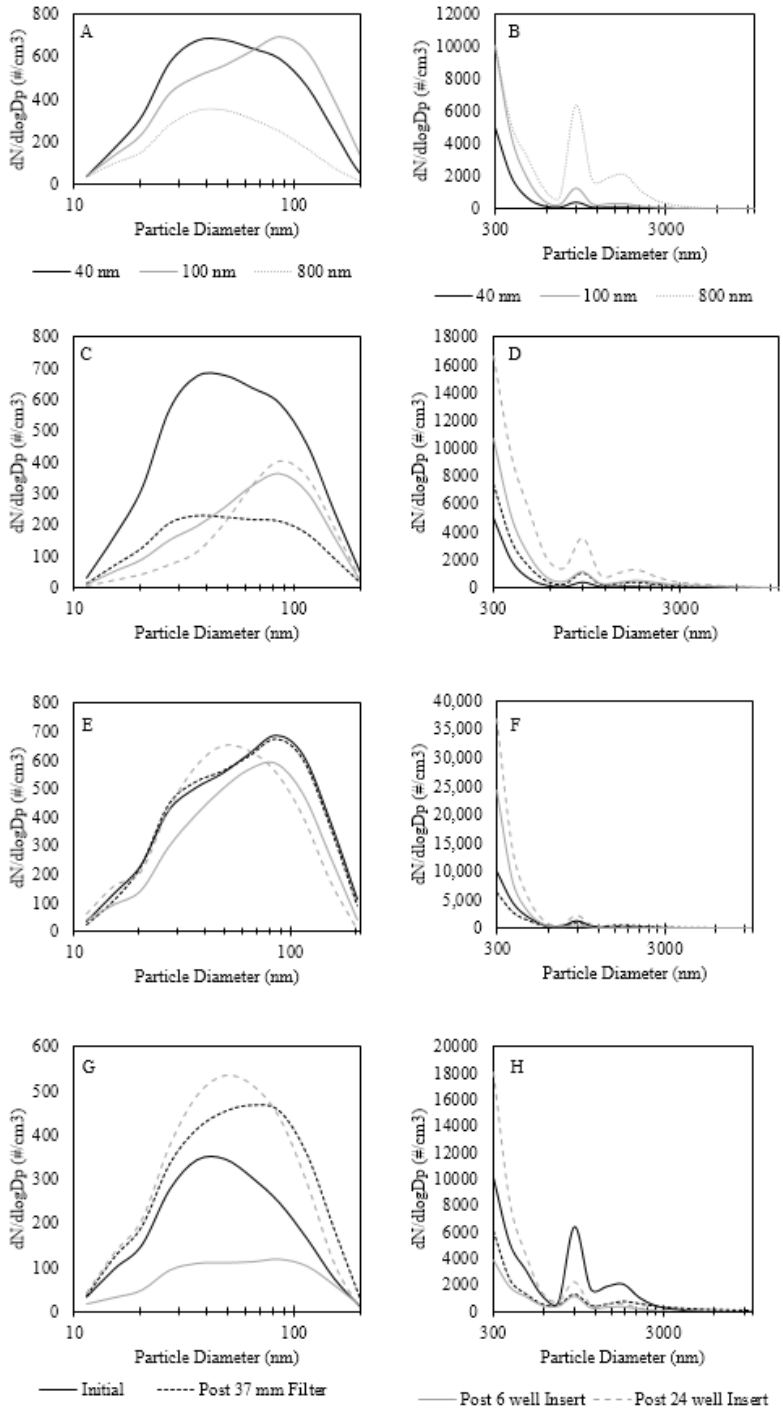

Figure 16. Aerodynamic particle sizes of copper nanoparticles as measured by SMPS and OPS. A. SMPS copper nanoparticle aerodynamic size comparison. B. OPS copper nanoparticle aerodynamic size comparison. C. SMPS comparison of 40 nm exposure particle size measurements before PIVEC (Initial) and post PIVEC. D. OPS comparison of 40 nm exposure particle size measurements before PIVEC (Initial) and post PIVEC. E. SMPS comparison of 100 nm exposure particle size measurements before PIVEC (Initial) and post PIVEC. F. OPS comparison of 100 nm exposure particle size measurements before PIVEC (Initial) and post

PIVEC G. SMPS comparison of 800 nm exposure particle size measurements before PIVEC (Initial) and post PIVEC. H. OPS comparison of 800 nm exposure particle size measurements before PIVEC (Initial) and post PIVEC

Post-exposure analysis can be expedited by determining the dose relationship between the 37 mm filter and the cell culture insert, decreasing the necessity to determine the dose after cellular exposure. Comparison of the deposition within the 37 mm filter cassette and the PIVEC shows a strong correlation for all sizes and wells with a Pearson correlation of above 0.7, however only for 800 nm is the correlation significant with a $p<0.05$, see Figure 17 and Table 8. Compared to similar systems throughout literature, including the Cultex CG[85], MINUCELL[93,111], NACIVT[87], and Vitrocell[81,86,90,111] systems, the deposition efficiency of the PIVEC over the range of particle sizes tested is comparable or increased over reported values, observed in Figure 18.

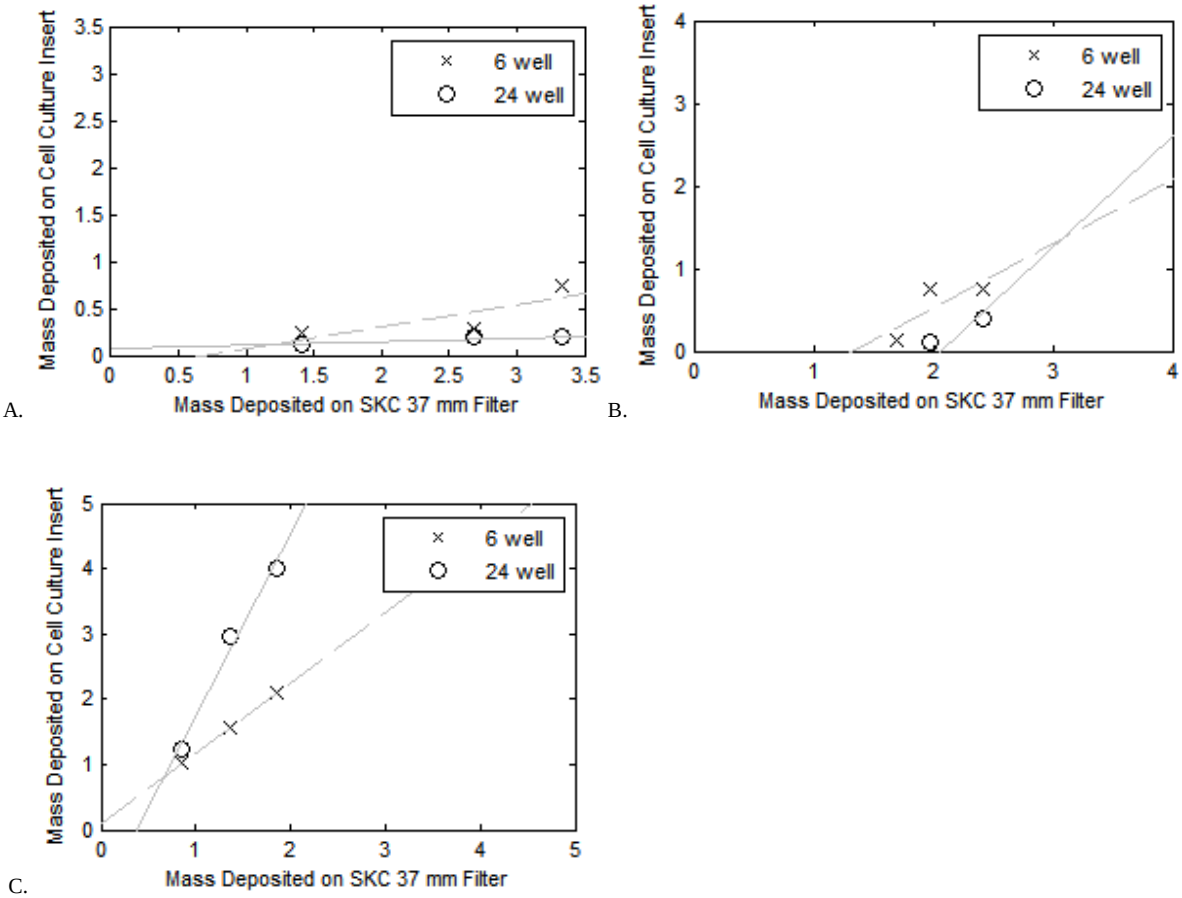

Figure 17. Relationship between deposition on cell insert and 37 mm filter. A) 40 nm copper particles. B) 100 nm copper particles. C) 800 nm copper particles.

Table 8. Correlation and significance of deposition relationships between 37 mm filter and cell culture insert.

Particle Size	Cell Culture Insert Size	Pearson Correlation	p-Value
40 nm	6 well	0.803	0.271
	24 well	0.811	0.260
100 nm	6 well	1.000	0.000
	24 well	0.943	0.065
800 nm	6 well	0.936	0.076
	24 well	0.993	0.004

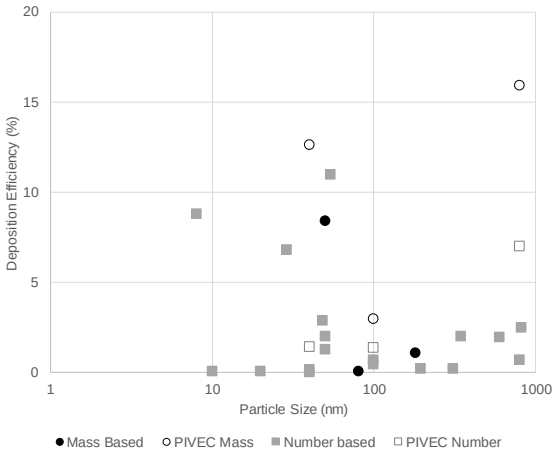

Figure 18. Deposition efficiency of PIVEC compared to perpendicular flow exposure systems in literature.

3.6 Cellular Exposures to Copper Nanoparticles

The cell model used for inhalation effects were the human alveolar epithelial adenocarcinomic A549 cell line[223]. The A549 cell line has been used by many exposure systems to test toxicity and for characterization[33,34,60,84,85,111,114]. Cells were cultured in Dulbecco's Modified Eagle Medium (Gibco) with 1% Penicillin-Streptomycin and 10% Fetal Bovine Serum (FBS, Gibco), together called culture media. After reaching confluency, cells were trypsinized, pelleted, and suspended to a concentration of 35,000 cells/mL using culture media. From this cell suspension, 0.25 mL was added to the apical side of a 24 well cell culture insert (Corning Costar, Collagen coated, 6.5 mm diameter, 0.4 µm pore size) with 0.5 mL of culture media on the basal side in the well. After seven days with media exchange every two days, the apical media was removed and cells were allowed to equilibrate at the air-liquid interface for 24 hours prior to exposure. This cell culture protocol has been shown to produce a cellular monolayer expressing tight junction proteins and a surfactant layer, similar to *in vivo* models[224].

To induce a biological response, copper nanoparticles of 40 nm, 100 nm, and 800 nm were used. The dry aerosol dispersal system connected to compressed air to generate a particle dispersion by opening the tank valve to start air flow, opening the valve closest to the high efficiency particulate air (HEPA) filter on the dry aerosol system, and then the valve closest to the vacuum generator to release the particles and create an aerosol. The tank air was then turned off and aerosol then traveled to the PIVEC as it was pulled through the system by a vacuum pump set at 500 mL/min and could exit through a HEPA filter. The full experimental set-up is described in Figure 15. Cells were exposed for a total of 10 minutes and returned to the incubator for post-exposure analysis.

3.6.1 Cytotoxicity and Oxidative Stress Assays

Cell death was determined using the lactate dehydrogenase (LDH) assay[225], which is a measure of cell membrane permeability through the diffusion of LDH outside of the cells. As LDH is a cytoplasmic enzyme generally present intracellularly, the presence of LDH can be correlated to membrane damage which is indicative of necrosis [226]. Briefly, immediately, four hours, and twenty-four hours after exposure, 50 μL of basal media was removed and placed into a white 96 well plate which was then set aside to incubate at room temperature for 20-30 minutes. Assay reagent was prepared per the assay manufacturer instructions (CytoTox-ONE Homogeneous Membrane Integrity Assay, Promega Inc.), 11 mL of assay buffer was added and mixed to dissolve the substrate buffer mix. After room temperature incubation, 50 μL of assay reagent was added and the reaction occurred for ten minutes, after which 25 μL of the provided stop solution was used to halt the reaction. Fluorescence of the generated resorufin was then measured using a plate reader (Cytation 3, BioTek) with excitation/emission wavelengths of 560/590 nm, respectively. Results are reported as a percent of the incubator control.

Generation of ROS was determined using 2',7'-dichlorodihydrofluoroscein diacetate (DCFH-DA, Sigma Aldrich) oxidation.[227] Intracellular ROS, such as hydrogen peroxide, super oxide radicals, and hydroxide radicals, are measured through the fluorescence of dichlorofluroscein that has been taken up by cells. The diacetate group is enzymatically cleaved from the compound within the cells, slowing the efflux of dye from the cells. Davies [151] reported on varying levels of equivalent hydrogen peroxide and the cellular effects of the oxidative stress. As ROS amounts increase intracellularly, the cell cycle begins to alter, initially pausing at low levels of ROS to inducing cell death through apoptosis or necrosis at high levels of ROS. Briefly, cells at the ALI were washed with phosphate buffered saline (PBS, Gibco) and a 1 mM stock

solution of DCFH-DA salt in methanol was diluted to 10 μM with Hank's Buffered Salt Solution (HBSS, Gibco) to dye the cells. A volume of 0.5 mL diluted DCFH-DA solution was added to the basal side of each ALI culture, the plate covered in foil, and placed in the incubator for an hour to allow the cells to take up the dye. After incubation, the diluted DCFH-DA solution was removed and replaced with 0.5 mL warmed HBSS and an initial reading taken. Fluorescence measurements of the oxidized DCF are taken using a plate reader (Cytation 3, BioTek) with excitation/emission wavelengths of 485/530 nm. After exposure, measurements are continued every 30 minutes for 2 hours, with a final measurement at 24 hours post exposure. Results are reported as fluorescence increase relative to the initial reading of each sample.

3.6.2 Statistical Analysis

Each experiment was run in triplicate unless otherwise noted. The average and standard deviation of each set was taken. With small data sets, analysis of variance (ANOVA) Single Factor analysis was performed to determine significance between data sets. Where applicable, student t-tests were performed to determine statistically significant data points. Data is reported as the average ± standard deviation.

3.6.4 Cellular Response

Cellular response will be affected by the deposited dose and may be affected by exposure duration if the cells are not properly maintained. Cells were exposed for 10 minutes to varying sizes of copper nanoparticles at a flow rate of 0.5 LPM. The particles were polydisperse ellipsoids forming aggregates with all manufacturer sizes, Figure 19. Primary particle sizes were determined using Image J software as approximately 73 nm (range 35-156 nm), 352 nm (range 153-2767 nm), and 520 nm (range 282-1107 nm) for the 40 nm, 100 nm, and 800 nm copper respectively. Full size distributions can be found in Figure 20 along with the EDS spectra, confirming copper particles, Figure 21. Energy dispersive spectroscopy (EDS) was used to confirm the presence of

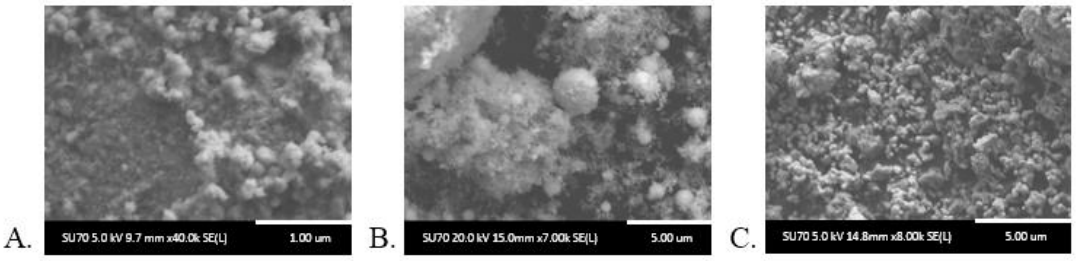

Figure 18. SEM images copper nanoparticles. A) Manufacturer size 40 nm. B) Manufacturer size 100 nm. C) Manufacturer size 800 nm.

copper in particles characterized using SEM. The 40 nm and 100 nm copper particles were >95% copper, Figure 21a and 21b. Due to spacing of particles, additional elements including sodium aluminum, and sulfur were detected with a significant copper peak (66%) for the 800 nm particles, Figure 21c. DLS was not representative of the true particle size as the copper was not stable in solution.

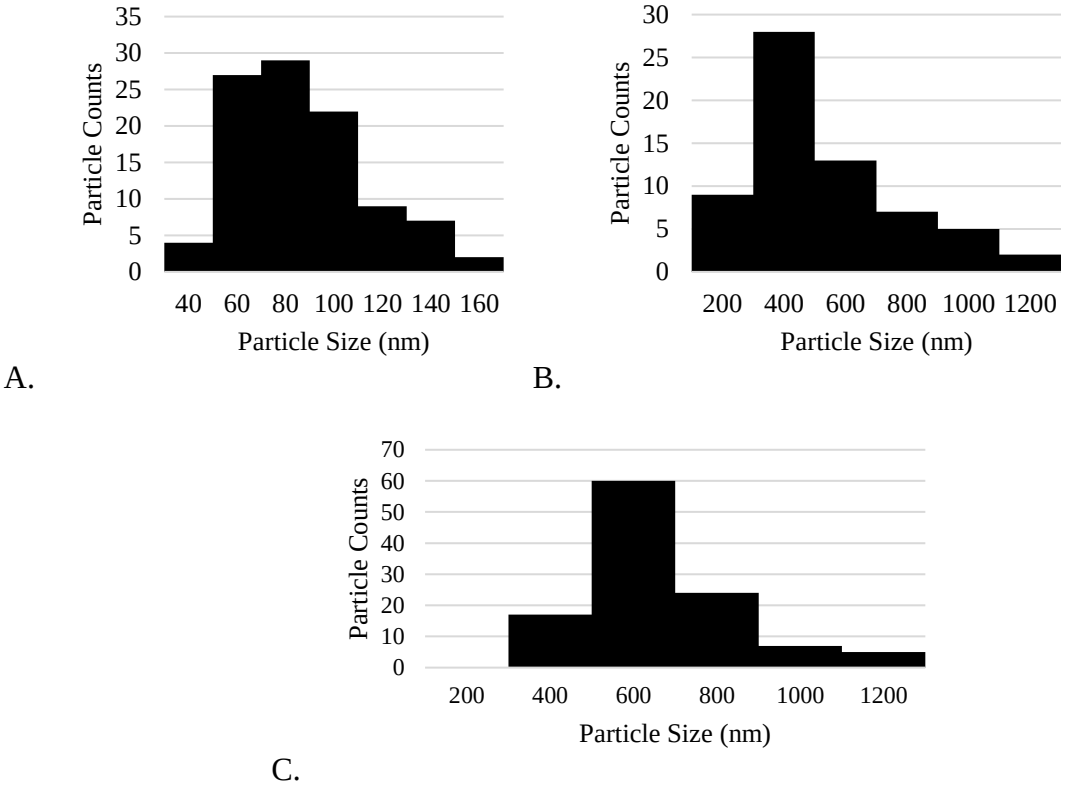

Figure 19. Particle size distribution from SEM images. A) 40 nm particles. B) 100 nm particles. C) 800 nm particles.

A.

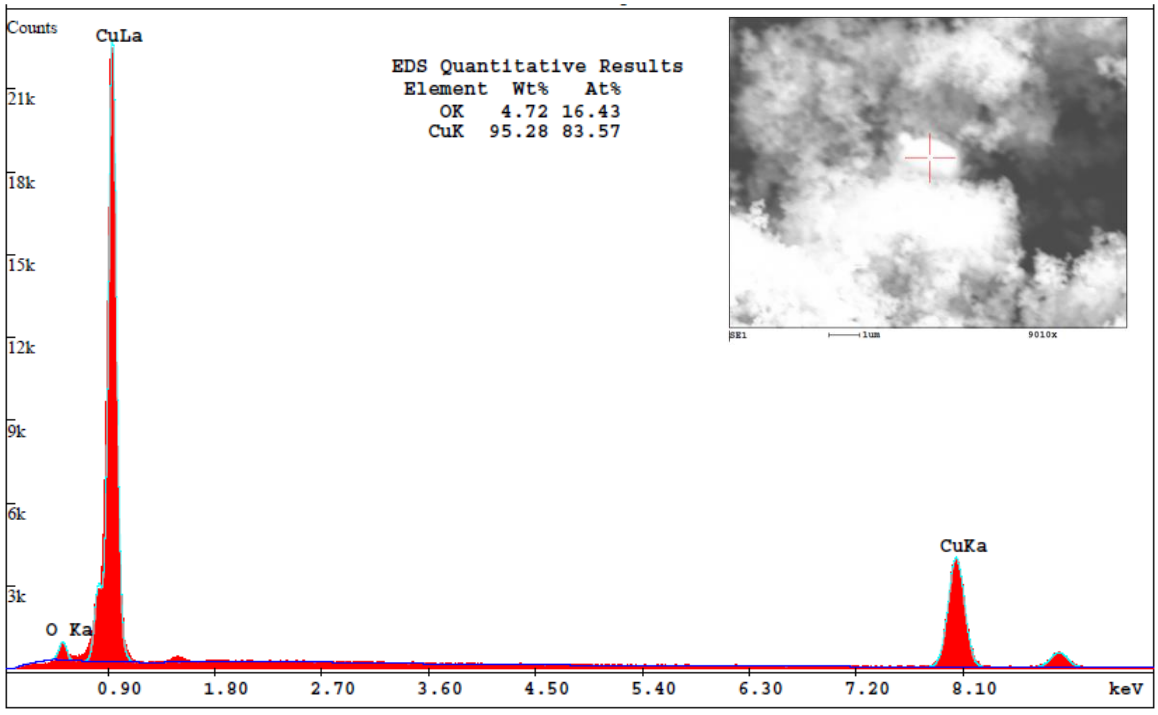
Counts
CuLa
EDS Quantitative Results
Element Wt% At%
OK 4.72 16.43
CuK 95.28 83.57
21k
18k
15k
12k
9k
6k
3k
O Ka
CuKa
0.90
1.80
2.70
3.60
4.50
5.40
6.30
7.20
8.10
keV

B.

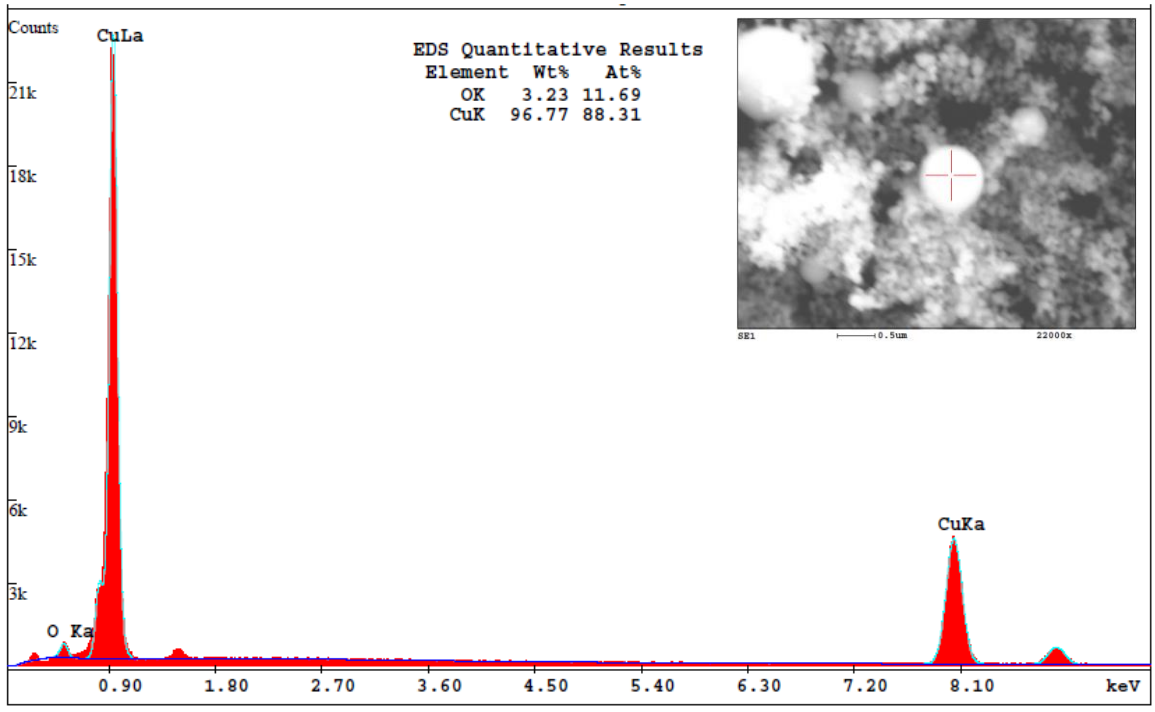
Counts
CuLa
EDS Quantitative Results
Element Wt% At%
OK 3.23 11.69
CuK 96.77 88.31
21k
18k
15k
12k
9k
6k
3k
O Ka
CuKa
0.90
1.80
2.70
3.60
4.50
5.40
6.30
7.20
8.10
keV

C.

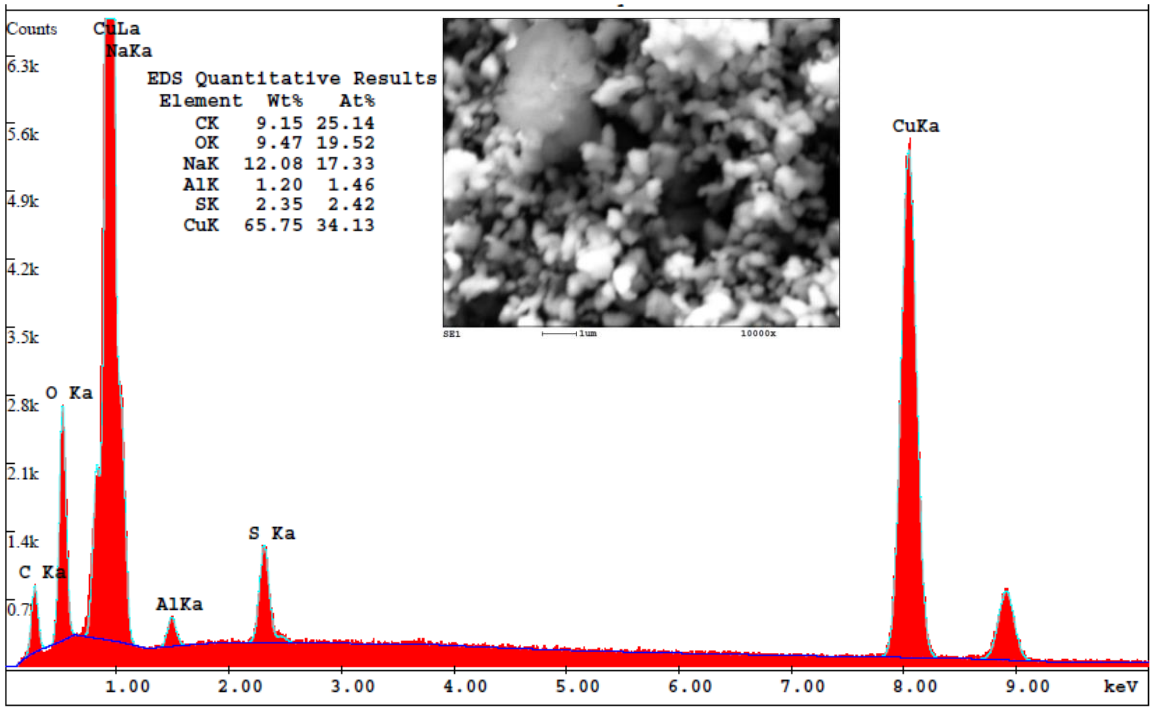

Figure 20. EDS patterns of copper nanoparticles. A) 40 nm particles. B) 100 nm particles. C) 800 nm particles.

Using the mass-based deposition efficiency measured and administered dose, 1.58 ± 0.04 mg/cm^2 of 40 nm copper, 0.30 ± 0.00 mg/cm^2 of 100 nm copper particles, and 0.32 ± 0.01 mg/cm^2 of 800 nm copper particles were deposited onto the cells. Cytotoxicity and oxidative stress were observed within the first twenty-four hours of exposure. Cytotoxicity was measured using the release of LDH from damaged cells immediately, 4 hours, and 24 hours post-exposure, Figure 22a. There was no significant toxicity from copper nanoparticles below 1.62 mg/cm^2 within 4 hours of exposure. Twenty-four hours post-exposure there was a statistically significant decrease in cell viability of less than 20% viability for cells exposed to copper nanoparticles. The intracellular oxidative stress was investigated using the DCFH-DA assay through the oxidation of DCFH by reactive oxygen species within the first two hours post-exposure, Figure 22b. Significant levels of

oxidative stress were measured at thirty minutes post-exposure for cells exposed to copper nanoparticles of all sizes. The level of oxidative stress continued to increase at similar rates for all sizes tested within the two hours observed without a dose-dependent response.

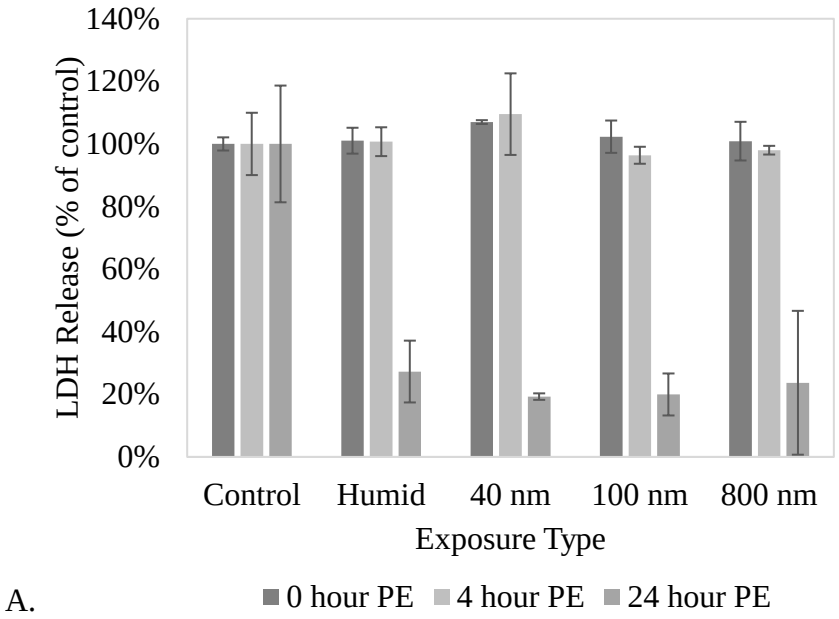

A.

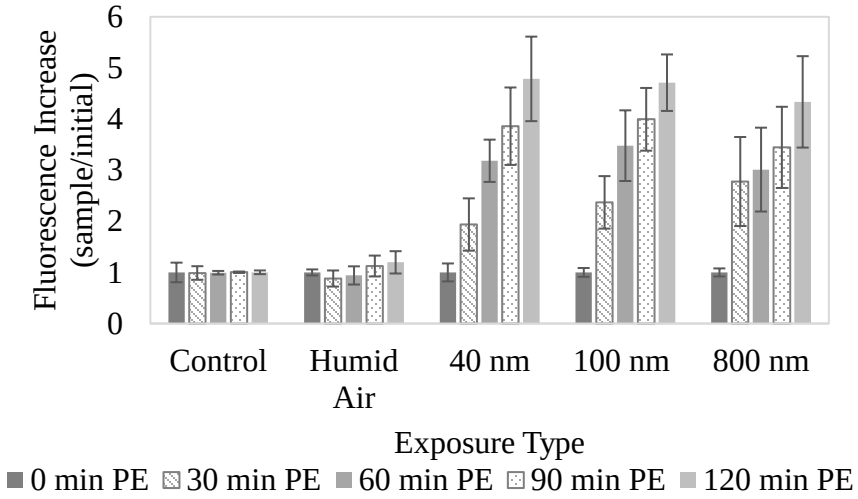

B.

Figure 21. Cellular response to copper nanoparticles. A) Cytotoxicity measured by the LDH assay. B) Oxidative stress measured by the DCFH-DA assay.

3.7 Discussion

Filter cassettes provide a simple, inexpensive method of collecting aerosols in the breathing zone; however, aerosol samples extracted from filters do not provide a complete picture of the entire aerosol (i.e. gases, volatiles, and particulates) and consequently limit the assessment of related biological effects. Using the initial design of the 37 mm filter cassette, the PIVEC is designed to maintain portability and mimic the *in vivo* deposition of particles from inhalation. The PIVEC is significantly smaller than current ALI exposure systems, approximately the size of a tissue box with temperature and humidity control included. The size is similar to personal cascade impactors while offering data on cellular response to the aerosol in addition. While the PIVEC contains space for one sample in comparison to other current exposure systems, the small size permits multiple systems to be used at once therefore increasing the sample size and allowing for spatial distribution to be monitored.

3.7.1 PIVEC Design and Optimization

The design of the PIVEC was based on perpendicular exposure systems and impaction models. The influence of design properties related to the aerosol delivery were investigated in relation to the deposition efficiency and theoretical deposited particle size at 50% efficiency. As discussed above, increasing the throat length while maintaining the aerosol inlet diameter leads to a smaller collected particle size. The same phenomenon is observed when the distance between the aerosol delivery point and the deposition area is decreased. As the 3D printed system (Figure 10) mimicking these changes was not physically stable, an alternative was used by incorporating a long, porous tube that also aided in maintaining cellular viability through increasing relative humidity. This system is not optimized for nanoparticle aerosols, yet when using a dry dispersal

system, the 20% deposition efficiency can nearly be achieved for a range of particle sizes using a 24 well cell culture insert.

Crucial to the design was maintaining cell viability throughout exposure, as significant cytotoxicity has been observed when cells are exposed at conditions with relative humidity below 75% .[228] Zavala et al.[228] performed a nice review of a sample of ALI exposures and the influence pre-conditioning the sample by adjusting temperature and humidity prior to exposure. Through the addition of a battery-operated resistive heater and a wetted, porous tube, the PIVEC maintains temperature at 37 ± 1°C and a relative humidity of >80%. No significant differences were observed between incubator controls and filtered air exposures after the temperature and humidity controls were implemented. Without these systems to maintain cell viability, the influences of removing the cells from the incubator will be observed. The influence of the aerosol itself can be determined by reducing these biological effects through maintaining temperature and humidity during exposure and using comparisons to the aerosol vehicle.

3.7.2 PIVEC Deposition

The PIVEC uses perpendicular flow to deposit particles via impaction, sedimentation, and diffusion onto the cells which has the potential to dry out cells through the flow and added stress on the cells. The deposition efficiency is dependent on the size of the particle due to the forces of deposition. The deposition forces become dominated by sedimentation as the particle size increases to 800 nm. At 40 nm diameter, the deposition forces are dominated by diffusion. At 100 nm, there is a decrease in deposition efficiency, due to the changing deposition forces and the inability of particles to escape the streamline. The large size distribution of the 100 nm particles could affect the deposition efficiency, helping to explain the decrease observed in Table 7. Many of the current exposure systems with perpendicular flow have a deposition efficiency of below

10% and much closer to 1%. The PIVEC has a deposition efficiency determined by gravimetric analysis of 3% to 16% for a 24 well cell culture insert. Using Equation 28, the particle number-based deposition efficiency is approximately 1% to 7% for the same insert. When using a 6 well cell culture insert, the deposition efficiency decreases, with the exception of the smallest particle size, due to the streamlining of the aerosol as more particles are confined in the cell culture insert without space for the flow to develop. These efficiencies are congruent with current perpendicular flow exposure systems available, as observed in Figure 18.[34,85,90,114,117] The Vitrocell has been characterized for deposition on a mass basis using 60 nm fluorescein particles providing an efficiency of approximately 70%[86]. Using a number basis, the deposition of the Vitrocell exposure system has been characterized using polystyrene particles between approximately 20 and 1000 nanometers in diameter[90,111], yielding efficiencies between approximately 0.2% and 7%, carbon nanotubes of varying sizes yielding efficiencies between 2 and 7%[111], and silica particles of 50 nm yielding an efficiency of 11%[81]. Few perpendicular systems report mass-based deposition efficiencies, ranging from 0.05% to 70.3%. The Cultex RFS and NACIVT exposure systems have also been evaluated on a mass basis using 80 nm and 180 nm copper particles yielding deposition efficiencies of 0.05% and 1.1% in the Cultex RFS[85] and 50 nm adipic acid particles yielding an efficiency of 8.4% in the NACIVT[87]. The PIVEC provides, similar or increased, deposition in comparison to available cellular exposure devices.

Deposition can be increased by changing the flow rate and exposure duration. This may also influence the cell viability with the potential of drying out the cells. The conditioning of aerosols is often performed to compensate for physiological attributes such as body temperature and humidification in the airways. Increased humidity, over 50%, mimics inhaled air and decreases cell death due to vehicle exposure.[228] When temperature and humidity are not well controlled, the

cellular response can be influenced. By decreasing the flow rate, additional particles of all sizes will deposit, increasing the deposition. Exposure duration is proportional to deposition, allowing more particles to deposit over an extended experimental period. Conditioning of the aerosol is important when increasing the exposure duration so that the cells do not dry out which can affect biological responses.

If filters are not well dried in a humidity-controlled environment before exposure, excess water increases the initial mass and can produce non-physical, negative deposited doses. Variable flow rates can also promote inconsistent deposited doses within the system. To avoid these issues, allow at least one day prior to and after exposure for filters to dry in a humidity-controlled environment.

3.7.3 PIVEC Cellular Responses

Cell exposures were performed using copper nanoparticles of 40 nm, 100 nm, and 800 nm. Cell viability was defined using the LDH assay with no significant decrease in viability within four hours post-exposure. The LDH assay was used with the Vitrocell exposure system for 74 ng/cm^2 after 2 hours and 148 ng/cm^2 after 4 hours of 9.2 nm[91] and 1 µg/cm^2 deposited after a sequential exposure 4 hours, incubation for 2 hours, then another exposure for 4 hours of 25 nm particles[86], both measuring significant decreases in cell viability. Cytotoxicity was observed in the Cultex for 1.6-7.6 µg/cm^2 of 180 nm particles[85] measured by trypan blue dye exclusion. Exposures of 15 minutes to 40-80 nm copper oxide nanoparticles decreased viability in the Cultex, measured 24 hours post exposure. The lower toxicity observed using the PIVEC was likely due to the shorter exposure time of 10 minutes and shorter post exposure measurement times. After four hours post-exposure, viability of cells exposed in the PIVEC decreased. Cells exposed to humid air controls observed no significant cytotoxicity, in agreement with other studies [34,36,86,91,93]. The oxidative

stress was determined using the DCFH-DA assay. The production of reactive oxygen species, such as hydrogen peroxide or oxygen radicals, generated an amount of stress that can lead to growth arrest or cell death. After the cell exposures, there was a minimal increase in oxidative stress for cells kept in the incubator as control and for cells exposed to humid air. Elevated oxidative stress occurred for all particle sizes, increasing within 30 minutes post-exposure. Within the Vitrocell system, 9.2 nm particles[91] and 25 nm particles[86] also induced oxidative stress measured via the carboxy-DCFH-DA assay. Increased exposure time from 2 hours to 4 hours elevated oxidative stress for 9.2 nm copper oxide particles[91]. After four hours of exposure, the 9.2 nm copper oxide particles produced a similar oxidative response as the sequential exposure of 25 nm copper oxide particles[86], suggesting that exposure duration has a higher influence on oxidative stress response than particle size. Cells exposed within the PIVEC produced elevated oxidative stress compared to the Vitrocell system, however the particles exposed in the Vitrocell are copper oxide and will dissolve less quickly than the copper exposed within the PIVEC. Studies performed on the dissolution of copper based on the composition and size of particles agree that larger particles and the metal oxides release ions slower than metal particles or their nanoparticle counterparts[85,229–231] In addition, Midander et al.[231] suggests that increased cytotoxicity is induced by the particle itself compared to the amount of released copper ions when through a comparison of nano-sized and micro-sized copper and copper oxide particles. As the humid air controls did not produce significant amounts of oxidative stress compared to the incubator control, the influence of copper particles to induce oxidative stress is consistent within the PIVEC to similar *in vitro* exposure systems. The biological responses observed using the PIVEC suggest that the PIVEC is an appropriate system for cellular exposure.

Results for the PIVEC exposures to the copper particles compared with results from direct suspension exposures and *in vivo* methods were also examined. A summary of *in vitro* methods of exposure are presented in Table 9. Similarly to the PIVEC, copper toxicity was observed from the exposure of bare particles[231–233]. The antioxidant capacity of cells was observed, leading to an increase in ROS generation[86,91,234]. Although particle size was observed to influence toxicity and response[231,233], this work is contradictory to that conclusion. The calculated surface area of the 40 nm copper particles is approximately six times greater than the 100 nm and 800 nm particle sizes, 1.41 m^2/g, 0.24 m^2/g, and 0.24 m^2/g, respectively. The lack of difference in surface area for the 100 nm and 800 nm particles supports the similar cellular responses.

A summary of copper particle exposures *in vivo* is presented in Table 10. *In vivo* toxicity[192] and increases in ROS generation[235,236] are also observed. Inhalation studies were performed at acute and sub-acute levels, producing a deposited dose of 10.8 µg to 63.6 µg[237] of copper nanoparticles or 0.2 mg of copper oxide particles[238]. The particles were between 9.2 nm[238] to 25 nm[237] in diameter. Sub-acute inhalation of copper based nanoparticles induced increases in macrophage, neutrophil, and lymphocyte response[237–239]. The LDH response determined by Kim et al.[239] was similar for inhaled particles and instillation, where there was an increase of approximately three times of deposited dose. Cytokine increases of IL-6, GM-CSF, and TNF-a, representing inflammation, were also observed in sub-acute dosages[237,239]. As copper ions are considered toxic, the dissolution of these particles was determined in Gamble's solution, a solution that mimics airway surface fluid. Within one hour of exposure of copper-based particles, there was an increase of copper ions of approximately 2%[237,238]. More acidic solutions completely dissolved the nanoparticles within twenty-four hours of exposure[237,238]. The similar cytotoxic effects

between *in vivo* inhalation studies and the PIVEC, suggest that the PIVEC is a reasonably representative exposure system for the transition between *in vitro* and *in vivo* models.

Table 9. In vitro exposures to copper based particles.

Nanoparticle	Size (nm)	Surface Coating	Cell Line	Exposure System	Exposure Duration (hr)	Deposition Efficiency Reported	Administered Dose	Deposited Dose	Results Summary	Ref.
Cu	DMPS: 80 180	Bare	A549	Cultex CG	4	0.05-1.1%	No Online Characterization Reported	Constant flow: 80 nm: 0.01 µg/cm^2 180 nm: 1.6-7.6 µg/cm^2 Pulsed flow: 80 nm: 0.01-0.05 µg/cm^2 180 nm: 0.3-2.6 µg/cm^2	Air exposed cells had 87 ± 5% viability, 4 h of constant exposure to 180 nm Cu exposure to 180 nm Cu had cytotoxicity (44 ± 7% viability), pulsed exposure and 80 nm Cu did not affect cells	85
	90	Oxidized shell	A549 THP-1	Direct	3 24	NR	0.1-3000 µg/mL	NR	Cu is highly toxic by both MTT and Neutral Red. Fair comparison across labs & cells	232
	SEM: 0.1 µm	Oxidized shell	A549	Direct	18	NR	40 µg/cm^2	NR	Nanoparticles were more potent than micron sized particles, greater toxicity induced by Cu nanoparticles than CuO.	231
	TEM: 100-200	Oxidized shell	A549	Direct	0.25	NR	10 µg/mL 20 µg/mL 40 µg/mL	NR	Membrane damage depends on chemical composition and surface area	233
CuO	Manufacturer: 42 TEM: 20-40 DLS: 220	NR	A549	Direct	4 18	NR	62 µg/mL 40 µg/mL 80 µg/mL	NR	Over 90% non-viable cells, approximately 10-15% oxidative lesions, highest DNA damage, highest increase in ROS, 8x steeper linear dose-response curve compared to Cu ions	234
	30	NR	HEP-2	Direct	4	NR	4 µg/cm^2 8 µg/cm^2 80 µg/cm^2 400 µg/cm^2	NR	Dose-dependent cellular viability was observed	240
	Nanopowder TEM: 20-40, DLS: 200 TEM: 0.5-10 µm	NR	A549	Direct	18	NR	20 µg/cm^2 40 µg/cm^2	NR	Size dependent toxicity	241
	30, 45.4	NR	A549 THP-1	Direct	3 24	NR	0.1-3000 µg/mL	NR	Cu is highly toxic by both MTT and Neutral Red. Fair comparison across labs & cells	232

Table 9 con't

Nanoparticle	Size (nm)	Surface coating	Cell line	Exposure system	Exposure duration (hr)	Deposition efficiency reported	Administered dose	Deposited dose	Results	Ref.
CuO	SEM: 0.05 µm	NR	A549	Direct	18	NR	40 µg/cm^2	NR	Nanoparticles were more potent than micron sized particles, greater toxicity induced by Cu nanoparticles than CuO.	231
	APS: 50	NR	A549	Direct	24	NR	10 µg/mL 25 µg/mL 50 µg/mL	NR	CuO can damage DNA through lipid peroxidation and oxidative stress	242
	Manufacturer: <50 DLS: 112.1 ± 17.3	29 m^2/g	A549	Direct	24	NR	3 cm^2/mL 10 cm^2/mL 30 cm^2/mL	NR	CuO toxic at both NP and aqueous extract in vitro and in vivo	192
	TEM: 23 DLS: 87	NR	A549	Direct	24	NR	5 µg/mL 10 µg/mL 15 µg/mL	NR	Dose dependent cytotoxicity (81% for 5 µg/mL, 56% for 10 µg/mL, 31% for 15 µg/mL), genotoxicity, and oxidative stress	243
	TEM: 23.1 ± 1.0 DLS: 95.6 ± 1.6		A549 16-HBE THP-1	Direct	24	NR	10.3 µg/mL 34.3 µg/mL 103 µg/mL	NR	Cytotoxicity due to water solubility of particles	244
	TEM: 20-50	NR	A549	Direct	0.25	NR	10 µg/mL 20 µg/mL 40 µg/mL	NR	Membrane damage depends on chemical composition and surface area	233
	Manufacturer: 25 TEM: 12 ± 1 SMPS: 30.2 ± 1.92	Oxidized shell	A549 HBEC	Vitrocell	8 (two 4h)	70.3 ± 3.4	1.0 µg/cm^2	262 ± 9.5 ng/cm^2 1.7 ± 0.1 µg/5.7 cm^2	Reduced cell viability (73%), increased LDH, ROS, and IL-8 amounts after exposure to Cu NPs. 63% of delivered Cu was found in basolateral medium, Cu NPS have increased cytotoxicity and increased ROS production	86
	NR	NR	A549	Cultex RFS	0.25 0.5 1	NR	6.856 x 10^5- 7.158 x 10^5 or 484 ± 20.03 µg/L	25 µg/cm^2 50 µg/cm^2 100 µg/cm^2	Comparison of inter and intra lab results, decreased viability	36
	TEM: 11.9 nm, DLS: <250 nm	NR	A549 Caco 2 Balb/c 3T3	Direct	24	NR	1-100 µg/mL	NR	Toxic at concentration below 100 µg/mL	245

Table 9 con't

Nanoparticle	Size (nm)	Surface coating	Cell line	Exposure system	Exposure duration (hr)	Deposition efficiency reported	Administered dose	Deposited dose	Results	Ref.
CuO	SMPS: 9.2 ± 0.2	Bare	A549 HBEC	Vitrocell	0 2 4	50.0%	2.27 x 10^7/cm^3	74 ng/cm^2	A549 more affected than HBEC by CuO toxicity, NAC reduced cytotoxicity through inhibited generation of ROS, comparison of ALI to in vivo study found in "good agreement", dose dependent cytotoxicity (A549 more affected than HBEC), HBEC produced more ROS, NAC inhibits ROS production in A549	91
	TEM: 23 DLS: 87	NR	A549	Direct	24	NR	5 µg/mL 10 µg/mL 15 µg/mL	NR	Genotoxic effect was induced, potentially linked with oxidative stress and compromised antioxidant potential	246
	TEM: 4 ± 1 24 ± 9 DLS: 5.2 ± 0.2	NR	A549	Direct	1 4 24 48	NR	5-125 µg/mL	NR	Size is primary factor for cytotoxicity.	247
	22-25 DLS: 154.5 ± 1.7 NTA: 168.4 ± 3.9	NR	A549 reporter pIL8-luc NFkB-luc	NAVETTA	1	95% with electric field, 75% without EF	4 g/L 50 mL	1-23 µg/cm^2	NAVETTA has spatial variation that can affect cellular response, difference in reporter type for influence on viability & IL-8.	189
	20-200 nm 55 nm DLS: 146	NR	A549 HeLa S3 BEAS-2B	Direct	24	NR	1-50 µg/mL	NR	at 50 µg/mL CuO NP had less than 10% cell viability, discussion of Trojan horse effect of Cu	248
	500-10 µm 1289 nm	NR	A549 HeLa S3 BEAS-2B	Direct	24	NR	1-50 µg/mL	NR	at 50 µg/mL CuO NP had less than 10% cell viability, discussion of Trojan horse effect of Cu	248
CuO/ZnO	NR	NR	A549 THP-1	Direct	3 24	NR	0.1-3000 µg/mL	NR	Copper is highly toxic by both MTT and Neutral Red. Fair comparison across labs & cells	232
CuO/Cu_2O	22.9	NR	A549 THP-1	Direct	3 24	NR	0.1-3000 µg/mL	NR	Copper is highly toxic by both MTT and Neutral Red. Fair comparison across labs & cells	232

Table 9 con't

Nanoparticle	Size (nm)	Surface coating	Cell line	Exposure system	Exposure duration (hr)	Deposition efficiency reported	Administered dose	Deposited dose	Results	Ref.
Cu_2O	83-94	NR	A549 THP-1	Direct	3 24	NR	0.1-3000 µg/mL	NR	Copper is highly toxic by both MTT and Neutral Red. Fair comparison across labs & cells	232
	Manufacturer: 40-80 5 µm	NR	A549	Cultex RFS	0.25 0.5 1	NR	25 µg/cm^2/15 min	Chamber 1: 535 ± 11 µg Chamber 2: 540 ± 12 µg Chamber 3: 539 ± 16 µg	Cu compounds had significant dose related cytotoxicity	34
$CuZnFe_2O_4$	Manufacturer: 29 TEM: 10-100 DLS: 40-300	NR	A549	Direct	4 18	NR	2 µg/mL 40 µg/mL 80 µg/mL	NR	Less than 10% non-viable cells, approximately 15% FPG sites (oxidative lesions), some DNA damage, no statistically significant ROS changes	234

Table 10. In vivo exposures to copper based particles.

Nanoparticle	Size (nm)	Surface coating	Model, subject	Exposure duration	Exposure technique	Administered dose	Pulmonary dose	Results Summary	Ref.
Cu	25	NR	ICR Mice (n=6)	Single Dose	Oral Gavage	108 mg/kg 158 mg/kg 232 mg/kg 341 mg/kg 501 mg/kg 736 mg/kg 1080 mg/kg	NR	LD50 for nano is between micro and cupric ions (413, >5000, 110 mg/kg respectively), considered moderately toxic	249
	Manufacturer: 23.5	NR	Rat (n=NR)	Single Dose	Oral Gavage	108 mg/kg 158 mg/kg 232 mg/kg 341 mg/kg 501 mg/kg 736 mg/kg 1080 mg/kg	NR	More toxic at smaller sizes	250
	Manufacturer: 25	NR	C57Bl/6 Mice (Acute: n=5-6 Sub-acute: n=8)	Acute: 4 h/d Sub-acute: 4 h/d 10 d	Inhalation	Acute: 3.6 mg/m^3 Sub-acute: 3.68 mg/m^3	Acute: 10.8 µg (estimated) Sub-acute: 63.6 µg (estimated)	Cu induced inflammatory response based on neutrophilia, macrophage, and total cell count from BALF, histopathology showed no Cu	237
	TEM: 12 ± 1	Cu_2O CuO	C57Bl/6 Mice (n=6)	4 hr/d 10 d	Inhalation (whole body) Instillation	Inhalation: 3.5 ± 0.4 mg/m^3 Instillation: 3 µg/mouse 35 µg/mouse 100 µg/mouse	Inhalation: 32 µg Cu/mouse	Dose dependent response from instillation, inhalation also induced response.	239
CuO	Manufacturer: < 50 DLS: 112.1 ± 17.3	NR	Wistar Rats (n=5)	Single Dose Eight Doses	Intratracheal Instillation	Single Dose: 100 cm^2/mL 300 cm^2/mL Multi-Dose: 50 cm^2/rat 150 cm^2/rat	NR	Inflammatory response at higher doses.	251
	Manufacturer: <50 DLS: 112.1 ± 17.3	NR	Wistar Rats (n=5-6)	Single Dose	Intratracheal Instillation	3 cm^2/mL 10 cm^2/mL 30 cm^2/mL	150 cm^2/rat	Cu toxic at both NP and aqueous extract in vitro and in vivo	192

Table 10
con't

Nanoparticle	Size (nm)	Surface coating	Model, subject	Exposure duration	Exposure technique	Administered dose	Pulmonary dose	Results Summary	Ref.
CuO	Manufacturer: < 50	NR	Wistar Albino Rats (n=4)	Single Dose	Intratracheal Instillation	1 mg/kg 5 mg/kg	NR	Observed reduction in antioxidant capacity and similar toxicity to positive control	235
	SEM: 20 ± 10 340 ± 168	NR	Female outbred Rats (n=12)	Single Dose	Intratracheal Instillation	0.5 mg/rat	NR	Nanoparticles induce higher recruitment of alveolar macrophages. Cytotoxic effect is believed to be related to particle dissolution and intracellular localization.	252
	TEM: 9.2-14	NR	Male Outbred Rats (n=6)	0.3 h/d 5d 0.6 h/d 5d 1.5 h/d 5d 3h/d 5d 6h /d 5d	Inhalation (nose-only)	13.2 mg/m^3	NR	Dose-dependent increase in lung inflammation with no fibrotic response	238
	BET: 58.7 nm	NR	BALB/c Male Mouse (n=4)	24 h	Intratracheal Instillation	2.5 mg/kg	0.76 µg/cm^2 instilled mass/alveolar surface area	Effect of epigenome by CuO and in agreement with in vitro study, responses were congruent for expression of transposable elements and DNA methylation between primary small airway cells and mouse lung tissue	253
	TEM: 46.5 DLS: 590.9 (H_2O) 432.2 (10% FCS media)	NR	C57Bl/6 Mice (n=4)	Single Dose	Nasal instillation	1 mg/kg 2.5 mg/kg 5 mg/kg 10 mg/kg	NR	Acute inflammatory period, bronchial epithelial cells are injured by ROS, infiltration of inflammatory cells and cytokines.	236

Success of the exposure can be determined through the repeatability of cellular response. The Nanotechnology Characterization Laboratory (NCL) provides two acceptance criteria for cytotoxicity assays including: 1) The 48 hr% cell viability and % total LDH leakage for the APAP positive control should be less than 50% and greater than 50%, respectively, and 2) The positive and sample replicate coefficient of variations should be within 50%.[254] If these criteria are not met, this suggest differences between experiments, such as altered deposition amounts, or poor humidity or temperature control. In addition, observing cytotoxicity measurements can lead to understanding about the experimental controls and aid in determining the error. When the flow rate is too high, cells may die from high amounts of sheer stress. By lowering the flow rate, the stress upon the cells from the flow can be decreased.

3.7.4 PIVEC Uses and Limitations

While the characterization and cellular studies of the PIVEC agree well with literature,[34,36,85,86,91,93] the device has limitations. The small design decreases the number of samples that can be exposed simultaneously within a single device in comparison to other exposure systems. Other systems allow for at least three cellular exposures to the same aerosol[34,35,111] facilitating replicate measurements. Although the PIVEC only allows for one insert per system, the small size allows for multiple systems to easily be used, helping to mitigate this issue. While other personal monitoring systems do not use cells, the PIVEC must be kept near vertical to reduce spilling the cell culture media necessary to preserve cellular viability. Although the PIVEC has not yet been optimized for specific particle ranges (e.g. PM_{10}, $PM_{2.5}$, $PM_{0.1}$), the PIVEC has been characterized for a range of particle sizes. For examining the biological effects associated with complete aerosols, this may be unimportant. However, if a specific size or size range is influencing the cellular response, then the lack of optimization is limiting. The PIVEC has been characterized

for a range of particle sizes, and like many other perpendicular flow systems, the PIVEC shows a decreased ability to deposit particles near 100 nm in diameter, while 40 nm and 800 nm particles deposited with similar efficiency.

The analysis of cells post-exposure can be expedited by performing parallel collection of aerosols within the PIVEC and a 37 mm filter cassette. A high correlation of gravimetric based deposition allows for estimation of the particle mass collected on the cells from data collected using 37 mm filters. Comparison of the insert to the filter cassette reduces the need to collect additional samples and additional measurements to determine the dose. The small size of the PIVEC allows it to be used in a variety of settings, such as on the body as a personal monitor, on a drone above a chemical plant, or outside in the environment for spatial resolution.

The deposition within the PIVEC can be altered through the vehicle flow rate, the experiment duration, and the particle size distribution. As the flow rate or exposure duration increase, the amount of particles that pass through the system increases, allowing additional particles to deposit. Increasing the flow rate, while increasing the effect of impaction based deposition, will also increase the sheer stress on the cells and affect the biological response. As long as the cell viability is maintained throughout exposure, the exposure duration may be extended for a number of hours. The modification of the aerosol with 5% carbon dioxide will increase the length of time that cells may be maintained outside of the cell culture incubator. Finally, by changing the particle size distribution within the aerosol, using filters, cascade impactors, or alternative size separation and concentration methods, the system deposition will be related to the mixture. For example, a mixture of larger particles over 100 nm will deposit with greater efficiency than a mixture of particles between 10 nm and 100 nm in size.

3.8 Conclusions

This method has shown the use of the PIVEC for the collection of aerosol particles onto cell cultures grown at the ALI. By conditioning the aerosol to 37 ± 1°C and > 80% relative humidity, cellular viability can be maintained during acute exposures. The PIVEC is appropriate for both liquid droplet and solid particle-based aerosols and has been shown to deposit particles between 40 nm and 800 nm in cell culture inserts. The versatility of the PIVEC allows this method to be used in multiple settings with a variety of biological endpoints.

The PIVEC has similar deposition efficiency to current ALI exposure systems through the use of liquid-based aerosols and number-based deposition measurements. The use of dry aerosol dispersion increases the deposition efficiency above current systems, to what is considered a more physiologically relevant amount according to the IRCP model. However, the small size of the PIVEC restricts the system to a single sample measurement at a time compared to the multiple simultaneous sample collections available with other exposure systems. The PIVEC can be used to perform studies without the cost of alternative exposure systems.

Through miniaturization of an ALI exposure device, exposure assessment can be performed in the field with a focus on the biological response. Breathing zone assessment is crucial for determination of human exposure to aerosolized particles. The design of the PIVEC allows for these critical measurements through wearing the device. Utility of the PIVEC can be expanded outside of the breathing zone to spatial monitoring of aerosol dispersion using multiple systems, real-time observation of cellular response through incorporation of a monitoring system, or even chemical plant safety assessment through mounting the PIVEC on drones.

CHAPTER 4: IN VITRO RESPONSE TO EXPOSURES OF NANOCERIA CONTAINING DIESEL EXHAUST VALIDATION OF THE PIVEC SYSTEM

4.1 Introduction

Diesel exhaust is a major component of air pollution, known to correlate with increased cardiovascular disease [2,255,256], respiratory morbidity [4,193,257], and lung cancer [258,259]. Mitigation of emissions has been pursued through diesel particulate filters (DPFs) [260–264] and fuel additives [5,92,265–268] based on cerium oxide or iron. DPFs include substrates of different porosities, such as metal foam [269], fibrous felts [270], sintered metal [271,272], or honeycomb ceramics [262], which contribute to the filtration efficiency and need to regenerate. Improvements to DPFs have been made through the integration of catalysts to induce soot oxidation at lower temperatures, decreasing the temperatures needed for DPF during regeneration, and increasing accumulation tolerances [260,263,264]. Diesel oxidation catalysts are needed for the removal of harmful gaseous emissions. Regulations vary by fuel use (e.g. passenger, heavy duty, or non-road), particle size, gaseous emission, and country [273–275]. Fuel additives have an advantage of reducing the overall greenhouse gas and soot particle emissions and will therefore be the focus of this research.

In the United States, there are more gasoline-based cars than diesel based on economics, however throughout the rest of the world, the situation is often reversed, Figure 23[276,277]. Over 60% of U.S. diesel fuel generated in 2014 was sold for use in on-highway vehicles[278], see Figure 24 for the entire break down. The World Health Organization has performed at least two multiple city study in Europe to monitor the ambient air quality. The first covered 357 cities in 33 counties, where 83% of these cities did not meet the air standards of 5 mg/m^3. The most

recent study covered 25 cities in the European Union and found that if the cities were able to reduce the $PM_{2.5}$ to air quality standards that the life expectancy increased by 22 months[279,280].

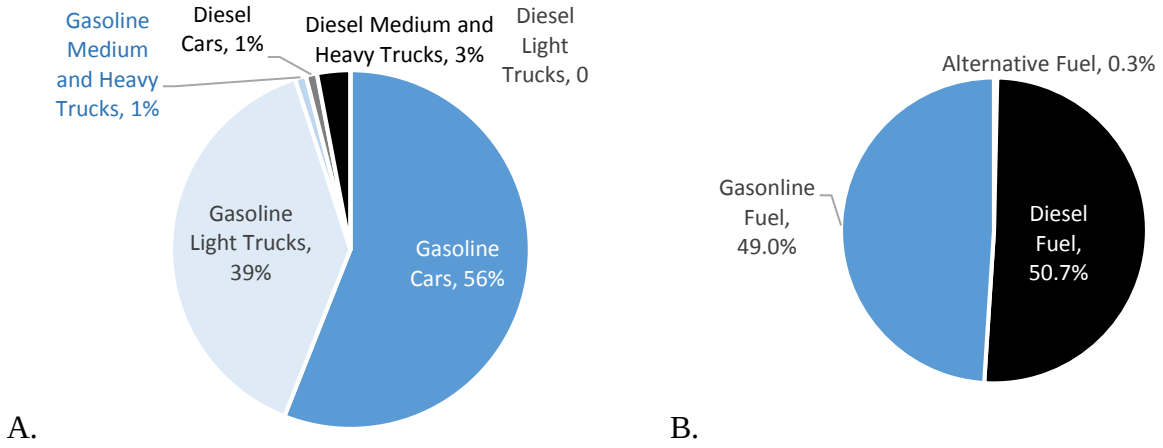

Figure 22. Comparison of diesel and gasoline vehicles in the USA and the UK. A. Breakdown of vehicle fuels in the USA in the year 2014. Adapted from U.S.D.O.T. 2015. B. Comparison of fuels used by registered vehicles in the year 2014 in the UK. Adapted from Guardian, 2015.

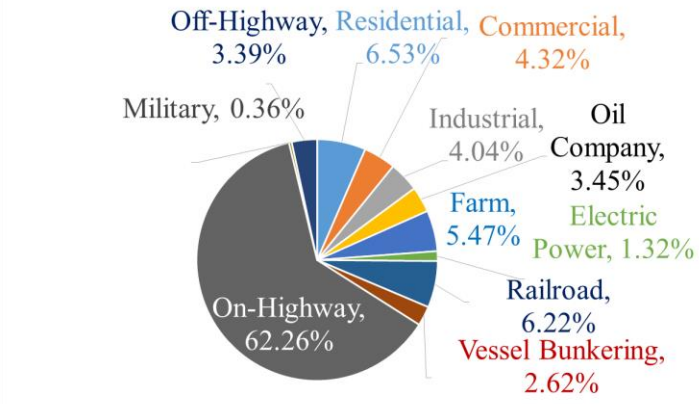

Figure 23. Breakdown of industries to which U.S. diesel fuel was sold in 2014.

Ceria first made its debut as a diesel fuel additive in 1999, designed to increase combustion efficiency [5]. The fuel additive also reduces greenhouse gases such as carbon dioxide, carbon monoxide, sulfur oxides, and nitrous oxides. A by-product of increasing the combustion

efficiency is reducing the amount of soot in the exhaust, and therefore the overall particulate matter. It has been shown in literature that decreases in particle mass correlate to a mean particle size shift into the nanoscale [10,281,282]. In addition, ceria can escape through the particle filter as it is not combusted, often being released as free particles or decorating carbonaceous matter [281,283,284]. Once emitted, the ceria nanoparticles can be inhaled and may alter biological responses to diesel exhaust. The mixture of ceria and diesel exhaust has not been extensively studied, in particular post combustion. As the particle changes through combustion, the studies performed on pristine nanoceria may not provide an accurate description of toxicity of the fuel additive.

In 2012, diesel exhaust was classified as carcinogenic to humans (Group 1); in contrast toxicity from ceria has conflicting results throughout literature. Diesel exhaust is considered to have negative biological effects including cytotoxicity [9,39,65,285–288], oxidative stress [39,285,286], and inflammation [289]. For *in vivo* exposures, the results consistently demonstrate that diesel exhaust produces increased oxidative stress [290,291] and inflammation in the lungs [290,292–294]. Ceria has mixed results throughout *in vitro* literature. Many studies show that ceria, typically tested between 2.5 µg/mL [295] and 500 µg/mL [296], does not produce cytotoxicity [108,295–300] and has anti-oxidant properties [295,301,302]. However, several toxicology studies for inhalation over the same concentration ranges show increases in cell death and an increase in reactive oxygen species (ROS), including hydrogen peroxide and hydroxyl or oxygen based radicals [37,204,303–305].

Human cells have been exposed to diesel exhaust particles at the ALI using filtered and denuded exhaust [306], model exhaust [291], and whole exhaust [80,88,138,288,306–310]. Some of these experiments used collected exhaust from bags that was reconstituted to an aerosol for experimentation [138,288,307]. Other experiments used freshly generated exhaust from engines with varying operational loads (0%, 38%, 47%, or 75%), dilution factors (6 fold to 20 fold), use of

particulate filters and oxidative catalysts, all of which can affect the particle sizes and concentrations in the aerosol introduced to the cells. Ceria has been tested at the ALI in cloud settling [108,115] or perpendicular flow patterns [36,37]. While Rothen-Rutishauser et al. [108] and Raemy et al. [115] observed no significant changes to the cells cytotoxicity from cloud settling at concentrations between 0.36 μg/cm^2 to 24 μg/cm^2, when the cells were exposed using perpendicular flow there was dose dependent cell death between 25 100 μg/cm^2 and 100 μg/cm^2 [36,37]. Few additional ALI experiments have been conducted with the addition of ceria additives. Steiner et al. [311] exposed cells to filtered air and full diesel exhaust at a particle number concentration of 4.8 x 10^8 particles/cm^3 from an engine for either 2 hours or 6 hours and then aerosolized synthesized ceria at two concentrations over the cells post diesel exhaust exposure. With the addition of 20 μg/mL or 60 μg/mL of ceria to filtered air and diesel exhaust, elevated levels of lactate dehydrogenase were observed and pro-apoptotic responses were reduced. Comparing similar exposures with and without ceria, ceria exposure increases glutathione responses. Zhang et al. [312] captured diesel exhaust that had been generated by a diesel generator at 25%, 50%, and 75% load (low, medium, and high), with varying amounts of manufactured ceria added to the fuel. Ceria amounts included 25 ppm, 50 ppm, and 100 ppm in the fuel. Low loads increased particle concentrations below 20 nm with the addition of ceria as low as 25 ppm, whereas this peak disappeared at medium load for 25 ppm ceria. There was no change in size distribution at high load for all ceria concentrations. Toxicology studies were performed on A549 cells using filter captured exhaust from the 100 ppm ceria. After reconstitution in cell culture media, the suspension was applied to cells at doses of 25 μg/mL, 50 μg/mL, 100 μg/mL, and 200 μg/mL and exposed for 24 hours. Cell viability measured via the MTT assay was decreased compared to diesel exhaust exposure up to 200 μg/mL. Genes were upregulated for

inflammatory response compared to the control and exposure to diesel exhaust alone. Both groups observed increases in cytotoxicity, oxidative stress, and inflammatory markers of the A549 cells dosed [311,312].

There have been few direct exposures of diesel fuel with nanoceria fuel additives [313], but none to ALI cells. An *ex vivo* exposure to rat lung slices was performed with 5 ppm Envirox and 2% to 20% diluted exhaust by Fall et al.[313], producing a significant decrease in intracellular ATP levels for all exposures and a significant decrease in intracellular glutathione for the highest dilution factor both with and without Envirox. The oxidative stress response is not well understood as ceria itself is often considered to scavenge radicals; however, the addition of ceria has previously lead to increases in oxidative stress. The aim of this pilot study was to investigate the potential for increased oxidative stress in lung cells exposed to diesel exhaust at the ALI resulting from the use of a nanoceria-based fuel additive. This study directly exposes lung cells at the ALI to exhaust generated from the combustion of diesel with and without the addition of a nanoceria-based fuel additive. Envirox was used as it is a commercial additive based on nanoceria used in Europe, particularly the United Kingdom in bus fleets [11,282]. Two exposure systems with different flow patterns, perpendicular flow and parallel flow, were used to expose the cells and were studied using dosimetry methods. Cellular responses of oxidative stress and cytotoxicity were measured post exposure.

4.2 Methods

Engine-based experiments were performed at the Centre for Research and Technology Hellas-Thessaloniki (CERTH) Chemical Energy and Processes Institute's Aerosol and Particle Technology Lab.

4.2.1 Cell Models

The cells used in the exposures were the A549 adenocarcinomic alveolar epithelial cell line [223] and the BEAS-2B normal bronchial line. The A549 alveolar epithelial cell line was chosen as it is widely used and represents cells at the air-blood barrier [18,37,39,59,91,93,103,114,132,285,287]. The BEAS-2B bronchial epithelial cell line has been widely used in suspension exposures to ceria [295–297,301,314]. Cells were cultured in Dulbecco's Modified Eagle Medium (DMEM, Gibco), with 10% fetal bovine serum (FBS, Life Technologies) and 1% penicillin-streptomycin (Life Technologies), then seeded at a density of 35,000 cells/well (A549) onto a 24 well cell culture insert (Corning or BD Falcon, 6.5 mm diameter, PET track-etched, 0.4 µm pore size) for ALI exposures. After 7 days of incubation with media exchange every two days, the apical media was removed and the cells left to equilibrate at the ALI for 48 hours prior to exposure. Following this method, it has been shown that A549 cells will grow into a tight monolayer and secrete a thin surfactant layer on the apical side of cells, mimicking conditions found *in vivo* [224].

For suspension exposures, the cells are seeded in a black 96 well plate with clear bottom with 500,000 cells per plate at 5,000 cells per well. Rows B-G are filled with 200 µL of cell suspension in columns 3-6 and 8-10. Columns 2, 7, and 11, and the perimeter are filled with 200 µL of PBS and the plate is placed on a paper towel that has been dampened with deionized (DI) water under sterile flow for 15 minutes. Once cells are confluent, usually after 24 hours, the cells were dosed with the appropriate particles in suspension and endpoints observed.

4.2.2 Model Particles

The particles used for laboratory validation of the PIVEC system were the Standard Reference Material (SRM) 2975 (NIST) and a 10 nm primary particle size ceria powder (U.S. Research Nanomaterials Inc.).

The SRM 2975 is a homogenized mixture of particles generated from a diesel-powered forklift. Characterized by NIST, the mixture includes polycyclic aromatic hydrocarbons (PAHs) and nitro-PAHs that are adsorbed during the collection process (SRM 2975, 2013). The homogeneous mixture is designed to have a diameter of 1.62 ± 0.01 μm, measured using a Microtrac particle analyzer, and a BET surface area 0.538 ± 0.006 m^2/cm^3. Size characterization was performed using TEM (Zeiss Libra 120) and DLS (Malvern Zetasizer Nano ZS).

The ceria particles were chosen to mimic the common nanoceria fuel additive Envirox [315]. Characterization of size was performed using TEM and DLS. Further characterization to determine the crystalline structure was performed using x-ray diffraction (XRD, PANalytical MPD X-ray diffractometer).

4.2.3 Model Particle Exposure

Particles used in exposures were SRM 2975, ceria, or a combination of SRM 2975 and ceria. SRM 2975 and ceria suspensions were prepared at concentrations of 100 µg/mL in solutions of 5% dimethylsulfoxide (DMSO) and Hank's Buffered Salt Solution (HBSS). The solutions were then sonicated at room temperature for 15 minutes to decrease aggregation and generate a suspension. Creating a combination of SRM 2975 and ceria, the individual suspensions are generated and then 2 µg of ceria are added for every 100 µg of DEP. The combined suspension was then sonicated to mix and suspend the particles. Cells were exposed in suspension to concentrations of 1, 10, 25, 50, or 100 µg particles/mL, Figure 25.

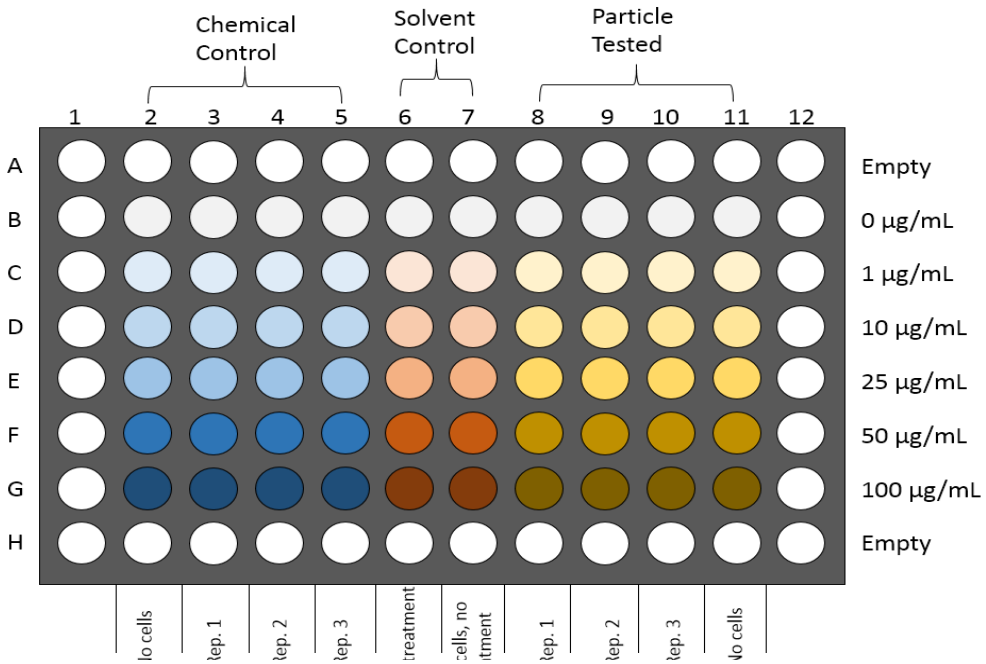

Figure 24. Design of 96 well plate experiment for suspension exposures.

Dosing the cells follows a serial dilution pattern with repetition of a positive control in columns 2-5 and particle repetition in columns 8-11. The positive control depends on the assay, whereas there is one particle added per plate. In row G, the particle concentration should be 100

µg/mL, diluted in an appropriate medium for the assay. Following Table 11, add the appropriate amount of media, positive control, and particle dilution into a round bottom 96 well plate. Once mixed, remove the supernatant from wells B2-G11 in the cell plate and add 100 µL from the dosing plate to the cell plate from low to high concentration. Return to incubator before post-exposure analysis.

Table 11. Dilution pattern for suspension exposures within a 96 well plate.

Row #	Dilute Media Columns 2-5 (µL)	Positive Control Columns 2-5 (µL)	Dilute Media Columns 8-11 (µL)	NP Dilutions Columns 8-11 (µL)
B	250	0	250	0
C	125	125 of row D	225	25 of row D
D	125	125 of row E	150	100 of row E
E	125	125 of row F	125	125 of row F
F	125	125 of row G	125	125 of row G
G	0	250	0	250

The ALI exposure system uses a nebulizer, dispersion chamber, and vacuum pump. A 3-jet BGI nebulizer produces droplets using compressed breathing air at 20 PSI which generates a flow rate of 6 LPM. Post nebulization, the aerosol flows into a 12 L dispersion chamber where it is contained by a valve and warmed to 37 ± 1°C. After a given nebulization time the nebulizer is turned off, the valve is opened, and the vacuum pump is started at 2 LPM. This begins the exposure time for the cells within the PIVEC system [316]. Two HEPA filters are used in the system, one to protect the dispersion chamber from outside air and another to protect the vacuum pump from particles.

4.2.4 Systems for Exhaust Exposure

Cells were exposed in two ALI exposure systems, the PIVEC[316] and the Multiculture cell Exposure Chamber (MEC), designed by Papaioannou and Konstandopoulos [317] and evaluated by Asimakopoulou et al. [84,147]. In the MEC, aerosol enters the device parallel to the cell surface,

allowing the aerosol to deposit through sedimentation, diffusion, and Brownian motion. The PIVEC operates with a perpendicular flow pattern where the aerosol is directed at the surface of the cells, with particles depositing by impaction in addition to sedimentation, diffusion, and Brownian motion. The MEC has been designed to have a uniform flow profile throughout the entire system such that each insert receives the same dosage [84,147,317]. The PIVEC was designed for portability and includes one insert which has been demonstrated to result in reproducible deposition across devices [316].

4.2.5 Engine Set-Up and Exposure

Diesel exhaust was generated using a partly loaded, single cylinder, four-stroke, air cooled, direct inject diesel power generator (5kW; by Hatz Diesel, Model 1B30) fueled with commercial low-sulfur diesel (LSD, Diesel Ekonomy by EKO), with 6 ppm sulfur content. The nanoceria fuel additive used was Envirox DPF Assist (Energenics, UK), added at 1 mL additive/L fuel, the "corrective" and highest dosage amount as suggested by the manufacturer. The exhaust entered a dilution tunnel heated to 150 °C to avoid condensation of exhaust volatile species. Gas levels and composition, including CO_2, CO, NO, NO_x, NO_2, and total hydrocarbon (THC), were monitored in the undiluted exhaust by an Fourier-Transform Infrared Spectroscopy (FTIR) analyzer (Gasmet^{TM}, Model CR2000), while CO_2 concentration of the diluted exhaust was simultaneously monitored by an IR gas sensor (Edinburgh Instruments, Model Gascard NG) in order to determine the 40-90 fold dilution ratio (after subtracting the background 500 ppm CO_2 content of dilution air). Particle total number concentration was of 1.5×10^6 pt/cm^3 as measured by a scanning mobility particle sizer (SMPS, TSI Inc., Model 3936L22). The exhaust then entered the exposure systems held in a conditioning chamber, heated to 37 °C, and naturally humidified. A process flow diagram of the set-up is found in Figure 26.

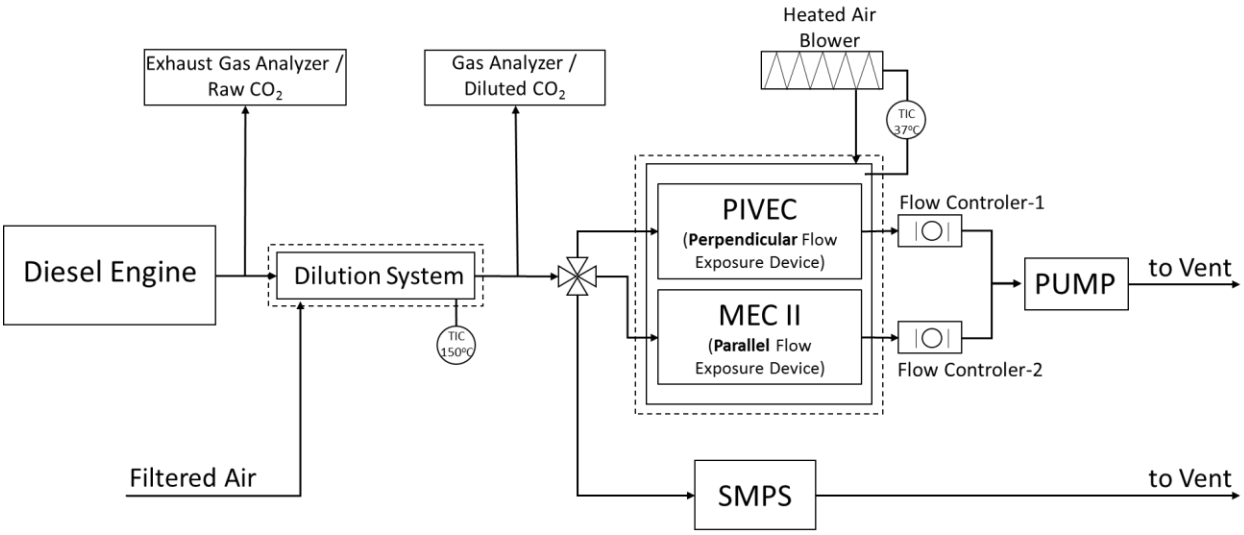

Figure 25. Schematic of experimental process. All exhaust streams are vented to the outside.

A flow rate of 2 LPM was maintained through each exposure system using rotameters, set prior to the start of exposure. A549 cells grown at the ALI were loaded into the PIVEC and MEC 60 minutes before exposure. The duration of exhaust exposure was 1 hour and the experiment was repeated three times for each fuel mixture.

Particle sizes were characterized using TEM (JEOL JEM 2010). The dose in the MEC was determined using a QCM mass sensor (OpenQCM 10MHz). Finally, the concentration of ceria in the Envirox was measured by inductively coupled plasma - optical emission spectrometer (ICP-OES) (Perkin Elmer, Model Optima 4300 DV). Gravimetric analysis of total particulate matter was determined using 37 mm diameter glass fiber filters (SKC Inc., 1 μm pore diameter). The filters were stored in an environmental chamber and weighed three times prior to exposure. Filters were then placed in 37 mm filter cassettes and exposed to diesel exhaust for a total of three hours. Residual water that was adsorbed during exposure was then removed through return to the environmental chamber for 24 hours post exposure. Collected mass was compared to the mass of particulate matter deposited within bare cell culture inserts.

4.2.6 Oxidative Stress

The oxidative stress was measured using the DCFH-DA assay [227]. This assay measures the intracellular generation of ROS, focusing on hydrogen peroxide, H_2O_2, as it is the most stable ROS, via a cell permeable dye that fluoresces after being cleaved and oxidized. To minimize oxidative stresses in the baseline exposure due to dye addition, the dye solution was added to the basolateral side of the cell culture insert. The fluorescence intensity was then measured prior to exposure and 2 hours post exposure.

Briefly, the cells were preloaded with indicator dye by incubating the cells with a diluted solution of 10 µM DCFH-DA in HBSS for 1 hour after being rinsed with PBS to remove adhered serum and phenol red from media that could interfere with the measurements. Initial fluorescence was measured and the cells were exposed to diesel exhaust for 1 hour. Cells were kept under normal culture conditions for two hours post exposure and the fluorescence was measured again. The fluorescence measurements were taken at excitation/emission wavelengths of 485/530 nm, respectively, in a BioTek Cytation 3 plate reader (model particle system) or a Perkin-Elmer Victor3 plate reader (engine exhaust). Results are reported as the increase in fluorescence from the baseline measurement.

4.2.7 Cellular Toxicity

Cytotoxicity was measured through the metabolic conversion of 3-(4,5-dimethylthiazol-2-yl)-2,5-diphenyltetrazolium bromide (MTT) or 3-(4,5-dimethylthiazol-2-yl)-5-(3-carboxymethoxyphenyl)-2-(4-sulfophenyl)-2H-tetrazolium (MTS) in living cells [318] and the leakage of LDH from damaged cell membranes [319]. For the MTT assay, mitochondria in living cells convert the tetrazolium salt into a purple, insoluble formazan product that can be

solubilized with dimethyl sulfoxide (DMSO) and measured with absorbance. Briefly, cytotoxicity is determined 24 hours post exposure through the addition of 200 µL media and 50 µL of a 5 mg/mL MTT solution then incubation at 37 °C for four hours to generate the formazan product. Following, 200 µL of DMSO and 25 µL of a glycine buffer were added to stabilize the suspension and the absorbance was measured at 562 nm using a plate reader (ELX-800, BioTek Instruments, Inc.). Results are reported as a cell viability by calculating the ratio of sample absorbance to the absorbance of the untreated cells.

The MTS assay is based on the same principles as the MTT, although is simplified in number of steps. The MTS assay reagent (Cell Titer 96 AQueous One Solution Cell Proliferation Assay, Promega) is diluted with complete media and 120 µL is added to cells without supernatant. The plate is wrapped in foil and incubated for 1 hour before being placed in the plate reader where it is shaken for 10 seconds and the absorbance is measured and read at 490 nm.

As LDH is stored within cells, leakage is generally considered proportional to membrane damage. The LDH reagent (CytoTox-ONE Homogeneous Membrane Integrity Assay, Promega) is prepared by following the manufacturer protocol. Twenty-four hours post exposure 50 µL aliquots of supernatant or basolateral media are transferred to a white 96 well plate. After the aliquots equilibrate to room temperature, 50 µL of LDH reagent is added to each well and allowed to react for 10 minutes before adding 25 µL of stop solution. The fluorescence is measured at excitation/emission wavelengths of 560/590 nm, respectively. Results are reported as LDH activity with respect to the unexposed cells.

4.2.8 Statistics

Experiments were repeated at minimum of three times. Single factor ANOVA was performed to determine statistical differences between the data sets. Where appropriate, student t-tests were performed to determine statistically significant data points. Data is reported as the mean ± standard deviation. The value of significance was held at 0.05 unless otherwise noted.

4.3 Results

4.3.1 Particle Characterization

The model particles were characterized for size to determine primary particle size and hydrodynamic size, Figure 27. The primary particle size measured via TEM of the SRM 2975 model particle was 31.0 ± 16.8 nm, smaller than many aerosolized exhaust particles. This is possible due to the homogenization process that the SRM 2975 particles undergo prior to consumer purchase. The DLS measured a hydrodynamic diameter of over 3 microns and a high polydispersity index (PI) of 0.7. Similarly, for the ceria particles, the TEM primary particle size was 10.8 ± 4.1 nm while the hydrodynamic particle size was near 3 microns with a high PI of 0.4. The large PI indicates a wide spread of particle sizes measured, which is verified through the DLS charts, and visually confirmed due to difficulty dispersing the two particles within the solutions. This difficulty in dispersal could also lead to the increased PI as over the measurement duration, the particles can agglomerate and settle, leading to increased particle size and the increased PI.

The ceria particles were measured by XRD to confirm crystallinity, which plays a role in the oxidation state and therefore the potential use as a fuel additive. The XRD measurement confirmed cerium (IV) oxide which can be used for the reduction-oxidation reaction between cerium III/IV.

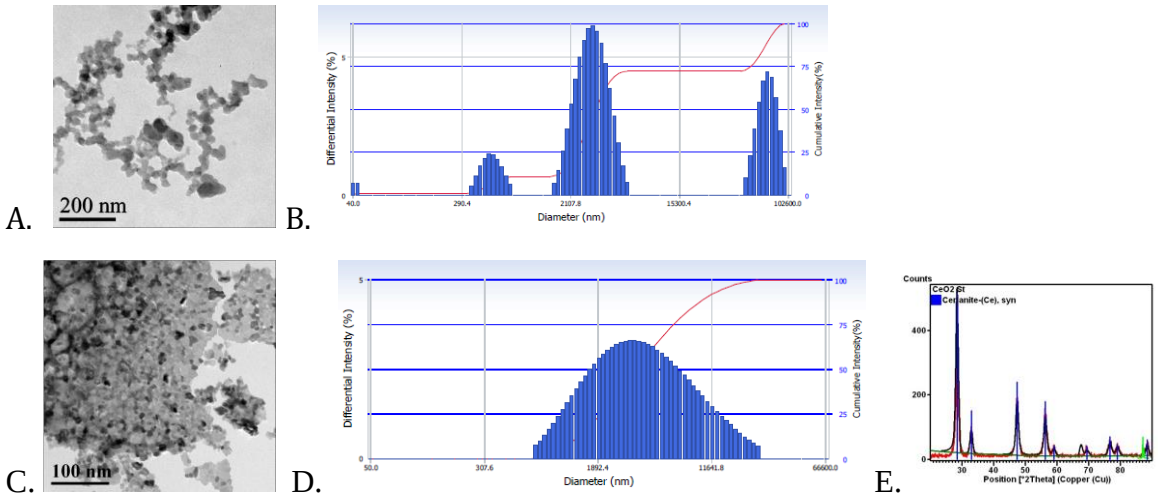

Figure 26. Characterization of model nanoparticles. A. TEM micrograph of SRM 2975. B. DLS plot of SRM 2975 in HBSS with 0.5% DMSO. C. TEM micrograph of ceria particles. D. DLS plot of ceria particles in HBSS with 0.5% DMSO. E. XRD of ceria particles.

4.3.2 Cellular Exposure to Model Particles

Intracellular oxidative stress was measured for suspension exposures of model particles using the DCFH-DA assay, Figure 28a. The diesel exhaust model particles generate oxidative stress within both cell lines at an administered dose of 25 µg/mL and above. When exposed to ceria particles alone, statistically significant levels of oxidative stress increases were observed at concentrations above 25 µg/mL. The amount of fluorescence increase was not as drastic for ceria exposure compared to SRM 2975 exposure, with the average fluorescence values for ceria exposures below the 1 µg/mL SRM 2975 fluorescence measurement. A co-exposure of SRM

2975 and ceria generated statistically significant increases in oxidative stress similar to an additive response of the two particles.

Cytotoxicity was measured using two assays, the LDH assay, Figure 28b, and the MTS assay. No significant cytotoxicity was observed from exposure to SRM 2975 at administered doses of 100 µg/mL and below for as measured by the LDH assay for either the A549 or the BEAS-2B cell lines. Similarly, no cytotoxicity was observed for ceria exposure within the A549 cells. The highest exposure concentration of 100 µg/mL of ceria increased LDH activity in BEAS-2B cells. Although slight increases in LDH activity was measured from a co-exposure to A549 cells, no measurements were statistically significant at a level of 0.05. The MTS assay was not well suited to determine cytotoxicity with SRM 2975 at concentrations above 10 µg/mL. Measurement interference from the particle was observed at the higher concentrations. There was no significant cytotoxicity measured using the MTS assay from exposure to ceria particles within A549 cell line, however the BEAS-2B cell line observed a significant decrease in viability.

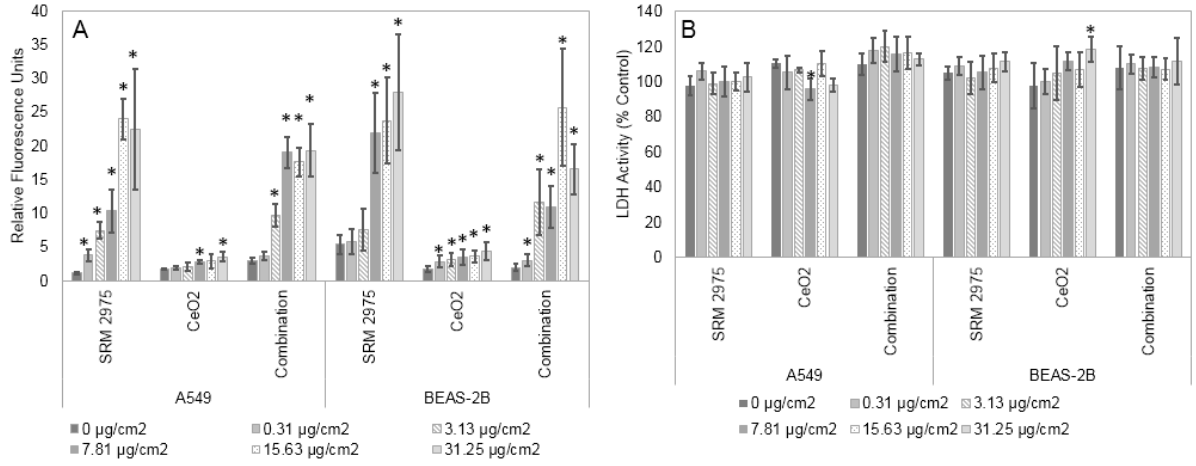

Figure 27. Suspension exposure toxicological results. A. Oxidative stress measured through the DCFH-DA assay. B. Cytotoxicity measured through the LDH assay. Runs performed with 3 experimental replicates.

The oxidative stress generated by radical oxygen species was measured in ALI exposures using the DCFH-DA assay, observed in Figure 29a. A slight increase of 20% from initial measurements was observed after exposure to SRM 2975 at the ALI. Cytotoxicity was measured via the LDH assay, Figure 29b, and MTS assay, Figure 29c. Exposure to 0.79 µg/cm^2 of SRM 2975 led to a 334% LDH activity and 0.70 µg/cm^2 ceria led to 233% LDH activity, whereas the co-exposure of the two particles did not increase LDH activity significantly from the incubator

control. When measured using the MTS assay, there was a significant decrease in cell viability to 29.4% after exposure to SRM 2975 at the ALI.

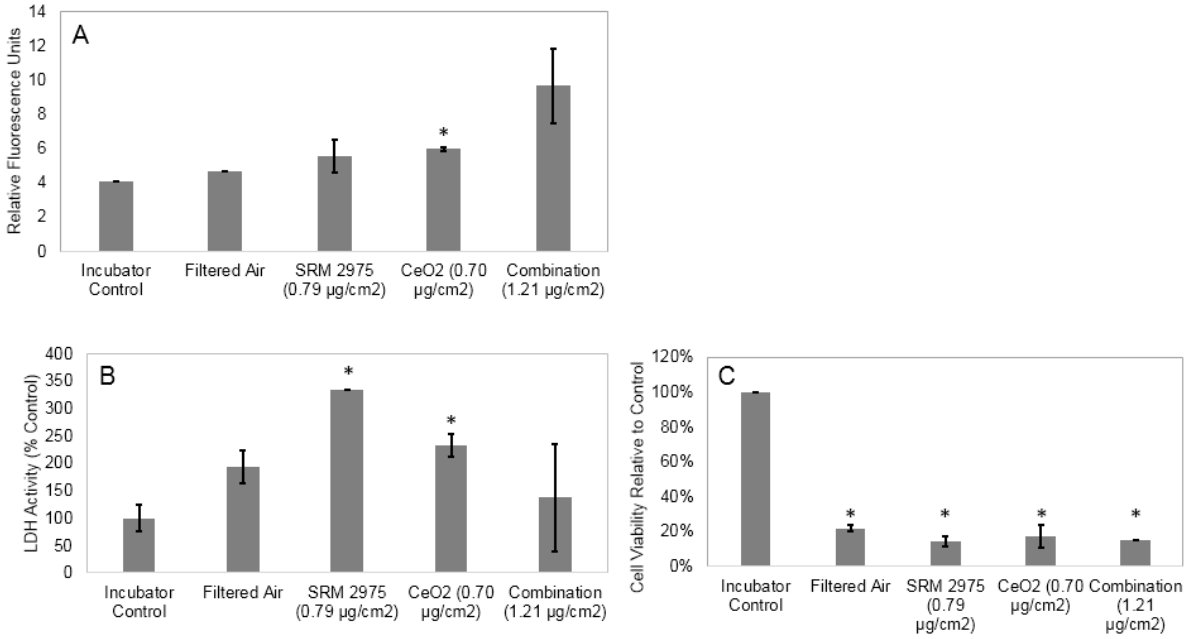

Figure 28. ALI exposure toxicological results. A. Oxidative stress measured through the DCFH-DA assay. B. Cytotoxicity measured through the LDH assay. C. Cytotoxicity measured through the MTS assay. Runs performed with 3 experimental replicates.

4.3.3 Engine Exhaust Characterization

Particles for exposure were characterized for size and shape using TEM and for metal concentration using ICP-OES. Soot particles were observed as 80 nm aggregates of roughly spherical particles of 20 nm primary particle diameter, as seen in Figure 30a. When Envirox is added at 1 mL additive/L fuel, smaller particles of 5 nm diameter are observed and believed to be free ceria, Figure 30b. The presence of free ceria was confirmed at higher doses of Envirox that were out of the scope of this study (data not shown) using TEM. Envirox was characterized as received with ICP-OES to determine the initial concentration of ceria within the additive, which was found to be 18,000 ± 500 ppm, assuming that all Ce measured appears as ceria. The 1 mL/L "corrective" dosage was determined to have 17 ± 0.8 ppm of ceria.

A. 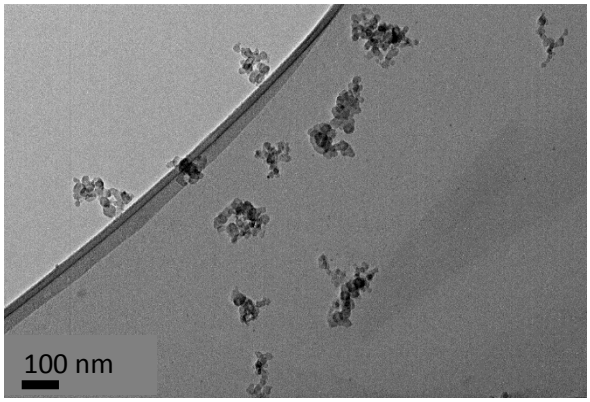

B. 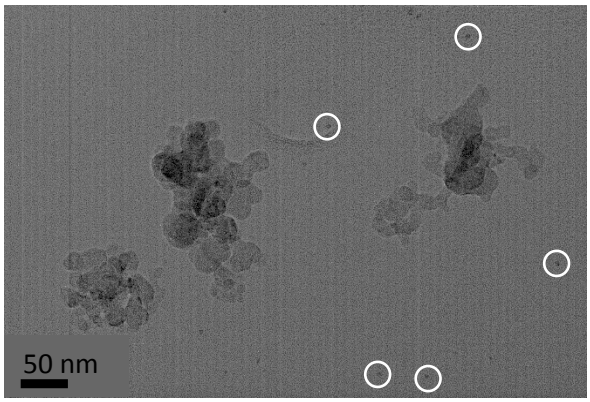

Figure 29. TEM micrographs of diesel exhaust. A. Low-sulfur diesel exposure. B. Exposure with nanoceria additized low-sulfur diesel.

Two conditions were investigated: (1) Low-Sulfur Diesel (LSD) and (2) LSD with 1 mL Envirox additive/L fuel, the manufacturer recommended "corrective" condition. Particle concentration of the diluted exhaust was held at 1.5 x 10^6 particles/cm^3 as measured via SMPS. The particle mean diameter as measured by SMPS did not change significantly with the addition of Envirox, from 80 ± 5 nm to 82 ± 3 nm, respectively, as the number concentrations were held constant, 1.5 x 10^6 pt/cm^3 without additive and 1.54 x 10^6 pt/cm^3 with Envirox, Table 12. There is a typical particle size distribution with or without use of the additive, Figure 31. Due to the deviation of gases measured throughout the experimental procedure, only a statistically significant decrease in CO (-24.91%) is observed with the addition of Envirox. This data is summarized in Table 12. The dose determined by QCM was measured within the MEC system, Figure 32. For the LSD fuel case, the dose was 0.104 µg/cm^2/h; whereas the dose increased to 0.126 µg/cm^2/h with the addition of the Envirox at 1 mL/L. This leads to an increased deposition over the same time period when Envirox is added to the fuel. Based on the deposition efficiency provided by Secondo et al.[316] for the PIVEC and density of exhaust particles[320], the dose was approximately 5.15 µg/cm^2/h for both fuel cases.

Table 12. Comparison of exhaust characteristics based on fuel type.

	Case I: Low-sulfur Diesel	**Case II: Low-sulfur Diesel with Envirox**	**% Difference**
Particle Size Distribution			
Mean Diameter (nm)	80 ± 5	82 ± 3	2 ± 6
Geom. Mean Diameter (nm)	71 ± 5	72 ± 4	1 ± 6
Standard Deviation, σ_g	1.8	1.8	-
Particle Concentration			
Number Concentration ($\#/cm^3$)	1.50E+06	1.54E+06	2.60
Coefficient Variation (%)	4.4	3.5	-
Diluted Gas Composition			
CO_2 (%)	4.82	5.26	8.37
CO (ppm)	262	210	-24.91
NO (ppm)	247	239	-3.32
NO_x (ppm)	290	300	3.13
THC (ppm)	37	40	8.60

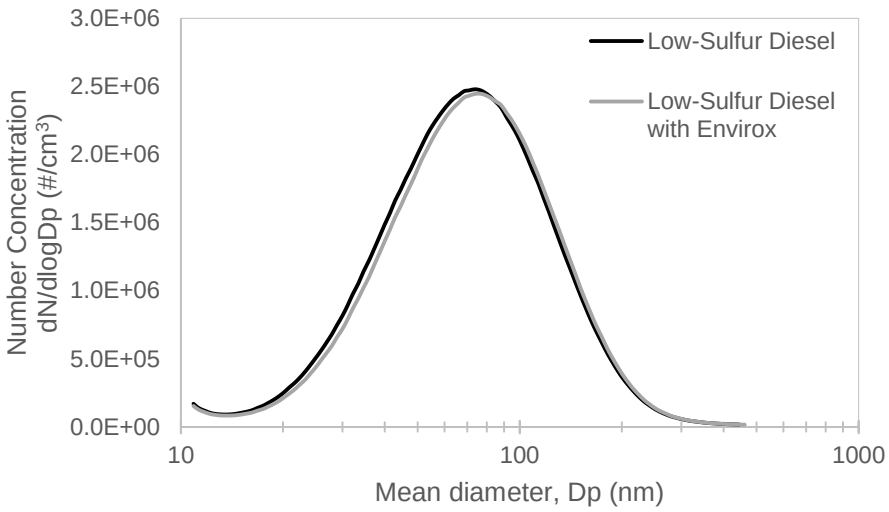

Figure 30. Particle size distribution as measured by SMPS comparing the two fuel cases.

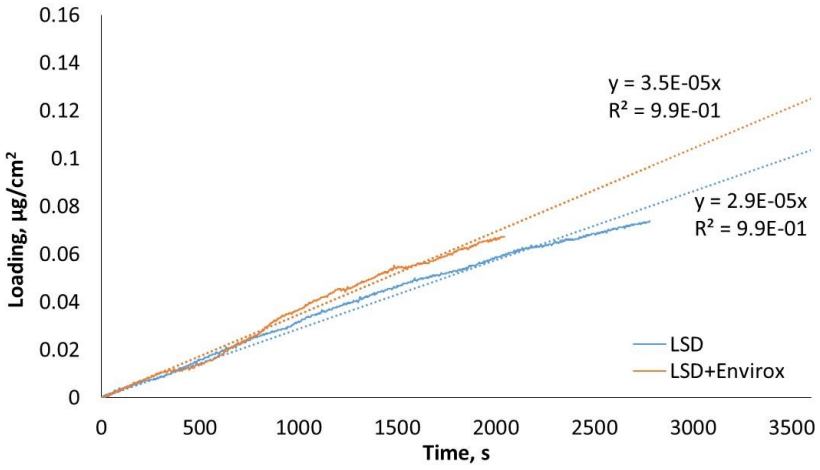

Figure 31. Loading of soot particles within MEC exposure system of each fuel case, based on QCM measurements.

Within the PIVEC, the deposition within the system was compared to the filter-based deposition and the variability between multiple PIVECs during a simultaneous exposure was investigated. There was a strong correlation between the mass collected on the filter and that within the insert, Figure 33a. On average, the mass collected within the 24 well cell culture insert

was approximately half of that collected by the 37 mm filter. There was a less than 0.07 mg difference between the maximum and minimum collected amounts of three simultaneously exposed PIVEC systems, Figure 33b. The deposition was increased during diesel exhaust exposure compared to the use of the additive. Visually, there was a significant deposition of

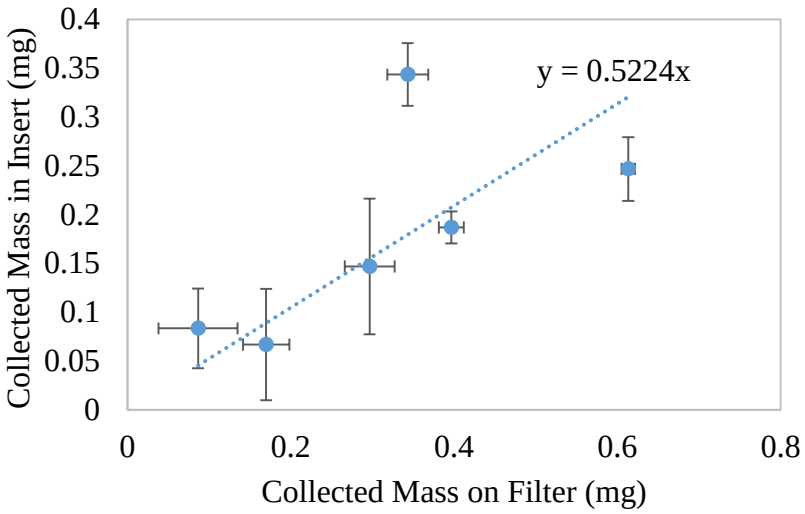

A.

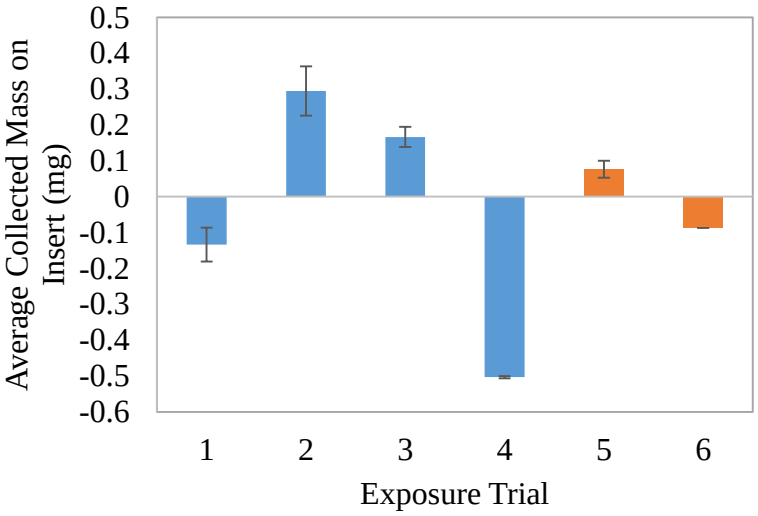

B.

Figure 32. PIVEC Collected Mass Comparison. A. Comparison of 37 mm filter and cell culture insert exposed to diesel exhaust. B. Average collected mass within insert. Blue bars relate to diesel exhaust exposure. Orange bars represent exposure to Envirox.

diesel exhaust on the 37 mm filter; whereas the deposition within the cellular inserts included a small number of larger aggregate particles, Figure 34.

A. 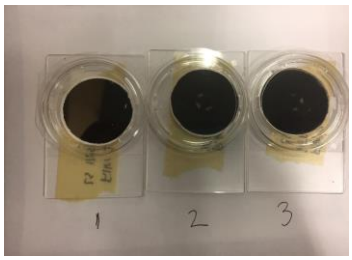

B. 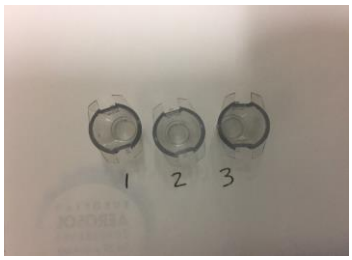

Figure 33. Visual inspection of collected mass during diesel exhaust exposure on January 25, 2017. All six samples were collected simultaneously at 2 LPM. A. 37 mm filters. B. 24 well cell culture inserts.

4.3.3 Cellular Exposures to Engine Exhaust

Oxidative stress was measured with the DCFH-DA assay 2 hours post-exposure. In the cells exposed using the PIVEC system, there was a significant increase in ROS generation after exposure to exhaust containing the additive, Figure 35a. In cells exposed using the MEC, a significant increase in ROS generation was also observed after the exposure to exhaust containing Envirox; however, there was no statistical difference between the intracellular ROS generation measured when comparing the two fuel types. Cytotoxicity was measured 24 hours post-exposure via the MTT assay. The cells exposed using the PIVEC system had a significant decrease in cell viability and without a difference between fuel types, Figure 35b. In cells exposed using the MEC system, differences in the fuel type is observed with an additional decrease in viability from Envirox exposure. Cells exposed to the LSD showed statistical differences in cellular viability between the two exposure systems with a higher viability from the MEC than the PIVEC. Significant increases in oxidative stress generally correlate to a

decrease in cellular viability, thus exposure with the Envirox led to both an increased oxidative stress and decreased viability in both exposure systems.

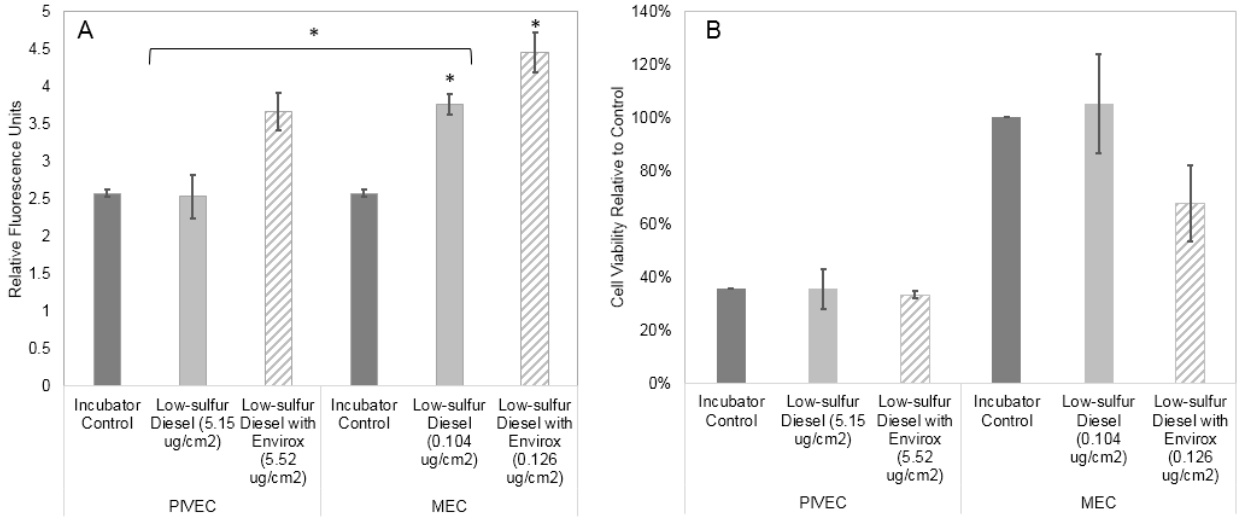

*Figure 34. Cellular responses to diesel exhaust. A. Oxidative stress response two hours post-exposure compared to initial measurements at time zero for varying fuel types and exposure systems. Low-sulfur diesel n=4, Low-sulfur diesel with Envirox n=3. B. Cellular viability response 24 hours post-exposure compared to incubator control for varying fuel types and exposure systems. n=3, *p<0.05*

4.4 Discussion

This pilot study investigates the influence of ceria particles on the response of diesel exhaust *in vitro*. Initial exploration was performed using model diesel and ceria particles with suspension and ALI exposure techniques. Model particles allow for the study of single compound interactions and control over material ratios within the system. In addition, this study compares the cellular response to exhaust emitted by diesel engine operated with commercial low sulfur fuel with and without a nanoceria based additive. By exposing cells to diluted exhaust, the response observed can be attributed to not only particulate matter but also VOCs and gases.

Complex aerosols can be investigated from either a top-down or a bottom-up approach, depending on if experiments are started with the full aerosol or an important compound within the aerosol. By identifying specific compounds of interest within the aerosol, the complexity can be reduced, allowing specific interactions between particles and cells to be investigated. These interactions can be investigated by altering the administration of the aerosol, for example in this study the ceria particles can be administered alone, prior to the diesel, or after the diesel, which may change the cellular response. This variability, however, may not fully replicate the exact ratios of the aerosol and does not account for any changes to the particles during combustion. The model particles used are pristine and do not go through the same processes the complex aerosol does, therefore there will be differences in the cellular response.

The model particles were chosen based on relation to literature on diesel exhaust particles and the nanoceria based diesel fuel additive, Envirox. It is known that diesel exhaust contains carbon, sulfur and oil materials, PAHs, and nitro-PAHs as particles [321] which are represented in SRM 2975. In addition, the influence of particles alone is determined through the use of diesel exhaust particles (DEP) instead of diesel exhaust, as the exhaust is a complex aerosol which contains many gases that can also influence cytotoxicity and oxidative stress. The ceria was chosen based on the primary particle size, near 9 nm in diameter, reported for the fuel additive Envirox [282]. Although it is possible, likely even, that the nanoceria in fuel additives has undergone some physical or chemical change such as agglomeration, oxidation, or sintering, the ceria model has not undergone these changes. These differences may affect the cells' biological endpoints which can be determined through on-engine testing.

At the concentrations investigated in suspension, there was an increase in oxidative stress that led to no significant change in cellular viability. Reactive oxygen species generation

increases have been observed from the use of SRM 2975 and spin trapping compounds [291,322]. The increased ROS generation leads to the elevated oxidative stress observed in this study and by Jantzen et al. [323]. The oxidative stress generated by exposure to ceria particles was similar to previous studies of A549 [304,305] and BEAS-2B cells [295,297]. The cytotoxicity responses are congruent with *in vitro* literature for DEP [39,285,286] and for ceria [295–297,324,325]. Cells exposed in suspension to SRM 2975 have generally not observed increases in extracellular LDH [288,326,327], likely due to the removed gases that are no longer present from the exhaust. The combination of DEP and ceria was determined using reported data from Gantt et al.[328]. Near road ambient particles generated from buses using diesel with the Envirox additive, were collected and the composition determined, observing that non-crustal ceria is approximately 10,000 times less than the amount of carbon black released [328]. Co-exposures of diesel and ceria in suspension have been performed by collecting the exhaust from diesel fuel spiked with 100 ppm ceria onto filters and reconstituting into media [312]. Zhang and Balasubramanian[11] observed increases in cell death with no change in response to ROS from the cells exposed. This is contradictory to this study's results, however, as discussed previously, differences could be due to the model particles used or due to changes that occurred during capture of the aerosol from the engine compared to the standardized SRM 2975.

Cells grown at the ALI are generally considered to be more sensitive to exposure than cells in suspension [41–43,132], inducing similar responses at lower deposited doses. This is supported by the LDH activity promoted by the model particle in this study, as increases in LDH are observed at three times less the minimum administered dose in suspension. Similar increases in cell death observed from the exposure of diesel exhaust have been reported [39,285]. Oxidative stress has been generated at the ALI marked by measurements of DCFH-DA and the heme

oxygease-1 (HO-1) protein [39,285]. As discussed previously, combined, *in vitro* responses are often difficult to determine. Steiner et al. (2012) use staggered dosing to attempt to understand the different effects of the particles by first dosing with DEP and then ceria. There were small increases in toxicity and oxidative stress, however the inflammatory markers did not provide a clear response before and post ceria addition [311]. The use of the model particles allow for easy investigation with varying concentration and determining appropriate assays. The model particles do not, however, allow for the full complexity of the aerosol to be studied, suggesting the need for direct exposure to diesel engine exhaust.

The diesel engine produced diesel exhaust with a composition that is consistent with literature [321]. With the addition of 1 mL Envirox/L fuel, 5 nm particles were observed, which is consistent with free nanoceria reported in literature [284,315,329]. Ceria allows for the oxidation of soot and gases via the movement of electrons throughout the metal-oxide lattice structure [330–332]. It is known that engine age and differences in load can lead to differences in exhaust characteristics [321] and the diesel engine used in this exposure scenario does not produce a high concentration of small particles, under 20 nm under typical operating conditions, as observed via SMPS and TEM. This supports the higher dosage observed via QCM with the addition of Envirox as the density of ceria is over three times greater than that of soot. At this concentration of Envirox, 17 ppm, we observed a typical particle size distribution. Throughout literature, ceria-based additive concentrations over 25 ppm are necessary to produce a bimodal distribution [11,281,333].

Cellular response is heavily influenced by exposure controls and dosage. As particles enter the body through inhalation, the temperature increases and the air gains moisture after entering the nose before continuing to the lower airways [146]; mimicking these *in vivo* conditions

is critical for *in vitro* ALI exposures. Zavala et al. [334] performed a study on the influence of temperature and humidity on the cytotoxicity of lung cells exposed by perpendicular flow and observed a significant decrease in cell viability after one hour of exposure when the temperature of the exposure stream was at room temperature and below 70% relative humidity [228]. Cellular exposure systems that pre-condition the exposure aerosol typically do not observe large differences between incubator controls and aerosol vehicle controls [33,35,137,228]. The effect of pre-conditioning of the aerosol is believed to be observed via the cytotoxicity as the aerosol stream was not adjusted for relative humidity which could dry out the cells. The filtered air stream was not heated prior to introduction to the cellular exposure chamber introducing a rise in cell death. Any variation in the deposition due to these parameters would lead to changes in the response. Additionally, the response could be affected by the number of cells in the cell culture insert or the treatment of the cells post exposure.

Variability between PIVEC systems during a simultaneous exposure was investigated as part of this study. Each PIVEC was labeled to ensure the same set-up from exposure to exposure. There was no significant difference in the collected mass within the three exposed cell culture inserts. The deposition within these inserts was able to be confirmed visually, therefore negative mass differences were determined non-physical and likely due to improper drying of the insert during the procedure. Variability is expected within the current PIVEC due to using 3D printing as the prototyping method as well as differences in materials. Two of the PIVEC systems were printed in Thessaloniki using ABS and one system was printed at VCU using ABSPlus. This supports the use of the PIVEC to investigate spatial differences and the ability to expose multiple systems at once.

Each dose observed, measured via TEM, filter, or QCM, is consistent with a human inhalation worst case scenario [56,140]. Assuming that in a 24 well insert the typical cell population at 80% confluency is 3 x 10^5 cells/cm^2 [335], the observed deposition of soot particles is 3,000 pt/cell/h. According to Paur et al. [56], a worst-case inhalation scenario example is 6,700 pt/cell/day. Paur et al. [56] also refer to the worst-case inhalation scenario as 0.12 µg/cm^2/day. At the lowest dose, the PIVEC gravimetric measurements corresponded to 91 µg/cm^2/h using LSD; therefore, is significantly higher than the worst-case scenario. In terms of MEC and according to the QCM based measurements, dose during typical 1 hour exposure corresponds to the accumulated daily dose of human inhalation worst case scenario.

Often exposure systems are defined by the deposition efficiency, a ratio of the deposited dose, that adsorbs to or internalizes within a cell, to the administered dose, the amount which is added to the system throughout the exposure duration. Deposition efficiency, calculated using a particle number concentration basis for the MEC and PIVEC, was approximately 35% for the MEC and 4.2% for the PIVEC.

Based on literature review, each system can act as a model for the flow pattern, as most parallel flow systems have a deposition efficiency near 35% and perpendicular flow systems are often between 1 and 10% efficient [31].

Oxidative stress is considered to be a pathway involved with the onset of respiratory diseases linked with air pollution [290]. The interaction of diesel exhaust with cells appears to induce ROS generation. The amount and significance is dependent on the system used. Cells exposed in both systems, the PIVEC at perpendicular flow and the MEC at parallel flow, reported increased oxidative stress at a significance of $p<0.1$ and $p<0.05$ respectively, when comparing the incubator to the Envirox additive case. However, using a parallel flow system,

there is no longer the oxidative stress difference between the LSD and Envirox cases. As the increase in oxidative stress due to the addition of Envirox is consistent regardless of flow profile, it is likely that this rise is due to the ceria in the exhaust.

Cell death was measured through the mitochondrial activity 24 hours post exposure using the MTT assay. Unlike the oxidative stress, cytotoxic differences were mostly observed in the MEC system. The MEC showed differences between the filtered air control and Envirox case and the two fuel cases. The deposition of fuel with Envirox additive was higher than diesel fuel alone, decreasing cell viability. In addition, the PIVEC and MEC had significant difference between the LSD exposures, suggesting an influence from the flow choice. The deposition was approximately the same for each fuel scenario within the PIVEC, which could attribute to the lack of difference in cell viability. The perpendicular aerosol flow into the cells produces more force onto the cells than a parallel aerosol flow which can produce more stress and in turn more cell death. This is supported by the lower cell viability from the PIVEC exposure system rather than the MEC system.

As observed within the PIVEC system, there was significant cytotoxicity from filtered air alone. This is due to the use of the non-optimized, original PIVEC design during exposure. This design did not sufficiently maintain the relative humidity at an increased level to sustain cell viability. Prior to the final design, the relative humidity was maintained by an excess of liquid within the well, increasing the natural humidity to over 50% at 37 °C. In addition, the use of a 2 LPM flow rate induces a high amount of stress onto the cells when used in the perpendicular flow profile. This flow rate was chosen to match previously used flow rates within the MEC system[84,147]. Using the same flow rate, the same administered dose was used and the differences between the systems were probed. These differences included stresses upon the cells exposed

due to the variances in deposition forces as parallel flow has negligible inertial impaction unlike perpendicular flow. These changes in deposition forces also led to varying deposition amounts and efficiencies of the system. Due to the strong influence of the vehicle control within the PIVEC, the influence of particles from exposure is difficult to determine. The MEC system exposures, however, support the hypothesis that the use of the nanoceria fuel additive induces additional biological responses measured by oxidative stress and cytotoxicity.

This study allowed for insight into the design and use of the PIVEC. The influence of the vehicle control led to the investigation of the relative humidity within the PIVEC, discussed in Chapter 2, leading to the final design of the system. Using multiple PIVEC systems at once afforded the examination of the reproducibility of the system and repeatability of exposure between systems. Two of the PIVEC systems used were 3D printed in Thessaloniki and the third was brought from the Lewinski Lab in Richmond, Virginia. There was, at maximum, a 0.07 mg difference between PIVEC exposed simultaneously. This suggests strong reproducibility of the PIVEC system when 3D printed by different systems. Finally, the flow rate used was elevated from many perpendicular flow systems observed in Table 3. By reducing the flow rate in future exposures, the influence of the vehicle can be reduced so that the biological response due to the particle can be well observed.

4.5 Conclusion

The determination of compounds of interest can be difficult with complex aerosols as cellular response can be influenced by the particle and gases. By using model particle systems of SRM 2975, ceria nanoparticles, and the combination of particles, the influence of particles alone and the material was investigated *in vitro*. In suspension, the combined exposure of SRM 2975 and ceria generated amounts of oxidative stress that were similar to an additive model of the two

particles individually. When the MTS assay was used in suspension, there was interference from the SRM 2975 particles due to the deposition on the cells which were measured along with the formazan crystals in solution, whereas for ALI exposure, only the formazan solution was measured, mitigating the potential for interference from diesel particles. This study supports the statement that cells grown at the ALI are more sensitive than cells in suspension.

Between the suspension and ALI exposures of model particles, the ALI exposures are much more sensitive than suspension for similar deposition values. The lower deposition amounts achieved from direct aerosol exposure leads to an increased cytotoxicity as cells are often more sensitive at the ALI and undergo additional stresses that are not felt in suspension. The A549 cell line is often less sensitive than the BEAS-2B cell line. Similar responses are observed for the model particles and engine exhaust scenarios for exposures within the PIVEC. This work is novel by exposing lung cells directly to diluted engine exhaust including a nanoceria based fuel additive at the ALI using exposure systems utilizing two methods of flow patterns. The volumetric flow rate was kept constant between the two flow systems, however the cellular assays showed that there can be significant influence from the flow pattern. As the perpendicular flow increased the stress on the cells, the effects were observed in the cytotoxic response compared to the parallel flow. The influence of the exposure scenario and exposure system can lead to significant differences in the cellular responses and should be considered in the design of experiment.

As this was a pilot study, the parameters were limited and improvements can be made. The aerosol flow profile should be matched in both the ALI and the exhaust exposures, including implementing a parallel flow device for the investigation of the model particles. Ensuring there is no significant effect from filtered air during experimental set-up will aid in determining the

effects from aerosols and particles rather than the vehicle itself. By matching these experimental parameters, including deposited dose, for the model system and exhaust exposures conclusions relating to the exposure technique, dose, and system can be reached. The cellular responses investigated were limited to cytotoxicity and oxidative stress; however, future studies should also consider inflammatory cytokines and antioxidant properties as ceria particles have been shown to reduce inflammation and stress effects *in vivo*. Although combined model particle systems may be unable to capture the full complexity of diesel exhaust, utilizing a bottom-up approach allows for investigation of specific interactions and remains important for risk assessment.

CHAPTER 5: AN ENZYMATIC BIOSENSOR FOR REAL-TIME MONITORING WITHIN THE PIVEC[3]

5.1 Introduction

Real-time monitoring allows for rapid determination of the biological influence of particles on the lungs. Typically, the concentration of particles is measured through particle number or mass but the biological influence is not measured until a significant time post-exposure. Handheld particle counters can be used to observe the particle concentrations[336,337], however these systems do not include exposure to cell cultures. In addition, handheld VOC monitors are available to monitor potentially dangerous gaseous compounds[338,339]. By integrating real-time monitoring of biological endpoints with cellular exposure, information relating to the particle-cell interactions can be gained.

Biological endpoints that are often measured include oxidative stress, cytotoxicity, and inflammation. Oxidative stress can be generated by an increase in ROS species generation, a decrease in antioxidative capacity, or a combination of these processes. ROS species include the highly reactive oxygen based radicals such as superoxide ($O_2^{\cdot -}$), the hydroxyl radical ($OH^{\cdot}$), and the more stable hydrogen peroxide (H_2O_2)[340]. As the balance between the generation of ROS species and the antioxidative capacity changes, the cell cycle is interrupted, and the cell may become damaged. Cytotoxicity can be triggered when particles interact with the cells, either

[3] This chapter is adapted from Secondo and Lewinski. Journal of Occupational and Environmental Hygiene. In Prep.

remaining on the outer membrane or being taken up by the cell. Methods of cell death include apoptosis, a programmed cell response, necrosis, an induced death generated by the cellular environment, and autophagy[56,151,341]. Inflammation is generated by the release of protective cells and marked by the excretion of cell-derived mediators including IL-8[342–345]. This chemokine is often derived from macrophages and epithelial cells and is known to stimulate the migration of granulocytes to the site of infection[346–348].

Oxidative stress and inflammation are closely linked endpoints within the biological response. There is often a cyclic relationship between increased oxidative stress and increased inflammation which has been implicated in adverse outcome pathways[349–352] leading to cancer, fibrosis, or pulmonary disorders. Once a tissue has been injured or is diseased, the activity of varying oxidases within the cells, including xanthine oxidase (XOD) and nicotinamide adenine dinucleotide phosphate (NADPH)[353–355]. Increasing oxidase activity generates more ROS and have been observed to significantly increase leading to additional damages[353]. The focus of this work will be on oxidative stress as it is intrinsically linked with both inflammation and cytotoxicity.

Reactive oxygen species are utilized within a cell for signaling purposes[352,356]; however, ROS can be generated in multiple ways inside or out of the cell. Mitochondria contain superoxide dismutase (SOD) and cytochrome c (cyt c) enzymes that interact with oxygen to produce superoxide and other ROS[356]. As these products permeate outside of the mitochondrial wall, signals to the cytosol, nucleus, and secondary redox signals occur, reflecting the state of the mitochondria. Alternatively, oxidative stress can be generated by the Fenton reaction, by which a transition metal reacts with hydrogen peroxide form a hydroxyl radical[352,357–360], equation 29.

$$M^n + H_2O_2 \rightarrow M^{n+1} + OH^- + OH^{\cdot} \quad (29)$$

The Haber-Weiss reaction also generates hydroxyl radicals[341,352,357,361–363], equation 30, and is catalyzed

$$O_2^{\cdot-} + H_2O_2 \rightarrow O_2 + OH^{\cdot} + OH^- \quad (30)$$

by transition metals that are present in biological systems at low levels. Outside of cells, radicals can also be generated via photocatalysis when ultraviolet light is absorbed resulting in the transition of an electron from the valance band to the conduction band, equation 31. This continues as water or hydroxide ions are trapped by the resulting holes and additional radicals are produced, equations 32-35. The production of ROS external to cells leads to considerations toward the particle-cell interactions based on compounds within the aerosol and the use of probes that may decrease activity or measure other radicals that are not related to exposure.

$$TiO_2 + h\nu \rightarrow h_{VB}^+ + e_{CB}^- \quad (31)$$

$$h_{VB}^+ + H_2O_{ads} \rightarrow OH^{\cdot} + H^+ \quad (32)$$

$$h_{VB}^+ + 2OH_{ads}^- \rightarrow OH^- + OH^{\cdot} \quad (33)$$

$$e_{CB}^- + O_2 \rightarrow O_2^{\cdot-} \quad (34)$$

$$O_2^{\cdot-} + 2H_2O \rightarrow 2OH^{\cdot} + 2OH^- + O_2 \quad (35)$$

Oxidative stress can be measured in a variety of ways including the use of fluorescent probes, electron spin resonance (ESR), and biosensors. Fluorescent probes, such as DCFH-DA, are often photosensitive in nature. There are multiple reviews within literature discussing advantages and disadvantages to the use of these probes[340,364,365]. The most popular fluorescent probe, DCFH-DA, is able to enter the cells where it accumulates to interact with reactive species. There are, however, contradictory conclusions on the ability for DCFH-DA to be oxidized by

hydrogen peroxide and other ROS species.[364,365] ESR detects the presence of unpaired electrons, however the ability to measure highly reactive radicals is quite low due to difficulties in maintaining these species for the duration of measurement. Many spin trapping compounds have unknown toxicity levels, limiting the *in vivo* applicability[340,366,367]. Biosensors for oxidative stress measurement can be focused toward the detection of specific ROS, with current systems designed to monitor hydrogen peroxide and superoxide[360,368]. Three main types of sensors have been developed for oxidative measurements using SOD, cyt c, and horseradish peroxidase (HRP). SOD is more specific and sensitive to superoxide radicals as SOD converts superoxide to oxygen and hydrogen peroxide cyclically[369,370]. However, SOD based sensors require operation at a high potential in order to oxidize hydrogen peroxide, however at these potentials, biologically available electroactive species are also oxidized causing interference[369,371]. HRP operates at a lower potential, decreasing the number of biological interferences[372–374]. HRP has the ability to reduce H_2O_2, thus limiting the application for specificity to superoxide radicals[360]. Cyt c is known to measure both H_2O_2 and superoxide radicals[375], following equations 36-38. Cyt c based sensors have been used *in vitro* and have been shown to have relatively fast electron shuttling, increasing the response time[368,376–379].

$$cyt\ c - Fe(III) + e^- \leftrightarrow cyt\ c - Fe(II) \tag{36}$$

$$2\ cyt\ c - Fe(II) + 2H^+ + H_2O_2 \rightarrow 2\ cyt\ c - Fe(III) + 2H_2O \tag{37}$$

$$cyt\ c - Fe(III) + O_2^{\cdot -} \rightarrow cyt\ c - Fe(II) + O_2 \tag{38}$$

Throughout literature, many biosensors have been produced with cyt c. Common methods for applying the enzyme to the working electrode include drop casting[353,375,377,379–381] and covalent bonding through immersion in a cyt c solution[376,382–388]. Cyt c has been shown to

have high selectivity against many biologically active compounds including dopamine, ascorbic acid, uric acid, oxygen, and reactive nitrate species[385,389]. In addition, cyt c based sensors have been used *in vitro* for the measurements of ROS in milk and mouthwash[377], bacterial cultures [378], and cancerous cell cultures[382,385,389], and *ex vivo* mouse brain slices[353]. Eguilaz et al.[377] made a biosensor by depositing a MWCNT-cyt c solution on a glassy carbon electrode and characterized the sensor in PBS up to 300 µM H_2O_2. The co-deposition of MWCNT and enzyme provided a highly reproducible and reusable electrode. The sensor was then used to determine the hydrogen peroxide content in mouthwash and spiked low-fat milk samples with a less than 2% deviation from standard values. Liu et al.[378] monitored the oxidative stress induced by antibiotics in a bacterial culture using a cytochrome c sensor. The sensor was designed on a gold wire working electrode, decorated with gold nanoparticles to which thiols were immobilized to enhance the covalent bonding of the enzyme. Using amperometry, the sensor was characterized in cell culture media at a theoretical concentration up to 1 µM superoxide generated by XOD. The oxidative stress generated by antibiotic interaction with the bacteria was not great enough to be the sole contribution to bacterial death. The hydrogen peroxide release of Hep G2 cells, a human hepatocellular carcinoma cell line, was measured by Rui et al.[389], Luo et al.[385], and Zhou et al.[382]. Sensors were fabricated through the covalent bonding of cyt c onto ZnO nanosheets[389] or TiO_2 nanoparticles[385] or the cross-linking of the enzyme within an hydrogel matrix[382]. Characterization was performed in PBS solutions with up to 1 mM of H_2O_2. Similar results were observed between each experimental set up, reducing current with the addition of phobol 12-myristate 13-acetate (PMA) and increasing with the addition of catalase to the cells[382,385,389]. Ganesana et al.[353] monitored the real-time release of superoxide in CD-1 mouse brain slices during normal physiological conditions, ischemia, and exposure to ceria nanoparticles. High

temporal resolution, sensitivity, and selectivity were observed in the normal conditions. Superoxide levels quickly increased during ischemia which were then reduced over 8% through the addition of ceria nanoparticles[353]. These studies provide a good basis for the design and testing of a cyt c based sensor.

There are no current ALI exposure systems that utilize real-time measurements. By adding a biosensor to the PIVEC, users of the PIVEC become more cognizant of their surroundings and the effects on their body. Focusing on oxidative stress allows insight toward the potential development of cancer, fibrosis, or pulmonary dysfunction, therefore a cyt c functionalized biosensor was incorporated to determine the concentration of ROS. The sensor was calibrated with hydrogen peroxide, tested in buffers for linearity of response, and compared to the traditional DCFH-DA assay post-exposure to 40 nm copper nanoparticles.

5.2 Methods and Materials

The design of an enzymatic biosensor is focused on the functionalized working electrode and the ability to transfer ions from the reaction substrate to the electrode for measurement. Nanostructures provide additional surface area for enzyme deposition and provide an opportunity for electron shuttling from the enzyme to the electrode[390]. After functionalization, the electrochemical response is measured and may vary with electrolyte composition, pH, and temperature[388,391–393].

5.2.1 Sensor Fabrication and Functionalization

The working electrode was grown on a patterned gold electrode on sapphire. Aqueous zinc nitrate hydrate, $Zn(NO_3)_2 \cdot 6H_2O$, was used to grow ZnO nanorods via electrodeposition at 90 °C.

Electrodeposition was performed using square pulses, 0.25 Hz frequency, 50% duty circle with varying peak currents. Moreover, ZnO can easily be produced in the form of various nanostructures (e.g. nanowires, nanobelts, nanotubes) with high surface-to-volume ratio that substantially enhance sensor sensitivity. The nanorods grown in this method were observed using SEM (Hitachi SU-7).

A coplanar, tri-electrode sensor is produced using three thin film metals, gold, platinum, and silver, on a sapphire wafer. Prior to functionalization, 32 gauge wire pieces are prepared and soldered to each electrode using indium. The solder is covered using a medical grade silicone (Silastic MDX 4-4210, Dow Corning), cured at 60 °C for 2 hours then room temperature for 8 hours, to provide a biocompatible barrier and enhance mechanical stability of the electrical connection. To functionalize the working electrode for H_2O_2 detection, 20 µL of a 0.67 mM (8 mg/1 mL) solution in 0.01 M PBS (pH 7.4) of cyt c (from equine heart, Sigma Aldrich) was drop cast onto the ZnO nanowires and allowed to dry. Unbound and loosely-adsorbed cyt c was then removed by rinsing the functionalized electrode with approximately 1 mL of 0.01 M PBS. Once dried, 20 µL of a 5 wt% Nafion solution (Sigma Aldrich) was spin coated to form a 40 nm thick membrane. The platinum and silver thin films were grown by electrodeposition to be used for counter and reference electrodes, respectively, using commercially available solutions (Pt: EPi 50/50 Ready to Plate, Ag: Technic Elevate). Anodization of the silver thin film occurred in a solution of 0.01 M PBS at 1.5 V for 3 minutes to form a layer of silver chloride. The functionalized working electrode, platinum thin film, and anodized silver thin film are then affixed to a sapphire wafer to produce a coplanar, tri-electrode sensor, Figure 36.

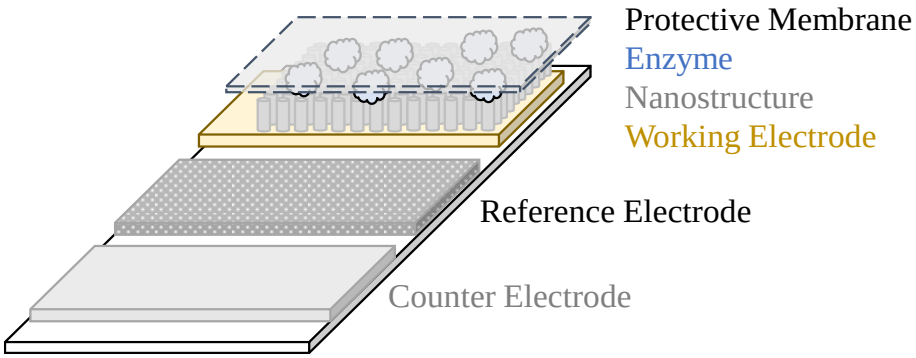

Figure 35. Design of coplanar tri-electrode sensor.

5.2.2 Electrochemical Testing of Cytochrome c Sensor

A 100 µM stock solution of H_2O_2 was used to simulate ROS increases in concentration and stimulate the electrochemical reactions observed in equations 36-38. All solutions were warmed to 37 °C prior to electrochemical testing and maintained during testing through the use of a resistive heater and direct current (DC) power supply set to 5 V providing roughly 0.55 A. The experimental set-up is presented in Figure 37. Baseline measurements were performed in 20 mL of either PBS or HBSS (Gibco) to which the stock solution of H_2O_2 is added. Cyclic voltammetry (CV) measurements were performed in buffer solution at 37 C. CV parameters were adjusted to

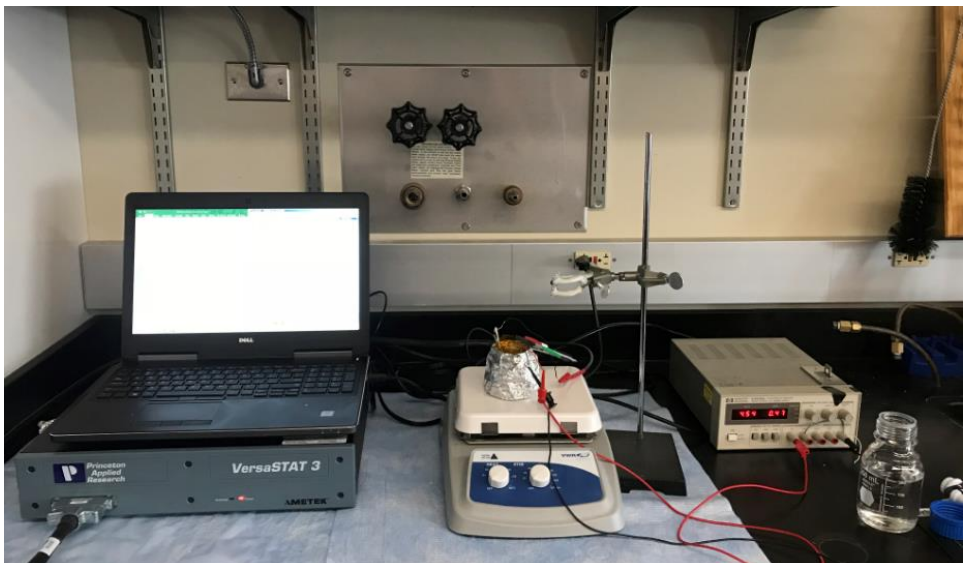

Figure 36. Bench top experimental set-up for electrochemical sensor testing.

Table 13. Experimental scheme for calibration curve using CV.

H_2O_2 Concentration (µM)	**Volume Added of H_2O_2 (mL)**	**Total Volume (mL)**
0	0.0000	20.0000
0.01	0.0020	20.0020
0.05	0.0120	20.0040
0.1	0.0300	20.0160
0.2	0.0602	20.0460
0.4	0.1208	20.1062
0.5	0.1819	20.2270
0.75	0.2547	20.4088
1	0.3608	20.6636
3	0.8521	21.0243
5	1.7705	21.8765
7.5	2.9563	23.6469
10	4.5980	26.6032

sweep from -1 V to 1.5 V versus Ag/AgCl at 50 mV/s and the concentration of H_2O_2 was altered following the test scheme found in Table 13, stirring between readings. Chronoamperometry was performed at 1 V versus Ag/AgCl and the H_2O_2 concentration adjusted following the test scheme found in Table 14 allowing 180 s between each concentration change for the reaction to occur. The solution was continuously stirred during chronoamperometric measurements. As amperometry is a reactant consuming detection method, the volumes necessary to produce the same concentrations is different than in CV testing. All electrochemical measurements were performed using a VersaStat 3 potentiostat galvanostat (Princeton Applied Research) that provides an accuracy of 0.2% of the current reading.

Table 14. Experimental scheme for calibration curve using chronoamperometry.

Time (s)	H_2O_2 Concentration (µM)	Volume Added of H_2O_2 (mL)	Total Volume (mL)
0	0	0.0000	20.0000
180	0.01	0.0020	20.002
360	0.05	0.0100	20.012
540	0.1	0.0200	20.032
720	0.2	0.0401	20.072
900	0.4	0.0803	20.152
1080	0.5	0.1005	20.253
1260	0.75	0.1511	20.404
1440	1	0.2020	20.606
1620	3	0.6186	21.225
1800	5	1.0526	22.277
1980	7.5	1.6216	23.899
2160	10	2.2222	26.121

5.2.3 Incorporation of Sensor within PIVEC

In order to place the sensor within the PIVEC, access to the well must be achieved such that the connections between PIVEC pieces remain tight. Thus a new bottom piece was designed, Figure 38, allowing the sensor wires to exit a designated port from the well. The coplanar sensor was positioned on the basolateral side of the ALI cells to measure the diffused hydrogen peroxide generated by the cells.

A.  B. 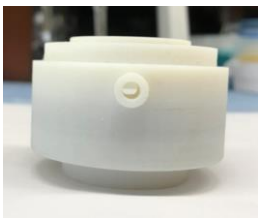 C. 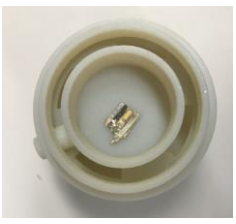 D. 

Figure 37. PIVEC designed for sensor use. A. Top view of bottom piece. B. Side view of bottom piece. C. Top view of bottom piece with sensor inside. D. Full PIVEC.

Prior to exposure, cells used for incubator control and DCFH-DA monitoring were dyed with DCFH-DA through the addition of 10 μM DCFH-DA solution on the basolateral side of the cells and incubation for 1 hour. Cells were then moved to a fresh plate of HBSS and an initial measurement of the DCFH-DA fluorescence was performed at 485/530 nm excitation/emission wavelength. The cell culture insert was loaded into the PIVEC with 2 mL of HBSS within the well with the sensor. The PIVEC set-up was completed and the resistive heater was attached and connected to the DC supply system held at 5 V to maintain temperature. After the wetted, porous tube was placed within the system, the PIVEC was connected to the dry air dispersal system and vacuum pump, Figure 39. Baseline electrochemical measurements were performed for 5 minutes prior to exposure using amperometry at 1 V versus Ag/AgCl.

Cells were exposed to 40 nm copper nanoparticles while continuing to monitor oxidative stress using the amperometric sensor. The administered dose of copper provided a deposited dose of 1.33 mg/cm^2 during the exposure of a flow rate of 0.5 LPM for 10 minutes. Post-exposure, cells exposed for DCFH-DA monitoring were returned to the well plate and fluorescence was measured every minute using a plate reader for 1 hour. For electrochemical monitoring, the cells and sensor remain inside the PIVEC post-exposure, maintained at 37 °C. The generation of ROS

was monitored through amperometric measurements every half second using the biosensor. This was continued for 1 hour post-exposure.

A.

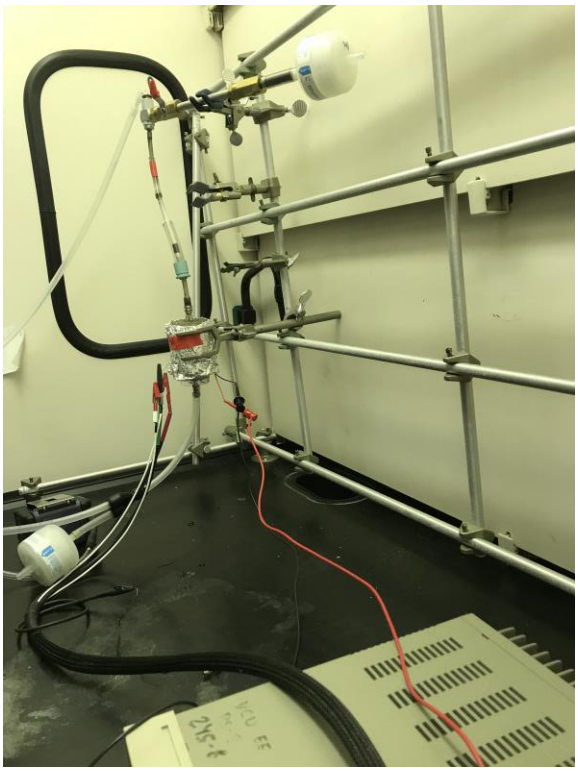

B.

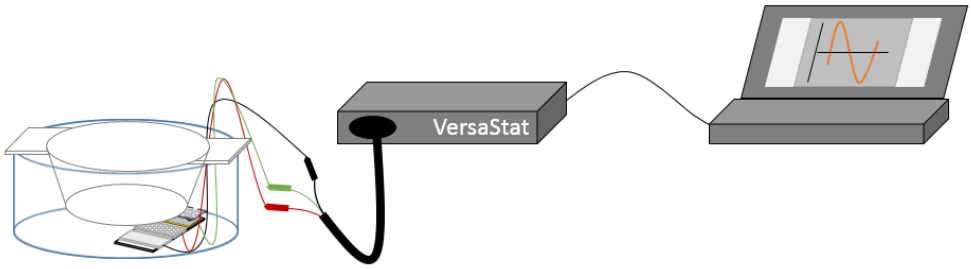

Figure 38. Experimental set-up of real-time monitoring within PIVEC. A. Bench-top set-up. B. Schematic of measurement.

5.3 Results

The sensor was functionalized with cyt c deposited on ZnO nanorods for the electrochemical detection of ROS generation. Calibration was performed with hydrogen peroxide

in multiple buffer solutions to determine the most appropriate for short term exposures. Finally, the sensor response was compared post-exposure to the traditional DCFH-DA assay.

5.3.1 Sensor Fabrication

The base working electrode was 50 nm of Au on 20 nm titanium deposited on a sapphire substrate. The nanorods grown in this method were rod-like with a hexagonal cross section, aligned perpendicularly to the substrate. The diameter was controlled through the peak current density measured with SEM, Figure 40. Nanorods used for the functionalization were grown at 0.625 mA/cm^2 to produce average diameter of approximately 100-150 nm and a length of 2 μm. The deposition of cyt c on the ZnO nanorods was determined using varying scan rates during the CV. Following an ideal Nernstian reaction under Langmuir isotherm conditions, the peak current observed is proportional to the scan rate applied using equation 39. In this equation, the number of electrons transferred, n, Faraday constant, F, and gas constant, R, are used to determine the molar concentration of enzyme, Γ. A low concentration of 5 nM/cm^2 was determined to be immobilized on the sensor.

$$i_p = \frac{n^2F^2}{4RT} A\nu\Gamma \tag{39}$$

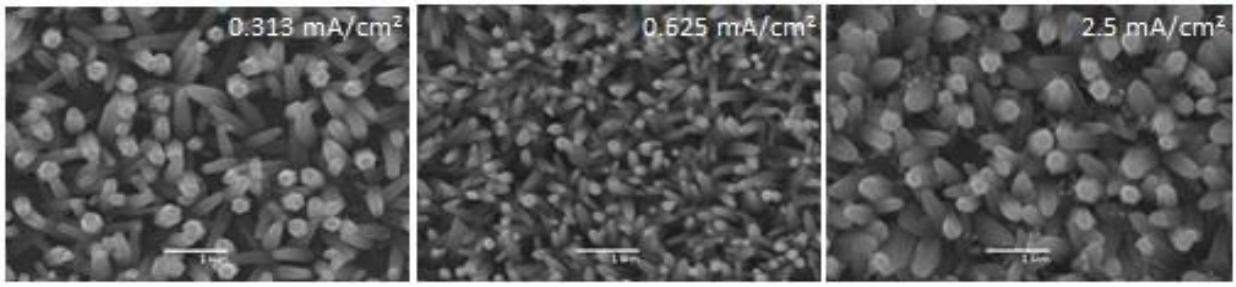

Figure 39. ZnO nanorods grown by electrochemical deposition on Au/Ti contact layers deposited on glass substrates using pulsed currents with different peak densities. A. Nanorods grown at 0.313 mA/cm^2. B. Nanorods grown at 0.625 mA/cm^2. C. Nanorods grown at 2.5 mA/cm^2.

5.3.2 Electrochemical Characterization

The sensor was tested using CV to determine the ability to measure H_2O_2 and the appropriate potential for amperometric testing. Initially, the sensor was tested in a solution of 0.1 M PBS and then in 1 M PBS. There was little sensor response in 0.01 M PBS as the measured current was less than 100 µA and no reaction peaks were observed. Increasing the ionic strength of the solution to approximately 0.151 M in 1 M PBS dramatically increased the measured current and redox peaks were observed near -0.5 V vs Ag/AgCl. When the sensor was run in HBSS the current decreased compared to the electrolyte of similar ionic strength (I_{HBSS}=0.155 M), however more defined redox peaks were observed near 1V and 0.3V. CV curves for each electrolyte are presented in Figure 41.

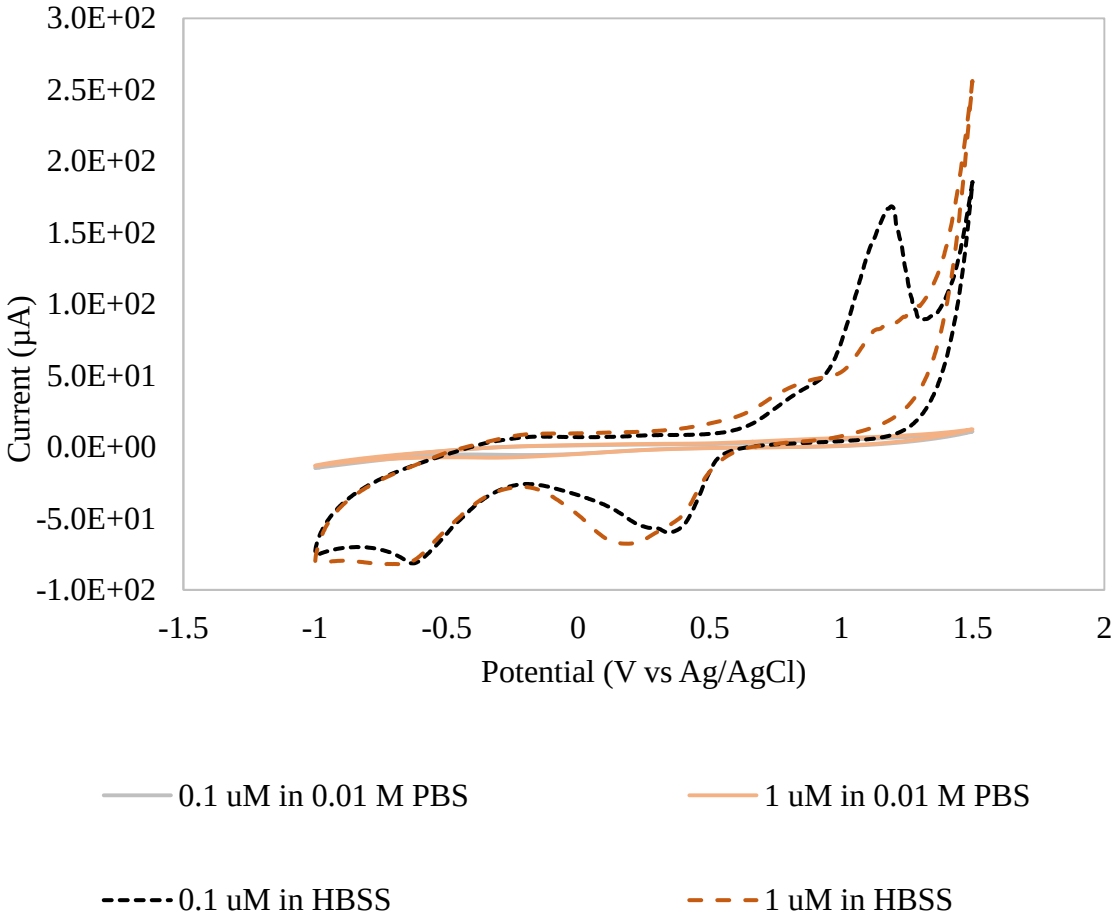

Figure 40. Comparison of CV curves at 0.1 µM and 1 µM H_2O_2 in 0.01 M PBS and HBSS.

Calibration curves were determined at 1V vs Ag/AgCl for both solvents, Figure 42. As observed, the current was increased overall within 1 M PBS, however there is little linearity over the desired concentration range. In the 0.01 M PBS, there is also little linearity observed from the response at the potential of interest. The HBSS response over the desired concentration range at the potential of interest includes a linear region from 0.01 µM to 7.5 µM. The sensor response measured from this experiment was 58.86 µA/µM/cm^2 for response in HBSS.

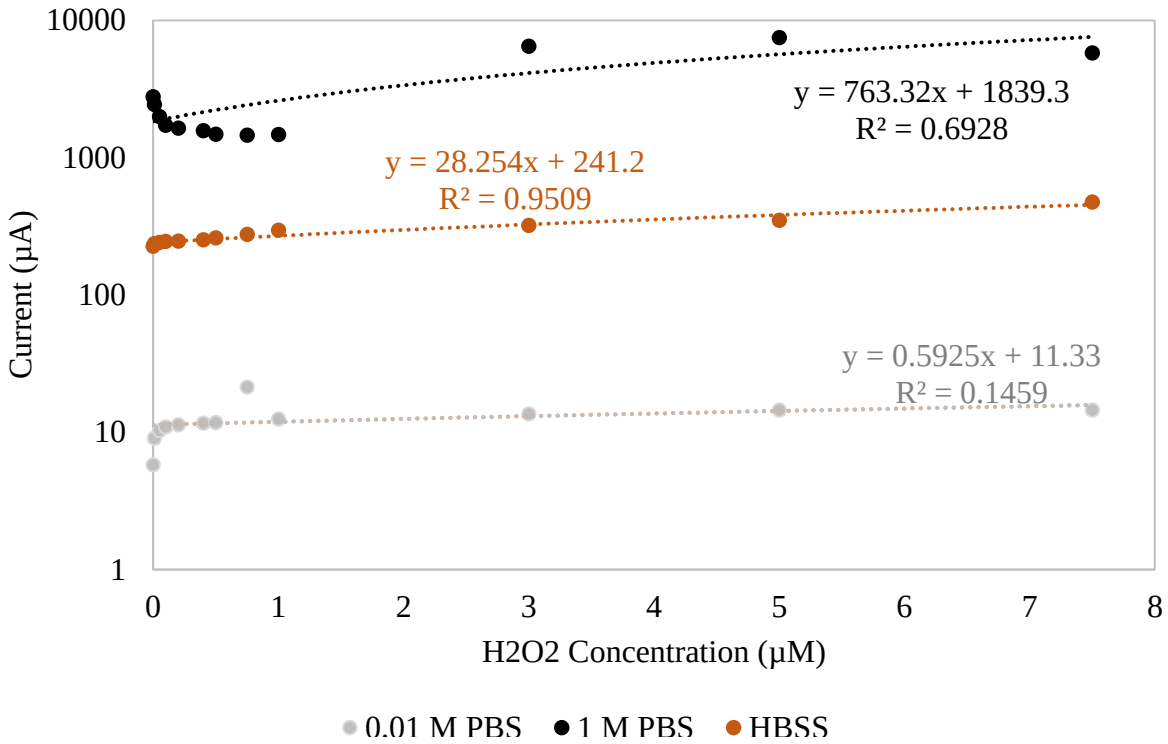

Figure 41. Comparison of sensor calibration in 0.1 µM and 1 µM H_2O_2 in 1 M PBS and HBSS.

5.3.3 Real-time monitoring within PIVEC

As the sensor was calibrated prior to exposure, observed in Figure 42, the sensor response was observed as 248.48 µA/µM/cm^2. This calibration curve was used to determine the H_2O_2 concentration during exposure. The H_2O_2 concentration was then normalized to the initial,

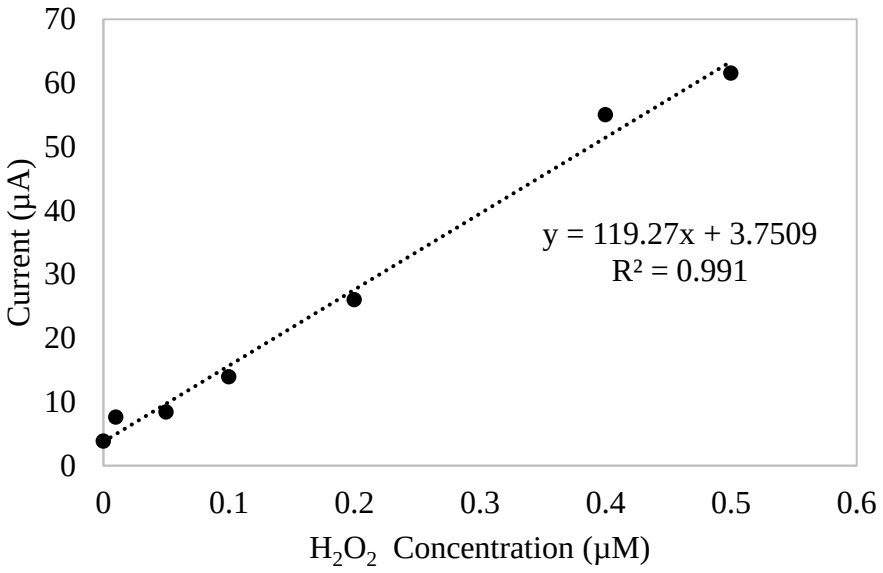

Figure 42. Calibration curve for ROS sensor prior to PIVEC exposure.

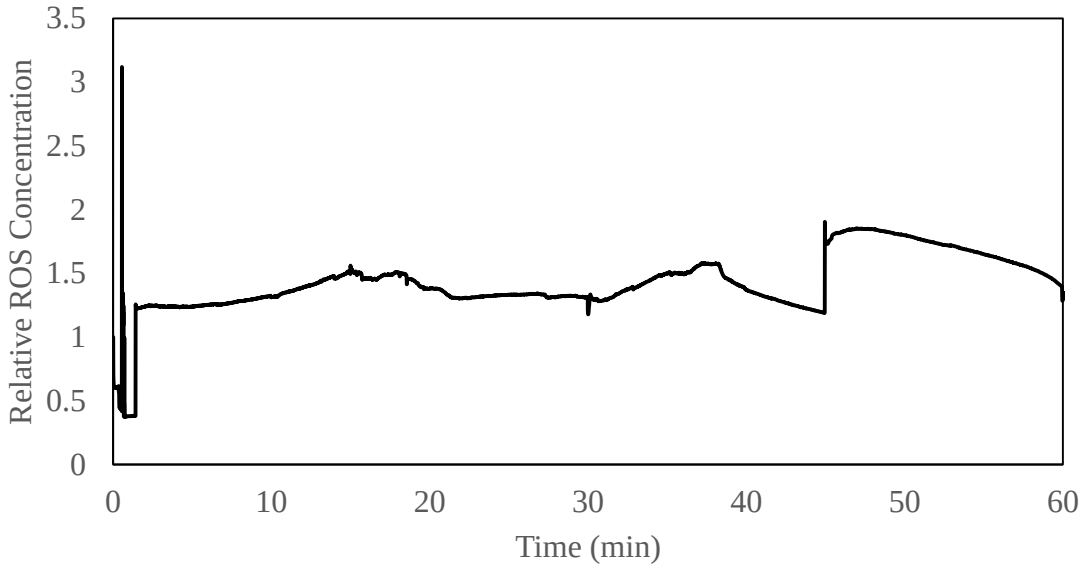

Figure 43. Real-time monitoring of H_2O_2 concentration within PIVEC using ROS sensor.

baseline concentration and reported as the relative accumulation. Exposure can be observed where the concentration spikes near 30 seconds, Figure 43. The real-time concentration of H_2O_2 was observed within two minutes of exposure.

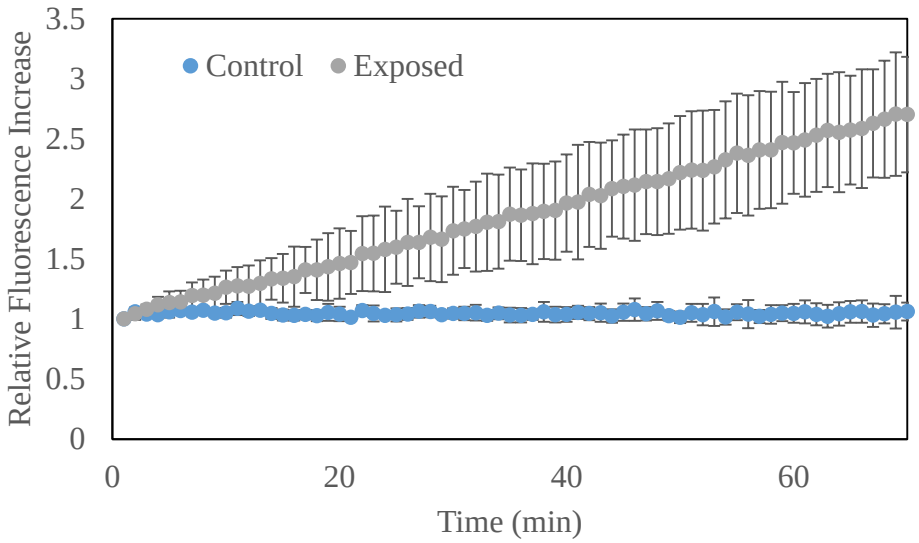

Figure 44. Intracellular ROS generation measured by the DCFH-DA assay.

Intracellular generation of ROS was measured using the DCFH-DA assay. There was a significant increase in fluorescence within 1 hour of exposure, Figure 44. The extracellular ROS generation was monitored using the cyt c sensor. Comparing these techniques, increases in ROS within and outside of the cell wall is observed after 30 minutes post-exposure. Accumulation of ROS measured using the biosensor is statistically significant compared to the intracellular ROS generation and control experiments.

5.4 Discussion

The generation of ROS can be measured through multiple methods, including the DCFH-DA assay and a cyt c functionalized biosensor. Measurements can be affected by the ionic strength of the electrolyte, observed through the response in PBS. A 100x increase in ionic strength was observed as a similarly proportional increase in current. The ionic strength of 1 M PBS and

HBSS are very similar, $I_{PBS,\ 1\ M}$ = 152 mM and I_{HBSS} = 155 mM. Additional ions within the electrolyte may affect the ability to shuttle ions as there is more affinity to the solution than at low ionic concentrations. This is consistent with the findings of Avila et al.[391]: solutions of low ionic strength provided near independence of electron transfer, whereas over 10 mM ionic strength affected the electron transfer, increasing the potential for cyt c to desorb from the electrode surface. Temperature, electrolytic compounds, and pH have also been shown to affect sensor response[388,391,393].

ROS generation was measured using two techniques. Intracellular measurement of ROS is performed through the DCFH-DA assay. The specificity of this assay is debated in literature[364,365,394]. Generation of ROS within the cell post-exposure can occur through particle or cell induced pathways. As the particle used is copper, a transition metal, the potential for the cell to utilize Fenton-like and Haber-Weiss reactions increases. Within the cell, the production of high levels of ROS have been shown to lead to cellular growth arrest at the equivalent of 120-150 μM H_2O_2, apoptosis at 0.5-1 mM H_2O_2 equivalent, or necrosis at levels 5-10 mM or higher equivalent H_2O_2[151]. Using the cyt c functionalized sensor, the generation of extracellular ROS and leakage of ROS through the cellular membrane is observed. Cyt c is non-selective toward hydrogen peroxide and superoxide ions and reflects the interaction with each species. The oxidative stress responses are similar to those presented in Chapter 3, however there is little information regarding the extracellular generation of ROS. Hydrogen peroxide can freely diffuse through the cell membrane, however superoxide must be shuttled through anion transport mechanisms[395,396]. This could account for the increase in ROS observed extracellularly.

Comparing the measurement techniques, increases in ROS are observed within the cell and in the basolateral fluid. There is approximately a 30 minute period where ROS is not observed

within the basolateral fluid. This is likely due to the time for ROS to diffuse out of the cell, across the permeable membrane, and through the basolateral fluid to the sensor. Modeling the system with Fick's second law, the time for diffusion to the sensor is approximately 5 minutes. However, once the signal begins to increase on the sensor, the rate and relative ROS accumulation is higher than that measured by DCFH-DA. It is possible that initially highly reactive radical species are observed followed by the slower decomposition of hydrogen peroxide.

5.5 Conclusions

Advantages of using real-time monitoring include the ability to observe the exposure and potential effects of the exposure process and duration on the generation of ROS. As observed in Figure 46, the exposure can be observed as a spike in current. While the vacuum pump did not induce changes in current, the air flow to aerosolize the nanopowder did. The change in current supports the increased stresses that occur from perpendicular flow. This response could be mitigated through the reduction in flow rate necessary to aerosolize the nanopowder. However, as the exposure duration lengthens, the vehicle becomes more likely to induce higher stresses on the culture. Therefore, low flow rates and characterization of the biological response to the vehicle is key.

While enzymatic biosensors are a promising method for real-time monitoring, limitations occur due to the enzyme and results can become convoluted. The enzymatic activity decreases over time due to stability, increasing the error and usefulness of the sensor. Throughout literature the stability of cyt c based sensors was measured typically at one week to one month depending on storage conditions and use[376,383]. The longest lasting sensor observed was for 180 days, however it was stored the majority of the time[381]. The use of a cytochrome c sensor allows for

monitoring multiple reactive oxygen species but does not allow for the specific determination of individual ROS.

This is one of the first studies to present a comparison of intracellular and extracellular ROS monitoring. The incorporation of a cytochrome c functionalized sensor allows for the real-time monitoring of oxidative stress generation within the PIVEC. The extracellular ROS generation observed using the biosensor was higher than the intracellular generation, likely due to the differences in transport mechanisms. By changing the enzyme immobilized on the sensor, alternative biological endpoints can be monitored during exposure. This process will allow for insight to the cellular response to particle interactions and pathways of toxicity.

CHAPTER 6: CONCLUSIONS AND FUTURE OUTLOOKS

6.1 Conclusions

The PIVEC allows for realistic exposure as a step between suspension and *in vivo* exposures. By taking the lab to the field, potential changes to the particles including size can be mitigated. Current exposure systems are large and bulky due to the additional instruments needed to maintain cell viability, making real-world exposure difficult. By miniaturizing the exposure system, the PIVEC can be worn for monitoring real-world aerosols and the effects of inhaled particles. Adding a real-time monitor allows for rapid determination of the biological response to aerosols.

6.1.1 PIVEC System

The PIVEC is a step between suspension exposures and *in vivo* exposures. This system was designed for personal sampling as the PIVEC may be worn on the body to monitor aerosols in the breathing zone. The major deposition methods within the PIVEC are sedimentation and diffusion, leading to 5-16% mass-based deposition efficiency. Compared to available systems, the PIVEC has been characterized over a variety of sizes. The deposition efficiency is similar or higher than current perpendicular flow systems. By measuring the deposition within the 37 mm filter cassette, shown to be highly correlated to the cell culture insert deposition amount, the dose within the PIVEC can be determined without the need for time and cost-intensive procedures. This can decrease the time necessary for analysis post-exposure.

The response of cells exposed within the PIVEC is similar to those exposed *in vivo* and through the traditional suspension methods for copper. Suspension methods induce high amounts of cytotoxicity, likely due to the high dissolution rates within the liquid covering the cells. Lower levels of cytotoxicity was observed *in vivo* with an increase in ROS generation and anti-oxidant depletion. As the responses to copper observed within the PIVEC were similar to *in vivo* exposures, this suggests the utility of the PIVEC to aid in bridging the gap between suspension and *in vivo* exposures.

6.1.2 Diesel Study

Model particles can be useful when evaluating a complex aerosol. The ceria system alone allows for the determination of the specific influence of the metal oxide within the diesel exhaust. Overall there was an increase in oxidative stress with the use of metal oxide nanoparticles. As the cells were exposed directly to fresh aerosol, the influence of combustion on the particles was considered including the gases in the aerosol. The aerosol was similar to real world exposures as cells were exposed directly to freshly generated diesel exhaust. Within this study, two different flow profiles were used for a comparison of the exposure systems. Parallel flow systems induce less stress on the cells and therefore higher flow rates can be used within the system. As perpendicular flow increases the stresses on the cells, the deposition efficiency is altered and lower flow rates should be used to mitigate the effects of the vehicle. The same flow rate was used in each system which provided insight to the design of the PIVEC. While exposing the cells in Greece, three systems were used at once, providing similar deposition efficiencies. Multiple systems were 3D printed for the system, including PIVECs of PLA and ABS.

6.1.3 Sensor Incorporation

The tri-electrode coplanar sensor was designed for monitoring the generation of ROS within the system post-exposure. Nanomaterials on the working electrode increase the active surface area, allowing for improved cytochrome c immobilization. Cytochrome c reacts with superoxide and hydrogen peroxide electrochemically, allowing the sensor to measure increases in these compounds extracellularly. To incorporate the sensor with the PIVEC, a new base piece was designed such that the airtight connection between pieces was not disturbed. The sensor was evaluated in buffer solutions and compared to a traditional assay method. During exposure, the oxidative stress was monitored and the exposure was observed. There was an increase over time of both intracellular and extracellular ROS. Comparison of the two measurement techniques yielded similar results with a delayed measurement from the sensor, likely due to diffusion time.

6.2 Limitations & Future Outlooks

The PIVEC system can be used for exposure of aerosols to ALI cells with the ability to monitor the production of reactive oxygen species in real-time. However, there are limitations to the current system that can continued to be improved. Refining the design and model of the PIVEC can be achieved. In addition, the sensor can be altered to monitor other endpoints which can then also be monitored *in vivo* through a side-by-side exposure using the PIVEC.

6.2.1 PIVEC Design

The major drawback of the PIVEC is the ability to only expose one sample at a time. Systems such as the NACIVT and MEC expose over 20 samples to a single aerosol, which can increase reproducibility of the biological effects as the deposition is similar for all samples. Using only one PIVEC, changes in the aerosol may occur during exposures, a concern when

using freshly generated aerosols in the lab. However, the small size of the system allows for multiple PIVECs to be used in conjunction with one another. These systems can be separated in area to determine spatial resolution of aerosol dispersal. This is particularly important for air pollution as the concentration of particles is much higher near the source of emission yet the biological response has not been investigated well using real-world concentrations. Currently there is one system available designed by splitting the exposure chamber in half, exposing cells to an aerosol on one side while maintaining a control area on the other side. The PIVEC can mimic this use through the use of two systems. Additionally, multiple exposure systems can be used for high-throughput evaluation of particles.

The design of the PIVEC produces a deposition efficiency below the target goal of 20% determined by the ICRP model. This efficiency can be increased by reducing the electrostatic deposition of particles within the PIVEC itself. The use of a conductive material will dissipate the charge build-up during exposure. Thus, options for fabrication include to print or mold a plastic with a metal or conductive filler or to make the design out of metal such as aluminum. As the connections between the PIVEC pieces will likely change with various materials, the use of o-rings is advised to maintain seal integrity. The material must be biocompatible due to contact of the PIVEC with cell culture media and the user. Appropriate, potential materials include aluminum or plexiglass which maintain the low-cost of the PIVEC. Alternatively, electric field or thermal gradients can also be implemented to enhance deposition, as observed in other systems in literature.

Another drawback of the PIVEC is the lack of specificity toward nanoparticle aerosols. The design can be refined for specific particle sizes through the incorporation of design aspects of cascade impactors or cyclone separators. Cascade impactors separate particles due to their

deposition forces with a focus on impaction as larger particles deposit on early stages and sizes decrease as the stage number increases. The incorporation of a stage within the PIVEC would increase the body length of the system while increasing the ability for smaller particles to deposit. This would come with the price of operating the system at a higher flow rate to induce the deposition which, as observed, may lead to an increase in cytotoxicity from the vehicle. Cyclone separators use high flow rates to separate particles on size. Considering these design principles, another option is lengthening the aerosol inlet to further streamline the aerosol and to maintain a higher velocity.

6.2.2 PIVEC Model

The PIVEC model is currently based on first principles and does not well capture the effect of streamlines within the system. To more appropriately represent the two-phase particle-fluid flow within the PIVEC, the use of computational tools such as COMSOL or ANSYS should be implemented. Base equations will be similar but these tools are able to incorporate Brownian motion, important for small particles. Previously, Brownian motion has been modeled using Monte-Carlo type methods. Implementation of these tools will allow insight on the design of the system.

Insight gained from expanding and refining the deposition model within the PIVEC will include size cutoffs due to design parameters. Use of a computational method will better capture the changes to fluid flow due to altered design parameters, such as the diameter of the aerosol inlet, distance between the aerosol inlet and the cells, and the interior diameter of the system. By evaluating these changes using simulation prior to fabrication, appropriate changes can be made while streamlining the design iteration process.

6.2.3 Sensor Incorporation

The cytochrome c based sensor is limited to monitoring the generation of hydrogen peroxide and superoxide species within the extracellular space and those species that migrate outside of the cell. This method does not allow for the deconvolution of the individual response from each ROS compound. An alternative to continue monitoring ROS generation and the ability to determine individual responses is the co-immobilization of SOD and HRP. These enzymes have selectivity toward individual ROS compounds and could be combined on a single sensor or two separate sensors. By initially working with a single sensor for each enzyme, the individual amounts of hydrogen peroxide or superoxide can be determined. After determining these responses, the sensors could be designed on the same platform or the enzymes could be co-immobilized on a single working electrode.

Inflammation and cytotoxicity are each important biological endpoints to be monitored after exposure to aerosols. As inflammation is marked by cytokine and chemokine excretion from cells, the real-time monitoring of these compounds can lead to information regarding inflammatory responses. An IL-8 response sensor has been designed in literature through the use of antibodies related to the cytokine. The antibody is immobilized on the working electrode and the electrochemical response of the reaction with the cytokine is determined. Cytotoxicity can be measured through the design of a sensor to monitor lactate release. Damaged cells release lactate dehydrogenase, which catalyzes the reaction from lactate to pyruvate.

6.2.4 Additional Testing

Other methods to test and validate the PIVEC would be to change the cell culture model, using a co-culture, or exposing primary cells. One change of the cell culture model is to use a

cell line with different sensitivity. A549 cells are considered to be sensitive to exposure at the ALI. In addition, the differentiation of A549 cells, a type two alveolar cell, will be different than other epithelial cell lines such as bronchial cells. The ability for the cells to develop tight junctions or secrete surfactant will influence the biological response. Using a co-culture model, multiple cell types can be studied allowing for insight to the pathway of biological response. As macrophage cells are known to interact with particles to induce inflammation, a common co-culture to investigate is a tri-culture of epithelial cells, macrophages, and dendritic cells. Use of a cell culture insert allows for investigation of the translocation of particles and therefore cells can also be seeded on each the apical and basolateral side of the membrane. Endothelial cells can be seeded on the basolateral side of the membrane for the investigation of translocation across the air-blood barrier. Primary cells cultures may include the over thirty types of cells found within the respiratory system, allowing for a more complex and physiologically relevant model.

Aerosols that the PIVEC could be used to study include mixed aerosols such as metal-oxide combusted particles, 3D printing exhaust, and electronic cigarette vapor. There is little understanding of the effects of metal-oxide fuel additives and the particle changes due to combustion. As suggested by our study, there are small metal-based particles emitted that may affect the biological response to exhaust. It is known that 3D printers emit particles during printing, with a concentration dependent on the color and type of filament used. The biological response to inhalation of these particles and their composition is unknown and requires further exploration. Finally, the exposure to electronic cigarette vapor is another area of research that includes mixed aerosols that the mechanism of cellular response is not well understood.

The PIVEC was designed for portable, personal measurements. Testing of the ability for the PIVEC to be assembled and used by an individual is an important step in the generation of

the system. The PIVEC could be worn during exposure within a laboratory setting, for example while weighing a powder, or in an occupational setting, for example during 3D printing. After approval, a human-based study could be performed that can relate the effects of aerosol exposure, deposition within the body, and the PIVEC *in vitro* study.

Finally, an important validation of the PIVEC is to perform a comparison to an *in vivo* study. To do this, the PIVEC could be placed in an inhalation chamber with the animal model and the deposition and cellular responses could be directly compared to the *in vivo* exposure. Monitoring the deposition of the 37 mm filter and the PIVEC could allow insight into the inhalable particles while helping to characterize the aerosol. Comparing the biological response *in vitro* to the response *in vivo* is a critical step in determining the toxicology of a compound. These experiments can also aid in refining the PIVEC design to help reproduce *in vivo* deposition.

6.3 Concluding Remarks

The PIVEC has been designed for the deposition of nanoparticle aerosols while mimicking *in vivo* exposure techniques. Characterized over a variety of particle sizes, the mass-based deposition efficiency is approximately 5-15%. This is, overall, an increase in deposition efficiency compared to current exposure systems. Multiple PIVECs that have been printed in different places have been shown to produce repeatable deposition. The design of the PIVEC can be further refined through the use of a CFD model and aspects of cyclone or cascade impactors. These alterations will aid in determining the differences in deposition based on particle size and design criteria. Improvement of the PIVEC can further increase deposition efficiency.

By incorporating an enzymatic biosensor, biological endpoints can be monitored during exposure. While real-time monitoring is currently set-up for ROS generation, the sensor can be

easily designed for the evaluation of inflammatory or cytotoxic responses. The sensor response is similar to a traditional assay technique, measuring similar ROS. Multi-analyte sensors will provide the opportunity to measure complex biological responses as they occur. With the small size of the PIVEC and incorporation of real-time monitoring, the PIVEC is a versatile system for aerosol exposure.

References

(1) Müller, L.; Gasser, M.; Raemy, D. O.; Herzog, F.; Brandenberger, C.; Schmid, O.; Gehr, P.; Rothen-Rutishauser, B.; Clift, M. J. D. Realistic Exposure Methods for Investigating the Interaction of Nanoparticles with the Lung at the Air-Liquid Interface In Vitro. *Insciences J.* **2011**, *1* (1), 30–64 DOI: 10.5640/insc.010130.

(2) Geiser, M.; Kreyling, W. G. Deposition and Biokinetics of Inhaled Nanoparticles. *Part. Fibre Toxicol.* **2010**, *7* (i), 2 DOI: 10.1186/1743-8977-7-2.

(3) Kuempel, E. D.; Sweeney, L. M.; Morris, J. B.; Jarabek, A. M. Advances in Inhalation Dosimetry Models and Methods for Occupational Risk Assessment and Exposure Limit Derivation. *J. Occup. Environ. Hyg.* **2015**, *12* (sup1), S18–S40 DOI: 10.1080/15459624.2015.1060328.

(4) Oberdörster, G.; Oberdörster, E.; Oberdörster, J. Nanotoxicology: An Emerging Discipline Evolving from Studies of Ultrafine Particles. *Environ. Health Perspect.* **2005**, *113* (7), 823–839 DOI: 10.1289/ehp.7339.

(5) Cassee, F. R.; van Balen, E. C.; Singh, C.; Green, D.; Muijser, H.; Weinstein, J.; Dreher, K. Exposure, Health and Ecological Effects Review of Engineered Nanoscale Cerium and Cerium Oxide Associated with Its Use as a Fuel Additive. *Crit. Rev. Toxicol.* **2011**, *41* (3), 213–229 DOI: 10.3109/10408444.2010.529105.

(6) Grass, R. N.; Limbach, L. K.; Athanassiou, E. K.; Stark, W. J. Exposure of Aerosols and Nanoparticle Dispersions to in Vitro Cell Cultures: A Review on the Dose Relevance of Size, Mass, Surface and Concentration. *J. Aerosol Sci.* **2010**, *41* (12), 1123–1142 DOI: 10.1016/j.jaerosci.2010.10.001.

(7) Klein, S. G.; Hennen, J.; Serchi, T.; Blömeke, B.; Gutleb, A. C. Potential of Coculture in Vitro Models to Study Inflammatory and Sensitizing Effects of Particles on the Lung. *Toxicol. Vitr.* **2011**, *25* (8), 1516–1534 DOI: 10.1016/j.tiv.2011.09.006.

(8) Klein, S. G.; Serchi, T.; Hoffmann, L.; Blömeke, B.; Gutleb, A. C. An Improved 3D Tetraculture System Mimicking the Cellular Organisation at the Alveolar Barrier to Study the Potential Toxic Effects of Particles on the Lung. *Part. Fibre Toxicol.* **2013**, *10*, 31 DOI: 10.1186/1743-8977-10-31.

(9) Sarkar, S.; Zhang, L.; Subramaniam, P.; Lee, K. B.; Garfunkel, E.; Strickland, P. a; Mainelis, G.; Lioy, P. J.; Tetley, T. D.; Chung, K. F.; Zhang, J.; Ryan, M.; Porter, a; Schwander, S. Variability in Bioreactivity Linked to Changes in Size and Zeta Potential of Diesel Exhaust Particles in Human Immune Cells. *PLoS One* **2014**, *9* (5), e97304 DOI: 10.1371/journal.pone.0097304.

(10) Snow, S. J.; McGee, J.; Miller, D. B.; Bass, V.; Schladweiler, M. C.; Thomas, R. F.; Krantz, T.; King, C.; Ledbetter, a. D.; Richards, J.; Weinstein, J. P.; Conner, T.; Willis, R.; Linak, W. P.; Nash, D.; Wood, C. E.; Elmore, S. a.; Morrison, J. P.; Johnson, C. L.; Gilmour, M. I.; Kodavanti, U. P. Inhaled Diesel Emissions Generated with Cerium Oxide Nanoparticle Fuel Additive Induce Adverse Pulmonary and Systemic Effects. *Toxicol. Sci.* **2014**, *142* (2), 403–417 DOI: 10.1093/toxsci/kfu187.

(11) Zhang, J.; Nazarenko, Y.; Zhang, L.; Calderon, L.; Lee, K. B.; Garfunkel, E.; Schwander, S.; Tetley, T. D.; Chung, K. F.; Porter, A. E.; Ryan, M.; Kipen, H.; Lioy, P. J.; Mainelis, G. Impacts of a Nanosized Ceria Additive on Diesel Engine Emissions of Particulate and Gaseous Pollutants. *Environ. Sci. Technol.* **2013**, *47* (22), 13077–13085 DOI: 10.1021/es402140u.

(12) Bachler, G.; Losert, S.; Umehara, Y.; von Goetz, N.; Rodriguez-Lorenzo, L.; Petri-Fink, A.; Rothen-Rutishauser, B.; Hungerbuehler, K. Translocation of Gold Nanoparticles across the Lung Epithelial Tissue Barrier: Combining in Vitro and in Silico Methods to Substitute in Vivo Experiments. *Part. Fibre Toxicol.* **2015**, *12* (1), 1–18 DOI: 10.1186/s12989-015-0090-8.

(13) Rothen-Rutishauser, B. M.; Kiama, S. G.; Gehr, P. A Three-Dimensional Cellular Model of the Human Respiratory Tract to Study the Interaction with Particles. *Am. J. Respir. Cell Mol. Biol.* **2005**, *32* (28), 281–289 DOI: 10.1165/rcmb.2004-0187OC.

(14) Braakhuis, H. M.; Kloet, S. K.; Kezic, S.; Kuper, F.; Park, M. V. D. Z.; Bellmann, S.; van der Zande, M.; Le Gac, S.; Krystek, P.; Peters, R. J. B.; Rietjens, I. M. C. M.; Bouwmeester, H. Progress and Future of in Vitro Models to Study Translocation of Nanoparticles. *Arch. Toxicol.* **2015**, *89* (9), 1469–1495 DOI: 10.1007/s00204-015-1518-5.

(15) Ji, J. H.; Jung, J. H.; Kim, S. S.; Yoon, J.-U.; Park, J. D.; Choi, B. S.; Chung, Y. H.; Kwon, I. H.; Jeong, J.; Han, B. S.; Shin, J. H.; Sung, J. H.; Song, K. S.; Yu, I. J. Twenty-Eight-Day Inhalation Toxicity Study of Silver Nanoparticles in Sprague-Dawley Rats. *Inhal. Toxicol.* **2007**, *19* (April), 857–871 DOI: 10.1080/08958370701432108.

(16) Takenaka, S.; Karg, E.; Roth, C.; Schulz, H.; Ziesenis, A.; Heinzmann, U.; Schramel, P.; Heyder, J. Pulmonary and Systemic Distribution of Inhaled Ultrafine Silver Particles in Rats. *Environ. Health Perspect.* **2001**, *109* (SUPPL. 4), 547–551 DOI: 10.2307/3454667.

(17) van Ravenzwaay, B.; Landsiedel, R.; Fabian, E.; Burkhardt, S.; Strauss, V.; Ma-Hock, L. Comparing Fate and Effects of Three Particles of Different Surface Properties: Nano-TiO2, Pigmentary TiO2 and Quartz. *Toxicol. Lett.* **2009**, *186* (3), 152–159 DOI: 10.1016/j.toxlet.2008.11.020.

(18) Brandenberger, C.; Rothen-Rutishauser, B.; Mühlfeld, C.; Schmid, O.; Ferron, G. A.; Maier, K. L.; Gehr, P.; Lenz, A. G. Effects and Uptake of Gold Nanoparticles Deposited at the Air-Liquid Interface of a Human Epithelial Airway Model. *Toxicol. Appl. Pharmacol.* **2010**, *242* (1), 56–65 DOI: 10.1016/j.taap.2009.09.014.

(19) Chithrani, B. D.; Chan, W. C. W. Elucidating the Mechanism of Cellular Uptake and Removal of Protein-Coated Gold Nanoparticles of Different Sizes and Shapes. *Nano Lett.* **2007**, *7* (6), 1542–1550 DOI: 10.1021/nl070363y.

(20) Cohen, J. M.; Teeguarden, J. G.; Demokritou, P. An Integrated Approach for the in Vitro Dosimetry of Engineered Nanomaterials. *Part. Fibre Toxicol.* **2014**, *11* (1), 20 DOI: 10.1186/1743-8977-11-20.

(21) Deloid, G.; Cohen, J. M.; Darrah, T.; Derk, R.; Rojanasakul, L.; Pyrgiotakis, G.; Wohlleben, W.; Demokritou, P. Estimating the Effective Density of Engineered Nanomaterials for in Vitro Dosimetry. *Nat. Commun.* **2014**, *5*, 3514 DOI:

10.1038/ncomms4514.

(22) Lee, Y. K.; Choi, E. J.; Webster, T. J.; Kim, S. H.; Khang, D. Effect of the Protein Corona on Nanoparticles for Modulating Cytotoxicity and Immunotoxicity. *Int. J. Nanomedicine* **2015**, *10*, 97–113 DOI: 10.2147/IJN.S72998.

(23) Tenzer, S.; Docter, D.; Kuharev, J.; Musyanovych, A.; Fetz, V.; Hecht, R.; Schlenk, F.; Fischer, D.; Kiouptsi, K.; Reinhardt, C.; Landfester, K.; Schild, H.; Maskos, M.; Knauer, S. K.; Stauber, R. H. Rapid Formation of Plasma Protein Corona Critically Affects Nanoparticle Pathophysiology. *Nat. Nanotechnol.* **2013**, *8* (10), 772–781 DOI: 10.1038/nnano.2013.181.

(24) Walkey, C.; Olsen, J.; Song, F.; Liu, R.; Guo, H.; Olsen, D. W.; Cohen, Y.; Emili, A.; Chan, W. C. W. Protein Corona Fingerprinting Predicts the Cellular Interaction of Gold and Silver Nanoparticles. *ACS Nano* **2014**, *8* (3), 2439–2455 DOI: 10.1021/nn406018.

(25) de Souza Carvalho, C.; Daum, N.; Lehr, C. M. Carrier Interactions with the Biological Barriers of the Lung: Advanced in Vitro Models and Challenges for Pulmonary Drug Delivery. *Adv. Drug Deliv. Rev.* **2014**, *75*, 129–140 DOI: 10.1016/j.addr.2014.05.014.

(26) Fattal, E.; Grabowski, N.; Mura, S.; Vergnaud, J.; Tsapis, N.; Hillaireau, H. Lung Toxicity of Biodegradable Nanoparticles. *J. Biomed. Nanotechnol.* **2014**, *10* (10), 2852–2864 DOI: 10.1166/jbn.2014.1939.

(27) Grainger, C. I.; Greenwell, L. L.; Lockley, D. J.; Martin, G. P.; Forbes, B. Culture of Calu-3 Cells at the Air Interface Provides a Representative Model of the Airway Epithelial Barrier. *Pharm. Res.* **2006**, *23* (7), 1482–1490 DOI: 10.1007/s11095-006-0255-0.

(28) Fröhlich, E.; Salar-Behzadi, S. Toxicological Assessment of Inhaled Nanoparticles: Role of in Vivo, Ex Vivo, in Vitro, and in Silico Studies. *Int. J. Mol. Sci.* **2014**, *15*, 4795–4822 DOI: 10.3390/ijms15034795.

(29) Holder, A. L.; Lucas, D.; Goth-goldstein, R.; Koshland, C. P. Cellular Response to Diesel Exhaust Particles Strongly Depends on the Exposure Method. *Toxicol. Sci.* **2008**, *103* (1), 108–115 DOI: 10.1093/toxsci/kfn014.

(30) Oberdörster, G.; Maynard, A.; Donaldson, K.; Castranova, V.; Fitzpatrick, J.; Ausman, K.; Carter, J.; Karn, B.; Kreyling, W.; Lai, D.; Olin, S.; Monteiro-Riviere, N.; Warheit, D.; Yang, H. Principles for Characterizing the Potential Human Health Effects from Exposure to Nanomaterials: Elements of a Screening Strategy. *Part. Fibre Toxicol.* **2005**, *2*, 8 DOI: 10.1186/1743-8977-2-8.

(31) Secondo, L. E.; Liu, N. J.; Lewinski, N. A. Methodological Considerations When Conducting in Vitro, Air–liquid Interface Exposures to Engineered Nanoparticle Aerosols. *Crit. Rev. Toxicol.* **2016**, 1–32 DOI: 10.1080/10408444.2016.1223015.

(32) Broßell, D.; Tröller, S.; Dziurowitz, N.; Plitzko, S.; Linsel, G.; Asbach, C.; Azong-Wara, N.; Fissan, H.; Schmidt-Ott, a. A Thermal Precipitator for the Deposition of Airborne Nanoparticles onto Living Cells-Rationale and Development. *J. Aerosol Sci.* **2013**, *63*, 75–86 DOI: 10.1016/j.jaerosci.2013.04.012.

(33) de Bruijne, K.; Ebersviller, S.; Sexton, K. G.; Lake, S.; Leith, D.; Goodman, R.; Jetters, J.;

Walters, G. W.; Doyle-Eisele, M.; Woodside, R.; Jeffries, H. E.; Jaspers, I. Design and Testing of Electrostatic Aerosol in Vitro Exposure System (EAVES): An Alternative Exposure System for Particles. *Inhal. Toxicol.* **2009**, *21*, 91–101 DOI: 10.1080/08958370802166035.

(34) Aufderheide, M.; Halter, B.; Möhle, N.; Hochrainer, D. The CULTEX RFS: A Comprehensive Technical Approach for the in Vitro Exposure of Airway Epithelial Cells to the Particulate Matter at the Air-Liquid Interface. *Biomed Res. Int.* **2013**, *2013* (1), 1–15 DOI: 10.1155/2013/734137.

(35) Jeannet, N.; Fierz, M.; Kalberer, M.; Geiser, M.; Burtscher, H. Nano Aerosol Chamber for In-Vitro Toxicity (NACIVT) Studies. *Nanotoxicology* **2014**, *5390*, 1–9 DOI: 10.3109/17435390.2014.886739.

(36) Steinritz, D.; Möhle, N.; Pohl, C.; Papritz, M.; Stenger, B.; Schmidt, A.; Kirkpatrick, C. J.; Thiermann, H.; Vogel, R.; Hoffmann, S.; Aufderheide, M. Use of the Cultex Radial Flow System as an in Vitro Exposure Method to Assess Acute Pulmonary Toxicity of Fine Dusts and Nanoparticles with Special Focus on the Intra- and Inter-Laboratory Reproducibility. *Chem. Biol. Interact.* **2013**, *206* (3), 479–490 DOI: 10.1016/j.cbi.2013.05.001.

(37) Rach, J.; Budde, J.; Möhle, N.; Aufderheide, M.; M??hle, N.; Aufderheide, M. Direct Exposure at the Air-Liquid Interface: Evaluation of an in Vitro Approach for Simulating Inhalation of Airborne Substances. *J. Appl. Toxicol.* **2014**, *34* (April 2013), 506–515 DOI: 10.1002/jat.2899.

(38) Cassee, F. R.; Campbell, A.; Boere, A. J. F.; McLean, S. G.; Duffin, R.; Krystek, P.; Gosens, I.; Miller, M. R. The Biological Effects of Subacute Inhalation of Diesel Exhaust Following Addition of Cerium Oxide Nanoparticles in Atherosclerosis-Prone Mice. *Environ. Res.* **2012**, *115*, 1–10 DOI: 10.1016/j.envres.2012.03.004.

(39) Cooney, D. J.; Hickey, A. J. Cellular Response to the Deposition of Diesel Exhaust Particle Aerosols onto Human Lung Cells Grown at the Air-Liquid Interface by Inertial Impaction. *Toxicol. Vitr.* **2011**, *25* (8), 1953–1965 DOI: 10.1016/j.tiv.2011.06.019.

(40) Jie, Y.; Isa, Z. M.; Jie, X.; Ju, Z. L.; Ismail, N. H. *Urban vs. Rural Factors That Affect Adult Asthma*; 2013; Vol. 226.

(41) Holder, A. L.; Marr, L. C. Toxicity of Silver Nanoparticles at the Air-Liquid Interface. *Biomed Res. Int.* **2013**, *2013*, 1–11 DOI: 10.1155/2013/328934.

(42) Mihai, C.; Chrisler, W. B.; Xie, Y.; Hu, D.; Szymanski, C. J.; Tolic, A.; Klein, J. A.; Smith, J. N.; Tarasevich, B. J.; Orr, G. Intracellular Accumulation Dynamics and Fate of Zinc Ions in Alveolar Epithelial Cells Exposed to Airborne ZnO Nanoparticles at the Air-Liquid Interface. *Nanotoxicology* **2015**, *9* (1), 9–22 DOI: 10.1038/nature13527.Structure.

(43) Xie, Y.; Williams, N. G.; Tolic, A.; Chrisler, W. B.; Teeguarden, J. G.; Maddux, B. L. S.; Pounds, J. G.; Laskin, A.; Orr, G. Aerosolized ZnO Nanoparticles Induce Toxicity in Alveolar Type II Epithelial Cells at the Air-Liquid Interface. *Toxicol. Sci.* **2012**, *125* (2), 450–461 DOI: 10.1093/toxsci/kfr251.

(44) Vance, M. E.; Kuiken, T.; Vejerano, E. P.; McGinnis, S. P.; Hochella, M. F.; Rejeski, D.; Hull, M. S. Nanotechnology in the Real World: Redeveloping the Nanomaterial Consumer Products Inventory. *Beilstein J. Nanotechnol.* **2015**, *6* (October 2013), 1769–1780 DOI: 10.3762/bjnano.6.181.

(45) Schütz, C. a.; Juillerat-Jeanneret, L.; Soltmann, C.; Mueller, H. Toxicity Data of Therapeutic Nanoparticles in Patent Documents. *World Pat. Inf.* **2013**, *35* (2), 110–114 DOI: 10.1016/j.wpi.2012.12.008.

(46) Schütz, C.; Juillerat-Jeanneret, L.; Mueller, H.; Lynch, I.; Riediker, M. Therapeutic Nanoparticles in Clinics and under Clinical Evaluation. *Nanomedicine* **2013**, *8*, 449–467 DOI: 10.2217/nnm.13.8.

(47) Venditto, V. J.; Szoka, F. C. Cancer Nanomedicines: So Many Papers and so Few Drugs! *Adv. Drug Deliv. Rev.* **2013**, *65* (1), 80–88 DOI: 10.1016/j.addr.2012.09.038.

(48) Jones, C. F.; Grainger, D. W. In Vitro Assessments of Nanomaterial Toxicity. *Adv. Drug Deliv. Rev.* **2009**, *61* (6), 438–456 DOI: 10.1016/j.addr.2009.03.005.

(49) Sayes, C. M.; Reed, K. L.; Warheit, D. B. Assessing Toxicology of Fine and Nanoparticles: Comparing in Vitro Measurements to in Vivo Pulmonary Toxicity Profiles. *Toxicol. Sci.* **2007**, *97* (1), 163–180 DOI: 10.1093/toxsci/kfm018.

(50) Bakand, S.; Hayes, A. Troubleshooting Methods for Toxicity Testing of Airborne Chemicals in Vitro. *J. Pharmacol. Toxicol. Methods* **2010**, *61* (2), 76–85 DOI: 10.1016/j.vascn.2010.01.010.

(51) Bérubé, K.; Aufderheide, M.; Breheny, D.; Clothier, R.; Combes, R.; Forbes, B.; Gaça, M.; Gray, A.; Hall, I.; Kelly, M.; Lethem, M.; Liebsch, M.; Merolla, L.; Morin, J.; Seagrave, J.; Swartz, M. a; D, T. T.; Umachandran, M. In Vitro Models of Inhalation Toxicity and Disease. *Alta* **2009**, *37*, 89–141.

(52) Grabinski, C. M.; Hussain, S. M.; Mohan Sankaran, R. Simulations of Submicron Aerosol Deposition at an Air–liquid Interface for in Vitro Toxicology. *J. Aerosol Sci.* **2015**, *90*, 87–102 DOI: 10.1016/j.jaerosci.2015.08.005.

(53) Herzog, F.; Loza, K.; Balog, S.; Clift, M. J. D.; Epple, M.; Gehr, P.; Petri-Fink, A.; Rothen-Rutishauser, B. Mimicking Exposures to Acute and Lifetime Concentrations of Inhaled Silver Nanoparticles by Two Different in Vitro Approaches. *Beilstein J. Nanotechnol.* **2014**, *5*, 1357–1370 DOI: 10.3762/bjnano.5.149.

(54) Huh, D.; Matthews, B. D.; Mammoto, A.; Hsin, H. Y.; Ingber, D. E.; Montoya-Zavala, M.; Hsin, H. Y.; Ingber, D. E. Reconstituting Organ-Level Lung Functions on a Chip. *Science (80-.).* **2010**, *328*, 1662–1668 DOI: 10.1126/science.1188302.

(55) Nel, A.; Xia, T.; Meng, H.; Wang, X.; Lin, S.; Ji, Z.; Zhang, H. Nanomaterial Toxicity Testing in the 21st Century: Use of a Predictive Toxicological Approach and High-Throughput Screening. *Acc. Chem. Res.* **2013**, *46* (3), 607–621 DOI: 10.1021/ar300022h.

(56) Paur, H. R.; Cassee, F. R.; Teeguarden, J.; Fissan, H.; Diabate, S.; Aufderheide, M.; Kreyling, W. G.; Hänninen, O.; Kasper, G.; Riediker, M.; Rothen-Rutishauser, B.; Schmid, O. In-Vitro Cell Exposure Studies for the Assessment of Nanoparticle Toxicity in

the Lung-A Dialog between Aerosol Science and Biology. *J. Aerosol Sci.* **2011**, *42* (September 2009), 668–692 DOI: 10.1016/j.jaerosci.2011.06.005.

(57) Paur, H. R.; M??lhopt, S.; Weiss, C.; Diabat??, S.; Mülhopt, S.; Weiss, C.; Diabaté, S. In Vitro Exposure Systems and Bioassays for the Assessment of Toxicity of Nanoparticles to the Human Lung. *J. fur Verbraucherschutz und Leb.* **2008**, *3* (3), 319–329 DOI: 10.1007/s00003-008-0356-2.

(58) Raemy, D. O.; Grass, R. N.; Stark, W. J.; Schumacher, C. M.; Clift, M. J. D.; Gehr, P.; Rothen – Rutishauser, B. Effects of Flame Made Zinc Oxide Particles in Human Lung Cells - a Comparison of Aerosol and Suspension Exposures. *Part. Fibre Toxicol.* **2012**, *9* (1), 33 DOI: 10.1186/1743-8977-9-33.

(59) Herzog, F.; Clift, M. J.; Piccapietra, F.; Behra, R.; Schmid, O.; Petri-Fink, A.; Rothen-Rutishauser, B. Exposure of Silver-Nanoparticles and Silver-Ions to Lung Cells in Vitro at the Air-Liquid Interface. *Part. Fibre Toxicol.* **2013**, *10*, 11 DOI: 10.1186/1743-8977-10-11.

(60) Aufderheide, M.; Knebel, J. W.; Ritter, D. An Improved in Vitro Model for Testing the Pulmonary Toxicity of Complex Mixtures Such as Cigarette Smoke. *Exp. Toxicol. Pathol.* **2003**, *55*, 51–57 DOI: 10.1078/0940-2993-00298.

(61) Fukano, Y.; Ogura, M.; Eguchi, K.; Shibagaki, M.; Suzuki, M. Modified Procedure of a Direct in Vitro Exposure System for Mammalian Cells to Whole Cigarette Smoke. *Exp. Toxicol. Pathol.* **2004**, *55*, 317–323 DOI: 10.1078/0940-2993-00341.

(62) Fukano, Y.; Yoshimura, H.; Yoshida, T. Heme Oxygenase-1 Gene Expression in Human Alveolar Epithelial Cells (A549) Following Exposure to Whole Cigarette Smoke on a Direct in Vitro Exposure System. *Exp. Toxicol. Pathol.* **2006**, *57*, 411–418 DOI: 10.1016/j.etp.2005.12.001.

(63) Okuwa, K.; Tanaka, M.; Fukano, Y.; Nara, H.; Nishijima, Y.; Nishino, T. In Vitro Micronucleus Assay for Cigarette Smoke Using a Whole Smoke Exposure System: A Comparison of Smoking Regimens. *Exp. Toxicol. Pathol.* **2010**, *62* (4), 433–440 DOI: 10.1016/j.etp.2009.06.002.

(64) Olivera, D. S.; Boggs, S. E.; Beenhouwer, C.; Aden, J.; Knall, C. Cellular Mechanisms of Mainstream Cigarette Smoke-Induced Lung Epithelial Tight Junction Permeability Changes in Vitro. *Inhal. Toxicol.* **2007**, *19*, 13–22 DOI: 10.1080/08958370600985768.

(65) Tsukue, N.; Okumura, H.; Ito, T.; Sugiyama, G.; Nakajima, T. Toxicological Evaluation of Diesel Emissions on A549 Cells. *Toxicol. Vitr.* **2010**, *24* (2), 363–369 DOI: 10.1016/j.tiv.2009.11.004.

(66) Wolz, L.; Krause, G.; Scherer, G.; Aufderheide, M.; Mohr, U. In Vitro Genotoxicity Assay of Sidestream Smoke Using a Human Bronchial Epithelial Cell Line. *Food Chem. Toxicol.* **2002**, *40*, 845–850 DOI: 10.1016/S0278-6915(02)00034-0.

(67) Teeguarden, J. G.; Hinderliter, P. M.; Orr, G.; Thrall, B. D.; Pounds, J. G. Particokinetics in Vitro: Dosimetry Considerations for in Vitro Nanoparticle Toxicity Assessments. *Toxicol. Sci.* **2007**, *95* (2), 300–312 DOI: 10.1093/toxsci/kfl165.

(68) Cohen, J. M.; Deloid, G. M.; Demokritou, P. A Critical Review of in Vitro Dosimetry for Engineered Nanomaterials. *Nanomedicine* **2015**, *10* (19), 3015–3032.

(69) Fadeel, B.; Fornara, A.; Toprak, M. S.; Bhattacharya, K. Keeping It Real: The Importance of Material Characterization in Nanotoxicology. *Biochem. Biophys. Res. Commun.* **2015**, *468* (3), 498–503 DOI: 10.1016/j.bbrc.2015.06.178.

(70) Durán, N.; Silveira, C. P.; Durán, M.; Martinez, D. S. T. Silver Nanoparticle Protein Corona and Toxicity: A Mini-Review. *J. Nanobiotechnology* **2015**, *13* (1), 55 DOI: 10.1186/s12951-015-0114-4.

(71) Brandenberger, C.; Mühlfeld, C.; Ali, Z.; Lenz, A. G.; Schmid, O.; Parak, W. J.; Gehr, P.; Rothen-Rutishauser, B. Quantitative Evaluation of Cellular Uptake and Trafficking of Plain and Polyethylene Glycol-Coated Gold Nanoparticles. *Small* **2010**, *6* (x), 1669–1678 DOI: 10.1002/smll.201000528.

(72) Limbach, L. K.; Li, Y.; Grass, R. N.; Brunner, T. J.; Hintermann, M. a; Muller, M.; Gunther, D.; Stark, W. J. Oxide Nanoparticle Uptake in Human Lung Fibroblasts: Effects of Particle Size, Agglomeration, and Diffusion at Low Concentrations. *Environ. Sci. Technol.* **2005**, *39* (23), 9370–9376 DOI: 10.1021/es051043o.

(73) Waters, K. M.; Masiello, L. M.; Zangar, R. C.; Tarasevich, B. J.; Karin, N. J.; Quesenberry, R. D.; Bandyopadhyay, S.; Teeguarden, J. G.; Pounds, J. G.; Thrall, B. D. Macrophage Responses to Silica Nanoparticles Are Highly Conserved across Particle Sizes. *Toxicol. Sci.* **2009**, *107* (2), 553–569 DOI: 10.1093/toxsci/kfn250.

(74) Moher, D.; Liberati, A.; Tetzlaff, J.; Altman, D. G. Academia and Clinic Annals of Internal Medicine Preferred Reporting Items for Systematic Reviews and Meta-Analyses : *Ann. Intern. Med.* **2009**, *151* (4), 264–269 DOI: 10.7326/0003-4819-151-4-200908180-00135.

(75) Klimisch, H.-J.; Andreae, M.; Tillmann, U. A Systematic Approach for Evaluating the Quality of Experimental Toxicological and Ecotoxicological Data. *Regul. Toxicol. Pharmacol.* **1997**, *25* (25), 1–5 DOI: 10.1006/rtph.1996.1076.

(76) Linkov, I.; Bates, M. E.; Canis, L. J.; Seager, T. P.; Keisler, J. M. A Decision-Directed Approach for Prioritizing Research into the Impact of Nanomaterials on the Environment and Human Health. *Nat. Nanotechnol.* **2011**, *6* (12), 784–787 DOI: 10.1038/nnano.2011.163.

(77) Hinderliter, P. M.; Minard, K. R.; Orr, G.; Chrisler, W. B.; Thrall, B. D.; Pounds, J. G.; Teeguarden, J. G. ISDD: A Computational Model of Particle Sedimentation, Diffusion and Target Cell Dosimetry for in Vitro Toxicity Studies. *Part. Fibre Toxicol.* **2010**, *7* (1), 36 DOI: 10.1186/1743-8977-7-36.

(78) Brown, J. S.; Wilson, W. E.; Grant, L. D. Dosimetric Comparisons of Particle Deposition and Retention in Rats and Humans. *Inhal. Toxicol.* **2005**, *17*, 355–385 DOI: 10.1080/08958370590929475.

(79) Tippe, A.; Heinzmann, U.; Roth, C. Deposition of Fine and Ultrafine Aerosol Particles during Exposure at the Air/Cell Interface. *J. Aerosol Sci.* **2002**, *33*, 207–218.

(80) Steiner, S.; Czerwinski, J.; Comte, P.; Müller, L. L.; Heeb, N. V.; Mayer, A.; Petri-Fink, A.; Rothen-Rutishauser, B. Reduction in (pro-)Inflammatory Responses of Lung Cells Exposed Invitro to Diesel Exhaust Treated with a Non-Catalyzed Diesel Particle Filter. *Atmos. Environ.* **2013**, *81*, 117–124 DOI: 10.1016/j.atmosenv.2013.08.029.

(81) Panas, A.; Comouth, A.; Saathoff, H.; Leisner, T.; Al-Rawi, M.; Simon, M.; Seemann, G.; Dössel, O.; Mülhopt, S.; Paur, H.; Fritsch-Decker, S.; Weiss, C.; Diabaté, S. Silica Nanoparticles Are Less Toxic to Human Lung Cells When Deposited at the Air–liquid Interface Compared to Conventional Submerged Exposure. *Beilstein J. Nanotechnol.* **2014**, *5*, 1590–1602 DOI: 10.3762/bjnano.5.171.

(82) Volckens, J.; Dailey, L.; Walters, G.; Devlin, R. Particle-to-Cell Deposition of Coarse Ambient Particulate Matter Increases the Production If Inflammatory Mediators from Cultured Human Airway Epithelial Cells. *Environ. Sci. Technol.* **2009**, *43* (12), 4595–4599.

(83) Messing, M. E.; Svensson, C. R.; Pagels, J.; Meuller, B. O.; Deppert, K.; Rissler, J. Gas-Borne Particles with Tunable and Highly Controlled Characteristics for Nanotoxicology Studies. *Nanotoxicology* **2012**, No. September, 1–12 DOI: 10.3109/17435390.2012.697589.

(84) Asimakopoulou, A.; Daskalos, E.; Lewinski, N.; Riediker, M.; Papaioannou, E.; Konstandopoulos, A. G. Development of a Dose-Controlled Multiculture Cell Exposure Chamber for Efficient Delivery of Airborne and Engineered Nanoparticles. *J. Phys. Conf. Ser.* **2013**, *429*, 1–10 DOI: 10.1088/1742-6596/429/1/012023.

(85) Elihn, K.; Cronholm, P.; Karlsson, H. L.; Midander, K.; Odnevall Wallinder, I.; Möller, L. Cellular Dose of Partly Soluble Cu Particle Aerosols at the Air-Liquid Interface Using an In Vitro Lung Cell Exposure System. *J. Aerosol Med. Pulm. Drug Deliv.* **2013**, *26* (2), 84–93 DOI: 10.1089/jamp.2012.0972.

(86) Kim, J. S.; Peters, T. M.; O'Shaughnessy, P. T.; Adamcakova-Dodd, A.; Thorne, P. S. Validation of an in Vitro Exposure System for Toxicity Assessment of Air-Delivered Nanomaterials. *Toxicol. Vitr.* **2013**, *27* (1), 164–173 DOI: 10.1016/j.tiv.2012.08.030.

(87) Mertes, P.; Praplan, A. P.; Künzi, L.; Dommen, J.; Baltensperger, U.; Geiser, M.; Weingartner, E.; Ricka, J.; Fierz, M.; Kalberer, M. A Compact and Portable Deposition Chamber to Study Nanoparticles in Air-Exposed Tissue. *J. Aerosol Med. Pulm. Drug Deliv.* **2013**, *26* (0), 228–235 DOI: 10.1089/jamp.2012.0985.

(88) Steiner, S.; Czerwinski, J.; Comte, P.; Popovicheva, O.; Kireeva, E.; Müller, L.; Heeb, N.; Mayer, A.; Fink, A.; Rothen-Rutishauser, B. Comparison of the Toxicity of Diesel Exhaust Produced by Bio- and Fossil Diesel Combustion in Human Lung Cells Invitro. *Atmos. Environ.* **2013**, *81*, 380–388 DOI: 10.1016/j.atmosenv.2013.08.059.

(89) Braakhuis, H. M.; Gosens, I.; Krystek, P.; Boere, J. A. F.; Cassee, F. R.; Fokkens, P. H. B.; Post, J. A.; van Loveren, H.; Park, M. V. D. Z. Particle Size Dependent Deposition and Pulmonary Inflammation after Short-Term Inhalation of Silver Nanoparticles. *Part. Fibre Toxicol.* **2014**, *11*, 49 DOI: 10.1186/s12989-014-0049-1.

(90) Fujitani, Y.; Sugaya, Y.; Hashiguchi, M.; Furuyama, A.; Hirano, S.; Takami, A. Particle

Deposition Efficiency at Air–liquid Interface of a Cell Exposure Chamber. *J. Aerosol Sci.* **2015**, *81*, 90–99 DOI: 10.1016/j.jaerosci.2014.10.012.

(91) Jing, X.; Park, J. H.; Peters, T. M.; Thorne, P. S. Toxicology in Vitro Toxicity of Copper Oxide Nanoparticles in Lung Epithelial Cells Exposed at the Air – Liquid Interface Compared with in Vivo Assessment. *Toxicol. Vitr.* **2015**, *29* (3), 502–511 DOI: 10.1016/j.tiv.2014.12.023.

(92) Steiner, S.; Czerwinski, J.; Comte, P.; Heeb, N. V.; Mayer, A.; Petri-Fink, A.; Rothen-Rutishauser, B. Effects of an Iron-Based Fuel-Borne Catalyst and a Diesel Particle Filter on Exhaust Toxicity in Lung Cells in Vitro. *Anal. Bioanal. Chem.* **2015**, *407* (20), 5977–5986 DOI: 10.1007/s00216-014-7878-5.

(93) Bitterle, E.; Karg, E.; Schroeppel, a.; Kreyling, W. G.; Tippe, a.; Ferron, G. a.; Schmid, O.; Heyder, J.; Maier, K. L.; Hofer, T. Dose-Controlled Exposure of A549 Epithelial Cells at the Air-Liquid Interface to Airborne Ultrafine Carbonaceous Particles. *Chemosphere* **2006**, *65*, 1784–1790 DOI: 10.1016/j.chemosphere.2006.04.035.

(94) Möller, W.; Felten, K.; Seitz, J.; Sommerer, K.; Takenaka, S.; Wiebert, P.; Philipson, K.; Svartengren, M.; Kreyling, W. G. A Generator for the Production of Radiolabelled Ultrafine Carbonaceous Particles for Deposition and Clearance Studies in the Respiratory Tract. *J. Aerosol Sci.* **2006**, *37*, 631–644 DOI: 10.1016/j.jaerosci.2005.05.010.

(95) Geiser, M.; Casaulta, M.; Kupferschmid, B.; Schulz, H.; Semmler-Behnke, M.; Kreyling, W. The Role of Macrophages in the Clearance of Inhaled Ultrafine Titanium Dioxide Particles. *Am. J. Respir. Cell Mol. Biol.* **2008**, *38* (3), 371–376 DOI: 10.1165/rcmb.2007-0138OC.

(96) Stevens, J. P.; Zahardis, J.; MacPherson, M.; Mossman, B. T.; Petrucci, G. a. A New Method for Quantifiable and Controlled Dosage of Particulate Matter for in Vitro Studies: The Electrostatic Particulate Dosage and Exposure System (EPDExS). *Toxicol. In Vitro* **2008**, *22* (7), 1768–1774 DOI: 10.1016/j.tiv.2008.05.013.

(97) Pauluhn, J. Subchronic 13-Week Inhalation Exposure of Rats to Multiwalled Carbon Nanotubes: Toxic Effects Are Determined by Density of Agglomerate Structures, Not Fibrillar Structures. *Toxicol. Sci.* **2010**, *113* (1), 226–242 DOI: 10.1093/toxsci/kfp247.

(98) Ma-Hock, L.; Strauss, V.; Treumann, S.; Küttler, K.; Wohlleben, W.; Hofmann, T.; Gröters, S.; Wiench, K.; van Ravenzwaay, B.; Landsiedel, R. Comparative Inhalation Toxicity of Multi-Wall Carbon Nanotubes, Graphene, Graphite Nanoplatelets and Low Surface Carbon Black. *Part. Fibre Toxicol.* **2013**, *10* (1), 23 DOI: 10.1186/1743-8977-10-23.

(99) Landsiedel, R.; Ma-Hock, L.; Hofmann, T.; Wiemann, M.; Strauss, V.; Treumann, S.; Wohlleben, W.; Gröters, S.; Wiench, K.; van Ravenzwaay, B. Application of Short-Term Inhalation Studies to Assess the Inhalation Toxicity of Nanomaterials. *Part. Fibre Toxicol.* **2014**, *11*, 16 DOI: 10.1186/1743-8977-11-16.

(100) Pauluhn, J.; Rosenbruch, M. Lung Burdens and Kinetics of Multi-Walled Carbon Nanotubes (Baytubes) Are Highly Dependent on the Disaggregation of Aerosolized MWCNT. *Nanotoxicology* **2015**, *9* (2), 242–252 DOI: 10.3109/17435390.2014.918204.

(101) Noel, A.; Maghni, K.; Cloutier, Y.; Dion, C.; Wilkinson, K. J.; Hall??, S.; Tardif, R.; Truchon, G. Effects of Inhaled Nano-TiO2 Aerosols Showing Two Distinct Agglomeration States on Rat Lungs. *Toxicol. Lett.* **2012**, *214* (2), 109–119 DOI: 10.1016/j.toxlet.2012.08.019.

(102) Kim, S.; Ryu, D.-Y. Y. Silver Nanoparticle-Induced Oxidative Stress, Genotoxicity and Apoptosis in Cultured Cells and Animal Tissues. *J. Appl. Toxicol.* **2013**, *33* (2), 78–89 DOI: 10.1002/jat.2792.

(103) Lenz, A.-G.; Stoeger, T.; Cei, D.; Schmidmeir, M.; Semren, N.; Burgstaller, G.; Lentner, B.; Eickelberg, O.; Meiners, S.; Schmid, O. Efficient Bioactive Delivery of Aerosolized Drugs to Human Pulmonary Epithelial Cells Cultured in Air-Liquid Interface Conditions. *Am. J. Respir. Cell Mol. Biol.* **2014**, *51* (4), 526–535 DOI: 10.1165/rcmb.2013-0479OC.

(104) Beckett, W. S.; Chalupa, D. F.; Pauly-Brown, A.; Speers, D. M.; Stewart, J. C.; Frampton, M. W.; Utell, M. J.; Huang, L. S.; Cox, C.; Zareba, W.; Oberd??rster, G. Comparing Inhaled Ultrafine versus Fine Zinc Oxide Particles in Healthy Adults: A Human Inhalation Study. *Am. J. Respir. Crit. Care Med.* **2005**, *171* (10), 1129–1135 DOI: 10.1164/rccm.200406-837OC.

(105) Ellinger-Ziegelbauer, H.; Pauluhn, J. Pulmonary Toxicity of Multi-Walled Carbon Nanotubes (Baytubes®) Relative to α-Quartz Following a Single 6 h Inhalation Exposure of Rats and a 3 Months Post-Exposure Period. *Toxicology* **2009**, *266* (1–3), 16–29 DOI: 10.1016/j.tox.2009.10.007.

(106) Stebounova, L. V; Adamcakova-dodd, A.; Kim, J. S.; Park, H.; Shaughnessy, P. T. O.; Grassian, V. H.; Thorne, P. S. Nanosilver Induces Minimal Lung Toxicity or Inflammation in a Subacute Murine Inhalation Model. *Part. Fibre Toxicol.* **2011**, *8* (1), 5 DOI: 10.1186/1743-8977-8-5.

(107) Baisch, B. L.; Corson, N. M.; Wade-mercer, P.; Gelein, R.; Kennell, A. J.; Oberdörster, G. Equivalent Titanium Dioxide Nanoparticle Deposition by Intratracheal Instillation and Whole Body Inhalation : The Effect of Dose Rate on Acute Respiratory Tract Inflammation. *Part. Fibre Toxicol.* **2014**, *11* (5), 1–16 DOI: 10.1186/1743-8977-11-5.

(108) Rothen-Rutishauser, B.; Grass, R.; Blank, F.; Lk. Direct Combination of Nanoparticle Fabrication and Exposure to Lung Cell Cultures in a Closed Setup as a Method To Simulate Accidental Nanoparticle Exposure. *Environ. Sci. Technol.* **2009**, *43* (7), 2634–2640.

(109) Ahmad, S.; Raemy, D. O.; Loader, J. E.; Kailey, J. M.; Neeves, K. B.; White, C. W.; Ahmad, A.; Gehr, P.; Rothen-Rutishauser, B. M. Interaction and Localization of Synthetic Nanoparticles in Healthy and Cystic Fibrosis Airway Epithelial Cells: Effect of Ozone Exposure. *J. Aerosol Med. Pulm. Drug Deliv.* **2012**, *25* (1), 7–15 DOI: 10.1089/jamp.2011.0889.

(110) Endes, C.; Müller, S.; Schmid, O.; Vanhecke, D.; Foster, E. J.; Petri-Fink, A.; Rothen-Rutishauser, B.; Weder, C.; Clift, M. J. D. Risk Assessment of Released Cellulose Nanocrystals – Mimicking Inhalatory Exposure. *J. Phys. Conf. Ser.* **2013**, *429*, 012008 DOI: 10.1088/1742-6596/429/1/012008.

(111) Fröhlich, E.; Bonstingl, G.; Höfler, A.; Meindl, C.; Leitinger, G.; Pieber, T. R.; Roblegg, E. Comparison of Two in Vitro Systems to Assess Cellular Effects of Nanoparticles-Containing Aerosols. *Toxicol. Vitr.* **2013**, *27*, 409–417 DOI: 10.1016/j.tiv.2012.08.008.

(112) Chortarea, S.; Clift, M. J. D.; Vanhecke, D.; Endes, C.; Wick, P.; Petri-Fink, A.; Rothen-Rutishauser, B. Repeated Exposure to Carbon Nanotube-Based Aerosols Does Not Affect the Functional Properties of a 3D Human Epithelial Airway Model. *Nanotoxicology* **2015**, *5390* (November), 1–11 DOI: 10.3109/17435390.2014.993344.

(113) Grigg, J.; Tellabati, A.; Rhead, S.; Howes, P.; Almeida, G.; Higgins, J.; Bowman, K.; Jones, G.; Almeida, G. DNA Damage of Macrophages at an Air-Tissue Interface Induced by Metal Nanoparticles Macrophage. *Nanotoxicology* **2009**, *3* (4), 348–354 DOI: 10.3109/17435390903276917.

(114) Lenz, A. G.; Karg, E.; Lentner, B.; Dittrich, V.; Brandenberger, C.; Rothen-Rutishauser, B.; Schulz, H.; Ferron, G. a; Schmid, O. A Dose-Controlled System for Air-Liquid Interface Cell Exposure and Application to Zinc Oxide Nanoparticles. *Part. Fibre Toxicol.* **2009**, *6*, 32 DOI: 10.1186/1743-8977-6-32.

(115) Raemy, D. O.; Limbach, L. K.; Rothen-Rutishauser, B.; Grass, R. N.; Gehr, P.; Birbaum, K.; Brandenberger, C.; Günther, D.; Stark, W. J. Cerium Oxide Nanoparticle Uptake Kinetics from the Gas-Phase into Lung Cells in Vitro Is Transport Limited. *Eur. J. Pharm. Biopharm.* **2011**, *77* (3), 368–375 DOI: 10.1016/j.ejpb.2010.11.017.

(116) Stoehr, L. C.; Endes, C.; Radauer-Preiml, I.; Boyles, M. S. P.; Casals, E.; Balog, S.; Pesch, M.; Petri-Fink, A.; Rothen-Rutishauser, B.; Himly, M.; Clift, M. J. D.; Duschl, A. Assessment of a Panel of Interleukin-8 Reporter Lung Epithelial Cell Lines to Monitor the pro-Inflammatory Response Following Zinc Oxide Nanoparticle Exposure under Different Cell Culture Conditions. *Part. Fibre Toxicol.* **2015**, *12* (1), 29 DOI: 10.1186/s12989-015-0104-6.

(117) Savi, M.; Kalberer, M.; Lang, D.; Ryser, M.; Fierz, M.; Gaschen, A.; Rička, J.; Geiser, M. A Novel Exposure System for the Efficient and Controlled Deposition of Aerosol Particles onto Cell Cultures. *Environ. Sci. Technol.* **2008**, *42*, 5667–5674 DOI: 10.1021/es703075q.

(118) Schleh, C.; Mühlfeld, C.; Pulskamp, K.; Schmiedl, A.; Nassimi, M.; Lauenstein, H. D.; Braun, A.; Krug, N.; Erpenbeck, V. J.; Hohlfeld, J. M. The Effect of Titanium Dioxide Nanoparticles on Pulmonary Surfactant Function and Ultrastructure. *Respir. Res.* **2009**, *10*, 90 DOI: 10.1186/1465-9921-10-90.

(119) Comouth, A.; Saathoff, H.; Naumann, K. H.; Muelhopt, S.; Paur, H. R.; Leisner, T. Modelling and Measurement of Particle Deposition for Cell Exposure at the Air-Liquid Interface. *J. Aerosol Sci.* **2013**, *63*, 103–114 DOI: 10.1016/j.jaerosci.2013.04.009.

(120) Jeannet, N.; Fierz, M.; Schneider, S.; Künzi, L.; Baumlin, N.; Salathe, M.; Burtscher, H.; Geiser, M. Acute Toxicity of Silver and Carbon Nanoaerosols to Normal and Cystic Fibrosis Human Bronchial Epithelial Cells. *Nanotoxicology* **2015**, No. September, 1–13 DOI: 10.3109/17435390.2015.1049233.

(121) Henderson, R. F.; Driscoll, K. E.; Harkema, J. R.; Lindenschmidt, R. C.; Chang, I.-Y.; Maples, K. R.; Barr, E. B. A Comparison of the Inflammatory Response of the Lung to

Inhaled versus Instilled Particles in F344 Rats. *Fundam. Appl. Toxicol.* **1995**, *24* (2), 183–197.

(122) Sung, J. H.; Ji, J. H.; Yoon, J. U.; Kim, D. S.; Song, M. Y.; Jeong, J.; Han, B. S.; Han, J. H.; Chung, Y. H.; Kim, J.; Kim, T. S.; Chang, H. K.; Lee, E. J.; Lee, J. H.; Yu, I. J. Lung Function Changes in Sprague-Dawley Rats After Prolonged Inhalation Exposure to Silver Nanoparticles Lung Function Changes in Sprague-Dawley Rats After Prolonged Inhalation Exposure to Silver Nanoparticles. *Inhal. Toxicol.* **2008**, *20* (6), 567–574 DOI: 10.1080/08958370701874671.

(123) Sung, J. H.; Ji, J. H.; Park, J. D.; Yoon, J. U.; Kim, D. S.; Jeon, K. S.; Song, M. Y.; Jeong, J.; Han, B. S.; Han, J. H.; Chung, Y. H.; Chang, H. K.; Lee, J. H.; Cho, M. H.; Kelman, B. J.; Yu, I. J. Subchronic Inhalation Toxicity of Silver Nanoparticles. *Toxicol. Sci.* **2009**, *108* (2), 452–461 DOI: 10.1093/toxsci/kfn246.

(124) Sung, J. H.; Ji, J. H.; Song, K. S.; Lee, J. H.; Choi, K. H.; Lee, S. H.; Yu, I. J. Acute Inhalation Toxicity of Silver Nanoparticles. *Toxicol. Ind. Health* **2011**, *27* (2), 149–154 DOI: 10.1177/0748233710382540.

(125) Song, K. S.; Sung, J. H.; Ji, J. H.; Lee, J. H.; Lee, J. S.; Ryu, H. R.; Lee, J. K.; Chung, Y. H.; Park, H. M.; Shin, B. S.; Chang, H. K.; Kelman, B.; Yu, I. J. Recovery from Silver-Nanoparticle-Exposure-Induced Lung in Flammation and Lung Function Changes in Sprague Dawley Rats. *Nanotoxicology* **2013**, *7* (May 2011), 169–180 DOI: 10.3109/17435390.2011.648223.

(126) Nurkiewicz, T. R.; Porter, D. W.; Hubbs, A. F.; Cumpston, J. L.; Chen, B. T.; Frazer, D. G.; Castranova, V. Nanoparticle Inhalation Augments Particle-Dependent Systemic Microvascular Dysfunction. *Part. Fibre Toxicol.* **2008**, *5*, 1 DOI: 10.1186/1743-8977-5-1.

(127) Ma-Hock, L.; Burkhardt, S.; Strauss, V.; Gamer, A. O.; Wiench, K.; van Ravenzwaay, B.; Landsiedel, R. Development of a Short-Term Inhalation Test in the Rat Using Nano-Titanium Dioxide as a Model Substance. *Inhal. Toxicol.* **2009**, *21* (2), 102–118 DOI: 10.1080/08958370802361057.

(128) Lindberg, H. K.; Falck, G. C.-M.; Catalán, J.; Koivisto, A. J.; Suhonen, S.; Järventaus, H.; Rossi, E. M.; Nykäsenoja, H.; Peltonen, Y.; Moreno, C.; Alenius, H.; Tuomi, T.; Savolainen, K. M.; Norppa, H. Genotoxicity of Inhaled Nanosized TiO2 in Mice. *Mutat. Res. Toxicol. Environ. Mutagen.* **2012**, *745* (1–2), 58–64 DOI: 10.1016/j.mrgentox.2011.10.011.

(129) Adamcakova-Dodd, A.; Stebounova, L. V; Kim, J. S.; Vorrink, S. U.; Ault, A. P.; O'Shaughnessy, P. T.; Grassian, V. H.; Thorne, P. S. Toxicity Assessment of Zinc Oxide Nanoparticles Using Sub-Acute and Sub-Chronic Murine Inhalation Models. *Part. Fibre Toxicol.* **2014**, *11* (1), 15 DOI: 10.1186/1743-8977-11-15.

(130) Bermudez, E.; Mangum, J. B.; Asgharian, B.; Wong, B. A.; Reverdy, E. E.; Janszen, D. B.; Hext, P. M.; Warheit, D. B.; Everitt, J. I. Long-Term Pulmonary Responses of Three Laboratory Rodent Species to Subchronic Inhalation of Pigmentary Titanium Dioxide Particles. *Toxicol. Sci.* **2002**, *70* (1), 86–97 DOI: 10.1093/toxsci/70.1.86.

(131) Bermudez, E.; Mangum, J. B.; Wong, B. A.; Asgharian, B.; Hext, P. M.; Warheit, D. B.;

Everitt, J. I. Pulmonary Responses of Mice, Rats, and Hamsters to Subchronic Inhalation of Ultrafine Titanium Dioxide Particles. *Toxicol. Sci.* **2004**, *77* (2), 347–357 DOI: 10.1093/toxsci/kfh019.

(132) Lenz, A. G.; Karg, E.; Brendel, E.; Hinze-heyn, H.; Maier, K. L.; Eickelberg, O.; Stoeger, T.; Schmid, O. Infammatory and Oxidative Stress Responses of an Alveolar Epithelial Cell Line to Airborne Zinc Oxide Nanoparticles at the Air-Liquid Interface : A Comparison with Conventional , Submerged Cell-Culture Conditions. *Biomed Res. Int.* **2013**, *2013*, 1–12.

(133) Baber, O.; Jang, M.; Barber, D.; Powers, K. Amorphous Silica Coatings on Magnetic Nanoparticles Enhance Stability and Reduce Toxicity to in Vitro BEAS-2B Cells. *Inhal. Toxicol.* **2011**, *23* (May), 532–543 DOI: 10.3109/08958378.2011.592869.

(134) He, C.; Morawska, L.; Hitchins, J.; Gilbert, D. Contribution from Indoor Sources to Particle Number and Mass Concentrations in Residential Houses. *Atmos. Environ.* **2004**, *38*, 3405–3415 DOI: 10.1016/j.atmosenv.2004.03.027.

(135) Wehner, B.; Birmili, W.; Gnauk, T.; Wiedensohler, A. Particle Number Size Distributions in a Street Canyon and Their Transformation into the Urban-Air Background: Measurements and a Simple Model Study. *Atmos. Environ.* **2002**, *36*, 2215–2223 DOI: 10.1016/S1352-2310(02)00174-7.

(136) Grabinski, C. M.; Hussain, S. M.; Mohan Sankaran, R. Simulations of Submicron Aerosol Deposition at an Air-Liquid Interface for In Vitro Toxicology. *J. Aerosol Sci.* **2015**, 1–30 DOI: 10.1016/j.jaerosci.2015.08.005.

(137) Zavala, J.; Lichtveld, K.; Ebersviller, S.; Carson, J. L.; Walters, G. W.; Jaspers, I.; Jeffries, H. E.; Sexton, K. G.; Vizuete, W. The Gillings Sampler - An Electrostatic Air Sampler as an Alternative Method for Aerosol in Vitro Exposure Studies. *Chem. Biol. Interact.* **2014**, *220C*, 158–168 DOI: 10.1016/j.cbi.2014.06.026.

(138) Stoehr, L. C.; Madl, P.; Boyles, M. S. P.; Zauner, R.; Wimmer, M.; Wiegand, H.; Andosch, A.; Kasper, G.; Pesch, M.; Lütz-Meindl, U.; Himly, M.; Duschl, A. Enhanced Deposition by Electrostatic Field-Assistance Aggravating Diesel Exhaust Aerosol Toxicity for Human Lung Cells. *Environ. Sci. Technol.* **2015**, *49* (14), 8721–8730 DOI: 10.1021/acs.est.5b02503.

(139) Schroeter, J. D.; Kimbell, J. S.; Bonner, A. M.; Roberts, K. C.; Andersen, M. E.; Dorman, D. C. Incorporation of Tissue Reaction Kinetics in a Computational Fluid Dynamics Model for Nasal Extraction of Inhaled Hydrogen Sulfide in Rats. *Toxicol. Sci.* **2006**, *90* (1), 198–207 DOI: 10.1093/toxsci/kfj072.

(140) Mulhopt, S.; Diabaté, S.; Krebs, T.; Weiss, C.; Paur, H.-R.; Mülhopt, S.; Diabaté, S.; Krebs, T.; Weiss, C.; Paur, H.-R. Lung Toxicity Determination by in Vitro Exposure at the Air Liquid Interface with an Integrated Online Dose Measurement. *J. Phys. Conf. Ser.* **2009**, *170*, 1–4 DOI: 10.1088/1742-6596/170/1/012008.

(141) Desantes, J. M.; Margot, X.; Gil, a.; Fuentes, E. Computational Study on the Deposition of Ultrafine Particles from Diesel Exhaust Aerosol. *J. Aerosol Sci.* **2006**, *37* (12), 1750–1769 DOI: 10.1016/j.jaerosci.2006.07.002.

(142) Chang, E.; Thekkek, N.; Yu, W. W.; Colvin, V. L.; Drezek, R. Evaluation of Quantum Dot Cytotoxicity Based on Intracellular Uptake. *Small* **2006**, *2* (12), 1412–1417 DOI: 10.1002/smll.200600218.

(143) Schaudien, D.; Knebel, J.; Creutzenberg, O. In Vitro Study Revealed Different Size Behavior of Different Nanoparticles. *J. Nanoparticle Res.* **2012**, *14*, 1–9 DOI: 10.1007/s11051-012-1039-6.

(144) Lehmann, A. D.; Daum, N.; Bur, M.; Lehr, C. M.; Gehr, P.; Rothen-Rutishauser, B. An in Vitro Triple Cell Co-Culture Model with Primary Cells Mimicking the Human Alveolar Epithelial Barrier. *Eur. J. Pharm. Biopharm.* **2011**, *77* (3), 398–406 DOI: 10.1016/j.ejpb.2010.10.014.

(145) Hayes, A. J.; Bakand, S. Toxicological Perspectives of Inhaled Therapeutics and Nanoparticles. *Expert Opin. Drug Metab. Toxicol.* **2014**, *10* (7), 933–947.

(146) Hayes, A.; Bakand, S. Inhalation Toxicology. *Mol. Clin. Environ. Toxicol.* **2010**, *100*, 461–488 DOI: 10.1007/978-3-7643-8338-1_13.

(147) Asimakopoulou, A.; Daskalos, M.; Chasapidis, L.; Akritidis, T.; Vlachos, N. D.; Papaioannou, E.; Konstandopoulos, A. G. Characterization of a Multiculture In-Vitro Cell Exposure Chamber for Assessing the Biological Impact of Diesel Engine Exhaust. *J. Phys. Conf. Ser.* **2011**, *304*, 1–9 DOI: 10.1088/1742-6596/304/1/012005.

(148) Adamson, J.; Azzopardi, D.; Errington, G.; Dickens, C.; McAughey, J.; Gaça, M. D. Assessment of an in Vitro Whole Cigarette Smoke Exposure System: The Borgwaldt RM20S 8-Syringe Smoking Machine. *Chem. Cent. J.* **2011**, *5* (1), 50 DOI: 10.1186/1752-153X-5-50.

(149) Schumacher, K.; Strehl, R.; De Vries, U.; Minuth, W. W. Advanced Technique for Long Term Culture of Epithelia in a Continuous Luminal-Basal Medium Gradient. *Biomaterials* **2002**, *23*, 805–815 DOI: 10.1016/S0142-9612(01)00186-7.

(150) Clift, M. J. D.; Gehr, P.; Rothen-Rutishauser, B. State of the Art Toxicological and Microscopic Assessment of Biomedical Nanocrystals on the Lung in Vitro. *Prog. Biomed. Opt. Imaging - Proc. SPIE* **2011**, *7909*, 1–16 DOI: 10.1117/12.875369.

(151) Davies, K. J. The Broad Spectrum of Responses to Oxidants in Proliferating Cells: A New Paradigm for Oxidative Stress. *IUBMB Life* **1999**, *48* (1), 41–47 DOI: 10.1080/713803463.

(152) Jang, M.; Ghio, A. J.; Cao, G. Exposure of BEAS-2B Cells to Secondary Organic Aerosol Coated on Magnetic Nanoparticles. *Chem. Res. Toxicol.* **2006**, *19*, 1044–1050 DOI: 10.1021/tx0503597.

(153) Sellgren, K. L.; Butala, E. J.; Gilmour, B. P.; Randell, S. H.; Grego, S. A Biomimetic Multicellular Model of the Airways Using Primary Human Cells. *Lab Chip* **2014**, 3349–3358 DOI: 10.1039/c4lc00552j.

(154) Stucki, A. O.; Stucki, J. D.; Hall, S. R. R.; Felder, M.; Mermoud, Y.; Schmid, R. A.; Geiser, T.; Guenat, O. T. A Lung-on-a-Chip Array with an Integrated Bio-Inspired Respiration Mechanism. *Lab Chip* **2015**, *15* (5), 1302–1310 DOI: 10.1039/c4lc01252f.

(155) Gernand, J. M.; Casman, E. A. A Meta-Analysis of Carbon Nanotube Pulmonary Toxicity Studies-How Physical Dimensions and Impurities Affect the Toxicity of Carbon Nanotubes. *Risk Anal.* **2014**, *34* (3), 583–597 DOI: 10.1111/risa.12109.

(156) Krug, H. F. Nanosafety Research-Are We on the Right Track? *Angew. Chemie Int. Ed.* **2014**, n/a-n/a DOI: 10.1002/anie.201403367.

(157) Mitchell, L. A.; Gao, J.; Wal, R. Vander; Gigliotti, A.; Burchiel, S. W.; McDonald, J. D. Pulmonary and Systemic Immune Response to Inhaled Multiwalled Carbon Nanotubes. *Toxicol. Sci.* **2007**, *100* (1), 203–214 DOI: 10.1093/toxsci/kfm196.

(158) Ryman-Rasmussen, J. P.; Tewksbury, E. W.; Moss, O. R.; Cesta, M. F.; Wong, B. A.; Bonner, J. C. Inhaled Multiwalled Carbon Nanotubes Potentiate Airway Fibrosis in Murine Allergic Asthma. *Am. J. Respir. Cell Mol. Biol.* **2009**, *40* (3), 349–358 DOI: 10.1165/rcmb.2008-0276OC.

(159) Landsiedel, R.; Ma-Hock, L.; Kroll, A.; Hahn, D.; Schnekenburger, J.; Wiench, K.; Wohlleben, W. Testing Metal-Oxide Nanomaterials for Human Safety. *Adv. Mater.* **2010**, *22* (24), 2601–2627 DOI: 10.1002/adma.200902658.

(160) Kim, J. S.; Sung, J. H.; Song, K. S.; Lee, J. S. J. H.; Kim, S. M.; Lee, G. H.; Ahn, K. H.; Lee, J. S. J. H.; Shin, J. H.; Park, J. D.; Yu, I. J. Persistent DNA Damage Measured by Comet Assay of Sprague Dawley Rat Lung Cells after Five Days of Inhalation Exposure and 1 Month Post-Exposure to Dispersed Multi-Wall Carbon Nanotubes (MWCNTS) Generated by New MWCNT Aerosol Generation System. *Toxicol. Sci.* **2012**, *128* (2), 439–448 DOI: 10.1093/toxsci/kfs161.

(161) Porter, D. W.; Wu, N.; Hubbs, A. F.; Mercer, R. R.; Funk, K.; Meng, F.; Li, J.; Wolfarth, M. G.; Battelli, L.; Friend, S.; Andrew, M.; Hamilton, R.; Sriram, K.; Yang, F.; Castranova, V.; Holian, A. Differential Mouse Pulmonary Dose and Time Course Responses to Titanium Dioxide Nanospheres and Nanobelts. *Toxicol. Sci.* **2013**, *131* (1), 179–193 DOI: 10.1093/toxsci/kfs261.

(162) Xu, J.; Futakuchi, M.; Shimizu, H.; Alexander, D. B.; Yanagihara, K.; Fukamachi, K.; Suzui, M.; Kanno, J.; Hirose, A.; Ogata, A.; Sakamoto, Y.; Nakae, D.; Omori, T.; Tsuda, H. Multi-Walled Carbon Nanotubes Translocate into the Pleural Cavity and Induce Visceral Mesothelial Proliferation in Rats. *Cancer Sci.* **2012**, *103* (12), 2045–2050 DOI: 10.1111/cas.12005.

(163) Mercer, R. R.; Scabilloni, J. F.; Hubbs, A. F.; Battelli, L. a; McKinney, W.; Friend, S.; Wolfarth, M. G.; Andrew, M.; Castranova, V.; Porter, D. W. Distribution and Fibrotic Response Following Inhalation Exposure to Multi-Walled Carbon Nanotubes. *Part. Fibre Toxicol.* **2013**, *10* (1), 33 DOI: 10.1186/1743-8977-10-33.

(164) Treumann, S.; Ma-Hock, L.; Gr??ters, S.; Landsiedel, R.; van Ravenzwaay, B. Additional Histopathologic Examination of the Lungs from a 3-Month Inhalation Toxicity Study with Multiwall Carbon Nanotubes in Rats. *Toxicol. Sci.* **2013**, *134* (1), 103–110 DOI: 10.1093/toxsci/kft089.

(165) Umeda, Y.; Kasai, T.; Saito, M.; Kondo, H.; Toya, T.; Aiso, S.; Okuda, H.; Nishizawa, T.; Fukushima, S. Two-Week Toxicity of Multi-Walled Carbon Nanotubes by Whole-Body

Inhalation Exposure in Rats. *J Toxicol Pathol* **2013**, *26* (2), 131–140 DOI: 10.1293/tox.26.131.

(166) Kasai, T.; Gotoh, K.; Nishizawa, T.; Sasaki, T.; Katagiri, T.; Umeda, Y.; Toya, T.; Fukushima, S. Development of a New Multi-Walled Carbon Nanotube (MWCNT) Aerosol Generation and Exposure System and Confirmation of Suitability for Conducting a Single-Exposure Inhalation Study of MWCNT in Rats. *Nanotoxicology* **2014**, *8* (2), 169–178 DOI: 10.3109/17435390.2013.766277.

(167) Kim, J. S.; Sung, J. H.; Choi, B. G.; Ryu, H. Y.; Song, K. S.; Shin, J. H.; Lee, J. S.; Hwang, J. H.; Lee, J. H.; Lee, G. H.; Jeon, K.; Ahn, K. H.; Yu, I. J. In Vivo Genotoxicity Evaluation of Lung Cells from Fischer 344 Rats Following 28 Days of Inhalation Exposure to MWCNTs, plus 28 Days and 90 Days Post-Exposure. *Inhal. Toxicol.* **2014**, *26* (April 2016), 222–234 DOI: 10.3109/08958378.2013.878006.

(168) Kasai, T.; Umeda, Y.; Ohnishi, M.; Kondo, H.; Takeuchi, T.; Aiso, S.; Nishizawa, T.; Matsumoto, M.; Fukushima, S. Thirteen-Week Study of Toxicity of Fiber-like Multi-Walled Carbon Nanotubes with Whole-Body Inhalation Exposure in Rats. *Nanotoxicology* **2015**, *9* (4), 1–10 DOI: 10.3109/17435390.2014.933903.

(169) Baggs, R. B.; Ferin, J.; Oberdörster, G. Regression of Pulmonary Lesions Produced by Inhaled Titanium Dioxide in Rats. *Vet Pathol* **1997**, *34*, 592–597.

(170) Kapp, N.; Kreyling, W.; Schulz, H.; Im Hof, V.; Gehr, P.; Semmler, M.; Geiser, M. Electron Energy Loss Spectroscopy for Analysis of Inhaled Ultrafine Particles in Rat Lungs. *Microsc. Res. Tech.* **2004**, *63* (5), 298–305 DOI: 10.1002/jemt.20044.

(171) Geiser, M.; Rothen-Rutishauser, B.; Kapp, N.; Sch??rch, S.; Kreyling, W.; Schulz, H.; Semmler, M.; Im Hof, V.; Heyder, J.; Gehr, P. Ultrafine Particles Cross Cellular Membranes by Nonphagocytic Mechanisms in Lungs and in Cultured Cells. *Environ. Health Perspect.* **2005**, *113* (11), 1555–1560 DOI: 10.1289/ehp.8006.

(172) Ferin, J.; Oberdörster, G.; Penney, D. P. Pulmonary Retention of Ultrafine and Fine Particles in Rats. *Am. J. Respir. Cell Mol. Biol.* **1992**, *6* (5), 535–542 DOI: 10.1165/ajrcmb/6.5.535.

(173) Oberdorster, G.; Ferin, J.; Lehnert, B. E. Correlation between Particle Size, in Vivo Particle Persistence, and Lung Injury. *Environ. Health Perspect.* **1994**, *102* (SUPPL. 5), 173–179 DOI: 10.1289/ehp.94102s5173.

(174) Grassian, V. H.; O'Shaughnessy, P. T.; Adamcakova-Dodd, A.; Pettibone, J. M.; Thorne, P. S. Inhalation Exposure Study of Titanium Dioxide Nanoparticles with a Primary Particle Size of 2 to 5 Nm. *Environ. Health Perspect.* **2007**, *115* (3), 397–402 DOI: 10.1289/ehp.9469.

(175) Grassian, V. H.; Adamcakova-Dodd, A.; Pettibone, J. M.; O'shaughnessy, P. I.; Thorne, P. S. Inflammatory Response of Mice to Manufactured Titanium Dioxide Nanoparticles: Comparison of Size Effects through Different Exposure Routes. *Nanotoxicology* **2007**, *1* (3), 211–226 DOI: 10.1080/17435390701694295.

(176) Heinrich, U.; Fuhst, R.; Rittinghausen, S.; Creutzenberg, O.; B, B.; Koch, W.; Levsen, K.

Chronic Inhalation Exposure of Wistar Rats and Two Different Strains of Mice to Diesel Engine Exhaust, Carbon Black, and Titanium Dioxide. *Inhal. Toxicol.* **1995**, *7* (4), 533–556 DOI: doi.org/10.3109/08958379509015211.

(177) Oosthuizen, M. A.; Oberholzer, H. M.; Scriba, M. R.; van der Spuy, W. J.; Pretorius, E. Evaluation of the Morphological Changes in the Lungs of BALB/c Mice after Inhalation of Spherical and Rod-Shaped Titanium Nanoparticles. *Micron* **2012**, *43* (8), 863–869 DOI: 10.1016/j.micron.2012.02.003.

(178) Lee, J. F.; Tung, S. P.; Wang, D.; Yeh, D. Y.; Fong, Y.; Young, Y. C.; Leu, F. J. Lipoxygenase Pathway Mediates Increases of Airway Resistance and Lung Inflation Induced by Exposure to Nanotitanium Dioxide in Rats. *Oxid. Med. Cell. Longev.* **2014**, *2014* DOI: 10.1155/2014/485604.

(179) Warheit, D. B.; Sayes, C. M.; Reed, K. L. Nanoscale and Fine Zinc Oxide Particles: Can in Vitro Assays Accurately Forecast Lung Hazards Following Inhalation Exposures? *Environ. Sci. Technol.* **2009**, *43* (20), 7939–7945 DOI: 10.1021/es901453p.

(180) Ho, M.; Wu, K.-Y.; Chein, H.-M.; Chen, L.-C.; Cheng, T.-J. Pulmonary Toxicity of Inhaled Nanoscale and Fine Zinc Oxide Particles: Mass and Surface Area as an Exposure Metric. *Inhal. Toxicol.* **2011**, *23* (17), 947–956 DOI: 10.3109/08958378.2011.629235.

(181) Ma-Hock, L.; Treumann, S.; Strauss, V.; Brill, S.; Luizi, F.; Mertler, M.; Wiench, K.; Gamer, A. O.; van Ravenzwaay, B.; Landsiedel, R. Inhalation Toxicity of Multiwall Carbon Nanotubes in Rats Exposed for 3 Months. *Toxicol. Sci.* **2009**, *112* (2), 468–481 DOI: 10.1093/toxsci/kfp146.

(182) Porter, D. W.; Hubbs, A. F.; Chen, B. T.; McKinney, W.; Mercer, R. R.; Wolfarth, M. G.; Battelli, L.; Wu, N.; Sriram, K.; Leonard, S.; Andrew, M.; Willard, P.; Tsuruoka, S.; Endo, M.; Tsukada, T.; Munekane, F.; Frazer, D. G.; Castranova, V. Acute Pulmonary Dose-Responses to Inhaled Multi-Walled Carbon Nanotubes. *Nanotoxicology* **2013**, *54* (7), 1179–1194 DOI: 10.1021/acs.biochem.5b00087.

(183) Delorme, M. P.; Muro, Y.; Arai, T.; Banas, D. A.; Frame, S. R.; Reed, K. L.; Warheit, D. B. Ninety-Day Inhalation Toxicity Study with a Vapor Grown Carbon Nanofiber in Rats. *Toxicol. Sci.* **2012**, *128* (2), 449–460 DOI: 10.1093/toxsci/kfs172.

(184) Stapleton, P. A.; Minarchick, V. C.; Cumpston, A. M.; McKinney, W.; Chen, B. T.; Sager, T. M.; Frazer, D. G.; Mercer, R. R.; Scabilloni, J.; Andrew, M. E.; Castranova, V.; Nurkiewicz, T. R. Impairment of Coronary Arteriolar Endothelium-Dependent Dilation after Multi-Walled Carbon Nanotube Inhalation: A Time-Course Study. *Int. J. Mol. Sci.* **2012**, *13* (11), 13781–13803 DOI: 10.3390/ijms131113781.

(185) Rosslein, M.; Elliott, J. T.; Salit, M.; Petersen, E. J.; Hirsch, C.; Krug, H. F.; Wick, P. Use of Cause-and-Effect Analysis to Design a High-Quality Nanocytotoxicology Assay. *Chem. Res. Toxicol.* **2014**, *28*, 21–30.

(186) Toman, B.; Rösslein, M.; Elliott, J. T.; Petersen, E. J. Estimation and Uncertainty Analysis of Dose Response in an Inter-Laboratory Experiment. *Metrologia* **2016**, *53* (1), S40–S45 DOI: 10.1088/0026-1394/53/1/S40.

(187) Lewinski, N. A.; Secondo, L. E.; Ferri, J. K. Enabling Real-Time Hazard Assessment at the Workplace Enabling Real-Time Hazard Assessment at the Workplace. In *14th Global Congress on Process Safety*; American Institute of Chemical Engineers: Orlando, 2018; pp 1–9.

(188) Bakand, S.; Winder, C.; Khalil, C.; Hayes, A. Toxicity Assessment of Industrial Chemicals and Airborne Contaminants: Transition from in Vivo to in Vitro Test Methods: A Review. *Inhal. Toxicol.* **2005**, *17*, 775–787 DOI: 10.1080/08958370500225240.

(189) Frijns, E.; Verstraelen, S.; Stoehr, L. C.; Van Laer, J.; Jacobs, A.; Peters, J.; Tirez, K.; Boyles, M. S. P.; Geppert, M.; Madl, P.; Nelissen, I.; Duschl, A.; Himly, M. A Novel Exposure System Termed NAVETTA for in Vitro Laminar Flow Electrodeposition of Nanoaerosol and Evaluation of Immune Effects in Human Lung Reporter Cells. *Environ. Sci. Technol.* **2017**, *51* (9), 5259–5269 DOI: 10.1021/acs.est.7b00493.

(190) Vincent, J. H. *Aerosol Science for Industrial Hygienists*; Elsevier, 1995.

(191) *Aerosols Handbook Measurement, Dosimetry, and Health Effects*; Ruzer, L. S., Harley, N. H., Eds.; CRC Press: Boca Raton, 2005.

(192) Cho, W. S.; Duffin, R.; Poland, C. A.; Duschl, A.; Oostingh, G. J.; MacNee, W.; Bradley, M.; Megson, I. L.; Donaldson, K. Differential Pro-Inflammatory Effects of Metal Oxide Nanoparticles and Their Soluble Ions in Vitro and in Vivo; Zinc and Copper Nanoparticles, but Not Their Ions, Recruit Eosinophils to the Lungs. *Nanotoxicology* **2012**, *6* (1), 22–35 DOI: 10.3109/17435390.2011.552810.

(193) Maier, K. L.; Alessandrini, F.; Beck-Speier, I.; Hofer, T. P. J.; Diabaté, S.; Bitterle, E.; Stöger, T.; Jakob, T.; Behrendt, H.; Horsch, M.; Beckers, J.; Ziesenis, A.; Hültner, L.; Frankenberger, M.; Krauss-Etschmann, S.; Schulz, H. Health Effects of Ambient Particulate Matter--Biological Mechanisms and Inflammatory Responses to in Vitro and in Vivo Particle Exposures. *Inhal. Toxicol.* **2008**, *20* (May 2007), 319–337 DOI: 10.1080/08958370701866313.

(194) Seagrave, J.; McDonald, J. D.; Mauderly, J. L. In Vitro versus in Vivo Exposure to Combustion Emissions. *Exp. Toxicol. Pathol.* **2005**, *57*, 233–238 DOI: 10.1016/j.etp.2005.05.011.

(195) Sanderson, P.; Su, S. S.; Chang, I. T. H.; Delgado Saborit, J. M.; Kepaptsoglou, D. M.; Weber, R. J. M.; Harrison, R. M. Characterisation of Iron-Rich Atmospheric Submicrometre Particles in the Roadside Environment. *Atmos. Environ.* **2016**, *140*, 167–175 DOI: 10.1016/j.atmosenv.2016.05.040.

(196) Zavala, J.; Obrien, B.; Lichtveld, K.; Sexton, K. G.; Rusyn, I.; Jaspers, I.; Vizuete, W. Assessment of Biological Responses of EpiAirway 3-D Cell Constructs versus A549 Cells for Determining Toxicity of Ambient Air Pollution. *Inhal. Toxicol.* **2016**, *28* (6) DOI: 10.3109/08958378.2016.1157227.

(197) Elder, A.; Couderc, J.-P.; Gelein, R.; Eberly, S.; Cox, C.; Xia, X.; Zareba, W.; Hopke, P.; Watts, W.; Kittelson, D.; Frampton, M.; Utell, M.; Oberdörster, G. Effects of On-Road Highway Aerosol Exposures on Autonomic Responses in Aged, Spontaneously Hypertensive Rats. *Inhal. Toxicol.* **2007**, *19* (1), 1–12 DOI: 10.1080/08958370701490262.

(198) Burtscher, H. Physical Characterization of Particulate Emissions from Diesel Engines: A Review. *J. Aerosol Sci.* **2005**, *36* (7), 896–932 DOI: 10.1016/j.jaerosci.2004.12.001.

(199) Cho, S. H.; Tong, H.; McGee, J. K.; Baldauf, R. W.; Krantz, Q. T.; Gilmour, M. I. Comparative Toxicity of Size-Fractionated Airborne Particulate Matter Collected at Different Distances from an Urban Highway. *Environ. Health Perspect.* **2009**, *117* (11), 1682–1689 DOI: 10.1289/ehp.0900730.

(200) Greenwood-Smith, B.; Sadleir, B.; Durrheim, D. N.; M., G. J.; Braack, L. E. O.; Gericke, A.; Speare, R.; Canyon, D.; Tindall, H. J.; Raw, L.; Overton, M.; Muller, R.; Boyle, S.; Low, S.; Taylor, V.; Melrose, W.; Harrison, S. *Rural and Remote Health I*; Australasian College of Tropical Medicine Publications, 2001.

(201) Ris, C. U.S. EPA Health Assessment for Diesel Engine Exhaust: A Review. *Inhal. Toxicol.* **2007**, *19* (Suppl. 1), 229–239 DOI: 10.1080/08958370701497960.

(202) Im Hof, V.; Patrick, G. Particle Retention and Clearance. *J. Aerosol Med.* **1994**, *7* (1), 39–47.

(203) Kreyling, W. G.; Semmler-Behnke, M.; M??ller, W. Health Implications of Nanoparticles. *J. Nanoparticle Res.* **2006**, *8* (5), 543–562 DOI: 10.1007/s11051-005-9068-z.

(204) Wiemann, M.; Vennemann, A.; Sauer, U. G.; Wiench, K.; Ma-Hock, L.; Landsiedel, R. An in Vitro Alveolar Macrophage Assay for Predicting the Short-Term Inhalation Toxicity of Nanomaterials. *J. Nanobiotechnology* **2016**, *14* (1), 16 DOI: 10.1186/s12951-016-0164-2.

(205) Kenny, L. C.; Aitken, R.; Chalmers, C.; Fabriès, J. F.; Gonzalez-Fernandez, E.; Kromhout, H.; Lidén, G.; Mark, D.; Riediger, G.; Prodi, V. A Collaborative European Study of Personal Inhalable Aerosol Sampler Performance. *Ann. Occup. Hyg.* **1997**, *41* (2), 135–153 DOI: 10.1016/S0003-4878(96)00034-8.

(206) Liu, G.; Li, X.; Qin, B.; Xing, D.; Guo, Y.; Fan, R. Investigation of the Mending Effect and Mechanism of Copper Nano-Particles on a Tribologically Stressed Surface. *Tribol. Lett.* **2004**, *17* (4), 961–966.

(207) Aruoja, V.; Dubourguier, H.-C.; Kasemets, K.; Kahru, A. Toxicity of Nanoparticles of CuO, ZnO and TiO 2 to Microalgae Pseudokirchneriella Subcapitata. **2008** DOI: 10.1016/j.scitotenv.2008.10.053.

(208) Wang, H.; Huang, Y.; Tan, Z.; Hu, X. Fabrication and Characterization of Copper Nanoparticle Thin-Films and the Electrocatalytic Behavior. *Anal. Chim. Acta* **2004**, *526*, 13–17 DOI: 10.1016/j.aca.2004.08.060.

(209) Farsalinos, K. E.; Voudris, V.; Poulas, K. Are Metals Emitted from Electronic Cigarettes a Reason for Health Concern? A Risk-Assessment Analysis of Currently Available Literature. *Int. J. Environ. Res. Public Heal.* **2015**, *12*, 5215–5232 DOI: 10.3390/ijerph120505215.

(210) Armstrong, C.; Moore, L. J.; Hackler, R.; Miller, G. J.; Stroube, R. An Outbreak of Metal Fume Fever. Diagnostic Use of Urinary Copper and Zinc Determinations. *J. Occup. Med.* **1983**, *25* (12), 886–888.

(211) Peoples, S.; McCarthy, J.; Chen, L.; Eppelsheimer, D.; Amdur, M. Copper Oxide Aerosol: Generation and Characterization. *Am. Ind. Hygeine Assoc.* **1988**, *49* (6), 271–276.

(212) Protection, I. C. on R. Human Respiratory Model for Radiological Protection. *Ann ICRP* **1994**, *24*, 1–300.

(213) Marple, V. a.; Willeke, K. *Inertial Impactors: Theory, Design and Use*; ACADEMIC PRESS, INC., 1976.

(214) Aufderheide, M.; Ritter, D.; Knebel, J. W.; Scherer, G. A Method for in Vitro Analysis of the Biological Activity of Complex Mixtures Such as Sidestream Cigarette Smoke. *Exp. Toxicol. Pathol.* **2001**, *53* (2–3), 141–152.

(215) Hebisch, R.; Frick, H.-H.; Hahn, J.-U.; Lahaniatis, M.; Maschmeier, C.-P.; Mattenklott, M. *Part III: Air Monitoring Methods*; Wiley, 2005; Vol. 9.

(216) Desantes, J. M.; Payri, R.; Salvador, F. J.; Gil, a. Development and Validation of a Theoretical Model for Diesel Spray Penetration. *Fuel* **2006**, *85* (7–8), 910–917 DOI: 10.1016/j.fuel.2005.10.023.

(217) Marple, V. a. *History of Impactors—The First 110 Years*; 2004; Vol. 38.

(218) Marple, V. a; Roberts, D. L.; Romay, F. J.; Miller, N. C.; Truman, K. G.; Van Oort, M.; Olsson, B.; Holroyd, M. J.; Mitchell, J. P.; Hochrainer, D. Next Generation Pharmaceutical Impactor (a New Impactor for Pharmaceutical Inhaler Testing). Part I: Design. *J. Aerosol Med.* **2003**, *16* (3), 283–299 DOI: 10.1089/089426803769017659.

(219) Lucci, F.; Castro, N. D.; Rostami, A. A.; Oldham, M. J.; Hoeng, J.; Pithawalla, Y. B.; Kuczaj, A. K. Characterization and Modeling of Aerosol Deposition in Vitrocell® Exposure Systems - Exposure Well Chamber Deposition Efficiency. *J. Aerosol Sci.* **2018**, *123* (March), 141–160 DOI: 10.1016/j.jaerosci.2018.06.015.

(220) Hinds, W. C. *Aerosol Technology Properties, Behavior, and Measurement of Airborne Particles*; John Wiley & Sons: New York, 1982.

(221) Secondo, L. E.; Liu, N. J.; Lewinski, N. A. Methodological Considerations When Conducting in Vitro, Air–liquid Interface Exposures to Engineered Nanoparticle Aerosols. *Crit. Rev. Toxicol.* **2017**, *47* (3), 225–262 DOI: 10.1080/10408444.2016.1223015.

(222) Tiwari, A. J.; Fields, C. G.; Marr, L. C. A Cost-Effective Method of Aerosolizing Dry Powdered Nanoparticles. *Aerosol Sci. Technol.* **2013**, *47* (11), 1267–1275 DOI: 10.1080/02786826.2013.834292.

(223) Lieber, M.; Smith, B.; Szakal, A.; Nelson-Rees, W.; Todaro, G. A Continuous Tumor-Cell Line from a Human Lung Carcinoma with Properties of Type II Alveolar Epithelial Cells. *Int. J. Cancer* **1976**, *17* (1), 62–70 DOI: 10.1002/ijc.2910170110.

(224) Blank, F.; Rothen-Rutishauser, B. M.; Schurch, S.; Gehr, P. An Optimized In Vitro Model of the Respiratory Tract Wall to Study Particle Cell Interactions. *J. Aerosol Med.* **2006**, *19* (3), 392–405.

(225) Decker, T.; Lohmann-Matthes, M. L. A Quick and Simple Method for the Quantification

of Lactate Dehydrogenase Release in Measurements of Cellular Cytotoxicity and Tumor Necrosis Factor (TNF) Activity. *J. Immunol. Methods* **1988**, *151*, 61–69.

(226) Chan, F. K.-M.; Moriwaki, K.; De Rosa, M. J. Detection of Necrosis by Release of Lactate Dehydrogenase (LDH) Activity. *Methods Mol Biol* **2013**, *979*, 65–70 DOI: 10.1007/978-1-62703-290-2.

(227) Carter, W. O.; Narayanan, P. K.; Robinson, J. P. Intracellular Hydrogen Peroxide and Superoxide Anion Detection in Endothelial Cells. *J. Leukoc. Biol.* **1994**, *55* (2), 253–258.

(228) Zavala, J.; Greenan, R.; Krantz, Q. T.; DeMarini, D. M.; Higuchi, M.; Gilmour, M. I.; White, P. A. Regulating Temperature and Relative Humidity in Air–liquid Interface in Vitro Systems Eliminates Cytotoxicity Resulting from Control Air Exposures. *Toxicol. Res. (Camb).* **2017**, *6*, 448–459 DOI: 10.1039/C7TX00109F.

(229) Cronholm, P.; Karlsson, H. L.; Hedberg, J.; Lowe, T. A.; Winnberg, L.; Elihn, K.; Wallinder, I. O.; Möller, L. Intracellular Uptake and Toxicity of Ag and CuO Nanoparticles: A Comparison between Nanoparticles and Their Corresponding Metal Ions. *Small* **2013**, *9* (7), 970–982 DOI: 10.1002/smll.201201069.

(230) Cronholm, P.; Midander, K.; Karlsson, H. L.; Elihn, K.; Wallinder, I. O.; Möller, L. Effect of Sonication and Serum Proteins on Copper Release from Copper Nanoparticles and the Toxicity towards Lung Epithelial Cells. *Nanotoxicology* **2011**, *5* (2), 269–281 DOI: 10.3109/17435390.2010.536268.

(231) Midander, K.; Cronholm, P.; Karlsson, H. L.; Elihn, K.; Möller, L.; Leygraf, C.; Wallinder, I. O. Surface Characteristics, Copper Release, and Toxicity of Nano- and Micrometer-Sized Copper and Copper(Ll) Oxide Particles: A Cross-Disciplinary Study. *Small* **2009**, *5* (3), 389–399 DOI: 10.1002/smll.200801220.

(232) Lanone, S.; Rogerieux, F.; Geys, J.; Dupont, A.; Maillot-Marechal, E.; Boczkowski, J.; Lacroix, G.; Hoet, P. Comparative Toxicity of 24 Manufactured Nanoparticles in Human Alveolar Epithelial and Macrophage Cell Lines. *Part. Fibre Toxicol.* **2009**, *6*, 1–12 DOI: 10.1186/1743-8977-6-14.

(233) Karlsson, H. L.; Cronholm, P.; Hedberg, Y.; Tornberg, M.; De Battice, L.; Svedhem, S.; Wallinder, I. O. Cell Membrane Damage and Protein Interaction Induced by Copper Containing Nanoparticles-Importance of the Metal Release Process. *Toxicology* **2013**, *313* (1), 59–69 DOI: 10.1016/j.tox.2013.07.012.

(234) Karlsson, H. L.; Cronholm, P.; Gustafsson, J.; Moeller, L. Copper Oxide Nanoparticles Are Highly Toxic: A Comparison between Metal Oxide Nanoparticles and Carbon Nanotubes. *Chem. Res. Toxicol.* **2008**, *21* (9), 1726–1732 DOI: 10.1021/tx800064j.

(235) Rani, V. S.; Kumar, A. K.; Kumar, P. C.; Reddy, A. R. N. Pulmonary Toxicity of Copper Oxide (CuO) Nanoparticles in Rats. *Journal of Medical Sciences*. 2013, pp 571–577.

(236) Lai, X.; Zhao, H.; Zhang, Y.; Guo, K.; Xu, Y.; Chen, S.; Zhang, J. Intranasal Delivery of Copper Oxide Nanoparticles Induces Pulmonary Toxicity and Fibrosis in C57BL/6 Mice. *Sci. Rep.* **2018**, *8* (1), 1–12 DOI: 10.1038/s41598-018-22556-7.

(237) Pettibone, J. M.; Adamcakova-Dodd, A.; Thorne, P. S.; O'Shaughnessy, P. T.; Weydert, J.

A.; Grassian, V. H. Inflammatory Response of Mice Following Inhalation Exposure to Iron and Copper Nanoparticles. *Nanotoxicology* **2008**, *2* (4), 189–204 DOI: 10.1080/17435390802398291.

(238) Gosens, I.; Cassee, F. R.; Zanella, M.; Manodori, L.; Brunelli, A.; Costa, A. L.; Bokkers, B. G. H.; de Jong, W. H.; Brown, D.; Hristozov, D.; Stone, V. Organ Burden and Pulmonary Toxicity of Nano-Sized Copper (II) Oxide Particles after Short-Term Inhalation Exposure. *Nanotoxicology* **2016**, *10* (8), 1084–1095 DOI: 10.3109/17435390.2016.1172678.

(239) Kim, J. S.; Adamcakova-Dodd, A.; O'Shaughnessy, P. T.; Grassian, V. H.; Thorne, P. S. Effects of Copper Nanoparticle Exposure on Host Defense in a Murine Pulmonary Infection Model. *Part. Fibre Toxicol.* **2011**, *8*, 1–14 DOI: 10.1186/1743-8977-8-29.

(240) Fahmy, B.; Cormier, S. A. Copper Oxide Nanoparticles Induce Oxidative Stress and Cytotoxicity in Airway Epithelial Cells. *Toxicol. Vitr.* **2009**, *23* (7), 1365–1371 DOI: 10.1016/j.tiv.2009.08.005.

(241) Karlsson, H. L.; Gustafsson, J.; Cronholm, P.; Möller, L. Size-Dependent Toxicity of Metal Oxide Particles-A Comparison between Nano- and Micrometer Size. *Toxicol. Lett.* **2009**, *188* (2), 112–118 DOI: 10.1016/j.toxlet.2009.03.014.

(242) Ahamed, M.; Siddiqui, M. A.; Akhtar, M. J.; Ahmad, I.; Pant, A. B.; Alhadlaq, H. A. Genotoxic Potential of Copper Oxide Nanoparticles in Human Lung Epithelial Cells. *Biochem. Biophys. Res. Commun.* **2010**, *396* (2), 578–583 DOI: 10.1016/j.bbrc.2010.04.156.

(243) Akhtar, M. J.; Kumar, S.; Alhadlaq, H. a; Alrokayan, S. a; Abu-Salah, K. M.; Ahamed, M. Dose-Dependent Genotoxicity of Copper Oxide Nanoparticles Stimulated by Reactive Oxygen Species in Human Lung Epithelial Cells. *Toxicol. Ind. Health* **2013**, *32* (5), 809–821 DOI: 10.1177/0748233713511512.

(244) Cho, W.-S.; Duffin, R.; Bradley, M.; Megson, I. L.; Macnee, W.; Lee, J. K.; Jeong, J.; Donaldson, K. Predictive Value of in Vitro Assays Depends on the Mechanism of Toxicity of Metal Oxide Nanoparticles. *Part. Fibre Toxicol.* **2013**, *10* (1), 55 DOI: 10.1186/1743-8977-10-55.

(245) Ivask, A.; Titma, T.; Visnapuu, M.; Vija, H.; Kakinen, A.; Sihtmae, M.; Pokhrel, S.; Madler, L.; Heinlaan, M.; Kisand, V.; Shimmo, R.; Kahru, A. Toxicity of 11 Metal Oxide Nanoparticles to Three Mammalian Cell Types In V.Itro. *Curr. Top. Med. Chem.* **2015**, *15* (18), 1914–1929 DOI: 10.2174/1568026615666150506150109.

(246) Akhtar, M. J.; Kumar, S.; Alhadlaq, H. A.; Alrokayan, S. A.; Abu-Salah, K. M.; Ahamed, M. Dose-Dependent Genotoxicity of Copper Oxide Nanoparticles Stimulated by Reactive Oxygen Species in Human Lung Epithelial Cells. *Toxicol. Ind. Health* **2016**, *32* (5), 809–821 DOI: 10.1177/0748233713511512.

(247) Wongrakpanich, A.; Mudunkotuwa, I. A.; Geary, S. M.; Angie, S.; Mapuskar, K. A.; Spitz, D. R.; Grassian, V. H.; Aliasger, K.; Therapeutics, E.; States, U.; States, U.; Jolla, L. Size-Dependent Cytotoxicity of Copper Oxide Nanoparticles in Lung Epithelial Cells. *Nano* **2017**, *3* (2), 365–374 DOI: 10.1039/C5EN00271K.Size-dependent.

(248) Strauch, B. M.; Niemand, R. K.; Winkelbeiner, N. L.; Hartwig, A. Comparison between Micro- and Nanosized Copper Oxide and Water Soluble Copper Chloride: Interrelationship between Intracellular Copper Concentrations, Oxidative Stress and DNA Damage Response in Human Lung Cells. *Part. Fibre Toxicol.* **2017**, *14* (1), 28 DOI: 10.1186/s12989-017-0209-1.

(249) Chen, Z.; Meng, H.; Xing, G.; Chen, C.; Zhao, Y.; Jia, G.; Wang, T.; Yuan, H.; Ye, C.; Zhao, F.; Chai, Z.; Zhu, C.; Fang, X.; Ma, B.; Wan, L. Acute Toxicological Effects of Copper Nanoparticles in Vivo. *Toxicol. Lett.* **2006**, *163* (2), 109–120 DOI: 10.1016/j.toxlet.2005.10.003.

(250) Meng, H.; Chen, Z.; Xing, G.; Yuan, H.; Chen, C.; Zhao, F.; Zhang, C.; Wang, Y.; Zhao, Y. Ultrahigh Reactivity and Grave Nanotoxicity of Copper Nanoparticles. *J. Radioanal. Nucl. Chem.* **2007**, *272* (3), 595–598 DOI: 10.1007/s10967-007-0630-2.

(251) Cho, W. S.; Duffn, R.; Poland, C. A.; Howie, S. E. M.; Macnee, W.; Bradley, M.; Megson, I. L.; Donaldson, K. Metal Oxide Nanoparticles Induce Unique Infammatory Footprints in the Lung: Important Implications for Nanoparticle Testing. *Environ. Health Perspect.* **2010**, *118* (12), 1699–1706 DOI: 10.1289/ehp.1002201.

(252) Privalova, L. I.; Katsnelson, B. A.; Loginova, N. V.; Gurvich, V. B.; Shur, V. Y.; Beikin, Y. B.; Sutunkova, M. P.; Minigalieva, I. A.; Shishkina, E. V.; Pichugova, S. V.; Tulakina, L. G.; Beljayeva, S. V. Some Characteristics of Free Cell Population in the Airways of Rats after Intratracheal Instillation of Copper-Containing Nano-Scale Particles. *Int. J. Mol. Sci.* **2014**, *15* (11), 21538–21553 DOI: 10.3390/ijms151121538.

(253) Lu, X.; Miousse, I. R.; Pirela, S. V.; Moore, J. K.; Melnyk, S.; Koturbash, I.; Demokritou, P. In Vivo Epigenetic Effects Induced by Engineered Nanomaterials: A Case Study of Copper Oxide and Laser Printer-Emitted Engineered Nanoparticles. *Nanotoxicology* **2016**, *10* (5), 629–639 DOI: 10.1016/j.antiviral.2015.06.014.Chronic.

(254) Laboratory, N. C. NCL Method GTA-2 HEP G2 Hepatocarcinoma Cytotoxicity Assay. 2015, pp 1–9.

(255) Gorr, M. W.; Youtz, D. J.; Eichenseer, C. M.; Smith, K. E.; Nelin, T. D.; Cormet-Boyaka, E.; Wold, L. E. In Vitro Particulate Matter Exposure Causes Direct and Lung-Mediated Indirect Effects on Cardiomyocyte Function. *Am. J. Physiol. Heart Circ. Physiol.* **2015**, *309* (1), H53-62 DOI: 10.1152/ajpheart.00162.2015.

(256) Brook, R. D.; Franklin, B.; Cascio, W.; Hong, Y.; Howard, G.; Lipsett, M.; Luepker, R.; Mittleman, M.; Samet, J.; Smith, S. C.; Tager, I. Air Pollution and Cardiovascular Disease: A Statement for Healthcare Professionals from the Expert Panel on Population and Prevention Science of the American Heart Association. *Circulation* **2004**, *109* (71), 2655–2671 DOI: 10.1161/01.CIR.0000128587.30041.C8.

(257) Patel, M. M.; Chillrud, S. N.; Correa, J. C.; Hazi, Y.; Feinberg, M.; Deepti, K.; Prakash, S.; Ross, J. M.; Levy, D.; Kinney, P. L. Traffic-Related Particulate Matter and Acute Respiratory Symptoms among New York City Area Adolescents. *Environ. Health Perspect.* **2010**, *118* (9), 1338–1343 DOI: 10.1289/ehp.0901499.

(258) Pope III, C. A.; Burnett, R. T.; Thun, M. J.; Calle, E. E.; Krewski, D.; Ito, K.; Thurston, G.

D. Lung Cancer, Cardiopulmonary Mortality, and Long-Term Exposure to Fine Particulate Air Pollution. *JAMA* **2002**, *287* (9), 1132–1141.

(259) Oeder, S.; Kanashova, T.; Sippula, O.; Sapcariu, S. C.; Streibel, T.; Arteaga-Salas, J. M.; Passig, J.; Dilger, M.; Paur, H.-R.; Schlager, C.; Mülhopt, S.; Diabaté, S.; Weiss, C.; Stengel, B.; Rabe, R.; Harndorf, H.; Torvela, T.; Jokiniemi, J. K.; Hirvonen, M.-R.; Schmidt-Weber, C.; Traidl-Hoffmann, C.; BéruBé, K. A.; Wlodarczyk, A. J.; Prytherch, Z.; Michalke, B.; Krebs, T.; Prévôt, A. S. H.; Kelbg, M.; Tiggesbäumker, J.; Karg, E.; Jakobi, G.; Scholtes, S.; Schnelle-Kreis, J.; Lintelmann, J.; Matuschek, G.; Sklorz, M.; Klingbeil, S.; Orasche, J.; Richthammer, P.; Müller, L.; Elsasser, M.; Reda, A.; Gröger, T.; Weggler, B.; Schwemer, T.; Czech, H.; Rüger, C. P.; Abbaszade, G.; Radischat, C.; Hiller, K.; Buters, J. T. M.; Dittmar, G.; Zimmermann, R. Particulate Matter from Both Heavy Fuel Oil and Diesel Fuel Shipping Emissions Show Strong Biological Effects on Human Lung Cells at Realistic and Comparable In Vitro Exposure Conditions. *PLoS One* **2015**, *10* (6), e0126536 DOI: 10.1371/journal.pone.0126536.

(260) Konstandopoulos, A. G.; Papaioannou, E. Update on The Science and Technology of Diesel Particulate Filters. *KONA Powder Part. J.* **2008**, *26* (26), 36–65 DOI: 10.14356/kona.2008007.

(261) Tandon, P.; Heibel, A.; Whitmore, J.; Kekre, N.; Chithapragada, K. Measurement and Prediction of Filtration Efficiency Evolution of Soot Loaded Diesel Particulate Filters. *Chem. Eng. Sci.* **2010**, *65* (16), 4751–4760 DOI: 10.1016/j.ces.2010.05.020.

(262) Adler, J. Ceramic Diesel Particulate Filters. *Int. J. Appl. Ceram. Technol.* **2005**, *2* (6), 429–439 DOI: 10.1111/j.1744-7402.2005.02044.x.

(263) Van Setten, B.; Makkee, M.; Moulijn, J. Science and Technology of Catalytic Diesel Particulate Filters. *Catal. Rev.* **2001**, *43* (4), 489–564 DOI: 10.1081/CR-120001810.

(264) Kumar, P. A.; Tanwar, M. D.; Bensaid, S.; Russo, N.; Fino, D. Soot Combustion Improvement in Diesel Particulate Filters Catalyzed with Ceria Nanofibers. *Chem. Eng. J.* **2012**, *207–208*, 258–266 DOI: 10.1016/j.cej.2012.06.096.

(265) Gantt, B.; Hoque, S.; Willis, R. D.; Fahey, K. M.; Delgado-Saborit, J. M.; Harrison, R. M.; Erdakos, G. B.; Bhave, P. V.; Zhang, K. M.; Kovalcik, K.; Pye, H. O. T. Near-Road Modeling and Measurement of Cerium-Containing Particles Generated by Nanoparticle Diesel Fuel Additive Use. *Environ. Sci. Technol.* **2014**, *48* (18), 10607–10613 DOI: 10.1021/es502169p.

(266) Zhang, J.; Lee, K.; He, L.; Seiffert, J.; Subramaniam, P.; Yang, L.; Chen, S.; Maguire, P.; Mainelis, G.; Schwander, S.; Tetley, T.; Porter, A.; Ryan, M.; Shaffer, M.; Hu, S.; Gong, J.; Chung, K. Effects of a Nanoceria Fuel Additive on Physicochemical Properties of Diesel Exhaust Particles. *Environ. Sci. Process. Impacts* **2016**, 1333–1342 DOI: 10.1039/C6EM00337K.

(267) Keskin, A.; Gürü, M.; Altıparmak, D. Influence of Metallic Based Fuel Additives on Performance and Exhaust Emissions of Diesel Engine. *Energy Convers. Manag.* **2011**, *52* (1), 60–65 DOI: 10.1016/j.enconman.2010.06.039.

(268) Wakefield, G.; Wu, X.; Gardener, M.; Park, B.; Anderson, S. Envirox(TM) Fuel-Borne

Catalyst: Developing and Launching a Nano-Fuel Additive. *Technol. Anal. Strateg. Manag.* **2008**, *20* (1), 127 DOI: 10.1080/09537320701726825.

(269) Pontikakis, G. N.; Koltikakis, G. C.; Stamatelos, A. M. Dynamic Filtration Modeling in Foam Filters for Diesel Exhaust. *Chem. Eng. Commun.* **2001**, *188* (1), 21–46 DOI: 10.1080/00986440108912894.

(270) Bensaid, S.; Russo, N.; Fino, D. CeO2 Catalysts with Fibrous Morphology for Soot Oxidation: The Importance of the Soot-Catalyst Contact Conditions. *Catal. Today* **2013**, *216*, 57–63 DOI: 10.1016/j.cattod.2013.05.006.

(271) Twigg, M. V.; Phillips, P. R. Cleaning the Air We Breathe - Controlling Diesel Particulate Emissions from Passenger Cars. *Platin. Met. Rev.* **2009**, *53* (1), 27–34 DOI: 10.1595/147106709X390977.

(272) Liati, A.; Eggenschwiler, P. D. Characterization of Particulate Matter Deposited in Diesel Particulate Filters: Visual and Analytical Approach in Macro-, Micro- and Nano-Scales. *Combust. Flame* **2010**, *157* (9), 1658–1670 DOI: 10.1016/j.combustflame.2010.02.015.

(273) Rogelj, J.; Den Elzen, M.; Höhne, N.; Fransen, T.; Fekete, H.; Winkler, H.; Schaeffer, R.; Sha, F.; Riahi, K.; Meinshausen, M. Paris Agreement Climate Proposals Need a Boost to Keep Warming Well below 2 °c. *Nature* **2016**, *534* (7609), 631–639 DOI: 10.1038/nature18307.

(274) Office of Air and Radiation; U.S. Environmental Protection Agency. *The Benefits and Costs of the Clean Air Act from 1990 to 2020*; 2011.

(275) European Parliament. Directive 2009/30/EC of the European Parliament and of the Council. *Off. J. Eur. Union* **2009**, No. April, L140/88-L140/113 DOI: 10.3000/17252555.L_2009.140.eng.

(276) Vidal, J. The rise of diesel in Europe: the impact on health and pollution https://www.theguardian.com/environment/2015/sep/22/the-rise-diesel-in-europe-impact-on-health-pollution.

(277) Chambers, M.; Schmitt, R. Diesel-powered Passenger Cars and Light Trucks.

(278) Administration, U. S. E. I. Consumption/Sales https://www.eia.gov/petroleum/data.php.

(279) Organization, W. H. World Health Organization Data and Statistics http://www.euro.who.int/en/health-topics/environment-and-health/air-quality/data-and-statistics.

(280) Organization, W. H. WHO's Ambient Urban Air Pollution database - Update 2016 http://www.who.int/phe/health_topics/outdoorair/databases/AAP_database_methods_2016_v03.pdf?ua=1.

(281) Jung, H.; Kittelson, D. B.; Zachariah, M. R. The Influence of a Cerium Additive on Ultrafine Diesel Particle Emissions and Kinetics of Oxidation. *Combust. Flame* **2005**, *142* (3), 276–288 DOI: 10.1016/j.combustflame.2004.11.015.

(282) Park, B.; Donaldson, K.; Duffin, R.; Tran, L.; Kelly, F.; Mudway, I.; Morin, J.-P.; Guest,

R.; Jenkinson, P.; Samaras, Z.; Giannouli, M.; Kouridis, H.; Martin, P. Hazard and Risk Assessment of a Nanoparticulate Cerium Oxide-Based Diesel Fuel Additive - a Case Study. *Inhal. Toxicol.* **2008**, *20* (January), 547–566 DOI: 10.1080/08958370801915309.

(283) Gantt, B.; Hoque, S.; Fahey, K. M.; Willis, R. D.; Delgado-Saborit, J. M.; Harrison, R. M.; Zhang, K. M.; Jefferson, D. A.; Kalberer, M.; Bunker, K. L.; Conny, J. M.; Bhave, P. V.; Weinstein, J. P.; Pye, H. O. T. Factors Affecting the Ambient Physicochemical Properties of Cerium-Containing Particles Generated by Nanoparticle Diesel Fuel Additive Use. *Aerosol Sci. Technol.* **2015**, *49* (6), 371–380 DOI: 10.1080/02786826.2015.1027809.

(284) Dale, J. G.; Cox, S. S.; Vance, M. E.; Marr, L. C.; Hochella, M. F. Diesel Fuel Additive during Combustion in a Diesel Engine Transformation of Cerium Oxide Nanoparticles from a Diesel Fuel Additive during Combustion in a Diesel Engine. *Environ. Sci. Technol.* **2017**, *51*, 1973–1980 DOI: 10.1021/acs.est.6b03173.

(285) Kooter, I. M.; Alblas, M. J.; Jedynska, A. D.; Steenhof, M.; Houtzager, M. M. G.; Ras, M. van. Alveolar Epithelial Cells (A549) Exposed at the Air–liquid Interface to Diesel Exhaust: First Study in TNO's Powertrain Test Center. *Toxicol. Vitr.* **2013**, *27* (8), 2342–2349 DOI: 10.1016/j.tiv.2013.10.007.

(286) Turner, J.; Hernandez, M.; Snawder, J. E.; Handorean, A.; McCabe, K. M. A Toxicology Suite Adapted for Comparing Parallel Toxicity Responses of Model Human Lung Cells to Diesel Exhaust Particles and Their Extracts. *Aerosol Sci. Technol.* **2015**, *49* (8), 599–610 DOI: 10.1080/02786826.2015.1053559.

(287) Seagrave, J.; Dunaway, S.; McDonald, J. D.; Mauderly, J. L.; Hayden, P.; Stidley, C. Responses of Differentiated Primary Human Lung Epithelial Cells To Exposure To Diesel Exhaust At an Air-Liquid Interface. *Exp. Lung Res.* **2007**, *33* (1), 27–51 DOI: 10.1080/01902140601113088.

(288) Hawley, B.; McKenna, D.; Marchese, A.; Volckens, J. Time Course of Bronchial Cell Inflammation Following Exposure to Diesel Particulate Matter Using a Modified EAVES. *Toxicol. Vitr.* **2014**, *28* (5), 829–837 DOI: 10.1016/j.tiv.2014.03.001.

(289) Cao, D.; Bromberg, P. a.; Samet, J. M. COX-2 Expression Induced by Diesel Particles Involves Chromatin Modification and Degradation of HDAC1. *Am. J. Respir. Cell Mol. Biol.* **2007**, *37* (19), 232–239 DOI: 10.1165/rcmb.2006-0449OC.

(290) Steiner, S.; Bisig, C.; Petri-Fink, A.; Rothen-Rutishauser, B. Diesel Exhaust: Current Knowledge of Adverse Effects and Underlying Cellular Mechanisms. *Arch. Toxicol.* **2016**, *90* (7), 1541–1553 DOI: 10.1007/s00204-016-1736-5.

(291) Park, S.; Nam, H.; Chung, N.; Park, J.-D.; Lim, Y. The Role of Iron in Reactive Oxygen Species Generation from Diesel Exhaust Particles. *Toxicol. Vitr.* **2006**, *20* (6), 851–857 DOI: 10.1016/j.tiv.2005.12.004.

(292) Ghio, A. J.; Smith, C. B.; Madden, M. C. Diesel Exhaust Particles and Airway Inflammation. *Curr. Opin. Pulm. Med.* **2012**, *18* (2), 144–150 DOI: 10.1097/MCP.0b013e32834f0e2a.

(293) Dybdahl, M.; Risom, L.; Bornholdt, J.; Autrup, H.; Loft, S.; Wallin, H. Inflammatory and Genotoxic Effects of Diesel Particles in Vitro and in Vivo. *Mutat. Res. - Genet. Toxicol. Environ. Mutagen.* **2004**, *562* (1–2), 119–131 DOI: 10.1016/j.mrgentox.2004.05.010.

(294) Hesterberg, T. W.; Long, C. M.; Bunn, W. B.; Sax, S. N.; Lapin, C. A.; Valberg, P. A. Non-Cancer Health Effects of Diesel Exhaust: A Critical Assessment of Recent Human and Animal Toxicological Literature. *Crit. Rev. Toxicol.* **2009**, *39* (3), 195–227 DOI: 10.1080/10408440802220603.

(295) Rubio, L.; Annangi, B.; Vila, L.; Hernández, A.; Marcos, R. Antioxidant and Anti-Genotoxic Properties of Cerium Oxide Nanoparticles in a Pulmonary-like Cell System. *Arch. Toxicol.* **2016**, *90* (2), 269–278 DOI: 10.1007/s00204-015-1468-y.

(296) Mazzolini, J.; Weber, R. J. M.; Chen, H.-S.; Khan, A.; Guggenheim, E.; Shaw, R. K.; Chipman, J. K.; Viant, M. R.; Rappoport, J. Z. Protein Corona Modulates Uptake and Toxicity of Nanoceria *via* Clathrin-Mediated Endocytosis. *Biol. Bull.* **2016**, *231* (1), 40–60 DOI: 10.1086/689590.

(297) Eom, H.-J.; Choi, J. Oxidative Stress of CeO2 Nanoparticles via P38-Nrf-2 Signaling Pathway in Human Bronchial Epithelial Cell, Beas-2B. *Toxicol. Lett.* **2009**, *187*, 77–83.

(298) Strobel, C.; Förster, M.; Hilger, I. Biocompatibility of Cerium Dioxide and Silicon Dioxide Nanoparticles with Endothelial Cells. *Beilstein J. Nanotechnol.* **2014**, *5*, 1795–1807 DOI: 10.3762/bjnano.5.190.

(299) Rotoli, B. M.; Bussolati, O.; Costa, A. L.; Blosi, M.; Cristo, L. Di; Zanello, P. P.; Bianchi, M. G.; Visigalli, R.; Bergamaschi, E. Comparative Effects of Metal Oxide Nanoparticles on Human Airway Epithelial Cells and Macrophages. *J. Nanoparticle Res.* **2012**, *14* (9) DOI: 10.1007/s11051-012-1069-0.

(300) Demokritou, P.; Gass, S.; Pyrgiotakis, G.; Cohen, J. M.; Goldsmith, W.; McKinney, W.; Frazer, D.; Ma, J. Y.; Schwegler-Berry, D.; Brain, J. D.; Castranova, V. An in Vivo and in Vitro Toxicological Characterization of Realistic Nanoscale CeO2 Inhalation Exposures. *Nanotoxicology* **2013**, *7* (8), 1338–1350 DOI: 10.3109/17435390.2012.739665.

(301) Xia, T.; Kovochich, M.; Liong, M.; Madler, L.; Gilbert, B.; Shi, H.; Yeh, J. I.; Zink, J. I.; Nel, A. E. Comparison of the Mechanism of Toxicity of Zinc Oxide and Cerium Oxide Nanoparticles Based on Dissolution and Oxidative Stress Properties. *ACS Nano* **2008**, *2* (10), 2121–2134 DOI: 10.1097/WAD.0b013e3181aba588.MRI.

(302) Wingard, C. J.; Walters, D. M.; Cathey, B. L.; Hilderbrand, S. C.; Katwa, P.; Lin, S.; Ke, P. C.; Podlia, R.; Rao, A.; Lust, R. M.; Brown, J. M. Mast Cells Contribute to Altered Vascular Reactivity and Ischemia-Reperfusion Injury Following Cerium Oxide Nanoparticle Instillation. *Nanotoxicology* **2011**, *5*, 531–545 DOI: 10.1016/j.pestbp.2011.02.012.Investigations.

(303) Kumari, M.; Singh, S. P.; Chinde, S.; Rahman, M. F.; Mahboob, M.; Grover, P. Toxicity Study of Cerium Oxide Nanoparticles in Human Neuroblastoma Cells. *Int J Toxicol* **2014**, *33* (2), 86–97 DOI: 10.1177/1091581814522305.

(304) Lin, W.; Huang, Y.-W.; Zhou, X.-D.; Ma, Y. Toxicity of Cerium Oxide Nanoparticles in

Human Lung Cancer Cells. *Int. J. Toxicol.* **2006**, *25* (6), 451–457 DOI: 10.1080/10915810600959543.

(305) Mittal, S.; Pandey, A. K. Cerium Oxide Nanoparticles Induced Toxicity in Human Lung Cells: Role of ROS Mediated DNA Damage and Apoptosis. *Biomed Res Int* **2014**, *2014*, 891934 DOI: 10.1155/2014/891934.

(306) Holder, A. L.; Lucas, D.; Goth-Goldstein, R.; Koshland, C. P. Inflammatory Response of Lung Cells Exposed to Whole, Filtered, and Hydrocarbon Denuded Diesel Exhaust. *Chemosphere* **2007**, *70*, 13–19 DOI: 10.1016/j.chemosphere.2007.07.036.

(307) Li, J.; Ghio, A. J.; Cho, S.-H.; Brinckerhoff, C. E.; Simon, S. a; Liedtke, W. Diesel Exhaust Particles Activate the Matrix-Metalloproteinase-1 Gene in Human Bronchial Epithelia in a Beta-Arrestin-Dependent Manner via Activation of RAS. *Environ. Health Perspect.* **2009**, *117* (3), 400–409 DOI: 10.1289/ehp.0800311.

(308) Steiner, S.; Heeb, N. V; Czerwinski, J.; Comte, P.; Mayer, A.; Petri-Fink, A.; Rothen-Rutishauser, B. Test-Methods on the Test-Bench: A Comparison of Complete Exhaust and Exhaust Particle Extracts for Genotoxicity/Mutagenicity Assessment. *Environ. Sci. & Technol.* **2014**, *48* (9), 5237–5244 DOI: 10.1021/es4056033.

(309) Hawley, B.; L'Orange, C.; Olsen, D. B.; Marchese, A. J.; Volckens, J. Oxidative Stress and Aromatic Hydrocarbon Response of Human Bronchial Epithelial Cells Exposed to Petro- or Biodiesel Exhaust Treated with a Diesel Particulate Filter. *Toxicol. Sci.* **2014**, *141* (2), 505–514 DOI: 10.1093/toxsci/kfu147.

(310) Zarcone, M. C.; Duistermaat, E.; van Schadewijk, A.; Jedynska, A.; Hiemstra, P. S.; Kooter, I. M. Cellular Response of Mucociliary Differentiated Primary Bronchial Epithelial Cells to Diesel Exhaust. *Am. J. Physiol. - Lung Cell. Mol. Physiol.* **2016**, *311* (1), L111–L123 DOI: 10.1152/ajplung.00064.2016.

(311) Steiner, S.; Mueller, L.; Popovicheva, O. B.; Raemy, D. O.; Czerwinski, J.; Comte, P.; Mayer, A.; Gehr, P.; Rothen-Rutishauser, B.; Clift, M. J. D. Cerium Dioxide Nanoparticles Can Interfere with the Associated Cellular Mechanistic Response to Diesel Exhaust Exposure. *Toxicol. Lett.* **2012**, *214* (2), 218–225 DOI: 10.1016/j.toxlet.2012.08.026.

(312) Zhang, Z. H.; Balasubramanian, R. Effects of Cerium Oxide and Ferrocene Nanoparticles Addition As Fuel-Borne Catalysts on Diesel Engine Particulate Emissions: Environmental and Health Implications. *Environ. Sci. Technol.* **2017**, *51* (8), 4248–4258 DOI: 10.1021/acs.est.7b00920.

(313) Fall, M.; Guerbet, M.; Park, B.; Gouriou, F.; Dionnet, F.; Morin, J.-P. Evaluation of Cerium Oxide and Cerium Oxide Based Fuel Additive Safety on Organotypic Cultures of Lung Slices. *Nanotoxicology* **2007**, *1* (3), 227–234 DOI: 10.1080/10643389.2012.728825.

(314) Veranth, J. M.; Kaser, E. G.; Veranth, M. M.; Koch, M.; Yost, G. S. Cytokine Responses of Human Lung Cells (BEAS-2B) Treated with Micron-Sized and Nanoparticles of Metal Oxides Compared to Soil Dusts. *Part. Fibre Toxicol.* **2007**, *4* (1), 2 DOI: 10.1186/1743-8977-4-2.

(315) Batley, G. E.; Halliburton, B.; Kirby, J. K.; Doolette, C. L.; Navarro, D.; Mclaughlin, M. J.; Veitch, C. Characterization and Ecological Risk Assessment Of Nanoparticulate CeO2 as a Diesel Fuel Catalyst. *Environ. Toxicol. Chem.* **2013**, *32* (8), 1896–1905 DOI: 10.1002/etc.2246.

(316) Secondo, L. E.; Wygal, N. J.; Lewinski, N. A. A New Portable in Vitro Exposure Cassette for Aerosol Sampling. *J. Vis. Exp.* **2018**, *Submitted*.

(317) Papaioannou, E.; Konstandopoulos, A. G.; Morin, J.; Preterre, D. A Selective Particle Size Sampler Suitable for Biological Exposure Studies of Diesel Particulate. *SAE Tech. Pap. Ser.* **2006**, No. April 3 DOI: 10.4271/2006-01-1075.

(318) Sieuwerts, A. M.; Klijn, J. G. M.; Peters, H. A.; Foekens, J. A. The MTT Tetrazolium Salt Assay Scrutinized: How to Use This Assay Reliably to Measure Metabolic Activity of Cell Cultures in Vitro for the Assessment of Growth Characteristics, IC50-Values and Cell Survival. *Clin. Chem. Lab. Med.* **1995**, *33* (11), 813–824 DOI: 10.1515/cclm.1995.33.11.813.

(319) Decker, T.; Lohmann-Matthes, M.-L. A Quick and Simple Method for the Quantitation of Lactate Dehydrogenase Release in Measurements of Cellular Cytotoxicity and Tumor Necrosis Factor (TNF) Activity. *J. Immunol. Methods* **1988**, *15*, 61–69 DOI: 10.1016/j.pcad.2015.11.006.

(320) Maricq, M. M.; Xu, N. The Effective Density and Fractal Dimension of Soot Particles from Premixed Flames and Motor Vehicle Exhaust. *J. Aerosol Sci.* **2004**, *35* (10), 1251–1274 DOI: 10.1016/j.jaerosci.2004.05.002.

(321) Kittelson, D. B. Engines and Nanoparticles: A Review. *J. Aerosol Sci.* **1998**, *29* (5–6), 575–588 DOI: 10.1016/S0021-8502(97)10037-4.

(322) Alaghmand, M.; Blough, N. V. Source-Dependent Variation in Hydroxyl Radical Production by Airborne Particulate Matter. *Environ. Sci. Technol.* **2007**, *41* (7), 2364–2370 DOI: 10.1021/es061902o.

(323) Jantzen, K.; Roursgaard, M.; Desler, C.; Loft, S.; Rasmussen, L. J.; Møller, P. Oxidative Damage to DNA by Diesel Exhaust Particle Exposure in Co-Cultures of Human Lung Epithelial Cells and Macrophages. *Mutagenesis* **2012**, *27* (6), 693–701 DOI: 10.1093/mutage/ges035.

(324) Zhang, H.; Ji, Z.; Xia, T.; Meng, H.; Low-Kam, C.; Liu, R.; Pokhrel, S.; Lin, S.; Wang, X.; Liao, Y. P.; Wang, M.; Li, L.; Rallo, R.; Damoiseaux, R.; Telesca, D.; M??dler, L.; Cohen, Y.; Zink, J. I.; Nel, A. E. Use of Metal Oxide Nanoparticle Band Gap to Develop a Predictive Paradigm for Oxidative Stress and Acute Pulmonary Inflammation. *ACS Nano* **2012**, *6* (5), 4349–4368 DOI: 10.1021/nn3010087.

(325) Demokritou, P.; Gass, S.; Pyrgiotakis, G.; Cohen, J. M.; Goldsmith, W.; McKinney, W.; Frazer, D.; Ma, J. Y.; Schwegler-Berry, D.; Brain, J. D.; Castranova, V. An in Vivo and in Vitro Toxicological Characterization of Realistic Nanoscale CeO2 Inhalation Exposures. *Nanotoxicology* **2013**, *7* (8), 1338–1350 DOI: 10.3109/17435390.2012.739665.An.

(326) Lehmann, A. D.; Blank, F.; Baum, O.; Gehr, P.; Rothen-Rutishauser, B. M. Diesel

Exhaust Particles Modulate the Tight Junction Protein Occludin in Lung Cells in Vitro. *Part. Fibre Toxicol.* **2009**, *6* (1), 26 DOI: 10.1186/1743-8977-6-26.

(327) Amara, N.; Bachoual, R.; Desmard, M.; Golda, S.; Guichard, C.; Lanone, S.; Aubier, M.; Ogier-Denis, E.; Boczkowski, J. Diesel Exhaust Particles Induce Matrix Metalloprotease-1 in Human Lung Epithelial Cells via a NADP(H) Oxidase/NOX4 Redox-Dependent Mechanism. *Am. J. Physiol. Lung Cell. Mol. Physiol.* **2007**, *293* (1), L170-81 DOI: 10.1152/ajplung.00445.2006.

(328) Gantt, B.; Hoque, S.; Willis, R. D.; Fahey, K. M.; Delgado-Saborit, J. M.; Harrison, R. M.; Erdakos, G. B.; Bhave, P. V.; Zhang, K. M.; Kovalcik, K.; Pye, H. O. T. Near-Road Modeling and Measurement of Cerium-Containing Particles Generated by Nanoparticle Diesel Fuel Additive Use. *Environ. Sci. Technol.* **2014**, *48* (18), 10607–10613 DOI: 10.1021/es502169p.

(329) Wakefield, G.; Wu, X.; Gardener, M.; Park, B.; Anderson, S. Envirox(TM) Fuel-Borne Catalyst: Developing and Launching a Nano-Fuel Additive. *Technol. Anal. Strateg. Manag.* **2008**, *20* (1), 127 DOI: 10.1080/09537320701726825.

(330) Bueno-López, A. Diesel Soot Combustion Ceria Catalysts. *Appl. Catal. B Environ.* **2014**, *146*, 1–11 DOI: 10.1016/j.apcatb.2013.02.033.

(331) Lahaye, J.; Boehm, S.; Chambrion, P. H.; Ehrburger, P. Influence of Cerium Oxide on the Formation and Oxidation of Soot. *Combust. Flame* **1996**, *104* (1), 199–207.

(332) Bokova, M. N.; Decarne, C.; Abi-Aad, E.; Pryakhin, A. N.; Lunin, V. V.; Aboukaïs, A. Kinetics of Catalytic Carbon Black Oxidation. *Thermochim. Acta* **2005**, *428* (1–2), 165–171 DOI: 10.1016/j.tca.2004.11.011.

(333) Skillas, G.; Qian, Z.; Baltensperger, U.; Matter, U.; Burtscher, H. The Influence of Additives on the Size Distribution and Composition of Particles Produced by Diesel Engines. *Combust. Sci. Technol.* **2000**, *154* (February 2015), 259–273 DOI: 10.1080/00102200008947279.

(334) Zavala, J.; Greenan, R.; Krantz, Q. T.; DeMarini, D. M.; Higuchi, M.; Gilmour, M. I.; White, P. A. Regulating Temperature and Relative Humidity in Air–liquid Interface in Vitro Systems Eliminates Cytotoxicity Resulting from Control Air Exposures. *Toxicol. Res.* **2017**, 448–459 DOI: 10.1039/C7TX00109F.

(335) Jiang, R. De; Shen, H.; Piao, Y. J. The Morphometrical Analysis on the Ultrastructure of A549 Cells. *Rom. J. Morphol. Embryol.* **2010**, *51* (4), 663–667.

(336) Mills, J. B.; Hong Park, J.; Peters, T. M. Comparison of the DiSCmini Aerosol Monitor to a Handheld Condensation Particle Counter and a Scanning Mobility Particle Sizer for Submicrometer Sodium Chloride and Metal Aerosols. *J. Occup. Environ. Hyg.* **2013**, *10* (5), 250–258 DOI: 10.1080/15459624.2013.769077.

(337) Matson, U.; Ekberg, L. E.; Afshari, A. Measurement of Ultrafine Particles: A Comparison of Two Handheld Condensation Particle Counters. *Aerosol Sci. Technol.* **2004**, *38* (5), 487–495 DOI: 10.1080/02786820490462200.

(338) Gerhardt, N.; Clothier, R.; Wild, G. Investigating the Practicality of Hazardous Material

Detection Using Unmanned Aerial Systems. *2014 IEEE Int. Work. Metrol. Aerospace, Metroaerosp. 2014 - Proc.* **2014**, 133–137 DOI: 10.1109/MetroAeroSpace.2014.6865908.

(339) Vilcekova, S.; Burdova, E. K.; Snopkova, M. Environmental Assessment of Selected Building - Case Study. In *GeoConference on Nano, Bio and Green - Technologies for a Sustainable Future*; 2013; pp 633–647.

(340) Halliwell, B.; Whiteman, M. Measuring Reactive Species and Oxidative Damage in Vivo and in Cell Culture: How Should You Do It and What Do the Results Mean? *Br. J. Pharmacol.* **2004**, *142*, 231–255 DOI: 10.1038/sj.bjp.0705776.

(341) Orrenius, S.; Nicotera, P.; Zhivotovsky, B. Cell Death Mechanisms and Their Implications in Toxicology. *Toxicol. Sci.* **2011**, *119* (1), 3–19 DOI: 10.1093/toxsci/kfq268.

(342) Zhang, L.; Ru, B.; Liu, Y.; Li, M.; Li, B.; Wang, L.; Xu, L.; Le Guyader, L.; Chen, C. The Dose-Dependent Toxicological Effects and Potential Perturbation on the Neurotransmitter Secretion in Brain Following Intranasal Instillation of Copper Nanoparticles. *Nanotoxicology* **2012**, *6* (5), 562–575 DOI: 10.3109/17435390.2011.590906.

(343) Ghio, A. J.; Kim, C.; Devlin, R. B. Pulmonary Inflammation in Healthy Human Volunteers. *Crit. Care Med.* **2000**, *162* (3), 981–988.

(344) Auger, F.; Gendron, M. C.; Chamot, C.; Marano, F.; Dazy, A. C. Responses of Well-Differentiated Nasal Epithelial Cells Exposed to Particles: Role of the Epithelium in Airway Inflammation. *Toxicol. Appl. Pharmacol.* **2006**, *215*, 285–294 DOI: 10.1016/j.taap.2006.03.002.

(345) Larsen, S. T.; Jackson, P.; Poulsen, S. S.; Levin, M.; Jensen, K. A.; Wallin, H.; Nielsen, G. D.; Koponen, I. K. Airway Irritation, Inflammation, and Toxicity in Mice Following Inhalation of Metal Oxide Nanoparticles. *Nanotoxicology* **2016**, *10* (9), 1254–1262 DOI: 10.1080/17435390.2016.1202350.

(346) Cromwell, O.; Hamid, Q.; Corrigan, C.; Barkans, J.; Meng, Q.; Collins, P. *Expression and Generation of Interleukin-8, IL-6 and Granulocyte-Macrophage Colony-Stimulating Factor by Bronchial Epithelial Cells and Enhancement by IL-1 and Tumour Necrosis Factor-A*; 1992; Vol. 77.

(347) Harada, A.; Sekido, N.; Akahoshi, T.; Wada, T.; Mukaida, N.; Matsushima, K. Essential Involvement of Interleukin-8 (IL-8) in Acute Inflammation. *J. Leukoc. Biol.* **1994**, *56* (5), 559–564.

(348) Strieter, R.; Kunkel, S. Acute Lung Injury: The Role of Cytokines in the Elicitation of Neutrophils. *J. Investig. Med. Off. Publ. Am. Fed. Clin. Res.* **1994**, *42* (4), 640–651.

(349) Vietti, G.; Lison, D.; Van Den Brule, S. Mechanisms of Lung Fibrosis Induced by Carbon Nanotubes: Towards an Adverse Outcome Pathway (AOP). *Part. Fibre Toxicol.* **2016**, *13* (11), 1–23 DOI: 10.1186/s12989-016-0123-y.

(350) Savolainen, K.; Backman, U.; Brouwer, D.; Fadeel, B.; Fernandes, T. *Nanosafety in Europe 2015-2025: Towards Safe and Sustainable Nanomaterials and Nanotechnology Innovations Nanosafety in Europe Towards Safe and Sustainable Nanomaterials and Nanotechnology Innovations*; 2013.

(351) Wittekindt, O. H.; Kinsner-Ovaskainen, A.; Colpo, P.; Ponti, J.; Rossi, F. *In Vitro Toxicology Systems*; 2014.

(352) Santschi, C.; Moos, N.; Koman, V. B.; Slaveykova, V. I.; Bowen, P.; Martin, O. J. F. Non-Invasive Continuous Monitoring of pro-Oxidant Effects of Engineered Nanoparticles on Aquatic Microorganisms. *J. Nanobiotechnology* **2017**, *15* (1), 1–18 DOI: 10.1186/s12951-017-0253-x.

(353) Ganesana, M.; Erlichman, J. S.; Andreescu, S. Real-Time Monitoring of Superoxide Accumulation and Antioxidant Activity in a Brain Slice Model Using an Electrochemical Cytochrome c Biosensor. *Free Radic. Biol. Med.* **2012**, *53* (12), 2240–2249 DOI: 10.1016/j.freeradbiomed.2012.10.540.

(354) Daiber, A.; Bachschmid, M. Enzyme Inhibition by Peroxynitrite-Mediated Tyrosine Nitration and Thiol Oxidation. *Curr. Enzym. Inhib.* **2007**, *3* (2), 15 DOI: 10.2174/157340807780598369.

(355) Daiber, A.; Frein, D.; Namgaladze, D.; Ullrich, V. Oxidation and Nitrosation in the Nitrogen Monoxide/Superoxide System* Downloaded From. *J. Biol. Chem.* **2002**, *277* (14), 11882–11888 DOI: 10.1074/jbc.M111988200.

(356) Murphy, M. P. How Mitochondria Produce Reactive Oxygen Species. *Biochem. J* **2009**, *417*, 1–13 DOI: 10.1042/BJ20081386.

(357) Curtin, J. F.; Donovan, M.; Cotter, T. G. Regulation and Measurement of Oxidative Stress in Apoptosis. *J. Immunol. Methods* **2002**, *265*, 49–72.

(358) Calas-Blanchard, C.; Cortina-Puig, M.; Barthelmebs, L.; Noguer, T. Electrochemical Biosensors for the Determination of the Antioxidant Capacity in Foods and Beverages Based on Reactive Oxygen Species. *Curr. Anal. Chem.* **2012**, *8* (4), 428–435 DOI: 10.2174/157341112803216852.

(359) Hurtado-Gallego, J.; Martín-Betancor, K.; Rodea-Palomares, I.; Leganés, F.; Rosal, R.; Fernández-Piñas, F. Two Novel Cyanobacterial Bioluminescent Whole-Cell Bioreporters Based on Superoxide Dismutases MnSod and FeSod to Detect Superoxide Anion. *Chemosphere* **2018**, *201*, 772–779 DOI: 10.1016/j.chemosphere.2018.03.012.

(360) Prieto-Simón, B.; Cortina, M.; Campàs, M.; Calas-Blanchard, C. Electrochemical Biosensors as a Tool for Antioxidant Capacity Assessment. *Sensors Actuators, B Chem.* **2008**, *129* (1), 459–466 DOI: 10.1016/j.snb.2007.08.004.

(361) Haber, V. F.; Weiss, J. Uber Die Katalyse Des Hydroperoxydes. *Naturwissenschaften* **1932**, *20* (51), 948–950.

(362) Kehrer, J. P. *The Haber-Weiss Reaction and Mechanisms of Toxicity*; 2000; Vol. 149.

(363) Brunner, T. J.; Wick, P.; Manser, P.; Spohn, P.; Grass, N.; Limbach, L. K.; Bruinink, A.; Stark, W. J. In Vitro Cytotoxicity of Oxide Nanoparticles : Comparison to Asbestos , Silica , and the Effect of Particle Solubility In Vitro Cytotoxicity of Oxide Nanoparticles : Comparison to Asbestos , Silica , and the Effect of Particle Solubility †. *Environ. Sci. Technol.* **2006**, *40* (14), 4374–4381 DOI: 10.1021/es052069i.

(364) Myhre, O.; Andersen, J. M.; Aarnes, H.; Fonnum, F. Commentary Evaluation of the Probes 2',7'-Dichlorofluorescin Diacetate, Luminol, and Lucigenin as Indicators of Reactive Species Formation. *2Biochemical Pharmacol.* **2003**, *65*, 1575–1582 DOI: 10.1016/S0006-2952(03)00083-2.

(365) Kalyanaraman, B.; Darley-Usmar, V.; Davies, K. J. A.; Dennery, P. A.; Forman, H. J.; Grisham, M. B.; Mann, G. E.; Moore, K.; Jackson, L.; Ii, R.; Ischiropoulos, H. Measuring Reactive Oxygen and Nitrogen Species with Fluorescent Probes: Challenges and Limitations. *Free Radic. Biol. Med.* **2012**, *52*, 1–6 DOI: 10.1016/j.freeradbiomed.2011.09.030.

(366) Monaghan, P.; Metcalfe, N. B.; Torres, R. Oxidative Stress as a Mediator of Life History Trade-Offs: Mechanisms, Measurements and Interpretation. *Ecol. Lett.* **2009**, *12* (1), 75–92 DOI: 10.1111/j.1461-0248.2008.01258.x.

(367) Wagner, B. A.; Witmer, J. R.; Van't Erve, T. J.; Buettner, G. R. An Assay for the Rate of Removal of Extracellular Hydrogen Peroxide by Cells. *Redox Biol.* **2013**, *1*, 210–217 DOI: 10.1016/j.redox.2013.01.011.

(368) Calas-Blanchard, C.; Catanante, G.; Noguer, T. Electrochemical Sensor and Biosensor Strategies for ROS/RNS Detection in Biological Systems. *Electroanalysis* **2014**, *26* (6), 1277–1286 DOI: 10.1002/elan.201400083.

(369) Braik, M.; Barsan, M. M.; Dridi, C.; Ben Ali, M.; Brett, C. M. A. Highly Sensitive Amperometric Enzyme Biosensor for Detection of Superoxide Based on Conducting Polymer/CNT Modified Electrodes and Superoxide Dismutase. *Sensors Actuators, B Chem.* **2016**, *236*, 574–582 DOI: 10.1016/j.snb.2016.06.032.

(370) Zhu, X.; Liu, T.; Zhao, H.; Shi, L.; Li, X.; Lan, M. Ultrasensitive Detection of Superoxide Anion Released from Living Cells Using a Porous Pt-Pd Decorated Enzymatic Sensor. *Biosens. Bioelectron.* **2016**, *79*, 449–456 DOI: 10.1016/j.bios.2015.12.061.

(371) Crulhas, B. P.; Recco, L. C.; Delella, F. K.; Pedrosa, V. A. A Novel Superoxide Anion Biosensor for Monitoring Reactive Species of Oxygen Released by Cancer Cells. *Electroanalysis* **2017**, *29* (5), 1252–1257 DOI: 10.1002/elan.201600767.

(372) Singh, P.; Srivastava, S.; Singh, S. H2O2 Sensing through Electrochemically Deposited Thionine Coated ITO Thin Film. *Cell. Mol. Biol.* **2017**, *63* (6), 60–62 DOI: 10.1016/j.pcad.2015.11.006.

(373) Bollella, P.; Fusco, G.; Tortolini, C.; Sanzò, G.; Favero, G.; Gorton, L.; Antiochia, R. Beyond Graphene: Electrochemical Sensors and Biosensors for Biomarkers Detection. *Biosens. Bioelectron.* **2017**, *89*, 152–166 DOI: 10.1016/j.bios.2016.03.068.

(374) Saha, S.; Arya, S. K.; Singh, S. P.; Sreenivas, K.; Malhotra, B. D.; Gupta, V. Zinc Oxide – Potassium Ferricyanide Composite Thin Film Matrix for Biosensing Applications. *Anal. Chim. Acta* **2009**, *653* (2), 212–216.

(375) Banan Sadeghian, R.; Han, J.; Ostrovidov, S.; Salehi, S.; Bahraminejad, B.; Ahadian, S.; Chen, M.; Khademhosseini, A. Macroporous Mesh of Nanoporous Gold in Electrochemical Monitoring of Superoxide Release from Skeletal Muscle Cells. *Biosens.*

Bioelectron. **2017**, *88*, 41–47 DOI: 10.1016/j.bios.2016.06.067.

(376) Thirumalai, D.; Kathiresan, V.; Lee, J.; Jin, S.-H.; Chang, S.-C. Electrochemical Reactive Oxygen Species Detection by Cytochrome *c* Immobilized with Vertically Aligned and Electrochemically Reduced Graphene Oxide on a Glassy Carbon Electrode. *Analyst* **2017**, *142* (23), 4544–4552 DOI: 10.1039/C7AN01387F.

(377) Eguílaz, M.; Gutiérrez, A.; Rivas, G. Non-Covalent Functionalization of Multi-Walled Carbon Nanotubes with Cytochrome c: Enhanced Direct Electron Transfer and Analytical Applications. *Sensors Actuators B* **2016**, *225*, 74–80 DOI: 10.1016/j.snb.2015.11.011.

(378) Liu, X.; Marrakchi, M.; Jahne, M.; Rogers, S.; Andreescu, S. Real-Time Investigation of Antibiotics-Induced Oxidative Stress and Superoxide Release in Bacteria Using an Electrochemical Biosensor. *Free Radic. Biol. Med.* **2016**, *91*, 25–33 DOI: 10.1016/j.freeradbiomed.2015.12.001.

(379) Sadeghian, R. B.; Ostrovidov, S.; Han, J.; Salehi, S.; Bahraminejad, B.; Bae, H.; Chen, M.; Khademhosseini, A. Online Monitoring of Superoxide Anions Released from Skeletal Muscle Cells Using an Electrochemical Biosensor Based on Thick-Film Nanoporous Gold. *ACS Sensors* **2016**, *1* (7), 921–928 DOI: 10.1021/acssensors.6b00325.

(380) Li, X.; Liu, Y.; Zhu, A.; Luo, Y.; Deng, Z.; Tian, Y. Real-Time Electrochemical Monitoring of Cellular H2O2 Integrated with In Situ Selective Cultivation of Living Cells Based on Dual Functional Protein Microarrays at Au-TiO 2 Surfaces. *Anal. Chem.* **2010**, *82*, 6512–6518 DOI: 10.1021/ac100807c.

(381) Rahimi, P.; Ghourchian, H.; Rafiee-Pour, H.-A. Superoxide Radical Biosensor Based on a Nano-Composite Containing Cytochrome C. *Analyst* **2011**, *136*, 3803–3808 DOI: 10.1039/c1an15380c.

(382) Zhou, J.; Liao, C.; Zhang, L.; Wang, Q.; Tian, Y. Molecular Hydrogel-Stabilized Enzyme with Facilitated Electron Transfer for Determination of H2O2 Released from Live Cells. *Anal. Chem.* **2014**, *86* (9), 4395–4401 DOI: 10.1021/ac500231e.

(383) Zhu, A.; Tian, Y.; Liu, H.; Luo, Y. Nanoporous Gold Film Encapsulating Cytochrome c for the Fabrication of a H2O2 Biosensor. *Biomaterials* **2009**, *30*, 3183–3188 DOI: 10.1016/j.biomaterials.2009.02.019.

(384) Tammeveski, K.; Tenno, T. T.; Mashirin, A. A.; Hillhouse, E. W.; Manning, P.; Mcneil, C. J. Superoxide Electrode Based on Covalently Immobilized Cytochrom c: Modelling Studies. *Free Radic. Biol. Med.* **1998**, *25* (8), 973–978.

(385) Luo, Y.; Liu, H.; Rui, Q.; Tian, Y. Detection of Extracellular H2O2 Released from Human Liver Cancer Cells Based on TiO2 Nanoneedles with Enhanced Electron Transfer of Cytochrome C. *Anal. Chem.* **2009**, *81*, 3035–3041 DOI: 10.1021/ac802721x.

(386) Chen, X. J.; West, A. C.; Cropek, D. M.; Banta, S. Detection of the Superoxide Radical Anion Using Various Alkanethiol Monolayers and Immobilized Cytochrome C. *Anal. Biochem.* **2008**, *80*, 9622–9629 DOI: 10.1021/ac800796b.

(387) Bowden, E. F.; Hawkridge, F. M.; Blount, H. N. Interfacial Electrochemistry of Cytochrome c at Tin Oxide, Indium Oxide, Gold, and Platinum Electrodes. *J. Electroanal.*

Chem **1984**, *161*, 355.

(388) Cai, C. X.; Ju, H. X.; Chen, H. Y. The Effects of Temperature and Electrolyte on the Redox Potential of Cytochrome c at a Chemically Modified Microband Gold Electrode. *Electrochim. Acta* **1995**, *40* (9), 1109–1112.

(389) Rui, Q.; Komori, K.; Tian, Y.; Liu, H.; Luo, Y.; Sakai, Y. Electrochemical Biosensor for the Detection of H2O2 from Living Cancer Cells Based on ZnO Nanosheets. *Anal. Chim. Acta* **2010**, *670*, 57–62 DOI: 10.1016/j.aca.2010.04.065.

(390) Scognamiglio, V. Nanotechnology in Glucose Monitoring: Advances and Challenges in the Last 10 Years. *Biosens. Bioelectron.* **2013**, *47*, 12–25 DOI: 10.1016/j.bios.2013.02.043.

(391) Avila, A.; Gregory, B. W.; Niki, K.; Cotton, T. M. An Electrochemical Approach to Investigate Gated Electron Transfer Using a Physiological Model System: Cytochrome c Immobilized on Carboxylic Acid-Terminated Alkanethiol Self-Assembled Monolayers on Gold Electrodes. *J. Phys. Chem. B* **2000**, *104*, 2759–2766 DOI: 10.1021/jp992591p.

(392) Gomez-Mingot, M. G.; Montiel, V.; Banks, C. E.; Iniesta, J. Screen-Printed Graphite Macroelectrodes for the Direct Electron Transfer of Cytochrome c: A Deeper Study of the Effect of PH on the Conformational States, Immobilization and Peroxidase Activity. *Analyst* **2014**, *139*, 1442–1448 DOI: 10.1039/c3an02137h.

(393) Allen, H.; Hill, O.; Hunt, N. I.; Bond, A. M. The Transient Nature of the Diffusion Controlled Component of the Electrochemistry of Cytochrome c at “bare” Gold Electrodes: An Explanation Based on a Self-Blocking Mechanism. *J. Electroanal. Chem.* **1997**, *436*, 17–25.

(394) Lebel, C. P.; Ischiropoulos, H.; Bondy8, S. C. *Evaluation of the Probe 2’,7’-Dichlorofluorescin as an Indicator of Reactive Oxygen Species Formation and Oxidative Stress*; 1992; Vol. 5.

(395) Fisher, A. B. Redox Signaling Across Cell Membranes. *Antioxid. Redox Signal.* **2009**, *11* (6), 1349–1356.

(396) Finkel, T. Oxidant Signals and Oxidative Stress. *Curr. Opin. Cell Biol.* **2003**, *15*, 247–254 DOI: 10.1016/S0955-0674(03)00002-4.